SUBCELLULAR DISTRIBUTION OF LIPID METABOLISING ENZYMES IN HUMAN SKELETAL MUSCLE

JULIETTE A CLARK

A thesis submitted to the

University of Birmingham

for the degree of

DOCTOR OF PHILOSOPHY

School of Sport and Exercise Sciences

The University of Birmingham,

April 2012

GENERAL ABSTRACT

In obesity, lipids stored in muscle as lipid droplets (LDs) lead to accumulation of fatty acid (FA) metabolites and insulin resistance. This research involves development of immunofluorescence microscopy methods to generate novel information on the subcellular content and distribution of key enzymes that play a role in the underlying mechanisms. Chapters 3 and 4 describe visualisation of two lipid synthesising enzymes. Both are more abundant in type I muscle fibres. Chapter 5 reveals no differences between these enzymes in non obese and obese elderly women. Chapter 6 reveals that a key lipolytic enzyme (ATGL) has a higher content in type I fibres, but its activator does not. Chapter 7 describes visualisation of SNAP23 and reveals a high content at the plasma membrane and mitochondria and low content in LDs. Chapter 8 fails to observe a difference between obese and non obese elderly women in plasma membrane SNAP23, and therefore fails to confirm the hypothesis that LDs hijack SNAP23. However, obese women have less SNAP23 in mitochondria and this may limit FA oxidation. In conclusion this thesis describes several novel mechanisms by which obesity leads to accumulation of FA metabolites and insulin resistance. The developed methods will be a valuable novel tool for future diabetes research.

ACKNOWLEDGMENTS

There are many people who I need to thank for their involvement in this PhD. Whether at an academic or personal level, there are many kind and generous people who have played a part in the completion of this thesis.

First and foremost I would like to thank my supervisors, Professor Anton Wagenmakers and Dr Chris Shaw for allowing me to study within such a respected research group. The support and guidance you have offered over the last few years have been paramount to the completion of this thesis and continues to be invaluable. Your knowledge and the time that you have invested in me has allowed me to develop in confidence as a researcher and has made my PhD an enjoyable endeavour.

I would also like to thank the members of the histology research group and those working in the Histology lab; Helen, Matt, Oliver, Stuart and Sam. I would also like to thank all the study participants who have given their time so willingly to be involved in the experiments contained within this thesis; without them, this research would not have been possible. I would also like to thank Faye Moore for her help with patient recruitment as well as Mr Ed Davis for his collaboration, kindly allowing us to obtain samples from his patients. Finally I would like to thank the theatre staff at Russells Hall Hospital for making me so welcome.

However, it is not only the people in the laboratory and those involved in the research that have provided support over the last three years. I would like to thank all my friends and colleagues within Sportex who have made my PhD experience so enjoyable especially those with whom I have shared an office; Cat, Elle, Sally, Sam and Pete. I also must thank Nic and Kim who have always been on hand to offer support and advice or a chat over a cup of tea during the highs and lows of PhD life.

Thank you also to Nicholas. Your unwavering love, support and patience have always been fantastic and have meant so much, especially during the last few years when I have been studying for this PhD. Also, your sense of humour truly has kept me sane during the more challenging times in completion of this thesis.

And finally, to my mum and dad, thank you for the belief and confidence you have always had in me and the enthusiasm and encouragement you have given to me to succeed, no matter what life throws at you. In particular, thank you for your love and support during my PhD; although a mere acknowledgement of thanks here could never be enough for the love and support you have shown me over the years.

Thank you all!

CONTENTS LISTING

LIST OF ABSTRACTS AND PUBLICATIONS

During the period of postgraduate study at The University of Birmingham, data from the current thesis resulted in the following abstract:

Shaw CS, **Clark JA** and Wagenmakers AJM. Fibre specific distribution of intramuscular triglyceride synthesizing enzymes in human skeletal muscle. Abstracts for the 14th International Conference Biochemistry of Exercise. *Applied Physiology, Nutrition and Metabolism* 2009, 34(6): 1117-1168

During the period of postgraduate study, the data in this thesis also resulted in the following conference communications:

Clark JA, Shaw CS, Davis E, Pilling J and Wagenmakers AJM. 'Association of SNAP23 with the mitochondrial network is reduced in skeletal muscle of obese females'. Accepted for presentation at the 17th Annual Congress of the European College of Sport Science, Bruges, 2012.

Clark JA, Shaw CS, Bradley H, Wilson OJ and Wagenmakers AJM. 'Visualising the subcellular distribution of SNAP23 in human skeletal muscle'. Accepted for presentation at the 15th International Biochemistry of Exercise, Stockholm, 2012.

Clark JA, Shaw CS, Davis E, Pilling J and Wagenmakers AJM. 'The association of SNAP23 with the mitochondrial network is reduced in the skeletal muscle of obese females'. 1st International Symposium on Advances in Human Metabolism Research, Warwick, 2011.

Clark JA, Shaw CS and Wagenmakers AJM. 'Visualisation of adipose triglyceride lipase and its activator CGI-58 in human skeletal muscle'. 16th Annual Congress of the European College of Sport Science, Liverpool, 2011.

Clark JA, Shaw CS and Wagenmakers AJM. 'Colocalisation of SNAP23 with mitochondria in skeletal muscle of physically active men'. 15th Annual Congress of the European College of Sport Science, Antalya, 2010.

Clark JA, Shaw CS and Wagenmakers AJM. 'SNAP23 colocalises with mitochondria and not with lipid droplets in human skeletal muscle'. UK Adipose Tissue Discussion Group, Alderley Park, Astra Zeneca, 2009.

Clark JA, Shaw CS and Wagenmakers AJM. 'The enzymes of intramuscular triglyceride synthesis exhibit fibre type specificity'. 14th Annual Congress of the European College of Sport Science, Oslo, 2009.

Clark JA, Shaw CS and Wagenmakers AJM. 'Mitochondrial glycerol-3-phosphate acyltransferase and diacylglycerol acyltransferase distribution in human skeletal muscle'. UK Adipose Tissue Discussion Group, University of Warwick, 2008.

The following paper was also published during the period of postgraduate study:

Shaw CS, **Clark JA** and Wagenmakers AJM. The effect of exercise and nutrition on intramuscular fat metabolism and insulin sensitivity. *Annual Review of Nutrition* 2010, 30: 13-34

TABLE OF CONTENTS

LIST OF FIGURES

LIST OF TABLES

CHAPTER 1

GENERAL INTRODUCTION

1.1 Obesity and Type 2 Diabetes: Rapidly Growing Global Human Health Threats

In the last three decades there has been a substantial and rapid rise in the prevalence of obesity and its related disorders. The prevalence of obesity has now reached epidemic levels with the World Health Organisation reporting in 2003 that 300 million adults were clinically obese (BMI $\geq$ 30) (World Health Organisation, 2003). Obesity can be defined as an excess accumulation of fat to the extent that it becomes detrimental to health. Obesity has also been shown to be associated with a higher risk of cardiovascular disease, a higher risk for functional disabilities limiting mobility and stability during old age, some forms of cancer, as well as chronic diseases such as type 2 diabetes, hypertension and hyperlipidaemia (NHS Information Centre, 2008). In fact, for every unit increase in BMI, the risk of type 2 diabetes is increased by 18 % (Helmrich *et al.*, 1991). According to the Foresight Report, obesity rates have trebled since the 1980's (Department for Health, 2007) and the Health Survey for England (2007) adds to this bleak picture, estimating that by 2050 60 % of men and 50 % of women would be obese (BMI $\geq$ 30) (NHS Information Centre, 2008). Furthermore, in 2008, almost a quarter of adults (24 % of men and 25 % of women) were obese, and 66 % of men and 57 % of women were either classified as overweight or obese (BMI $\geq$ 25.0). In comparison, only 33 % of men and 41 % of women had a BMI within the normal range (18.5 – 24.9) (NHS Information Centre, 2008).

Energy intake has not increased dramatically over the last 30 - 40 years, in fact some evidence has even reported a decrease in energy intake (Prentice & Jebb, 1995). However the population has become increasingly sedentary (Oja, 1995), with an increasing pressure to work long hours in sedentary jobs and with increased reliance on cars for transportation. This

compares to a time when many jobs were manual, either industry based or labour-intensive manual work in agriculture. In addition, anecdotally, although the total energy intake has possibly not changed, the quality of food consumed has changed from nutritious balanced meals to energy dense convenience foods with very poor nutritional value. These two factors in combination could have impacted on the increase in the prevalence of obesity.

Obesity is one of the many factors that contribute to the metabolic syndrome. The metabolic syndrome is a clustering of risk factors to include hypertension, hypertriglyceridaemia and hyperglycaemia which collectively increase the risk of developing cardiovascular disease. Obesity is associated with a decline in the ability to control blood glucose concentrations, termed insulin resistance. If this condition is not controlled it can progress into type 2 diabetes. Insulin resistance is associated with progression to cardiovascular disease and it is reported that the greatest risk for type 2 diabetic individuals are cardiovascular complications, with around half of all diabetics dying of cardiovascular disease (World Health Organisation, 2006).

As a result of the worldwide obesity epidemic there has also been a surge in the number of individuals diagnosed with type 2 diabetes each year. Until recently, this disease was known as ‘late onset diabetes’ but with the increased prevalence of obesity, in individuals of any age, that term is no longer applicable. Even young children are now presenting with type 2 diabetes. According to Fact Sheet No 312 (World Health Organisation, 2008) more than 180 million people worldwide have diabetes and this is predicted to double by 2030. In the UK, currently 2.25 million adults are diagnosed with diabetes, but the actual figure is likely to be much higher as many cases remain undiagnosed (Diabetes UK, 2010). Many complications

can occur as a result of diabetes; diabetic retinopathy, diabetic neuropathy (which increase the chances of blindness and amputations in the extremities, respectively), kidney failure, heart disease and stroke. In fact, the overall risk of dying prematurely is at least doubled in individuals with diabetes compared to their age-matched peers without the disease.

Type 2 diabetes does not just lead to a burden on health but is also an economic burden to national government with the NHS estimated to spend £7 billion annually on diabetes related illnesses. Approximately 5% of the NHS budget and 10% of NHS spend on hospital inpatients is the result of diabetes and its associated complications (Department for Health, 2007). New figures reveal that over 300 heart attacks, 300 strokes, 65 foot or toe amputations and 38 leg amputations occur among people with diabetes each week (NHS Information Centre, 2009).

1.2 Insulin Signaling in Skeletal Muscle

In healthy humans, resting blood glucose levels are approximately 5 mmol/L. Glucose is taken up into a variety of tissues such as liver, skeletal muscle, adipose tissue and the brain. Skeletal muscle accounts for 40 – 50 % of total body mass in man and is responsible for more than 50 % of glucose disposal in the postprandial period (Ferrannini *et al.*, 1985;Katz *et al.*, 1983) and this is even larger in the period after exercise. Thus skeletal muscle is of crucial importance when it comes to understanding the mechanisms of impaired glucose tolerance and insulin resistance in obesity and type 2 diabetes. When glucose is taken up into the muscle then it can either be used for glycolysis or be stored as glycogen. The main hormone responsible for the increased uptake of blood glucose in skeletal muscle and glucose homeostasis in the postprandial period is insulin. In the postprandial period, blood glucose

levels become elevated. Insulin is a hormone released by the pancreas in response to these glucose excursions. Insulin binds to the insulin receptor at the plasma membrane and t-tubuli of the skeletal muscle fibres (Wardzala & Jeanrenaud, 1981;Douen *et al.*, 1990), and to the plasma membrane of adipose tissue and liver cells enabling glucose to be taken up into these tissues.

The amount of free glucose in the blood under fasting conditions is small (~ 3.9 - 5.5 mmol/L). Following meal ingestion, large amounts of glucose are absorbed by the gut and appear in the blood. However, this does not result in substantial increases in blood glucose concentration due to the glucose buffering mechanisms that exist, leading to increased glucose disposal from plasma as well as suppression of the release of endogenous glucose stores (Fery *et al.*, 1990). In individuals with impaired glucose tolerance and type 2 diabetes however, these glucose buffering mechanisms become impaired such that, in response to a meal, plasma glucose concentrations become elevated and remain so for many hours. In uncontrolled diabetes postprandial glucose levels may be as high as 20 mmol/L. Eventually the circulating glucose concentration under basal conditions also becomes permanently elevated to levels $\geq$ 7 mmol/L.

1.2.1 Insulin Signaling Cascade

Insulin is a potent signal regulating metabolic events in the muscle. Two distinct insulin signalling pathways have been suggested to have involvement in insulin stimulated GLUT4 translocation and glucose uptake (Figure 1.1). The first pathway is the more established of the two; namely the IRS - phosphoinositide 3-kinase (PI3K) pathway. The second pathway involves the APS-CAP-Cbl complex. This latter pathway is currently less well understood

and its relative contribution in muscle less well established. The PI3K pathway has been shown to play a crucial role in insulin stimulated GLUT4 translocation through studies in which the catalytic activity of PI3K has been inhibited with wortmannin or overexpression of a dominant interfering mutant of the p85 regulatory subunit of PI3K. Both approaches have been shown to reduce glucose uptake and GLUT4 translocation (Cheatham *et al.*, 1994;Okada *et al.*, 1994).

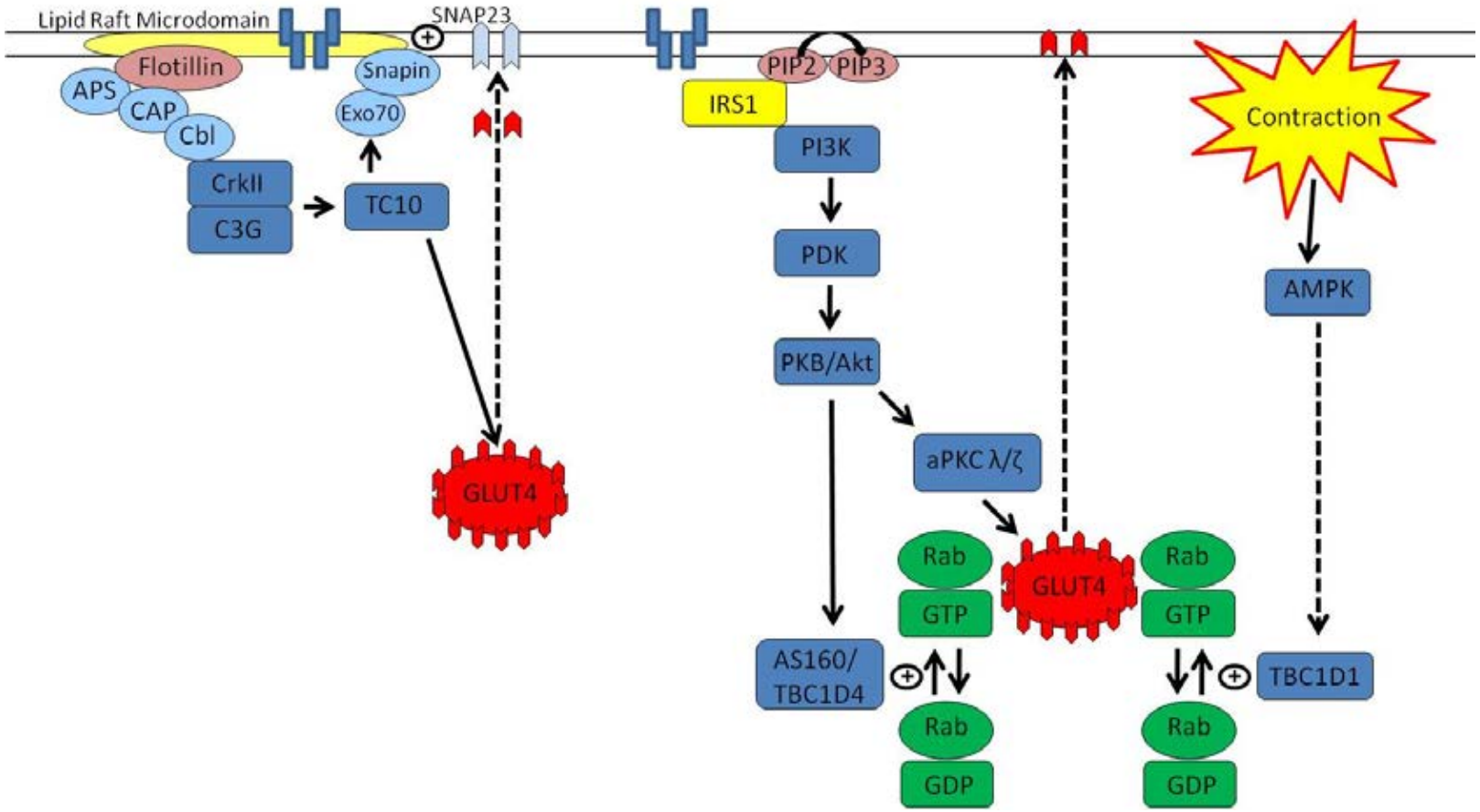

Figure 1.1. Insulin and contraction mediated GLUT4 translocation. IRS1, insulin receptor substrate 1; PIP2, PI 4,5-bisphosphate; PIP3, PI3,4,5-triphosphate; PI3K, phosphoinositide 3-kinase; PDK, phosphoinositide dependent kinase 1; PKB/Akt, protein kinase B; PKC, protein kinase C; AS160/TBC1D4, Akt substrate of 160 kDa; GTP, guanine triphosphate; AMPK, AMP dependent protein kinase; APS, adaptor protein containing a PH and SH2 domain; CAP, Cbl associated protein/Cbl complex; GLUT4, Glucose transporter 4.

1.2.2 The IRS-PI3K Insulin Signaling Pathway

On arrival at the muscle insulin binds to the α-subunits of the insulin receptor (IR). The IR is a tetrameric structure with two α and two β subunits which act allosterically. The α subunits cause a conformational change that triggers the activation of the β-subunits via the inhibition of its intrinsic tyrosine kinase activity. The IR then phosphorylates scaffold proteins such as the insulin receptor substrate family (IRS 1-4) and APS (adaptor protein containing a PH and SH2 domain) (White, 1998;Pessin & Saltiel, 2000). The tyrosine phosphorylation reveals 'docking sites' for the adaptor molecules containing SH2 domain binding sites such as the regulatory subunit (p85) of PI3K. The PI3K is then targeted to PI4,5-bisphosphate ($PI(4,5)P_2$) which is localised at the plasma membrane (Nebl *et al.*, 2000). This metabolite is then phosphorylated to form PI3,4,5-triphosphate ($PI(3,4,5)P_3$) in the plasma membrane. The formation of these molecules provide recognition sites for proteins by attracting pleckstrin homology (PH) domain containing proteins including phosphoinositide dependent kinase 1 (PDK1) and protein kinase B (PKB/Akt) to the inner surface of the plasma membrane to generate further signals including facilitating the PKB/Akt phosphorylation by PDK1.

1.2.3 The APS/CAP/Cbl Complex Pathway

Insulin signalling can also occur via the APS/CAP (Cbl associated protein)/Cbl complex pathway. This pathway is centred on lipid raft microdomains of the plasma membrane as this is where the initial insulin stimulated Cbl tyrosine phosphorylation is induced due to the association of CAP. The protein flotillin is present in the lipid rafts and its interaction with CAP results in the CAP/Cbl complex being recruited to and incorporated into the lipid rafts. Upon tyrosine phosphorylation of Cbl, the adaptor protein CrkII and the guanine nucleotide

exchange factor C3G are also recruited into the lipid rafts activating TC10. For a more detailed review see Chang *et al.,* (2004).

1.2.4 GLUT4 Translocation

In skeletal muscle, glucose uptake requires an insulin stimulated signalling cascade (Figure 1.1) which ultimately results in the translocation of a glucose transporter molecule to the cell surface (plasma membrane or t-tubuli) allowing glucose uptake via facilitative diffusion. It has been demonstrated that glucose transporter 4 (GLUT4) is primarily responsible for the insulin mediated glucose uptake in skeletal muscle (Watson & Pessin, 2001).

It has recently been demonstrated that AS160 is a substrate for PKB/Akt and plays a role in GLUT4 translocation, as overexpression of dominant interfering AS160 blocked GLUT4 uptake (Zeigerer *et al.*, 2004;Welsh *et al.*, 2005;Stockli *et al.*, 2008). AS160 (also known as TBC1D4) contains PKB/Akt phosphorylation sites as well as a Rab GAP (GTPase activating protein) domain. Rab proteins make up a group of proteins involved in secretory/endocytic pathways (Martinez & Goud, 1998). These Rab proteins cycle continually between a GDP-bound and a GTP-bound state and are involved in regulating several processes involved in membrane trafficking. Specifically Rab proteins 4, 5 and 11 (Kanzaki, 2006) and more recently Rab 13 (Sun *et al.*, 2010) have been implicated in GLUT4 trafficking processes. Insulin also causes polymerisation of the actin cytoskeleton which forms a mesh (track-like) structure to the plasma membrane (and likely to t-tubuli as well) allowing the targeted channelling of GLUT4 to the plasma membrane (Khayat *et al.*, 2000) by acting as a scaffold. The modelling of the cytoskeleton appears to be mediated via PI3K and atypical isoforms of PKC, namely lambda and zeta, but not Akt (Liu *et al.*, 2006). It appears that these enzymes are recruited to the plasma membrane (and t-tubuli) and are activated by PDK1 dependent

phosphorylation in response to insulin stimulation although the exact roles of these enzymes in glucose transport remain an ongoing area of research.

In the basal state, GLUT4 constantly recycles between intracellular storage vesicles and the plasma membrane with the majority localised to intracellular storage compartments as endocytosis exceeds exocytosis. In the basal state approximately 2 – 5 % of GLUT4 resides at the plasma membrane (Kanzaki, 2006). Upon insulin stimulation GLUT4 exocytosis increases dramatically resulting in a large proportion of GLUT4 becoming incorporated into the plasma membrane at the cell surface and the t-tubules thereby allowing glucose to enter the cell (Cushman & Wardzala, 1980;Lauritzen *et al.*, 2006;Marette *et al.*, 1992). The t-tubular network enlarges the surface area for glucose uptake as the t-tubular surface area is two to three fold larger than the sarcolemma (Knudson & Campbell, 1989). Recent immunofluorescence microscopy images in animals would suggest that the increase in surface area is even larger (Wang *et al.*, 1996;Ploug *et al.*, 1998;Lauritzen *et al.*, 2006;Lauritzen *et al.*, 2008b;Lauritzen *et al.*, 2010). In a mouse model, GLUT4 translocation to the t-tubules has been suggested to be delayed compared to translocation to the plasma membrane due to a time lag in insulin diffusion into the lumen of t-tubuli (Lauritzen *et al.*, 2006), however, there also appears to be a delay in the reinternalisation of GLUT4 following insulin stimulation in the t-tubuli (Lauritzen *et al.*, 2008b). Thus the GLUT4 response to insulin is compartmentalised.

1.2.5 GLUT4 tethering and fusion

Soluble N-ethylmaleimide sensitive factor (NSF) attachment protein receptor (SNARE) proteins play a crucial role in many docking and fusion processes in a variety of intracellular organelles, particularly contributing to docking and fusion processes with the plasma membrane. Although there are many SNARE proteins, it has been shown *in vitro* that

SNAP25, syntaxin 1A and VAMP2 alone are sufficient for docking and fusion (Weber *et al.*, 1998). SNARE proteins have a distinctive coiled coil structure (Figure 1.2) due to the polar nature of the amino acid chain which is 60 - 70 amino acids long and contains both hydrophobic and hydrophilic portions arranged in heptad repeats so that a stable coil structure forms.

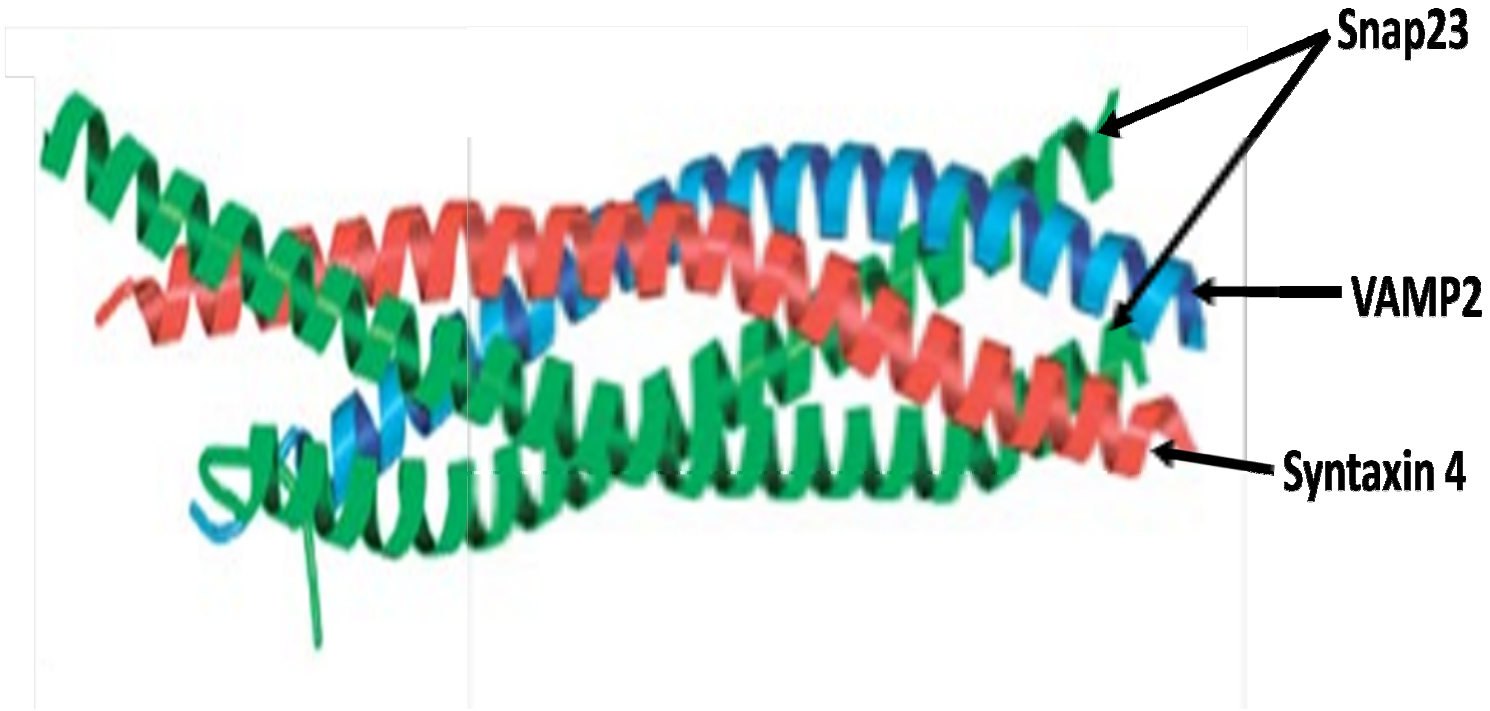

Figure 1.2. SNARE Complex Structure. The coiled coil structure of the SNARE complex is shown. Each individual SNARE protein has a coiled structure due to the polar nature of the amino acid sequence which is then intertwined with three other SNARE proteins to form this stable complex structure. Image adapted from Jahn and Scheller (2006).

SNARE proteins can be subdivided into two categories; target SNARE (tSNARE) and vesicle SNARE (vSNARE). tSNAREs are present on the target membrane and the vSNAREs are localised to the opposing vesicle membrane. As the SNARE proteins interact, the two membranes are drawn together; thus the SNARE proteins are crucial in many docking and fusion processes including GLUT4 translocation and lipid droplet fusion. This process however does not occur in isolation; NSF is also required and is found both on membranes and intracellularly. In order for NSF to interact and bind to a membrane it requires the interaction of alpha SNAP (soluble NSF associated protein). NSF is involved in providing the energy which is necessary for the SNARE proteins to change their conformational shape and thus become activated. However, once formed, the SNARE complex cannot disassemble without energy provided by NSF and alpha SNAP (Sollner *et al.*, 1993), thus NSF and alpha SNAP are involved in maintaining a supply of free SNARE proteins and ensuring they are activated.

The activation of TC10 *(see section 1.2.3)* results in the activation of Exo70 which also translocates to the lipid rafts binding to Snapin. It has been suggested that Exo70 arriving at the lipid rafts and interacting with Snapin may activate the SNARE protein SNAP23 (synaptosomal associated protein 23) (Bao *et al.*, 2008) which is required for the tethering of GLUT4 to the plasma membrane. SNAP23 has been shown to be involved in insulin mediated GLUT4 translocation and glucose uptake *in vitro.* SNAP23 was first identified in the membrane fraction of mouse adipocytes (Rea *et al.*, 1998) and microinjection of SNAP23 antibody directed towards the c-terminus of SNAP23 inhibited GLUT4 incorporation into the plasma membrane (Foster *et al.*, 1999) and reduced glucose uptake by ~ 40 % (Rea et al., 1998). Further, in adipocytes transfected with an inactive mutant SNAP23, insulin induced translocation of GLUT4 was reduced (Kawanishi *et al.*, 2000a) .

Animal studies have demonstrated a role for syntaxin 4 in insulin stimulated GLUT4 translocation, as syntaxin 4 null mice had an impaired insulin stimulated GLUT4 translocation and impaired glucose tolerance compared to their wild type counterparts (Yang *et al.*, 2001). VAMP2 has also been implicated in insulin stimulated GLUT4 translocation *in vitro* as insulin infusion resulted in an increased VAMP2 translocation to the plasma membrane (Martin *et al.*, 1996). However this was less than the increase in GLUT4 translocation suggesting that VAMP2 is not a limiting factor in the GLUT4 translocation process in response to insulin. The location of VAMP2 in adipocytes has also been proposed to differ from that of SNAP23 and syntaxin 4, both of which are proposed to reside on lipid rafts at the plasma membrane. VAMP2 resided in intracellular lipid rafts (Chamberlain & Gould, 2002).

1.2.6 Insulin Signaling in Endothelium

Insulin signalling is also known to occur at the level of the microvascular endothelium in muscle. It is thought that insulin regulates its own delivery to the muscle fibres via the activation of an insulin dependent pathway at the level of the endothelium (for a review see: (Barrett *et al.*, 2009)). Binding of insulin to the insulin receptor on endothelial cells in terminal arterioles in skeletal muscle eventually leads to the synthesis of the vasodilator nitric oxide, allowing relaxation of the vascular smooth muscle layer, dilation of terminal arterioles and increased blood flow and nutrient delivery to the muscle. This mechanism is clearly of importance in the delivery of insulin and glucose to the muscle fibres and therefore in the regulation of insulin action and therefore plasma glucose concentrations and muscle glucose uptake. However, this thesis will focus on factors influencing insulin signal transduction and glucose uptake in skeletal muscle fibres.

1.3 Insulin Resistance of Skeletal Muscle Fibres

In some individuals skeletal muscle fibres show an impaired signalling response after binding of insulin to the IR leading to a reduced glucose uptake and higher circulating levels of blood glucose (hyperglycaemia). This condition is termed insulin resistance. Skeletal muscle is a highly plastic tissue that adapts relatively rapidly to anabolic stimuli such as exercise (and catabolic stimuli such as disuse). This, taken together with its quantitative role in glucose uptake after meal ingestion, make skeletal muscle into an important target for understanding the mechanisms of insulin resistance as well as a potential therapeutic target for interventions designed for the treatment of type 2 diabetes. If insulin resistance is not treated successfully with lifestyle interventions such as a calorie controlled diet, exercise, the combination of the two or with antidiabetic drugs then type 2 diabetes will develop.

1.3.1 Lipid Induced Insulin Resistance

Acute increases in the concentration of plasma fatty acids (FA) achieved via intravenous intralipid-heparin infusions lead to impairments in glucose uptake in both rats (Nolte *et al.*, 1994;Jucker *et al.*, 1997), healthy human controls (Boden *et al.*, 1991;Kelley *et al.*, 1993;Boden *et al.*, 1994;Roden *et al.*, 1996;Roden *et al.*, 1999) and patients with type 2 diabetes (Boden, 1999). It has been proposed that these impairments in insulin signalling may be due to deleterious changes in the insulin signalling cascade and may be mediated via activation of protein kinase C (PKC) θ (Griffin *et al.*, 1999).

These lipid and heparin infusions, usually lasting approximately 5 hours, cause an elevation in plasma FA levels. It is mainly through these studies that PKC isoforms have been implicated

in the development of insulin resistance. It has been reported that 5 hour intravenous infusions of intralipid with heparin leads to increases in skeletal muscle of the FA metabolites: long chain fatty acyl coenzyme A (LCFACoA) (Griffin *et al.*, 1999;Yu *et al.*, 2002;Chalkley *et al.*, 1998) and diacylglycerol (DAG) (Itani *et al.*, 2002). These increases were associated with the activation and translocation of PKCθ to the plasma membrane leading to serine phosphorylation of IRS-1 (De & Roth, 1997;Yu *et al.*, 2002) and insulin resistance (Griffin *et al.*, 1999;Yu *et al.*, 2002;Chalkley *et al.*, 1998). Serine phosphorylation of IRS-1 has been suggested to lead to down regulation of the tyrosine phosphorylation and prevent downstream activation of the insulin signalling cascade (Yu *et al.*, 2002). Direct evidence of the role of PKCθ in lipid-induced insulin resistance in mice was illustrated through the use of PKCθ knock out mice which were protected against insulin resistance and serine phosphorylation of IRS-1 during a 5 hour intralipid-heparin infusion (Kim *et al.*, 2004b). In healthy humans a 6 hour intralipid-heparin infusion substantially reduced glucose clearance during a hyperinsulinaemic euglycaemic clamp and increased the protein content of PKCβ (specifically the βII isoform) eightfold in the membrane fraction of skeletal muscle (Itani *et al.*, 2002).

Similar deleterious effects have also been observed in response to dietary manipulations. Consumption of a high fat diet for three weeks has been shown to lead to skeletal muscle insulin resistance in rats and showed a positive correlation with the skeletal muscle LCFACoA (Oakes *et al.*, 1997a;Oakes *et al.*, 1997b;Ellis *et al.*, 2000) and DAG content (Oakes *et al.*, 1994;Schmitz-Peiffer *et al.*, 1997). Further, in human participants it was shown that the skeletal muscle LCFACoA content was inversely related to whole body insulin action (Ellis *et al.*, 2000).

1.3.2 Lipid Overflow Hypothesis

Adipose tissue is not simply a metabolically inert store of fat. It is metabolically flexible and plays a key role in regulating circulating levels of FA and TAG. In the postprandial period insulin inhibits the action of hormone sensitive lipase (HSL), a lipolytic hormone which breaks down TAG resulting in FA release into the circulation. The majority of the ingested fat is directed towards chylomicron-TAG synthesis in the gut. Lipoprotein lipase (LPL) which is present on the luminal site of endothelial cells in adipose tissue capillaries hydrolyses chylomicron-TAG and the FAs released are taken up by the adipocytes and re-esterified to form TAG. This process is mediated by the lipid synthesising enzymes glycerol-3-phosphate acyltransferase (GPAT) and diacylglycerol acyltransferase (DGAT). The postprandial clearance of chylomicron-TAG into the adipose tissue stores acts as a protective mechanism (Frayn, 2002), protecting the vascular wall, the liver and other tissues, including skeletal muscle, from increased FA and TAG exposure and deposition, which would impair endothelial function and increase the risk of atherosclerotic plaques (vasculature), steatosis and non alcoholic fatty liver disease (liver) and insulin resistance and type 2 diabetes (skeletal muscle).

In obesity, in the postprandial state, there is a large overspill of FA from the adipose tissue into the circulation (Opie & Walfish, 1963;Frayn, 2002;Mittendorfer *et al.*, 2009) and the clearance of chylomicron-TAG by adipose tissue has been suggested to be reduced (McQuaid *et al.*, 2011). This leads to increased concentrations of circulating FA (only marginally higher in insulin resistant obese individuals) and especially TAG (Potts *et al.*, 1995;Ruge *et al.*, 2009), which presents an increased risk for development of cardiovascular disease (Patsch *et al.*, 1992;Hokanson & Austin, 1996;Bansal *et al.*, 2007), and due to excessive deposition of

FA and lipids into skeletal muscle has been suggested to contribute to insulin resistance (Lewis *et al.*, 2002).

The intramuscular triglyceride (IMTG) pool in muscle has a limited storage capacity especially in sedentary and obese individuals and patients with type 2 diabetes. In obesity and type 2 diabetes, there is an imbalance between the uptake of FA and their use for oxidation and TAG synthesis in the muscle. This results in the accumulation of FA metabolites such as LCFACoA, DAG and ceramide which are thought to inhibit insulin signalling, thus leading to obesity induced insulin resistance (Figure 1.3). Trained individuals are able to maintain a low concentration of FA metabolites and high insulin sensitivity in spite of the fact that they have the largest IMTG stores (Goodpaster *et al.*, 2001;van Loon *et al.*, 2004).

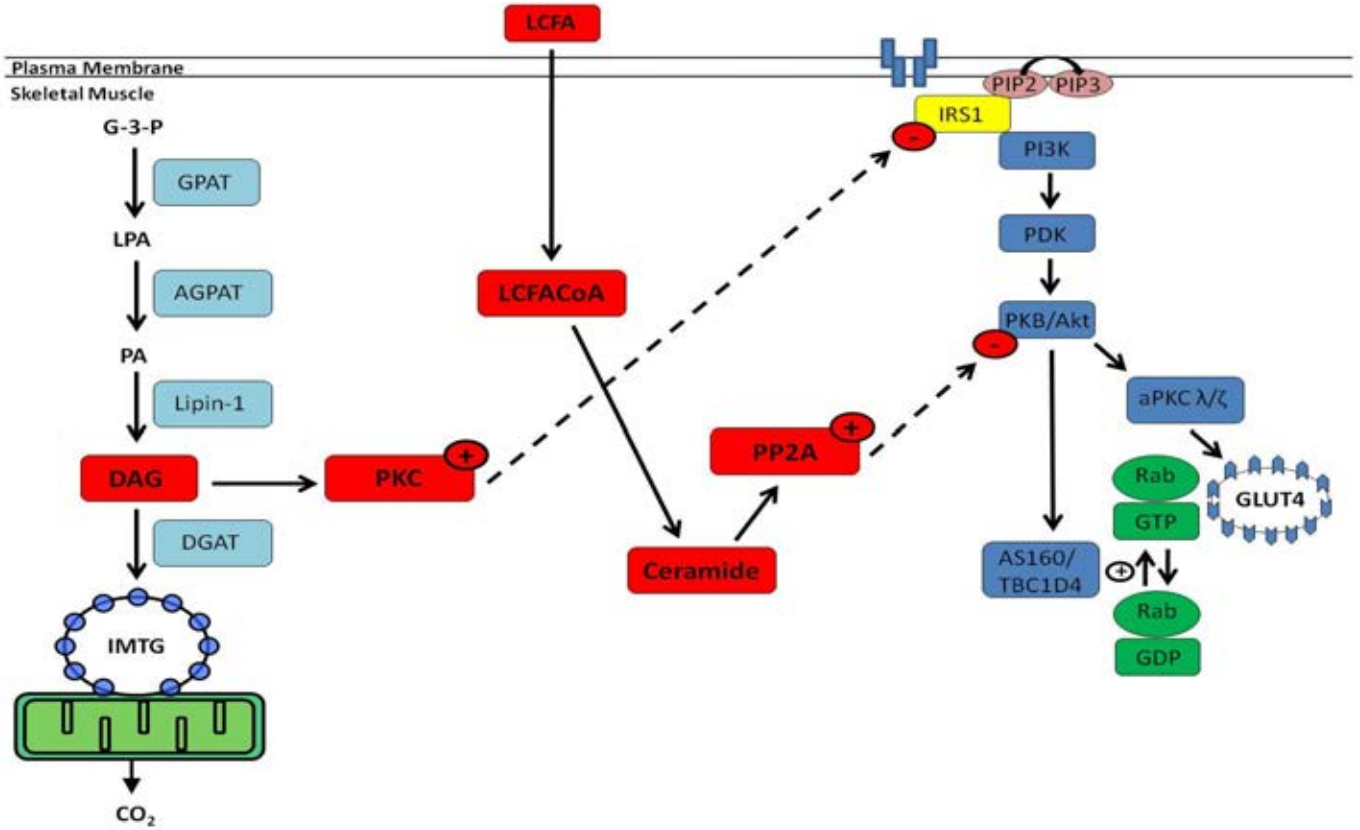

Figure 1.3. Fatty Acid Spillover Hypothesis. GPAT, glycerol-3-phosphate acyltransferase; LPA, lysophosphatidic acid; AGPAT, 1-acyl-glycerol-3-phosphate acyltransferase; PA, phosphatidic acid; DAG, diacylglycerol; DGAT, diacylglycerol acyltransferase; IMTG, intramuscular triglyceride; PKC, protein kinase C; PP2A protein phosphatase 2; IRS1, insulin receptor substrate-1; PIP2, PI 4,5-bisphosphate; PIP3, PI3,4,5-triphosphate; PI3K, phosphoinositide 3-kinase; PDK, phosphoinositide dependent kinase-1; PKB/Akt, protein kinase B; PKC, protein kinase C; AS160/TBC1D4, Akt substrate of 160 kDa; GTP, guanine triphosphate; GLUT4, glucose transporter-4.

Many years ago, the Randle cycle (Randle *et al.*, 1963) was proposed as an explanation for the impairment in glucose oxidation that occurs in the presence of elevated FA concentrations. It was thought that a series of negative feedback events led to the glucose concentration gradient between the circulation and the muscle being lost, thereby reducing the uptake of blood glucose into skeletal muscle. Randle *et al.,* (1963) suggested that high rates of FA oxidation led to an increase in the mitochondrial ratio of acetyl-CoA/CoA and $NADH/NAD^+$ which inhibit pyruvate dehydrogenase (PDH) and reduce pyruvate and therefore glucose oxidation. The high FA oxidation rate via the high acetyl-CoA/CoA ratio also results in citrate accumulation which inhibits phosphofructokinase (PFK). This in turn was assumed to lead to an accumulation of glucose-6-phosphate which then inhibits hexokinase II and results in an accumulation of intracellular glucose. Loss of the glucose gradient between the microvascular circulation and the cytosol of muscle fibres would then reduce glucose uptake via facilitated diffusion via GLUT4. This theory has however since been questioned as subsequent studies observed a decrease rather than an increase in glucose-6-phosphate concentrations (pointing at glucose transport as the limiting step) and also failed to observe an increase in citrate concentration when glucose metabolism was inhibited through the use of an intralipid-heparin infusion as a means to elevate plasma FA levels (Boden *et al.*, 1994;Boden, 1999;Roden *et al.*, 1999).

Metabolic flexibility is a term used to describe the ability of an individual to transiently switch fuel use from a fasted to fed state and from a fed to fasted state also (Storlien *et al.*, 2004;Corpeleijn *et al.*, 2009). It is likely that in obese, insulin resistant individuals this metabolic flexibility is compromised and the buffering capacity of FA/TAG in plasma is disrupted. Plasma FA can accumulate in obese individuals as the ability of insulin to suppress FA release from adipose tissue is blunted in the postprandial period (Groop *et al.*,

1989;Campbell *et al.*, 1994). Further, in obese individuals there is an impairment in insulin's ability to up-regulate the activity of LPL in adipose tissue (and therefore TAG clearance into adipose tissue) leading to increased circulating TAG (Sadur *et al.*, 1984;Ong & Kern, 1989;Richelsen *et al.*, 1993;Frayn, 2002). In obesity, FA release from the adipocytes is increased as the adipocyte becomes insulin resistant and HSL activity is not down-regulated in response to insulin, thus lipolysis continues in the postprandial period (Frayn, 2002;Lewis *et al.*, 2002;Corpeleijn *et al.*, 2009). Obesity is also associated with increased VLDL-TAG as the increased FA released from adipose are directed to the liver where VLDL-TAG synthesis is increased. Conversion of plasma FA into VLDL-TAG does explain why some studies fail to observe increased plasma FA levels but observe large increases in VLDL-TAG in obese insulin resistant individuals (Bickerton *et al.*, 2008). A high concentration of VLDL-TAG is a major risk factor for cardiovascular disease. In order to 'manage' the increase in circulating FA there may also be increased uptake of FA into other tissues such as liver, heart and muscle where they are either oxidised (Hodson *et al.*, 2010) or re-esterified into TAG. This ectopic fat accumulation has been associated with insulin resistance and is termed the lipid 'overflow' or 'spillover' hypothesis (Bays et al 2004; Lewis et al 2002).

1.4 Lipid Droplets

Lipid droplets are found in skeletal muscle and may act as a readily available fuel source in trained individuals during exercise. However, excessive storage of these lipid droplets is pivotal to the development of many metabolic diseases such as obesity, insulin resistance and type 2 diabetes (Guo *et al.*, 2009). For many years, lipid droplets were simply considered to be inert storage depots but more recently they have been demonstrated to be dynamic organelles with a direct role in the pathogenesis of metabolic disease.

1.4.1 Lipid Droplet Structure

Lipid droplets consist of a core of neutral lipids (mainly TAG), surrounded by a monolayer of phospholipids (Bartz *et al.*, 2007b). A large number of proteins have been identified in isolated lipid droplet fractions (Brown, 2001;Bartz *et al.*, 2007a). Most of these proteins are assumed to be functionally associated with or even embedded in the surrounding phospholipid monolayer. The proteins assumed to be functional include the PAT proteins, (perilipin, adipophilin/adipocyte differentiation related protein (ADRP), tail interacting protein of 47 kDa (TIP-47), muscle lipid droplet storage protein (MLDSP)/OXPAT), lipid synthetic enzymes such as acetyl-CoA carboxylase 1 (synthesising malonylCoA for de novo lipogenesis) and DGAT2 (Stone *et al.*, 2009), lipolytic proteins such as ATGL and membrane trafficking proteins such as Rabs. The proteins embedded in the phospholipid layer may have important regulatory functions. The PAT proteins for instance have been suggested to regulate the access of lipolytic enzymes to the TAG core (Brasaemle *et al.*, 2000b). Unfortunately, the majority of knowledge regarding lipid droplets has been discovered *in vitro* or in adipocytes and thus currently this information must be extrapolated to skeletal muscle. The core of the lipid droplets surprisingly has been shown to also contain proteins (Robenek *et al.*, 2005). However, further research is needed into how these proteins are transported into and out of the lipid core and whether they indeed are functional or artefacts.

1.4.2 Lipid Droplet Formation

Lipid droplets are thought to be formed in the vicinity of or within the endoplasmic reticulum (ER) although the exact mechanisms by which this occurs are unknown, particularly for skeletal muscle. Therefore, information must again be extrapolated from *in vitro* cell studies

or other tissues. Newly formed lipid droplets are known as 'primordial' and are approximately 0.1 - 0.4 µm in diameter (Marchesan *et al.*, 2003), however they have the capacity to greatly increase in size by up to 50 times in the majority of cell types (and even more in adipocytes). Primordial lipid droplets form from microsomes, having a diameter of approximately 0.1µm and contain ADRP, vimentin, caveolin and GRP78 (Marchesan *et al.*, 2003). Lipid droplets are formed of a core of neutral lipids and cholesterol esters encased by a phospholipid monolayer (Ohsaki *et al.*, 2009). Lipid droplets can increase in size via the process of TAG synthesis however it has been shown that lipid droplets can also form complexes as they fuse and thus their size can increase independent of this process. For example, *in vitro* inhibition of TAG biosynthesis using Triacsin C resulted in no increase in oil red O staining in response to 7 hours oleic acid incubation (Bostrom *et al.*, 2005). Lipid droplet size however did increase with an increase in number of the largest droplets (> 3µm in diameter).

There has been much controversy regarding the mechanisms of lipid droplet biogenesis. Until recently, the popular hypothesis was that lipid esters gradually accumulate between two leaflets of the ER membrane. The gradual accumulation of lipid esters allows the familiar globular shape to form until, on reaching a critical size, they are pinched off (Murphy & Vance, 1999). Recently however, unequivocal evidence has come to light using freeze fracture electron microscopy in macrophages suggesting that it is in fact ADRP enriched domains of the ER membrane that allow for the formation of lipid droplets which fit into the membrane (like an egg in an egg cup) (Robenek *et al.*, 2006). The lipid does not accumulate within the ER membrane as first hypothesised, instead it seems that both membranes lie external to, and follow the contour of the lipid droplet. ADRP has previously been implicated in lipid droplet biogenesis. ADRP co-exists with Rab18 in lipid droplets however

immunofluorescence microscopy shows a reciprocal relationship. That is, when the signal for Rab18 is strong, the signal for ADRP is weak (Ozeki *et al.*, 2005). Rab18 is found at the lipid droplet monolayer and this association is increased following stimulation of lipolysis in adipocytes (Martin *et al.*, 2005).

The microtubule network has also been implicated as playing a crucial role in the formation of lipid droplets. Incubation of adipocytes with the microtubule destroyer nocodazole decreased lipid droplet complex formation by 88 % as well as blunting the growth of existing lipid droplets (Bostrom *et al.*, 2005). The motor protein dynein co-immunoprecipitated with ADRP suggesting that it is the ADRP containing droplets that can be transported along the microtubule network leading to the formation of lipid droplet complexes. Dynein is thought to be phosphorylated by ERK2 (Andersson *et al.*, 2006) implicating ERK2 in the process of lipid droplet assembly. This has been clarified through its inhibition with Ste-Mek1$_{13}$ (Kelemen *et al.*, 2002) which resulted in a significant decrease in the rate of lipid droplet formation. This effect was independent of incubation in oleic acid. Using this inhibitor with insulin simulation, it was found that the insulin induced stimulation of lipid droplet formation was also reduced.

1.5 IMTG Metabolism

Throughout this thesis lipid droplets and IMTG are investigated. Whilst these terms are often used interchangeably, the difference for the purpose of this thesis is that the term lipid droplet describes the individual intracellular structure containing IMTG, surrounded by a phospholipid monolayer and a number of proteins such as perilipins. IMTG is used to describe the fuel source that these lipid droplets can collectively provide and is also used

when describing reactions of synthesis and lipolysis as these reactions work specifically to produce IMTG that fills the lipid droplet or to hydrolyse the IMTG stored within the lipid droplet.

The lipid levels within the muscle are tightly regulated by the balance of lipid synthesis and lipolysis. If this process becomes unbalanced, or FA uptake is not matched by FA oxidation, lipid metabolites can accumulate in the muscle, leading to insulin resistance. When FAs first enter the muscle they are diverted towards IMTG synthesis via the lipid synthetic pathway involving the lipid synthetic enzymes GPAT and DGAT and, when energy is required, the lipolytic pathway involving adipose triglyceride lipase (ATGL) and HSL allows for the release of FA from the IMTG stores to undergo mitochondrial β-oxidation (Figure 1.4).

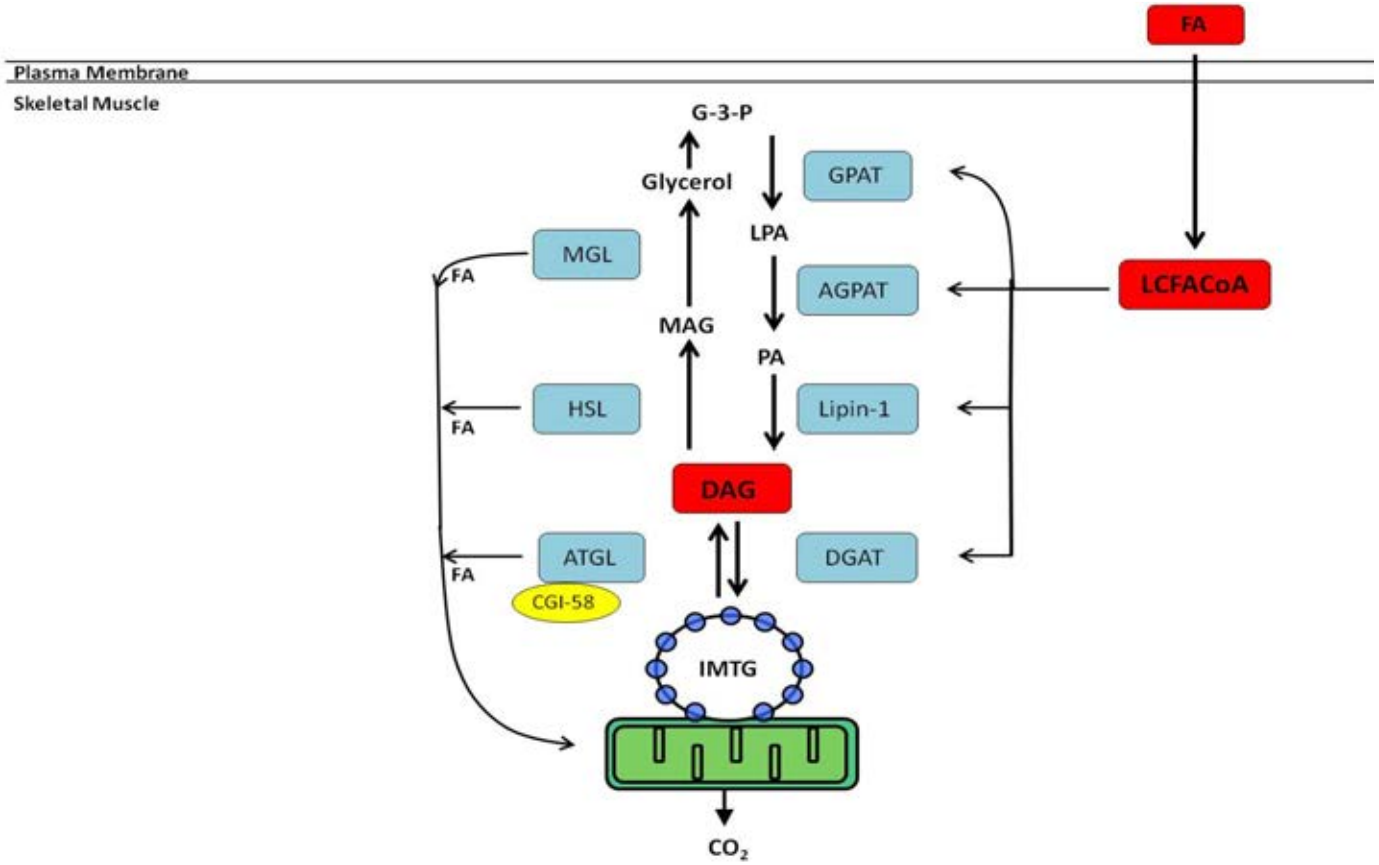

Figure 1.4. Lipid Turnover in Skeletal Muscle. G-3-P, glycerol-3-phosphate; GPAT, glycerol-3-phosphate acyltransferase; LPA, lysophosphatidic acid; AGPAT, 1-acyl-glycerol-3-phosphate-O-acyltransferase; PA, phosphatidic acid; DAG, diacylglycerol; DGAT, diacylglycerol acyltransferase; ATGL, adipose triglyceride lipase; CGI-58, comparative gene identification-58; HSL, hormone sensitive lipase; MGL, monoglyceride lipase.

1.5.1 IMTG Synthesis

The synthesis of IMTG in human skeletal muscle is an important process as it utilises the FA metabolites (LCFACoA and DAG) in the synthetic process thus reducing their levels and potentially protecting against insulin resistance. The process involves a series of sequential acylation reactions in which the ultimate product is TAG. The first committed step of TAG synthesis is the acylation of glycerol-3-phosphate with LCFACoA to form lysophosphatidic acid (LPA). This reaction is catalysed by GPAT (Figure. 1.3). The LPA product of this reaction is acylated to phosphatidic acid (PA) by 1-acyl-glycerol-3-phosphate-O-acyltransferase (AGPAT). A phosphate group is then removed from the PA to form DAG. The final step of TAG synthesis is the acylation of DAG to TAG which is catalysed by DGAT. Two of the enzymes involved in this process are investigated in further detail in this thesis, namely, GPAT1 and DGAT1.

1.5.1.1 Glycerol-3-Phosphate Acyltransferase

GPAT is responsible for catalyzing the first step of IMTG synthesis; the acylation of glycerol-3-phosphate with LCFACoA to form LPA. Currently four isoforms of GPAT are known to exist; two mitochondrial isoforms namely GPAT1 and GPAT2, (Monroy *et al.*, 1973;Shin *et al.*, 1991;Lewin *et al.*, 2004) were first described in mouse liver and were named mitochondrial isoforms as each was found to be present in a high concentration in liver mitochondria (Monroy *et al.*, 1973). Two microsomal isoforms also exist; GPAT3 and GPAT4 which were first measured in rat liver microsomes (Yamashita & Numa, 1972;Yamashita *et al.*, 1972) and have since been cloned (Cao *et al.*, 2006;Chen *et al.*, 2008). GPAT1 makes up less than 10% of total GPAT activity in adipocytes as well as hepatocytes and baby hamster kidney cells (Stern & Pullman, 1978;Bell & Coleman, 1980), however its

contribution in skeletal muscle is currently unknown. GPAT1 also shows a preference for saturated acyl-CoAs (Coleman & Lee, 2004). The enzymes involved in the latter stages of IMTG synthesis are present at the ER along with microsomal GPAT, thus the LPA produced must be transported from the mitochondria to the ER most probably via liver-fatty acid binding protein (Gonzalez-Baro *et al.*, 2007), however it is currently unknown how this process occurs in skeletal muscle.

The putative role of GPAT1 has previously been investigated in GPAT1 knockout mice. These mice demonstrated a reduced body mass, lower hepatic TAG content, lower plasma TAG and VLDL-TAG and decreased liver TAG secretion (Hammond *et al.*, 2002), suggesting that GPAT1 is important for liver VLDL-TAG production but that its role can at least in part be taken over by GPAT 2 - 4 as these mice are not totally devoid of TAG. In hepatocytes overexpressing GPAT1, TAG content has been shown to increase in response to oleate incubation (Lewin *et al.*, 2005). This response has also been shown in mice (Linden *et al.*, 2006) and Chinese hamster ovary cell (Igal *et al.*, 2001) models.

To date, few studies have measured the protein abundance of GPAT1 or 2 by Western blotting in human skeletal muscle. GPAT1 content was found to be increased the day following a bout of endurance exercise (45 min treadmill exercise and 45 min cycle ergometer exercise at 65% VO_{2peak}) (Schenk & Horowitz, 2007). The increase in GPAT1 was found to be concurrent with an increase in DGAT1 and was found to protect against insulin resistance induced by lipid-heparin infusion in non obese women. In a further study, using a similar exercise protocol, an increase in GPAT1 activity was observed, but there was no increase in GPAT protein content (Newsom *et al.*, 2010). Regardless of this, a 30 % increase in IMTG

content was seen following an overnight lipid-heparin infusion and the exercise again resulted in protection against lipid induced insulin resistance.

The location of GPAT1 at the outer mitochondrial membrane has recently come under scrutiny as a recent publication has demonstrated two storage sites for GPAT1 in rat liver (Pellon-Maison *et al.*, 2007). One storage site appears to be present in a vesicular membrane fraction associated with the mitochondria (MAV) however the GPAT specific activity in this fraction appeared low. The second store of GPAT1 appeared to be found at the mitochondrial outer membrane (OMM) and this was where the greatest specific GPAT activity was found. Therefore, it is possible that GPAT1 in rat liver translocates from the MAV to the OMM upon activation e.g. by insulin, where it is involved in synthesising IMTG in close proximity to the mitochondria. A more recent study in NIH 3T3 fibroblasts has shown that mitochondria may be coupled to lipid droplets in a process regulated by the SNARE protein SNAP23 (Jagerstrom *et al.*, 2009) and it is possible that GPAT1 is involved in the tightly regulated formation of lipid droplets in close proximity to the mitochondria which are then coupled to lipid droplets via SNAP23. There was no information on the spatial localisation of the GPAT1-4 isomers in skeletal muscle when beginning the research described in this thesis.

1.5.1.2 Diacylglycerol Acyltransferase

DGAT is the enzyme responsible for the final step of IMTG synthesis (Choi *et al.*, 2007), catalysing the acylation of DAG with LCFACoA resulting in TAG formation. In this role, DGAT can both increase the IMTG content and reduce the DAG content. As DAG, apart from being implicated in the mechanisms leading to insulin resistance, also exerts a variety of signalling roles, the latter role may be of equal or even greater importance. Two DGAT

isoforms are known to exist, DGAT1 and DGAT2 (Cases *et al.*, 1998;Cases *et al.*, 2001). Current evidence perhaps suggests that these two isoforms play differing roles in lipid metabolism as DGAT1 knockout mice have 50% less TAG in tissues and are protected from diet induced obesity and insulin resistance through a mechanism seemingly related to increased energy expenditure (Chen *et al.*, 2002). Overexpression of DGAT1 also has been suggested to have a protective effect against insulin resistance. Overexpression of myocellular DGAT1 by recombinant adenovirus in C2C12 myotubes resulted in a three - fold increase in DGAT activity and led to a six - fold increase in intracellular TAG and reduced DAG by 50 % (Liu *et al.*, 2007) . Further, it has recently been reported that an increase in the content of DGAT1 (and GPAT1) occurred the day following a single bout of endurance exercise and prevented insulin resistance induced by lipid-heparin infusion in healthy humans by reducing the content of DAG and ceramides, FA metabolites which are known to lead to insulin resistance (Schenk & Horowitz, 2007). However, in a follow up study of the same group no increase in DGAT1 activity and protein content was found, but an acute bout of exercise prior to an overnight lipid-heparin infusion still protected against lipid induced insulin resistance (Newsom *et al.*, 2010). These studies suggest that high levels of GPAT1 and DGAT1 may protect against the development of insulin resistance.

1.5.2 Lipolysis

Just as a high rate of triglyceride synthesis may protect against insulin resistance by reducing levels of FA metabolites, it is also possible that high rates of IMTG hydrolysis, not compensated by increased oxidation, may lead to insulin resistance, particularly if incomplete lipolysis to DAG and LCFACoA were to occur. Two enzymes responsible for hydrolysis of IMTG are ATGL and HSL.

1.5.2.1 Adipose Triglyceride Lipase

In adipocytes it has been shown that, in the basal state, ATGL is present both in the cytoplasm and attached to lipid droplets (Zimmermann *et al.*, 2004;Granneman *et al.*, 2007). Activation of PKA with adrenaline has been shown to lead to translocation of ATGL towards the lipid droplets (Granneman *et al.*, 2007). The hydrophobic region within the C-terminal of ATGL seems to be important for colocalisation with lipid droplets, although the mechanism by which this interaction facilitates lipid droplet colocalisation is still currently unknown (Kobayashi *et al.*, 2008;Schweiger *et al.*, 2008). Translocation to the lipid droplets also coincides with an increase in ATGL activity, but the increase in activity is not thought to be the result of the increase in PKA activity (Zimmermann *et al.*, 2004). The kinases that do regulate this process are currently unknown. ATGL phosphorylation leading to activation is thought to occur at residues Ser^{404} and Ser^{428} (Bartz *et al.*, 2007a). Maximal activation of ATGL requires the interaction of comparative gene identification 58 (CGI-58) (Lass *et al.*, 2006), increasing its activity up to 20 fold in a cultured kidney cell line. However it is currently not known if, and under which conditions, it activates ATGL in human skeletal muscle.

Rates of lipolysis are also mediated by the PAT proteins (Perilipin, ADRP and TIP-47) which regulate the access of the lipolytic enzymes ATGL and HSL to the TAG in the lipid core. Under basal conditions it is thought that CGI-58 is colocalised with the PAT protein perilipin on the surface of the lipid droplets. In the basal state, ATGL is proposed to be both found in the cytoplasm and bound to lipid droplets in adipose tissue, however upon adrenergic stimulation which causes phosphorylation of perilipin, CGI-58 dissociates from the lipid droplets into the cytoplasm (Brasaemle *et al.*, 2004;Granneman *et al.*, 2007;Yamaguchi *et al.*,

2007) to recruit and activate ATGL on the surface of the lipid droplets lacking perilipin (Granneman *et al.*, 2007;Yamaguchi *et al.*, 2007). However, this CGI-58 mediated activation is unlikely to occur in skeletal muscle as skeletal muscle lacks perilipin (Greenberg *et al.*, 1993;Londos *et al.*, 1995;Servetnick *et al.*, 1995;Sztalryd *et al.*, 2003). It may be that another of the PAT proteins present in skeletal muscle is involved in this process in that case.

1.5.2.2 Hormone Sensitive Lipase

Human HSL is 775 amino acids in length and is made up of three domains; a catalytic domain, a regulatory domain containing phosphorylation sites and an NH2-terminal domain involved in protein-protein and protein-lipid interactions (Watt & Spriet, 2010). In adipocytes, three phosphorylation sites are involved in PKA dependent increases in HSL activity (Ser^{563}, Ser^{659} and Ser^{660}) (Anthonsen *et al.*, 1998;Shen *et al.*, 1998). However, the importance of Ser^{563} is unclear (Anthonsen *et al.*, 1998). PKA phosphorylation leads to a 2 - 3 fold increase in HSL activity and promotes translocation of HSL to the lipid droplet in adipocytes (Egan *et al.*, 1992) in response to β-adrenergic stimulation. ERK also increases HSL activity via phosphorylation at Ser^{660} (Greenberg *et al.*, 2001). Ser^{565} is a site of negative regulation by AMPK in adipocytes (Garton *et al.*, 1989;Daval *et al.*, 2005). HSL activity is also negatively regulated by the action of insulin which causes its dephosphorylation in both adipose tissue and skeletal muscle (Enoksson *et al.*, 1998;Narkar *et al.*, 2008).

HSL was initially thought to be responsible for the first rate limiting step of lipolysis. However since the discovery of ATGL it is known that HSL is primarily responsible for the lipolysis of DAG, with its relative hydrolase activity *in vitro* 11-fold greater against DAG than TAG (Fredrikson *et al.*, 1981a). In intact rat adipocytes, phosphorylation of HSL has

been shown to take place on two residues ((Ser^{563} (Garton *et al.*, 1988) and Ser^{565} (Garton *et al.*, 1989)). Catecholamine stimulation of β-adrenergic receptors results in elevation of cAMP which activates PKA leading to phosphorylation of HSL (Stralfors *et al.*, 1984). In primary adipocytes this activation leads to an ~50 fold increase in lipolysis, however *in vitro* this increase in PKA mediated activation only results in a two-fold increase in HSL activity (Fredrikson *et al.*, 1981b). This is likely due to HSL translocation from the cytosol to the lipid droplets for lipolysis upon activation. *In vitro* studies have revealed the translocation of HSL from cytosolic fractions to the fat cake fraction of isolated rat adipocytes (Hirsch & Rosen, 1984;Egan *et al.*, 1992). This translocation from the cytosol to the lipid droplet surface has also been demonstrated in response to adrenergic stimulation in adipocytes (Brasaemle *et al.*, 2000a) as well as in response to adrenaline incubation and electrical stimulation in single fibres of rat skeletal muscle (Prats *et al.*, 2006). The exact mechanisms of the translocation are currently unknown however it has been shown that the translocation events do not rely on the cytoskeletal compartments; microfilaments or microtubules (Brasaemle *et al.*, 2000a). Therefore this spatial redistribution of HSL may be of crucial importance in the regulation of lipolysis; however this translocation is yet to be demonstrated in human skeletal muscle.

1.5.3 The Role of SNARE Proteins in IMTG Metabolism

In obese individuals the increased lipid spillover resulting from the reduced chylomicron-TAG clearance by adipose tissue as well as the increased VLDL-TAG production by the liver seems to lead to an increase in the size of IMTG stores. This may be accompanied by an increase in lipid droplet size. In obese and insulin resistant individuals it has been shown that there is a distinct increase in IMTG stores (Kelley *et al.*, 2002). Further, the severity of insulin

resistance is associated and correlated with the size of IMTG stores in obese individuals; the IMTG concentration being inversely related to insulin sensitivity (Pan *et al.*, 1997).

1.5.3.1 SNAP23 and its Role in Insulin Resistance

SNAP23 is a SNARE protein which has been identified in non neural tissues and has been found to be an analogue of SNAP25 sharing high sequence homology (Ravichandran *et al.*, 1996). In its role as a SNARE protein SNAP23 binds with VAMP1 and 2 and also Syntaxin1, 2, 3 and 4 and is the functional equivalent to SNAP25 in non-neural cells playing a role in targeted exocytosis. A hypothesis of highjacking of SNAP23 away from the plasma membrane to the lipid droplets has been put forward by Sollner (2007). A decreased content of SNAP23 at the plasma membrane would lead to a decreased availability of SNAP23 for transport, docking and fusion of GLUT4 and therefore could be a factor leading to the impairments in insulin mediated GLUT4 translocation seen in obesity and type 2 diabetes shown in Figure 1.5.

SNAP23 has also been shown to play a role in lipid droplet fusion in cardiomyocytes as knockdown of the genes for SNAP23, syntaxin-5 and VAMP4 or microinjection of mutant α-SNAP resulted in a decrease in the rate of lipid droplet fusion (Bostrom *et al.*, 2007). Furthermore, oleic acid incubation resulted in decreased insulin sensitivity; however this was overcome with transfection of SNAP23 to these cells, likely due to replenishment of the plasma membrane SNAP23 store. The exact mechanisms regulating the increase in insulin sensitivity with greater SNAP23 content had remained unclear until recently. Oleic acid incubation results in an increase in the volume of the lipid droplet pool in cardiomyocytes, leading to a decreased availability of SNAP23 at the plasma membrane and a concomitant decrease in insulin mediated glucose uptake. It is possible that the action of SNAP23 could

explain the increased lipid droplet size and the hijacking of SNAP23 by fusing lipid droplets could prevent GLUT4 docking with the plasma membrane resulting in decreased glucose uptake in response to insulin in obese and type 2 diabetic individuals.

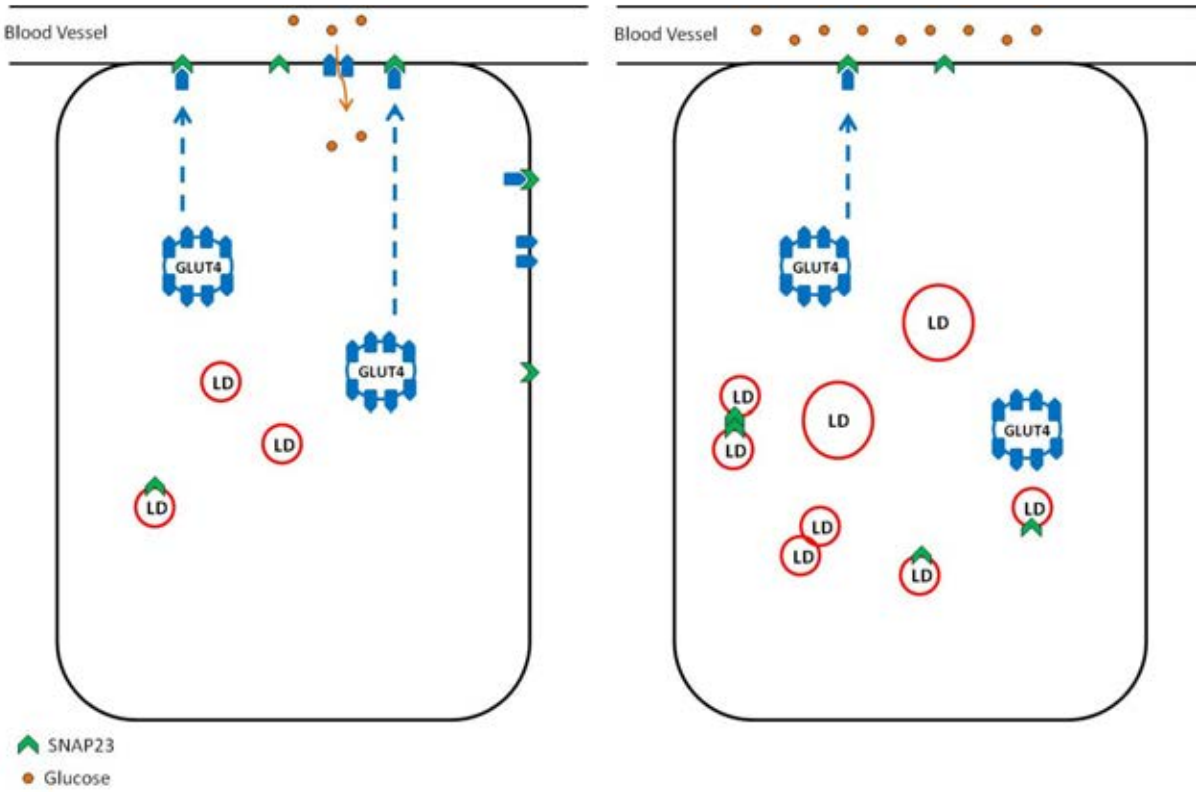

Figure 1.5. SNAP23 hijacking hypothesis. In response to insulin, GLUT4 translocates to the plasma membrane, docking with the aid of SNAP23 residing at the plasma membrane allowing glucose entry into the cell. However, in a cell with a high lipid droplet (LD) content (right panel) SNAP23 is sequestered away from the plasma membrane for lipid droplet fusion, limiting GLUT4 docking at the plasma membrane and leading to hyperglycaemia. Image adapted from Sollner (2007). Note that additional SNARE proteins (VAMP2, VAMP4, Syntaxin 4 and Syntaxin 5) also play a role n GLUT4 docking but have been excluded from the scheme to highlight the role of SNAP23.

1.6 IMTG Metabolism in Humans

1.6.1 High Fat Diets and IMTG Content

Many studies have investigated the effects of high fat diets on lipid metabolism and insulin resistance. Dietary intervention studies in human volunteers have ranged in time from 24 h to 7 days and the studies measuring the IMTG content via biochemical extraction methods observed a maximal increase by up to 90 % (Starling *et al.*, 1997;Zderic *et al.*, 2004). Other studies used ^{1}H-MRS for the determination of IMTG content and showed that consumption of a high fat (60 % of energy) diet in as little as 48 h increased resting IMTG levels by 45 % (Starling *et al.*, 1997;Johnson *et al.*, 2003;Zderic *et al.*, 2004). Further, in as little as 60 h after the start of the consumption of a high saturated fat diet (45 % energy from fat of which 60 % was saturated fat), insulin sensitivity, as measured by hyperinsulinaemic euglycaemic clamp, was reduced by 25 % (Stettler *et al.*, 2005). A consistent finding in these dietary intervention studies regardless of the length of the diet appears to be the increase in skeletal muscle lipids. In longer protocols of high fat feeding, a one week 60 % high fat diet led to a 54 % increase in IMTG (Schrauwen-Hinderling *et al.*, 2005) which was comparable to increases seen in the shorter term high fat feeding regimes. A 2.3 fold increase in IMTG content was seen after a 5 week high fat diet (53 % energy from fat) (Vogt *et al.*, 2003) and following 7 weeks of high fat feeding (65 % energy from fat) IMTG concentration was significantly elevated by 73 % (Helge *et al.*, 2001). Bachmann *et al.,* (2001) found a significant 50 % increase in IMTG in soleus muscle but only a 14 % increase in tibialis anterior muscle in response to a 3 day high fat diet (55 - 60 % energy from fat). However the soleus muscle is an oxidative muscle and relies on fat for energy, whereas the tibialis anterior has a lower initial content of IMTG and a much lower reliance on fat oxidation (Schrauwen-Hinderling *et al.*, 2005). It has been

reported that type I fibres contain approximately two fold more lipid than type II fibres (Malenfant *et al.*, 2001;van Loon *et al.*, 2004). The variation in the IMTG content in these studies may also, in part, be explained by the participants' diet prior to the intervention taking place which may have impacted the IMTG concentrations.

1.6.2 Lipid Infusion and Insulin Sensitivity in Humans

The content of TAG in skeletal muscle has previously been shown to be correlated with insulin resistance in obese individuals (Pan *et al.*, 1997). However well trained, insulin sensitive athletes also have high levels of TAG in skeletal muscle (van Loon & Goodpaster, 2006) suggesting that it is not the accumulation of lipid *per se* which leads to insulin resistance. Many studies have mimicked the large lipid flux seen in obesity via lipid-heparin infusion in both rodents and lean humans. However when these studies have been undertaken in obese or type 2 diabetic individuals, the results differ from those obtained using animal models, with increases in different lipid metabolites, discrepancies in the time course of the development of insulin resistance and also the specific signalling proteins which appear to be involved in the development of insulin resistance.

In male subjects intravenous lipid-heparin infusion (Itani *et al.*, 2002) led to an increase in plasma FA, albeit to supraphysiological levels, maximally 1200 μmol/L, which led to a 3 fold increase in DAG mass at 6 h. PKC activity has also been shown to be increased both in the cytosol and at the plasma membrane (Itani *et al.*, 2002). In similar protocols in which a 5 h (Dresner *et al.*, 1999) or 7.5 h (Kruszynska *et al.*, 2002) lipid-heparin infusion was administered, glucose oxidation and glycogen synthesis were 50 – 60 % lower, implying diminished glucose transport and reduced insulin action as a result of the lipid infusion. More

recently it has been shown that increasing FA levels to mimic values closer to physiological values (maximal increase to ~ 1 mmol/L) with an intravenous lipid-heparin infusion also led to a 30 % reduction in insulin sensitivity index (Schenk & Horowitz, 2007).

1.6.3 Dietary Fatty Acid Composition, IMTG and Insulin Sensitivity

It also appears that the composition of dietary fats can impact upon insulin sensitivity. However to date, the majority of the studies assessing FA composition have been carried out in cell culture with few investigating human participants. In C2C12 myotubes incubated for 18 hours either with or without FA prior to stimulation with insulin, it was found that palmitate elevated ceramide concentrations two fold and inhibited insulin stimulated phosphorylation of glycogen synthase kinase-3 (GSK-3) and PKB. These effects, however, were not seen with unsaturated FA (oleate or linoleate) incubation despite inhibition of PI3K activity (Schmitz-Peiffer *et al.*, 1999). More recently, palmitate incubation of mouse myotubes increased DAG content, PKCθ activation and decreased IMTG content due to downregulation of DGAT2. Incubation with the monounsaturated FA oleate however did not cause these changes (Coll *et al.*, 2008).

These effects have also been investigated in animals. Under conditions of hyperinsulinaemia chronic high fat feeding of either high saturated or polyunsaturated fat impaired insulin signal transduction at the level of IRS1 Tyr^{612} and PKB Ser^{473}. The findings of this study suggested that the amount of fat is crucial, more so than the type of fat delivered when it comes to insulin action (Frangioudakis *et al.*, 2005), although these findings appear to contradict those of others who found contrasting effects for saturated and unsaturated fatty acids. Therefore this is an area in need of further research.

A large scale study in which 162 human participants followed a diet high in either saturated FA or monounsaturated FA found that insulin sensitivity was 12.4 % lower on the diet high in saturated FA and 8.8 % higher on the diet high in monounsaturated FA (Vessby *et al.*, 2001). Whilst the animal data of Frangioudakis *et al.,* (2005) is of interest, it is the findings in humans of Vessby *et al.,* (2001) that are most relevant to this thesis. Thus it would seem that high fat diets do not by definition lead to increases in FA metabolites and insulin resistance but instead, the composition of FAs (whether saturated or unsaturated) appears to be a major factor in determining this effect. It would seem that diets high in saturated fat can impair insulin signalling through an increase in FA metabolites and decreased insulin sensitivity.

1.6.4 Calorie Restriction and Insulin Sensitivity

It is known that fasting for up to 72 hours reduced whole body glucose disposal and leads to insulin resistance (Mansell & Macdonald, 1990;Webber *et al.*, 1994). A 67 h starvation protocol led to an increase in IMTG when compared to a mixed carbohydrate diet and also induced insulin resistance which was measured using an intravenous glucose tolerance test (Johnson *et al.*, 2006). The similar IMTG content following short term starvation or short term high fat diet could perhaps be explained by the increased plasma FA in both conditions (during starvation there is an increase in adipose-derived FA) thereby increasing FA uptake into the muscle. Similar increases in IMTG have been found following a 72 h fast in non diabetic physically fit men which was again proposed to be due to the increase in plasma FA (Stannard *et al.*, 2002). None of these studies measured the LCFACoA, DAG and ceramide pool, nor PKC β and θ activities and IRS-1 serine phosphorylation, implying that the medium by which acute fasting reduces insulin stimulated glucose uptake in skeletal muscle is not currently known.

There is however substantial evidence to suggest that alternative weight loss interventions involving low or reduced calorie intakes can improve insulin sensitivity and decrease IMTG content. It is not clear though if the decrease in IMTG content is related to the improved insulin sensitivity or whether reductions in fat mass reduce the lipid spillover and fat deposition in non-adipose tissues. Following chronic calorie restriction over 4 months in patients with type 2 diabetes it has been reported that a decrease in IMTG occurs (Goodpaster *et al.*, 2000). However, in this study, the association between IMTG and insulin sensitivity was not evaluated. Bariatric surgery has also proved to be effective at improving insulin sensitivity from as little as 6 months follow up (when the first measurement was taken), although it is likely that improvements had already occurred much earlier. In a study comparing bariatric surgery or a 6 months hypocaloric diet, surgery resulted in significantly greater weight loss than calorie restriction alone and calorie restriction alone also only led to mild improvements in insulin sensitivity compared to insulin resistance being completely reversed 6 months following surgery (Greco *et al.*, 2002). This reversal of insulin resistance also coincided with a decrease in the size of the IMTG pool (1.63 ± 1.06 to 0.22 ± 0.44) which only occurred in patients who opted for surgery. No data were provided on the concentrations of the FA metabolites that lead to insulin resistance (Greco *et al.*, 2002). Furthermore there was a trend for GLUT4 expression to be increased following surgery. Significant improvements in insulin sensitivity have been seen one year following gastric bypass in morbidly obese patients (Houmard *et al.*, 2002;Gray *et al.*, 2003) along with decreases in BMI and fasting glucose. Bariatric surgery results in such a dramatic reduction in calorie intake that fat mass is reduced massively. The visceral adipose stores are often decreased rapidly in weight loss. Visceral fat accumulation may result in an increased flux of FA to the liver providing a source of FA for VLDL-TAG production and liver TAG

deposition (Hodson *et al.*, 2010). The loss of visceral fat stores reduces lipid spillover and therefore ectopic fat accumulation in muscle, liver and the vascular wall. Taken together these findings suggest that the weight loss brought about by bariatric surgery results in much greater improvements in insulin sensitivity than the more moderate calorie restriction achieved without surgery. Whether this is due solely to the extreme energy restriction and weight loss needs to be investigated.

Short term interventions involving more moderate calorie restrictions in combination with exercise also have been shown to improve glucose tolerance and insulin sensitivity. A two week diet and exercise intervention in type 2 diabetics resulted in a 19 % decrease in IMTG and a 57 % increase in insulin sensitivity as measured using a hyperinsulinaemic euglycaemic clamp (Tamura *et al.*, 2005). Additionally, insulin sensitivity, measured using a hyperinsulinaemic euglycaemic clamp, was improved and IMTG content was decreased in individuals following 12 weeks aerobic exercise training or a reduced calorie diet (~ 33 % calories less than normal) (Solomon *et al.*, 2008). However it was found that IMTG reduction did not have an association to insulin sensitivity but was associated with improvements in fat oxidation and IMTG utilisation. The increased IMTG oxidation was proposed to be the result of higher elevations in AMPK during exercise. AMPK is an enzyme which acts as a metabolic 'fuel-gauge' responding to changes in cellular energy. AMPK can increase FA oxidation in muscle through the inhibition of acetyl coenzyme A carboxylase, relieving the inhibition of malonylCoA on carnitine palmitoyl transferase 1, thus allowing FA to be shuttled efficiently into the mitochondria to undergo β-oxidation (Hardie *et al.*, 1998;Ruderman *et al.*, 1999;Winder & Hardie, 1999). Further research has looked more specifically at the morphological changes seen in the IMTG pool (He *et al.*, 2004). Four

months of weight loss via a combined caloric restriction (decrease by 500 - 1000 kcal/d) and exercise intervention resulted in ~ 10 % weight loss and a decrease in lipid droplet size. Interestingly, in this study IMTG content did not decrease. This decrease in lipid droplet size was correlated with an increase in insulin sensitivity and importantly the amount of physical activity (He *et al.*, 2004). Thus it seems that exercise is a key component to changes in IMTG metabolism with an impact on glucose tolerance and muscle insulin sensitivity.

A short term very low calorie diet (700 kcal/d for 6 days) in obese individuals with and without type 2 diabetes resulted in small but significant decreases in total body fat and BMI as well as a pronounced reduction in IMTG (56 % in non diabetics and 40 % in type 2 diabetics). Further, glucose disposal rate was increased by 9.3 % under oral glucose tolerance test conditions (Lara-Castro *et al.*, 2008) suggesting that a more robust calorie restriction may be necessary to initiate significant reductions in IMTG, if it is not combined with exercise. An arguably more realistic dietary protocol of 1200 kcal/d until euglycaemia was achieved (between 3 - 12 weeks) showed that normal fasting glucose levels can be achieved even with a more moderate weight loss protocol (Petersen et al., 2005). Average weight loss was 8 kg and whilst fasting plasma glucose was normalised, no changes were seen in insulin stimulated peripheral glucose uptake, measured by hyperinsulinaemic euglycaemic clamp or IMTG.

1.6.5 Gender Differences in IMTG Metabolism

It is known that there are differences in IMTG metabolism between males and females. Several studies have reported a higher total IMTG content in females than in males (Roepstorff *et al.*, 2002;Steffensen *et al.*, 2002;Roepstorff *et al.*, 2006;Tarnopolsky *et al.*, 2007). However, the higher IMTG content in females does not appear to impair insulin

signalling, in fact, with a 47 % higher IMTG content, women displayed a 22 % higher whole body insulin sensitivity during a hyperinsulinaemic euglycaemic clamp and 29 % higher insulin stimulated leg glucose uptake (Hoeg *et al.*, 2009). An explanation for this apparently paradoxical result has been discussed elsewhere in this introduction *(see section 1.3.2)*. It is likely that it is not the IMTG content *per se* that leads to the insulin resistance. Instead, the fractional synthesis rate of IMTG as well as the balance between lipolysis, IMTG synthesis and FA oxidation all impact the FA metabolite concentration (Moro *et al.*, 2008). In respect of the findings of Hoeg *et al.,* (2009), it therefore seems important that oxidative capacity is maintained and it was shown in non obese women that the increased IMTG was accompanied by a greater capillary density and a greater proportion of oxidative type I fibres than their male counterparts. Further, skeletal muscle HSL protein content is higher in women compared with men although HSL activity during 90 minutes of exercise at 60% VO_{2peak} was not different (Roepstorff *et al.*, 2006). No information is available today on differences in the concentration of LCFACoAs, DAGs and ceramides between the muscles of women and men.

IMTG metabolism does however differ when comparisons are made between lean and obese sedentary individuals of the same gender. It was first proposed over 15 years ago that obese individuals have a lower rate of IMTG turnover (Klein *et al.*, 1994). Lean men with impaired glucose tolerance recently were shown to have lower IMTG synthesis rates than their normally glucose tolerant counterparts however these differences did not exist in a female cohort (Perreault *et al.*, 2010). Similar to the relationship that exists in lean individuals, with lean women having twice as much IMTG as lean men, it has been shown that obese women have twice as much IMTG as obese men when matched for BMI (Haugaard *et al.*, 2009;Perreault *et al.*, 2010). Further, it has also been suggested that in females obesity is also

associated with extramyocellular triglycerides both within and between the muscles (Weis *et al.*, 2007). It is proposed that in obesity, a reduced oxidative capacity can lead to the accumulation of IMTG, possibly due to the position of the mitochondria in relation to the IMTG. In sedentary individuals the mean distance between the mitochondria and IMTG is large, leading to a larger diffusion distance which can lead to higher FA metabolite concentrations (Tarnopolsky *et al.*, 2007) whereas in trained individuals, the IMTG and mitochondria are distributed in close proximity (Tarnopolsky *et al.*, 2007;Shaw *et al.*, 2008).

Controversy exists as to the effects of weight loss on the IMTG pool between genders and seems to confirm that women can maintain insulin sensitivity for a higher IMTG set point. For example, an 11.5 % rapid (53 days) weight loss in obese women did not change the IMTG levels but still led to significant improvements in insulin sensitivity (Rabol *et al.*, 2009). A slower rate of weight loss in men (112 days vs. 53 days) resulted in a decrease in IMTG content and improved insulin sensitivity in a euglycaemic clamp in men (Toledo *et al.*, 2008). Thus it would seem that the gender differences in IMTG metabolism also exist during weight loss regimes. A proper evaluation of gender differences is difficult to make today as there is lack of information from properly controlled studies comparing the genders under exactly the same baseline conditions and using exactly the same intervention protocols.

1.6.6 The Athletes' Paradox

It has been noted that the skeletal muscle of endurance trained individuals contains large IMTG stores (Goodpaster *et al.*, 2001;van Loon *et al.*, 2004) comparable with or even higher than those observed in obese and type 2 diabetic individuals. In trained individuals, the IMTG stores tend to be localised in close proximity to the mitochondria with minimal distances

between these organelles (Hoppeler, 1999;Tarnopolsky *et al.*, 2007;Shaw *et al.*, 2008) so that they can be readily utilised as a fuel source during exercise. A further important difference between the lipid pools in obese sedentary individuals and endurance trained individuals is the turnover of the IMTG stores. When endurance athletes are training, their IMTG stores are regularly depleted and then replenished in the post exercise period. This allows for a major proportion of the meal derived FA to enter the muscle and be channelled into IMTG synthesis, thus keeping FA metabolite levels within the muscle low. In obese and type 2 diabetic individuals, the IMTG stores are not emptied during exercise (van Loon, 2004;van Loon *et al.*, 2005) potentially due to the fact that the mean distance between mitochondria and lipid droplets is larger (Tarnopolsky *et al.*, 2007). Thus when FA enter the muscle, they cannot be channelled to IMTG synthesis as these stores are already at their maximal volume. This then leads to increases in the concentration of FA metabolites within the muscle which inhibits the insulin signalling cascade *(see section 1.3.1)*.

1.7 The Importance of Immunofluorescence Microscopy as a Research Tool

The use of different methods to investigate IMTG content and use during exercise have lead to equivocal findings. For example, biochemical TAG extraction of human skeletal muscle biopsies obtained prior to and following an acute bout of moderate intensity exercise have shown contradictory findings between laboratories dependant on the training status or gender (Roepstorff *et al.*, 2002;Steffensen *et al.*, 2002) of the individuals for instance. The between biopsy coefficient of variation (CV) for this technique is approximately 20 – 26 %, and most likely is too large to tease out meaningful data about TAG utilisation between genders, training status, exercise and diet interventions. It has been suggested that the cause of the large CV is the presence of a variable extra myocellular lipid pool which is part of the total

IMTG estimate when analysed via the biochemical TAG extraction method (Guo, 2001). This problem can be overcome through the use of ^{1}HMRS. Studies using this technique have shown a 20 – 40 % decrease in IMTG following an acute bout of exercise in trained male and female participants (Boesch *et al.*, 1997;Boesch *et al.*, 1999;Krssak *et al.*, 2000;Rico-Sanz *et al.*, 2000;Brechtel *et al.*, 2001;Decombaz *et al.*, 2001;Larson-Meyer *et al.*, 2002;van Loon *et al.*, 2003b). However, a key limitation to both of these techniques is the lack of information on the different fibre types present in skeletal muscle. The different fibre types have different metabolic characteristics with potentially a large impact on lipid content, lipid turnover, FA oxidative capacity, and IMTG use during exercise.

Stable isotope tracers have also been used to examine IMTG utilisation when used in combination with indirect calorimetry. Intravenous infusions of tracer labelled FAs have been used to determine the rate of appearance/disappearance and oxidation of plasma FA. This method however cannot discriminate between plasma and muscle derived TAG, both of which contribute to total fat oxidation (Havel *et al.*, 1967;Oscai *et al.*, 1990;Helge *et al.*, 2001;van Loon *et al.*, 2001;van Loon *et al.*, 2003a).

Therefore, immunofluorescence microscopy may be proposed as the most powerful analytical method to investigate which impairments exist in lipid metabolism of skeletal muscle with a potential negative impact on glucose uptake and insulin sensitivity or action. The main advantage of immunofluorescence microscopy is that it provides additional information regarding fibre type differences in lipid distribution and usage during exercise (van Loon *et al.*, 2004;Koopman *et al.*, 2001;Shaw *et al.*, 2008). This is of importance given the differing metabolic characteristics that occur in type I and type II fibres for instance in terms of insulin

sensitivity with type I fibres being more insulin sensitive than type II fibres. As type I fibres utilise IMTG at a much higher rate than type II fibres (van Loon, 2004;Stellingwerff *et al.*, 2007), differences in fibre type distribution between individuals may also contribute to the large CV seen between repeated biopsies, between individuals and between the effects of interventions when using, for example, the biochemical extraction method to measure IMTG.

Immunohistochemistry is also an invaluable research tool when investigating the morphology of lipid droplets and their spatial distribution, including fibre type differences. Such differences cannot be studied with traditional methods applied to whole muscle homogenates and extracts such as is the case when using Western Blots, HPLC or Mass Spectrometry. For instance, it has been demonstrated using immunofluorescence microscopy that overall lipid droplet content did not change in response to weight loss and exercise in previously sedentary individuals, but that the individual lipid droplets appeared to be dispersed into a larger number of substantially smaller droplets (He *et al.*, 2004). This change in lipid droplet morphology could have crucial implications in terms of accessibility for the lipid metabolising enzymes and insulin resistance, for instance smaller lipid droplets may have greater rates of lipid turnover and, therefore, could be less subject to oxidative damage or result in lower levels of FA metabolites.

The protein content of the lipid droplets in skeletal muscle has also been identified with immunofluorescence microscopy. Recently, it has been shown that ADRP colocalised with ~60 % of the lipid droplets (Shaw *et al.*, 2009). The PAT protein TIP47 also colocalises with lipid droplets (Prats *et al.*, 2006). Immunofluorescence microscopy has also successfully identified that mitochondria and lipid droplets are present in a matrix structure with the lipid

droplets in close proximity to the mitochondria but filling only part of the spaces that are available between the mitochondria, which fill most of the available spaces on both sides of the Z-line in trained individuals (Tarnopolsky *et al.*, 2007;Shaw *et al.*, 2008).

Immunofluorescence microscopy has also been used to demonstrate the specific redistribution of proteins in response to stimuli such as the translocation of HSL to the lipid droplets in response to adrenaline incubation or contraction (Prats *et al.*, 2006) as well as the redistribution of SNAP23 and Munc18 in type 2 diabetic humans (Bostrom *et al.*, 2010). The value of immunofluorescence microscopy has also been shown in an elegant series of experiments investigating the dynamics of GLUT4 translocation both in basal conditions and in response to stimulation by both insulin (Lauritzen *et al.*, 2006;Lauritzen *et al.*, 2008b) and contraction (Lauritzen *et al.*, 2010). These studies imaged skeletal muscle from living GLUT4-enhanced green fluorescent protein–transfected mice. In these studies the dynamic nature of the GLUT4 vesicles can be visualised as well as clearly demonstrating the compartmentalised distribution of GLUT4 to the plasma membrane, t-tubules and the perinuclear regions. The fact that this technique can be used both for *in vitro* and *in vivo* work, is obviously of importance in order to investigate the pathogenic mechanisms.

Immunofluorescence microscopy is a valuable and powerful research technique that can provide (semi)quantitative data as well as producing informative images showing spatial distribution of specific proteins of interest. Therefore, this thesis shows the development of a number of new immunohistochemical methods which could be used in the future to address a number of research questions and hypotheses that might play a role in understanding the

mechanism by which impairment in lipid metabolism in obesity lead to insulin resistance in skeletal muscle.

1.8 Scope and Outline of the thesis

In order to develop therapies that may help to prevent obesity induced insulin resistance and the related pathologies, it is important to identify the main mechanisms that lead to impaired glucose tolerance in obese individuals. This thesis aims to generate novel methods by which obesity induced insulin resistance in skeletal muscle may be investigated in the future. In particular, this thesis aims to investigate the distribution of the enzymes that play a role in the regulation of lipid turnover (TAG synthesis and lipolysis) in skeletal muscle, that also determine the concentration of FA metabolites that previously have been suggested to lead to obesity induced insulin resistance *(explained in section 1.3.1)*. In the final two chapters the role of a protein (SNAP23) with a potentially parallel function in glucose uptake (GLUT4 docking) and fusion of lipid droplets in skeletal muscle as a limitation in glucose uptake in obesity and type 2 diabetes is explored. It is of key importance to know the subcellular localisation of these enzymes including colocalisation with organelles and membrane structures as this could provide crucial information on the regulation of lipid synthesis, hydrolysis and oxidation.

1.8.1 General Overview

Chapter 2 details the general methodology common to each of the experimental chapters and includes information on sample collection, sample treatment and detailed protocols for immunofluorescence microscopy and Western blotting.

The spatial distribution of the enzymes that control IMTG synthesis is investigated in Chapter 3 and Chapter 4 through immunofluorescence staining of GPAT1, GPAT4 and DGAT1 respectively in six lean, moderately active men. The difference between fibre types and the potential colocalisation of these enzymes with lipid droplets and mitochondria is also investigated. Chapter 5 investigates the distribution of both GPAT1 and DGAT1 in skeletal muscle obtained from ageing non obese and obese women in an attempt to establish whether there is a change in the localisation of these enzymes in response to obesity. Regulation of lipid turnover is also influenced by IMTG hydrolysis, thus in Chapter 6, the specific distribution of ATGL and CGI-58 (an activator of ATGL) are investigated together for the first time in human skeletal muscle of lean, moderately active males.

Chapter 7 investigates the distribution of SNAP23 in six healthy, moderately active males. The colocalisation of SNAP23 with mitochondria, lipid droplets and the plasma membrane is also investigated. Chapter 8 investigates whether there are differences in the distribution of SNAP23 between six non obese and six obese ageing women in skeletal muscle samples obtained during elective orthopaedic surgery.

In Chapter 9 (General Discussion) the findings of each of the experimental chapters is discussed and placed in the context of the general literature and proposals are made for future research in light of the findings of the studies within this thesis. Future studies should aim to generate further information from lean, obese and obese type 2 diabetic individuals using immunofluorescence microscopy and complementary techniques with a higher spatial resolution in order to identify differences in distribution and colocalisation and impairments in translocation/fusion in response to physiological stimuli (insulin, meal, exercise, adrenaline) that result from these conditions to deepen our current insight into the mechanisms that lead to glucose intolerance, insulin resistance, metabolic syndrome and type 2 diabetes and identify target enzymes or translocation/fusion processes for development of new drugs.

1.8.2 Aims of the Experimental Chapters

In *section 1.5.1.1* and *1.5.1.2* the recently published evidence is presented that a high content or activity of the lipid synthetic enzymes GPAT1 and DGAT1, which determine the major rate controlling steps of IMTG synthesis, can offer protection against lipid induced insulin resistance. The distribution of GPAT1 and DGAT1 has not been investigated in human skeletal muscle to date and so the aims of Chapters 3 and 4 are to establish a protocol to be used for immunofluorescence staining of the most important isoforms of these enzymes and also to investigate their fibre type and subcellular distribution to include potential colocalisation with lipid droplets and mitochondria. Chapter 5 aims to investigate whether there are differences in the distribution of these enzymes between non obese and obese women.

In *section 1.5* the arguments and rationale are given to underpin the view that a detailed understanding of the mechanisms that control lipid turnover (TAG synthesis, lipolysis and FA oxidation) is required to understand mechanisms responsible for insulin resistance in skeletal muscle. An imbalance between the components of lipid turnover could lead to an accumulation of FA metabolites which have been proposed to lead to insulin resistance through the activation of PKC (LCFACoA and DAG) and inactivation of Akt (ceramides). Chapter 6 aims to investigate the hydrolytic part of the lipid turnover pathway through the investigation of novel aspects of the distribution of ATGL and CGI-58 in human skeletal muscle.

The aim of Chapter 7 is to validate an antibody for immunohistochemical studies of sections of human skeletal muscle obtained from lean, active males in order to investigate the subcellular and fibre type specific distribution of SNAP23 and its potential colocalisation with the plasma membrane, lipid droplets and mitochondria. In *section 1.5.3.1* it was reported that lipid droplets in obese individuals and type 2 diabetes patients have been proposed to hijack part of the limited SNAP23 stores from the plasma membrane to lipid droplets where they might be required for lipid droplet fusion. Chapter 8 aims to investigate the distribution of SNAP23 in six non obese and six obese women in order to investigate if SNAP23 hijacking occurs in the obese women.

CHAPTER 2

GENERAL METHODS

2.1 Ethical Approval

Written informed consent was obtained from all participants. Approval for execution of the studies was obtained from NHS Research Ethics Committees in the Birmingham and Warwick region.

2.2 Muscle Samples

Percutaneous muscle biopsies were obtained from the *m. vastus lateralis* under local anaesthesia (~ 5 ml 1 % lidocaine) using the needle biopsy technique (Bergstrom, 1975). Following local anaesthesia, a small (~ 1 cm) incision was made in the skin and the fascia covering the central portion of the *m. vastus lateralis*. The biopsy needle was then inserted and sequential cuts were made with the application of suction (~ 100 mg). In addition, samples were obtained during elective orthopaedic surgery (Chapters 5 and 8 only) under general anaesthesia at Russells Hall Hospital, Dudley Group of Hospitals NHS Trust by Mr Edward Davis, Consultant Orthopaedic Surgeon. Following the initial incisions for the total hip arthroplasty surgery, a muscle biopsy (~ 200 mg) was obtained from the *m. gluteus maximus*. Following removal, samples were blotted of excess blood and any visible fat and collagen was separated from the sample and discarded. Part of the biopsy sample (~ 30 mg) was embedded in Tissue-Tek OCT Compound (Sakura Finetek Europe, Zoeterwoude, The Netherlands) on a cork board which was immediately frozen in liquid nitrogen-cooled isopentane (Sigma-Aldrich, Dorset, UK) and stored in pre-cooled cryotubes at - 80 ºC for histological analyses. The rest of the biopsy samples were snap frozen in liquid nitrogen and stored at – 80 ºC for subsequent Western blotting analyses.

2.2.1 Sample Preparation for Histology

Cryosections (5 µm) were cut using a microtome (Bright Instrument Company Limited, Huntingdon, England) housed within a cryostat at – 25 ºC. The sections were collected onto uncoated, pre-cleaned glass slides (VWR International Ltd, Leicestershire, UK), stored at room temperature and left to air dry for a maximum of one hour before treatment.

2.3 Immunofluorescence Method Development

2.3.1 Antibodies

2.3.1.1 Antibody Validation

The success of immunofluorescence staining techniques is critically reliant on the selection of an appropriate primary antibody which solely detects the target protein. Failure to critically analyse the specificity of the selected antibodies using a variety of techniques can lead to the generation of incorrect data and therefore pollution of the literature with artefacts. Fundamentally, all antibodies used in any antibody technology application must be specific to the protein of interest.

All of the antibodies targeting the key proteins of interest in this thesis were validated for use in immunofluorescence staining. This was primarily completed with the Basic Local Alignment Search Tool (BLAST), immunofluorescence staining and Western blotting. The BLAST was used in order to determine that the sequence against which the antibody was raised exists within the protein of interest only. The BLAST was completed using the online resource www.uniprot.org. The immunofluorescence staining was used in order to determine whether the images obtained were in line with the expected distribution as purported in the literature or the function of enzymes. Western blotting was used to check that a single band

was revealed at the correct molecular weight. Specific details of the Western blotting procedures can be found later in this chapter in section 2.6.

2.3.1.2 Primary Antibodies

Primary antibodies were obtained from a variety of sources, both commercial as well as kind donations from Astra Zeneca R&D. All antibodies were diluted to their predetermined optimal working concentration in phosphate buffered saline (PBS) (PBS, 137 mM sodium chloride, 3 mM potassium chloride, 8 mM disodium hydrogen phosphate and 3 mM potassium dihydrogen phosphate, pH 7.4) with the addition of 5 % normal goat serum (NGS) or normal donkey serum (NDS) as a blocking agent depending on the primary antibody. Cell borders were marked using wheat germ agglutinin (WGA) (Invitrogen, Paisley, UK) which binds to sialic acid and N-acetylglucosaminyl sugar residues which are located predominantly at the plasma membrane.

2.3.1.3 Secondary Antibodies

Appropriately targeted secondary antibodies were also obtained from a variety of sources (Invitrogen, Paisley, UK; Stratech Scientific, Suffolk, UK). All secondary antibodies were Alexa Fluor conjugated or DyLight conjugated and were selected to fluoresce either red (568/594 nm), green (488 nm) or blue (350 nm). All secondary antibodies were diluted (1:200 unless otherwise stated) in PBS as described above.

2.3.1.4 Oil Red O

Intramuscular triglycerides (IMTG) were stained using the neutral lipid dye oil red O in combination with immunofluorescence as developed by Koopman *et al.,* (2001). Oil red O stock solution was made up of 100 mg oil red O in 20 ml of 60 % triethylphosphate. A 60 % stock solution (in dd H_2O) was then filtered twice through 150 mm Whatman filter paper (VWR, Leicestershire, UK) to remove any residual oil red O crystals. Cryosections were incubated with oil red O working solution at room temperature for 30 minutes followed by 3, 30 second rinses in dd H_2O and a 10 minute rinse under slow running cold tap water.

2.3.2 Immunofluorescence Methods

For each of the antibodies used within this thesis, a series of method development steps were taken in order to ensure that the images obtained were of the best possible quality and clarity.

2.3.2.1 Sample Fixation

Cryosections (5 µm) were imaged both after 3.7 % formaldehyde fixation as well as after acetone : ethanol (3:1) fixation in order to determine the fixative that provided the highest quality images. Formaldehyde fixation was used in order to maintain the structural integrity and antigenicity of the tissue. In a diluted aqueous solution of formaldehyde such as that used in this protocol, the majority of the formaldehyde is present as methylene-glycol which is formed when a molecule of water is combined with a molecule of formaldehyde. This reaction is reversible but has a heavy bias to the right hence the large reservoir of methylene-glycol which is required to form the methylene (-CH_2-) bridges which form between the proteins of the tissue providing the additional structural integrity (Fox *et al.*, 1985). Alcohol

fixatives, such as the acetone : ethanol used, coagulate proteins rather than forming bonds, changing the shape of the molecules but not their chemical properties.

2.3.2.2 Permeabilisation

General membrane permeabilisation procedures often help to allow the fluorescent probes to reach and reveal epitopes hidden in the plasma membrane and the membranes of organelles and vesicles. This can be achieved using treatment with detergents such as Triton X-100 which is commonplace in immunofluorescence staining as it helps to partly solvate the cellular membranes without disruption of protein-protein interactions. Previous work from this laboratory (Shaw *et al.*, 2008;Shaw *et al.*, 2009) has used 0.5 % Triton-X as a means of permeabilisation and so, during method development, staining was attempted both with and without permeabilisation, as this process can affect the epitopes that are revealed for antibody binding. This could therefore influence the image obtained in immunofluorescence quite dramatically.

2.3.2.3 Antibody Dilution

The appropriate primary antibody dilution and incubation time and temperature were also determined. Antibodies were each tested at dilutions of 1:25, 1:50 and 1:100 with incubations both for 1 hour at room temperature as well as overnight at 4 °C.

2.3.2.4 Immunofluorescence Controls

For each antibody, negative control samples were run in which the immunofluorescence microscopy procedure was completed, however the primary antibody was omitted and PBS was applied in its place. This allowed for testing for any non specific staining that may occur.

Controls were also carried out to prevent the chance of data being confounded by bleedthrough of signal into different channels. For instance when using the DAPI filter following the application of Alexa Fluor 350 (as well as the full immunofluorescence staining procedure), these images were also acquired with the FITC and Texas red filters to ensure that no signal was detected in the other channels used to visualise other proteins. This procedure was also carried out for the other secondary antibodies used (Alexa Fluor 488 and 594) as well as for oil red O. Cryosections were tested for autofluorescence in the absence of any antibodies, simply applying PBS to the section following the fixing and permeabilisation steps required.

2.4 General Immunofluorescence Staining Method

Samples were fixed for either 1 hour in 3.7 % formaldehyde or for 5 minutes in acetone : ethanol (3:1). Following fixation (formaldehyde only), samples were either washed 3 times for 5 minutes in PBS (if no permeabilisation was required) or 3 times for 30 seconds in doubly distilled water (if permeabilisation was deemed necessary). In the studies in this thesis, samples that were incubated in 0.5 % Triton X-100 for 5 minutes were then washed three times, for 5 minutes each, in PBS. Following these initial preparation steps, regardless of the fixation method, appropriately targeted primary antibodies were then applied. The duration of this incubation depended on the optimal conditions determined for each individual antibody. Following three 5 minute washes in PBS, secondary antibodies appropriately targeted to the primary antibodies were then applied for 30 minutes. Samples were then washed again 3 times for 5 minutes in PBS before the coverslips were mounted onto the slides. The mounting medium was made from 6 g glycerol and 2.4 g mowiol 4-88 dissolved in 18 ml 0.2 M Tris-buffer (pH 8.5) with the addition of 0.1 % (0.026 g) 1,4-diazobicyclo-

[2,2,2]-octane (DABCO) antifade medium. The slides were then left to dry overnight in the dark room.

2.5 Fluorescence Microscopy

Images were captured using a Nikon E600 microscope coupled to a SPOT RT KE colour 3 shot CCD camera (Diagnostic instruments Inc, MI, USA). In order to visualise the Alexa Fluor 350 fluorophores, the DAPI (387/11) excitation filter was used. To visualize the Alexa Fluor 488 fluorophores the FITC (494/20) excitation filter was used. Alexa Fluor 568/594 as well as IMTG stained using oil red O were observed using the Texas Red filter. Digital images showing cross sections and longitudinal sections of skeletal muscle fibres were obtained using the 40 x (0.75 NA) objective. The filters used in this microscope system were 3 excitation filters and 1 dichroic and 1 emission filter ("Pinkel" Triple Set, Semrock, Kettering, UK) which allow for crude measures of colocalisation due to zero pixel shift. The slides were illuminated with a 170 W Xenon Light Source and the filters were controlled using a semi-automated filterwheel (10B 10 Position Filterwheel, Sutter, USA). Detailed digital images demonstrating the cellular distribution of target proteins were obtained using an inverted confocal microscope (Leica DMIRE2, Leica Microsystems) with a 63 x (1.4 NA) oil immersion objective which allows for a greater amount of clarity to be viewed in the images. The confocal microscope also allows the investigation of colocalisation at a greater resolution. Alexa fluor 488 fluorophores were excited with a 488 nm line of the argon laser for excitation and 510 - 555 nm for emission. Alexa fluor 594 fluorophores were excited with 594 nm line of the helium-neon laser for excitation and 617 nm for emission.

2.5.1 Image Analysis

Images were processed using Image-Pro Plus 5.1 software (Media Cybernetics, MD, USA). For the analysis of IMTGs, intensity thresholds were selected to represent minimum values for lipid droplets. These were kept consistent throughout all image analysis. For each image, the muscle fibre area and the area occupied by lipid droplets were measured and any comparisons were made with sections on the same slide. Lipid content was expressed as the area fraction by dividing the stained area in the fibre by the total area of that fibre. The fluorescence intensity of some stains was measured by selecting the whole of the fibre area of interest and using measures of optical density. Using this method in combination with a fibre type stain, it was possible to determine the fibre type differences of the proteins of interest. All images used for these analyses were oriented as cross-sections. Colocalisation analysis of confocal microscopy images was conducted in Image Pro Plus 5.1 using Pearson's correlation. The significance of the colocalisation was determined by overlaying non matched images and running the same Pearson's correlation analysis, a method proposed by Lachmanovich *et al.,* (2003). If these non matched images showed significantly less colocalisation (using a paired samples t-test) than the matched image pairs, the colocalisation was deemed significant.

2.5.2 Automated Image Capture and Analysis

The routine analysis of IMTG and mitochondria in Chapters 4, 5, 7 and 8 was completed using automated image analysis. Measures of fibre type specific fluorescence intensity were also completed using this automated system in Chapters 5 and 7. Images were captured using a Metafer Slide Scanning platform (MetaSystems, Bicester, UK) which is based on a Zeiss Imager Z2 microscope with an automated slide feeder and slide stage. Image acquisition was

controlled via Metafer 4 software. The process of image capture was completed through the pre-scanning of each slide at 5 x objective (Zeiss plan neofluar 5x) and automated analysis completed to determine which regions of the cell contain tissue. Subsequently the tissue containing regions were then captured using a 40 x oil objective (Zeiss plan-neofluar 40 x oil 1.3 NA).

2.5.3 Automated Image Processing

Images were then analysed in detail using Definiens Cellenger software (Munich, Germany). User defined thresholds were determined for the intensity and contrast of either mitochondria or lipid stained objects where contrast refers to the contrast between the object pixel intensities and the background pixel intensities in a greyscale image. The user value was determined on a scale from -10 – 0 and defined the minimum contrast between an object and its surroundings, where 0 means little or no contrast. The contrast value was then used later in the analysis in the ruleset in conjunction with other parameters to define the object detection.

If investigating fluorescence intensity, further thresholds were also determined for the intensity of myosin heavy chain type I staining to identify muscle fibre type and also a value for "muscle cell growth" which was required to adjust for the width of the WGA staining that can encroach into the cell area. In the rulesets, a number for muscle cell growth was determined. This value was always set to '5' which refers to the number of pixels to dilate the muscle fibre once it has been identified from the WGA stain. This was required because the WGA stain did not form a narrow, well defined border around the fibre and in some fibres the fibre specific staining occurred overlapping or outside of the WGA stain. Therefore the

"muscle cell growth" parameter was required to increase the muscle cell size in order to correct for this.

Once these settings were established, firstly, muscle cells were detected using a non-user defined threshold on the WGA staining. Subsequently, images were 'quality controlled' manually to ensure they only contained cells identified as muscle cells. The algorithm then assigned whether the cell was fast or slow type, then (depending on whether lipid or mitochondria analysis was required) the algorithm defined the fine detail objects using a watershed algorithm. This allowed the channel in which the objects of interest were identified to be considered a topographic surface, with gradients from the highest pixel intensities to the lowest intensities or local minima (background within a fibre). In the muscle, criteria were set that classified objects that were identified as the threshold decreased and emerging pixels that have common criteria and could be segmented. Therefore, as the threshold was decreased, each emerging object was analysed and its shape, relation to neighbouring pixels, intensity and contrast to neighbouring pixels was evaluated.

2.6 Western Blotting

Western blotting was used as a method to show specificity of the selected primary antibodies.

2.6.1 Muscle Extraction Protocol

Homogenisation buffer (50 mM Tris - HCl, 1 mM EDTA, 1 mM EGTA and 1 % Triton X-100 in dd H_2O) was used for dilution of lysis buffer (protease inhibitor cocktail, 10 mM β-glycerophosphate, 50 mM sodium fluoride and 0.5 mM sodium orthovanadate) in which the total protein fraction was isolated. A bicinchoninic acid (BCA) assay was then used to

determine the protein concentration of the homogenate in order that samples could then be normalised to all contain 2 µg of protein/µl.

2.6.2 Sample Preparation

Samples were made up from protein, homogenising buffer and Laemmli SDS Buffer (3.78 g (30%) glycerol, 2.6 mL 0.625 M Tris buffer, 3 mL 20 % sodium dodecyl sulphate, 0.5 mL 0.5 % bromophenol blue, 0.12 ml deionised water, 100 µl of β-mercaptoethanol per 900 µl of sample buffer). Finally samples were heated to 95 ºC for 4 minutes.

2.6.3 Western Blotting

Proteins were then loaded (35 µl) and separated in a Tris-HCl Polyacrylamide Gel (Biorad, Hertfordshire, UK) applying a 40 mA current for approximately 90 minutes. Proteins were then transferred for approximately 2 hours at a 350 mA current to a polyvinylidene fluoride (PVDF) membrane. The membrane was blocked in 5 % skimmed milk powder (Cell Signalling, New England Biolabs, Hertfordshire, UK) for 1 hour at room temperature and following three 10 minute washes in TBST (TBS in 1 % tween) the membrane was then incubated overnight at 4 °C in appropriately targeted primary antibodies at a dilution of 1:1000 . Following three 10 minute washes in TBST, membranes were then incubated for 1 hour with an appropriately targeted horseradish peroxidase linked secondary antibody. The membrane was then washed twice in TBST (each for 10 minutes) followed by one 10 minute wash in TBS. The signal was developed using Super signal West Dura chemiluminescent substrate (Pierce Scientific, Northumberland, UK) which was applied for 5 minutes. The membrane was dried and wrapped in cling film and then encased inside a developer with blue X-ray film and exposed for as long as necessary (usually 2 - 5 minutes). The X-ray film was

then developed in photographic developer (1:25), rinsed in water and then fixed (photographic fixer, 1:25) (Jessops, UK).

2.7 Acknowledgements

Colleagues at AstraZeneca (particularly Dr. Brendan Leighton) provided invaluable advice regarding validation of antibodies.

Dr. Melissa Grant also provided expert knowledge and advice for the progression of this work.

CHAPTER 3

GLYCEROL-3-PHOSPHATE ACYLTRANSFERASE EXHIBITS FIBRE TYPE SPECIFICITY IN HUMAN SKELETAL MUSCLE

3.1 Abstract

Intramuscular triglycerides (IMTG) accumulate in skeletal muscle as discrete lipid droplets that are in close proximity to the mitochondria. The key enzymes in IMTG synthesis are glycerol-3-phosphate acyltransferase (GPAT) (which exists in a mitochondrial (GPAT1) and a microsomal (GPAT4) isoform) and diacylglycerol acyltransferase 1. These enzymes catalyse acylations that consume the fatty acid (FA) metabolites that may lead to insulin resistance. The aim of the present study was to develop methods that allow the investigation of the spatial and fibre type distribution of the enzymes involved in the first catalytic stage of IMTG synthesis, GPAT1 and GPAT4, in human skeletal muscle. Percutaneous biopsies were obtained from the *m. vastus lateralis* of six lean, healthy males. Cryosections (5 µm) were stained using either rabbit anti-GPAT1 or rabbit anti-GPAT4 antibodies, each in combination with mouse anti-myosin heavy chain type I. IMTG were stained using the neutral lipid dye oil red O and images were viewed using widefield and confocal fluorescence microscopy. A strong GPAT1 signal was present in type I fibres, while GPAT1 staining was almost absent in type II fibres ($P < 0.001$). GPAT4 staining showed a diffuse signal throughout all fibres, however still with a stronger signal in type I compared to type II fibres ($P < 0.002$). These results demonstrate that type I fibres have a higher content of the enzymes involved in the first step of IMTG synthesis than type II fibres, which is in line with the observation that type I fibres contain more IMTG whilst being more insulin sensitive. The low content of GPAT1 in type II fibres despite the presence of IMTG suggests that GPAT4 may be responsible for the first step of IMTG synthesis in type II fibres.

3.2 Introduction

Lipid droplets are made up of a central core of neutral lipids (mainly triacylglycerols or cholesteryl esters) surrounded by a monolayer of phospholipids and associated proteins (Martin & Parton, 2006) and are present in numerous cell types. They are involved in many cellular processes including energy storage and lipid homeostasis. The accumulation and dysfunctional regulation of this lipid store in skeletal muscle is thought to play a role in the development of metabolic diseases such as type 2 diabetes (He *et al.*, 2001;Taskinen, 2003). It has been proposed that the inflexibility of this intramuscular triglyceride (IMTG) pool (reduced rates of fatty acid (FA) incorporation into IMTG and reduced FA oxidation) in sedentary obese individuals results in the accumulation of FA metabolites such as long chain fatty acyl CoA (LCFACoA) (Ellis *et al.*, 2000), diacylglycerol (DAG) and ceramides (Itani *et al.*, 2000;Itani *et al.*, 2001;Itani *et al.*, 2002). These FA metabolites appear to induce insulin resistance through the activation of protein kinase C-β and θ and serine phosphorylation of insulin receptor substrate-1 which leads to the inhibition of the insulin signalling cascade (Itani *et al.*, 2002).

IMTG are synthesised via a series of sequential acylation reactions. The first step of IMTG synthesis is the acylation of glycerol-3-phosphate with LCFACoA to form lysophosphatidic acid (LPA). This step is catalysed by mitochondrial glycerol-3-phosphate acyltransferase (mtGPAT) (Gonzalez-Baro *et al.*, 2007). To date, two mtGPAT isoforms have been identified, GPAT1 and GPAT2 (Lewin *et al.*, 2004;Shin *et al.*, 1991). There are also two microsomal isoforms of GPAT (micGPAT), GPAT3 and GPAT4 (Cao *et al.*, 2006;Chen *et al.*, 2008). In the majority of body tissues studied in animals, mtGPAT makes up less than 10% of total GPAT activity and shows a preference for saturated acyl-CoAs (Coleman & Lee,

2004). However in rat skeletal muscle mtGPAT has been demonstrated to be responsible for the majority of GPAT activity (Park *et al.*, 2002). The enzymes involved in the latter stages of triglyceride synthesis are present at the endoplasmic reticulum (ER) along with micGPAT, however it has been suggested, perhaps unexpectedly, that lipid formation is initially regulated by the mitochondrial isoform (Hammond *et al.*, 2002;Coleman & Lee, 2004;Igal *et al.*, 2001).

There has been little previous research into micGPAT as its isoforms are yet to be identified and cloned, however it has been proposed that 6-acylglycerol 3-phosphate acyltransferase (AGPAT6) should be re-classified as a micGPAT isoform (GPAT4) as it was found that purified AGPAT6 demonstrated GPAT activity but surprisingly no AGPAT activity (Chen *et al.*, 2008). It has also been identified that GPAT3 has 80 % gene sequence identity with the acyltransferase domain of AGPAT6 (Cao *et al.*, 2006) and also is closely related to GPAT4 (Gimeno & Cao, 2008). Overexpression of AGPAT6 increased LPA levels in HEK293 cells suggesting that AGPAT6 plays a role in the acylation of glycerol-3-phosphate (Chen *et al.*, 2008). Furthermore, COS-7 cells overexpressing AGPAT6 were found to have increased GPAT specific activity in the absence of an increase of AGPAT specific activity (Nagle *et al.*, 2008). This provides further support that AGPAT6 should be reclassified as an isoform of GPAT.

It has recently been reported that an increase in IMTG synthesis resulting from an increased content of GPAT1 (and another IMTG synthetic enzyme, diacylglycerol acyltransferase) occurs one day following a single bout of endurance exercise in untrained women and prevents insulin resistance induced by a lipid and heparin infusion by reducing the content of

the FA metabolites which lead to insulin resistance (Schenk *et al.*, 2005;Schenk & Horowitz, 2007;Newsom *et al.*, 2010). Thus it is possible that a high protein expression of GPAT1 and possibly GPAT4 plays a protective role in the development of insulin resistance. As there is currently little research (Schenk & Horowitz, 2007;Newsom *et al.*, 2010) into these enzymes in human skeletal muscle, the aim of the present study was to investigate the subcellular and fibre type distribution of GPAT1 and GPAT4 in skeletal muscle of healthy, male individuals.

3.3 Methods

Muscle Samples

Percutaneous muscle biopsies were obtained from the *m. vastus lateralis* of six lean, healthy male subjects using the needle biopsy technique (Bergstrom, 1975) in the overnight fasted state. Subject characteristics can be seen in Table 3.1. Samples were prepared and stored as described previously in Chapter 2.2.

Table 3.1 Subject Characteristics

	Male Participants
n	6
Age (y)	31 ± 2
Height (m)	1.78 ± 0.03
Body Mass (kg)	74.3 ± 2.9
Body Mass Index (BMI) (kg/m^2)	23.4 ± 0.4

Data are presented as means ± SEM.

Antibodies

Fibre type was determined by incubating sections in mouse anti-myosin heavy chain type I (MHCI) (A4.840 DSHB, developed by Dr. Blau). This antibody was added in combination with rabbit anti-GPAT1 (kind donation of Professor Jan Oscarsson, Astra Zeneca, Mölndal, Sweden) or rabbit anti-AGPAT6 (GPAT4) (Atlas Antibodies, Stockholm, Sweden) which was used to identify micGPAT, as AGPAT6 has previously been shown to have GPAT activity (Nagle *et al.*, 2008;Chen *et al.*, 2008). Mitochondria were also visualised using mouse anti-cytochrome c oxidase (COX) (Invitrogen, Paisley, UK). Subsequently, samples were incubated with appropriately targeted secondary Alexa Fluor conjugated antibodies for 30

minutes (goat anti-mouse IgM 350 and goat anti rabbit IgG 488, Invitrogen, UK). IMTGs were stained using the neutral lipid dye oil red O in combination with immunofluorescence originally developed by Koopman *et al.,* (2001), as described previously in Chapter 2.3.1.4.

Immunofluorescence Staining

Cryosections were treated using fixation, permeabilisation and antibody application methods described in Chapter 2.4. For both GPAT1 and GPAT4, primary antibodies were used at a 1:50 dilution and incubation time was 1 hour at room temperature and secondary antibody incubation time was 30 minutes at room temperature.

Fluorescence Microscopy

Images were captured using a Nikon E600 microscope coupled to a SPOT RT KE colour 3 shot CCD camera (Diagnostic instruments Inc, MI, USA) using the excitation filters described in Chapter 2.5 to visualise Alexa Fluor 350, 488 as well as oil red O. Digital images showing the distribution of GPAT1, GPAT4, and IMTG in longitudinally oriented and cross sections of muscle fibres were obtained. Detailed digital images demonstrating the subcellular distribution of GPAT1 were obtained using an inverted confocal microscope (Leica DMIRE2, Leica Microsystems) with a 63 x oil immersion objective. Alexa Fluor 488 fluorophore was excited with a 488 nm line of the argon laser for excitation and emits at 510-555 nm. Alexa Fluor 594 and oil red O was excited with the 594 nm line of the Helium–Neon laser for excitation.

Image Processing

Images were processed using Image-Pro Plus 5.1 software (Media Cybernetics, MD, USA) and intensity thresholds were selected to represent minimum values for lipid droplets. These were kept consistent throughout all image analysis. For each image, the muscle fibre area and the area occupied by lipid droplets was measured. Lipid content was expressed as the area fraction by dividing the stained area in the fibre by the total area of that fibre. Fibre type differences in GPAT1 and GPAT4 fluorescence intensity were quantified using measures of optical density.

Antibody Validation

Antibodies were validated using Western Blotting in order to check the molecular weight of the bands stained by the antibody against GPAT1. Proteins were extracted from the skeletal muscle sample as described in Chapter 2.6.1. Proteins were then loaded (70 µg) and separated in 10 % Tris - HCl Polyacrylamide Gel (Biorad, Hertfordshire, UK) and transferred to a PVDF membrane which was then blocked in 5 % milk powder (Cell Signaling, New England Biolabs, Hertfordshire, UK) for 1 hour at room temperature. Membranes were then incubated overnight at 4 °C in polyclonal rabbit anti-GPAT1 (Prof. Jan Oscarsson, Astra Zeneca R&D, Mölndal, Sweden) which was specifically targeted against the murine amino acid sequence 312-326 (IFLEGTRSRSGKTSC). Following washing, membranes were then incubated for 1 hour at room temperature with horseradish peroxidase linked goat anti-rabbit IgG and developed using Super signal West Dura chemiluminescent substrate (Pierce Scientific, Northumberland, UK).

The reported molecular weight of GPAT1 is 90 kDa (Shin *et al.*, 1991), but initial analysis of GPAT1 extracted from human muscle homogenate and subjected to Western blot analysis revealed a band just below 50 kDa (Figure 3.1A). The basic local alignment search tool (BLAST) was used to analyse the amino acid sequence against which the GPAT1 antibody was raised. The result showed that no other human protein contained the sequence against which the antibody was raised suggesting that GPAT1 in the muscle homogenate had been broken down by proteolysis. Western blot analysis of a rat liver homogenate showed a band at the expected molecular weight for GPAT1 (Figure 3.1B). Therefore, a sample of rat liver homogenate was mixed with human muscle homogenate and incubated overnight at 4 °C before the protein extraction and Western blot analysis. On the resultant Western blot the band at 90 kDa had disappeared, again leaving only the band at ~50 kDa (Figure 3.1C). This experiment provided convincing evidence that GPAT1 was broken down by remaining proteolytic activity in the muscle homogenate from the intact 90 kDa protein to a 50 kDa fragment despite the presence of a protease inhibitor cocktail in the extraction buffer.

In addition to the Western Blotting, a protein competition assay was also used to test the specificity of anti-GPAT1. Human GPAT1 protein was kindly donated by AstraZeneca R&D (Alderley Park, Macclesfield, UK) and following 5 minutes of boiling at 95 °C, was added in excess to the anti-GPAT1 and incubated together at 4 °C for 24 hours prior to experimentation. The mixed GPAT1-antibody solution was then added in place of the primary antibody during the immunohistochemical staining procedures and this resulted in total elimination of the staining (Figure 3.2) adding further evidence of the specificity of the GPAT1 antibody.

Anti-GPAT4 which targets a specific amino acid sequence of human AGPAT6 (FAWATLRMERGAKEKNHQLYKPYTNGIIAKDPTSLEEEIKEIRRSGSSKALDNTPEFELSDIFYFCRKGMETIMDDEVTKRFSAEELESW) has previously been validated for immunohistochemistry in human skeletal muscle in the human protein atlas (HPA) (see Ponten *et al.,* (2008) for more details of the HPA). BLAST analysis showed that this sequence is present in GPAT4 and that GPAT4 is the only human skeletal muscle protein that contains this sequence.

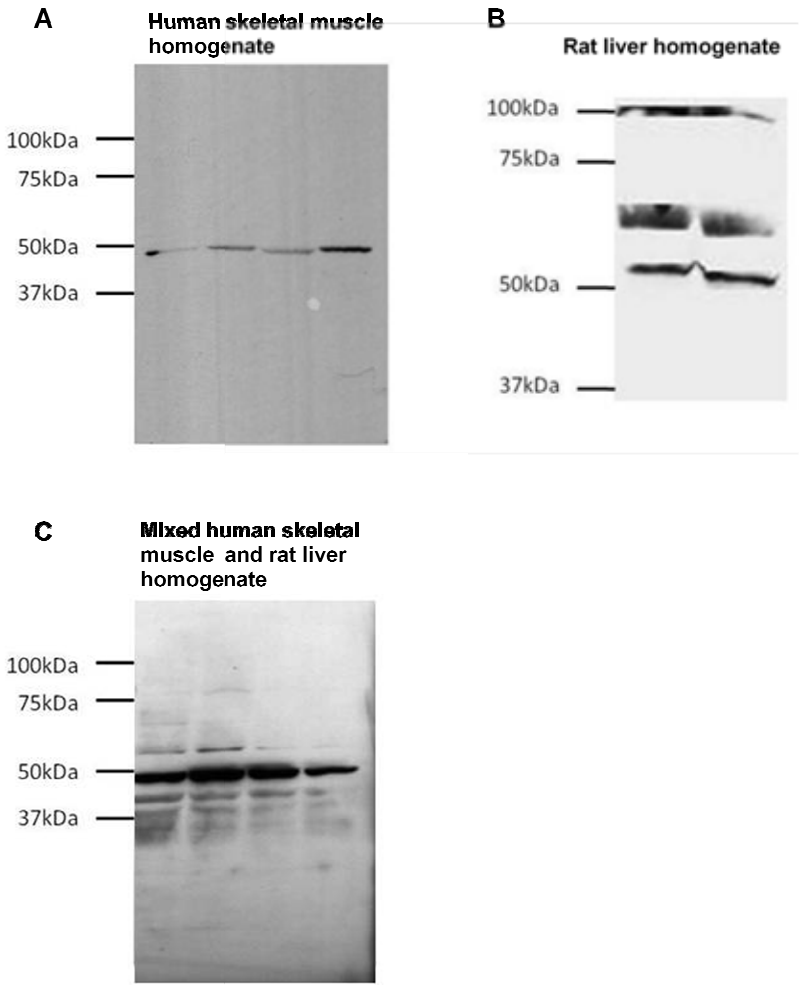

Figure 3.1. Western immunoblots demonstrating specificity of the GPAT1 antibody. A: Results generated using samples of human skeletal muscle homogenate. B: Results generated using rat liver homogenates. C: Results generated using a mixture of human skeletal muscle and rat liver homogenate.

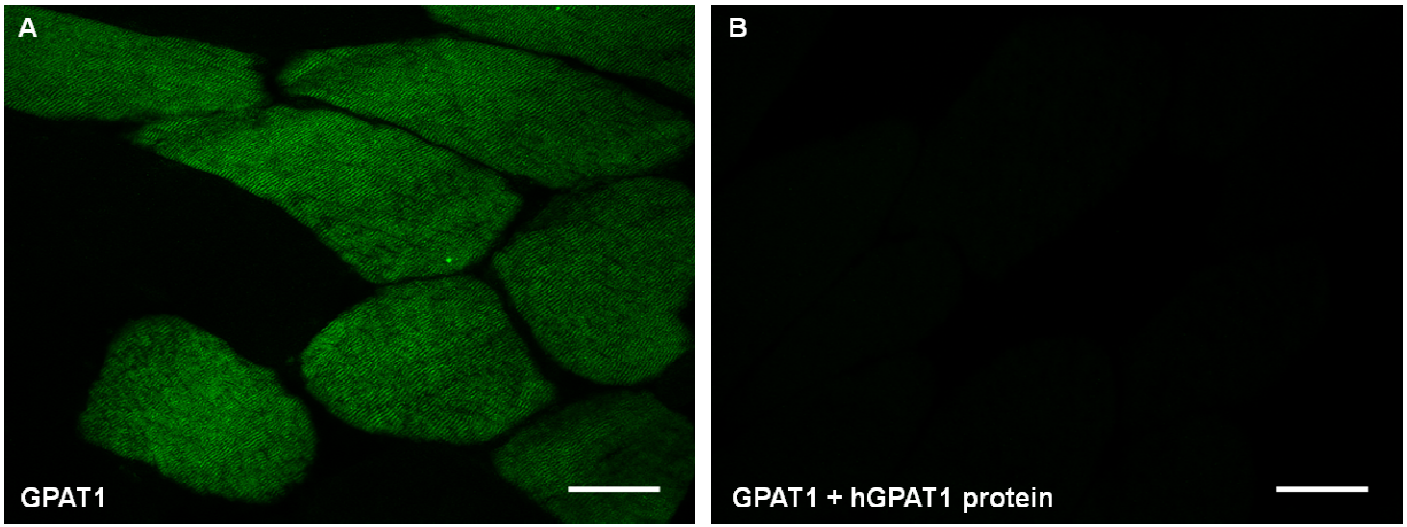

Figure 3.2. Immunofluorescence competition assay using human GPAT1 protein. Representative staining of GPAT1 in human skeletal muscle (A). Competition assay following overnight incubation of anti-GPAT1 with hGPAT1 protein (B). Note the reduction of signal in the competition assay suggesting specificity of anti-GPAT1 to human GPAT1. Bar is 50 µm.

Statistical analyses

A Student's paired samples t-test was used to investigate whether statistically significant differences existed between type I and type II fibres for the staining intensity of GPAT1 and GPAT4 and for the lipid droplet area fraction. Statistical significance was set at $P < 0.05$. All data are expressed as mean ± SEM unless otherwise stated.

3.4 Results

Representative images of human skeletal muscle using widefield immunofluorescence microscopy following incubation with rabbit anti-GPAT1, mouse anti-MHCI and oil red O staining of IMTG can be seen in Figure 3.3A. The GPAT1 staining showed a strong positive signal in type I muscle fibres and very little staining in type II fibres. The type I muscle fibres also had a stronger oil red O signal (Figure 3.3). Longitudinally oriented cryosections viewed with confocal microscopy also showed a distinct fibre type specific distribution of GPAT1 with a striated distribution pattern of GPAT1 running across the length of the muscle fibre (Figure 3.4).

Figure 3.3B shows representative images of human skeletal muscle viewed using a widefield immunofluorescence microscope following incubation with anti-GPAT4 in combination with mouse anti-MHCI and oil red O staining of IMTG. The GPAT4 staining showed a diffuse but weak signal distributed throughout all muscle fibres with no obvious fibre type difference.

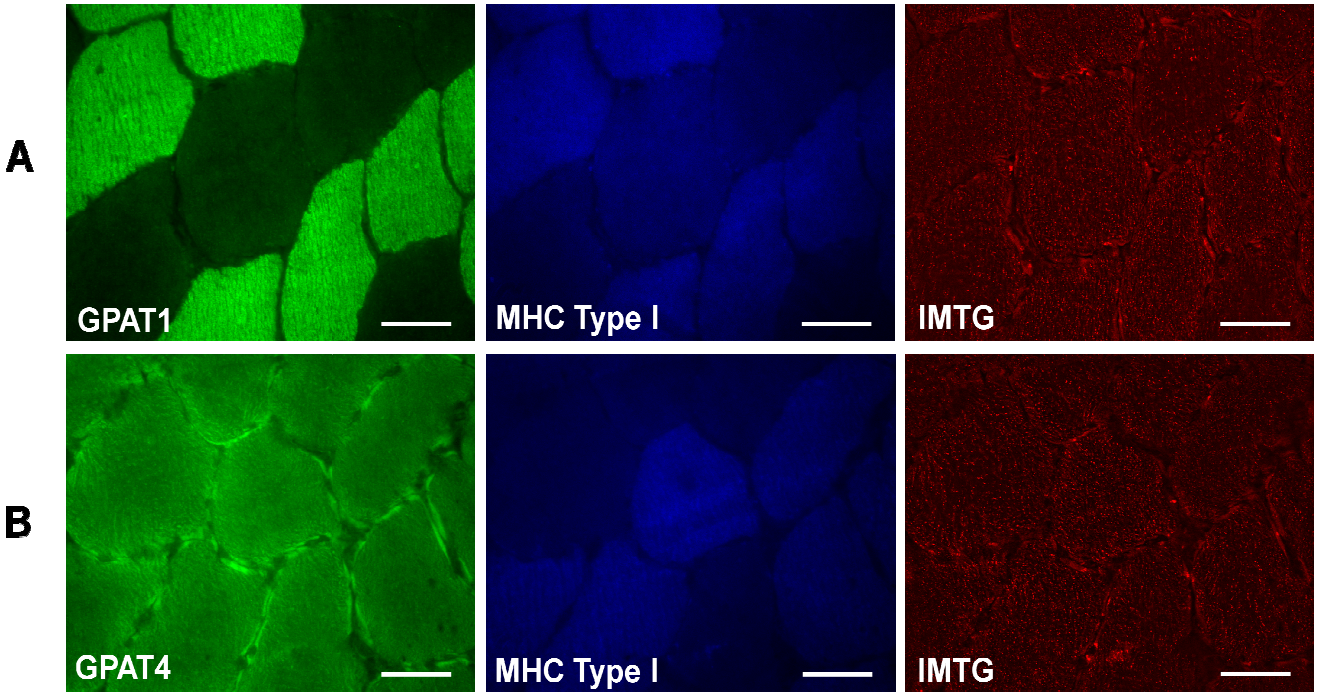

Figure 3.3. Widefield immunofluorescence microscopy images to show visualisation of GPAT1, MHCI and IMTG staining (section A). Visualisation of GPAT4, MHCI and IMTG is shown in section B. The diffuse stain of GPAT4 gives a weaker signal than that of GPAT1 and does not show an obvious fibre type difference. Bar represents 50µm.

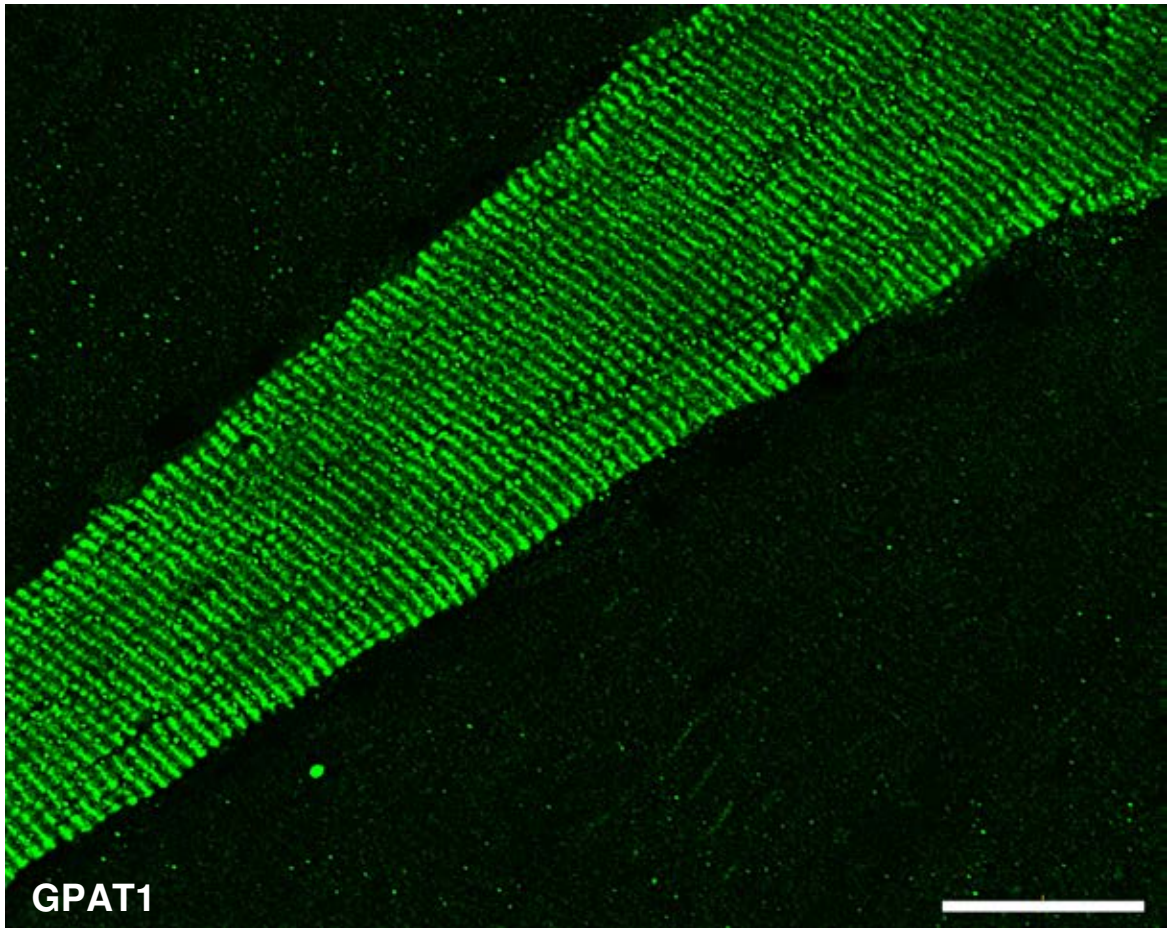

Figure 3.4. Confocal immunofluorescence microscopy to show visualisation of GPAT1 distribution in human skeletal muscle fibres. Bar represents 20µm. Note the striated spatial distribution of the stain.

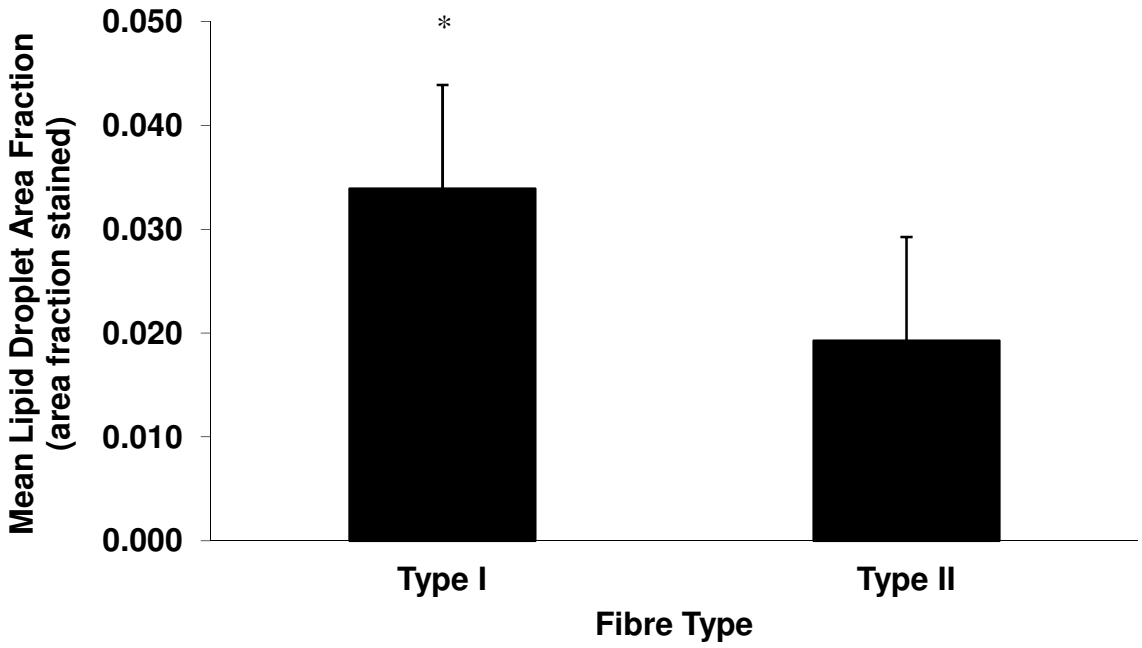

Figure 3.5. Mean lipid droplet area fraction in human skeletal muscle. Values are mean ± SEM. * Denotes significant difference between fibre type (P < 0.05).

In Figures 3.5 and 3.6 mean values of staining intensities for six subjects are presented. An ~two-fold greater IMTG content was seen in type I muscle fibres compared to type II muscle fibres (Figure 3.5) (mean lipid droplet area fraction 0.0365 ± 0.0155 vs. 0.0197 ± 0.0079, $P <$ 0.020). Figure 3.6A shows a significantly greater GPAT1 staining intensity in type I muscle fibres (mean fluorescence intensity 79 ± 10) than in type II muscle fibres (24 ± 5) ($P < 0.001$) which corresponded to the fibres with the greatest lipid content ($P < 0.020$). Figure 3.6B shows that the signal of GPAT4 was significantly more intense in type I muscle fibres than in type II muscle fibres (83 ± 7 vs. 74 ± 6) ($P < 0.002$).

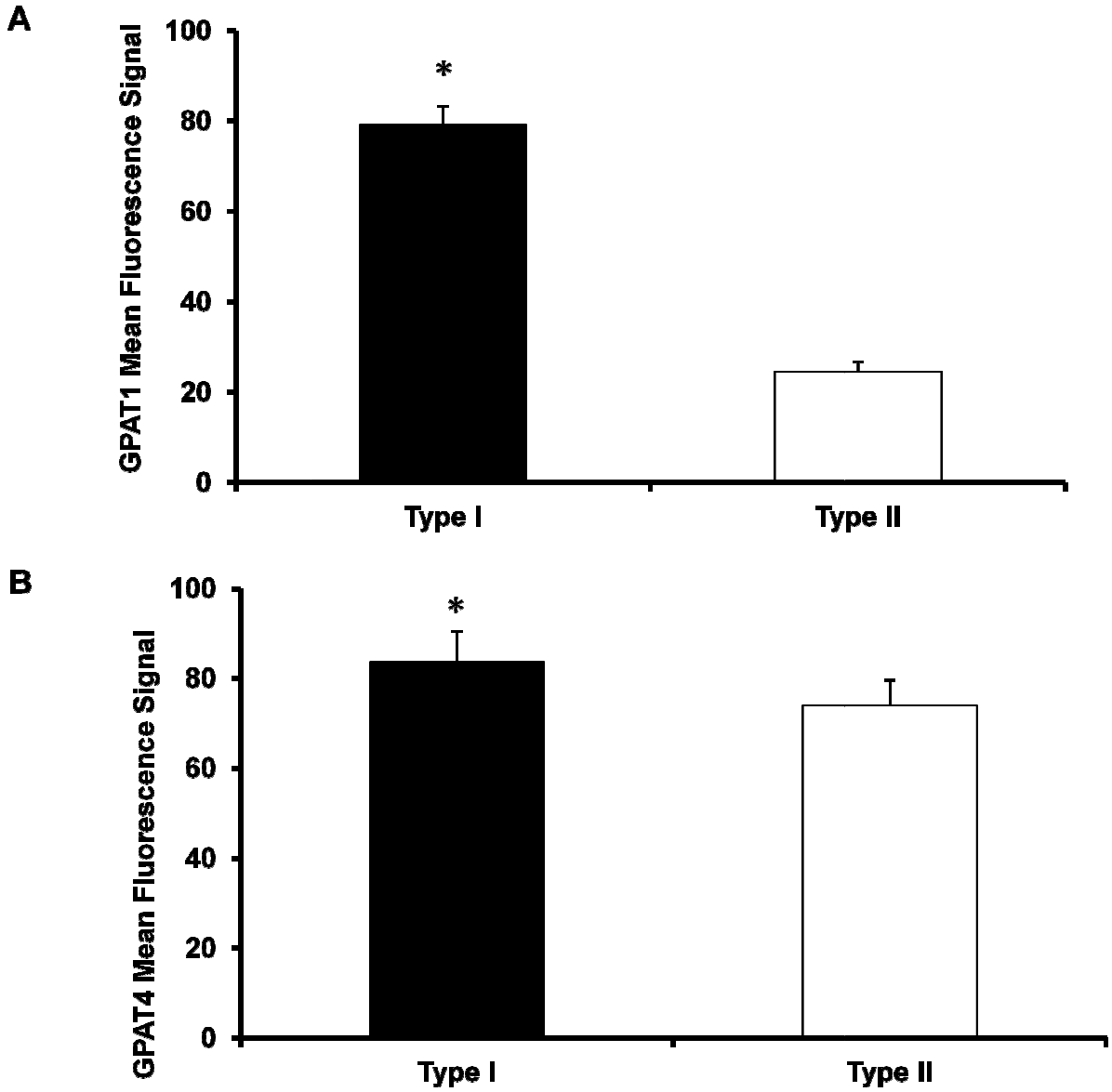

Figure 3.6. Mean fluorescence intensity measurements showing fibre type comparisons for GPAT1 (A) and GPAT4 (B) in human skeletal muscle fibres. Values are mean ± SEM. * Denotes significant difference between fibre type (P< 0.05).

Figure 3.7 shows confocal images of the subcellular distribution of GPAT1 and IMTG. It can be seen that the IMTG are distributed between the striations of the GPAT1 protein. This GPAT1 staining demonstrates the muscle fibre type specific nature of GPAT1 as the type II muscle fibre at the top of the image contains IMTG but lacks GPAT1 staining. Figure 3.8 is a representative confocal image displaying the subcellular distribution of GPAT1 and the mitochondrial network (stained using anti-COX). The image demonstrates that there is little colocalisation between GPAT1 and COX. The mitochondrial network seems to fit into the space between the striations of GPAT1.

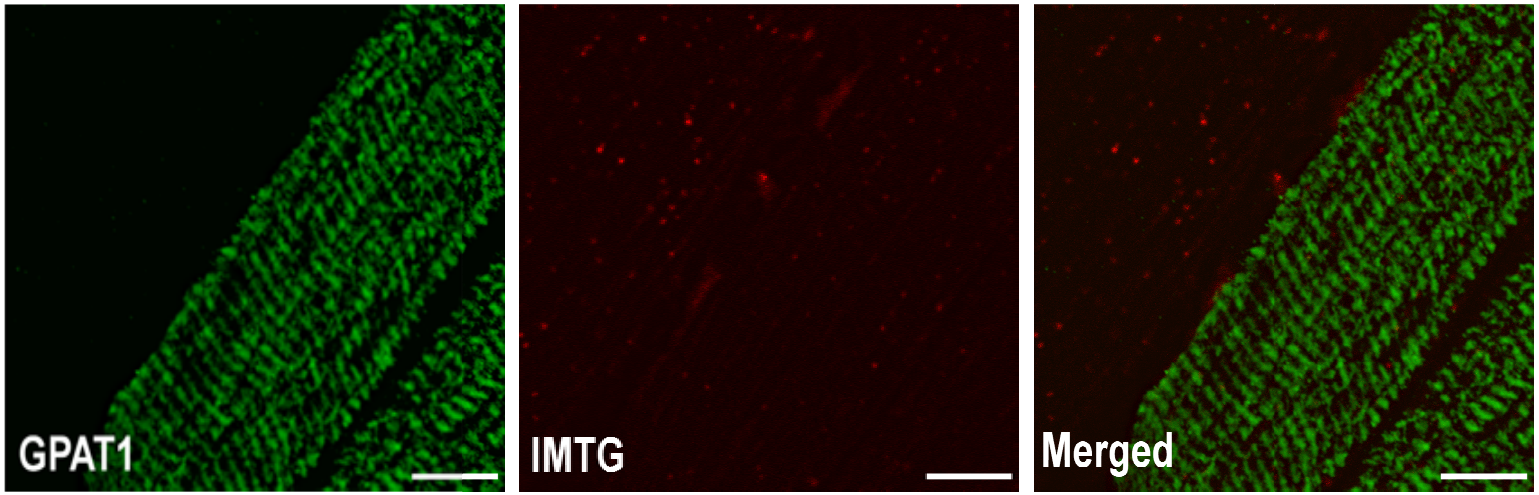

Figure 3.7. Confocal microscopy to demonstrate subcellular distribution of GPAT1 and IMTG. Bar represents 10 µm.

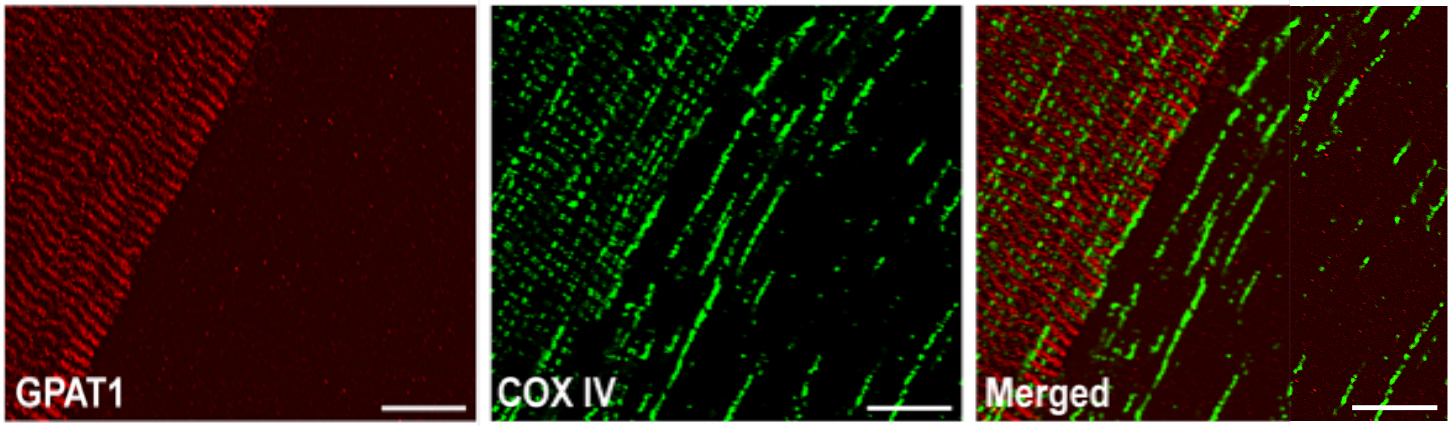

Figure 3.8. Confocal microscopy to demonstrate subcellular distribution of GPAT1 and COX. Bar represents 10 µm. Note the positioning of the mitochondria between the striations of GPAT1.

3.5 Discussion

GPAT isoforms are responsible for the initial committed step in IMTG synthesis; however, before completion of this study the subcellular distribution of these enzymes had yet to be identified in skeletal muscle. This study, therefore, aimed to visualise the subcellular and fibre type distribution of two GPAT isoforms namely GPAT1 and GPAT4. It was shown, using widefield immunofluorescence microscopy techniques, that GPAT1 and GPAT4 are each present in both type I and type II skeletal muscle fibres (to varying degrees) with both enzymes giving a greater signal in type I fibres compared to type II fibres (Figure 3.6). This is the first time that the distribution of these enzymes has been described in human skeletal muscle.

The finding that GPAT1 is highly expressed in type I muscle fibres is in line with a previous study that has demonstrated a higher GPAT1 expression (measured with Western blots) and enzyme activity in oxidative (soleus) compared to glycolytic rat muscle (extensor digitorum longus) (Lewin *et al.*, 2001). The high GPAT1 activity may also contribute to higher rates of IMTG synthesis in oxidative rat muscle (Budohoski *et al.*, 1996). Numerous previous human studies have demonstrated that type I muscle fibres have a 2-3-fold greater IMTG content than type II fibres (Malenfant *et al.*, 2001;van Loon *et al.*, 2004;Shaw *et al.*, 2008). The greater GPAT expression in type I muscle fibres is also likely to be part of the mechanism leading to a greater IMTG content in type I muscle fibres in basal conditions and higher IMTG resynthesis rates in the period following IMTG depleting exercise (van Loon *et al.*, 2003b). The most striking and perhaps unexpected finding of the present study was the distinctly weak GPAT1 signal in type II fibres (Figures 3.3A and 3.6A) despite the clear presence of IMTG in these fibres (Figure 3.3 and 3.5). The present study has also shown for

the first time that the GPAT4 protein is expressed in human skeletal muscle, with only a marginally lower protein content in type II than in type I muscle fibres. This seems to imply that GPAT4 is primarily responsible for the initial step of IMTG synthesis in type II fibres.

At rest, the majority of FAs taken up by the muscle enter esterification pathways and are incorporated into IMTGs (Sacchetti *et al.*, 2004), however during exercise the vast majority of FAs entering the muscle are oxidised and only ~ 10 % are incorporated into the IMTG pool (Sacchetti *et al.*, 2002). The apparent differences in IMTG synthetic enzyme content between muscle fibre types found in the present study could have important implications for differences between type I and type II fibres in FA handling in the postprandial period, during exercise and in the period after exercise.

In longitudinally oriented fibres stained for GPAT1, a striated pattern was seen (Figure 3.4). As it has been reported that GPAT1 is located at the outer mitochondrial membrane in rat liver mitochondria (Lewin *et al.*, 2004), GPAT1 colocalisation was investigated with COX as a marker of the mitochondrial network (Shaw et al 2008). However, no colocalisation of GPAT1 was observed with the COX stain indicating that in human skeletal muscle, in the resting fasted state, GPAT1 (also named mitochondrial GPAT) is not present in the outer mitochondrial membrane. However, the distribution in a striated pattern suggests that GPAT1 takes a regular place in the mitochondrial network and in some way is associated with the mitochondria (Figure 3.8). In rat liver it has been suggested that GPAT1 is present in part in the outer mitochondrial membrane and in part in mitochondria associated vesicles (MAVs) or membranes (MAMs) (Pellon-Maison *et al.*, 2007). The fraction in the outer mitochondrial membrane had by far the highest activity and Pellon-Maison *et al.,* (2007) therefore suggested

that a high activity in this fraction is crucial to direct LCFACoA away from carnitine palmitoyl transferase 1 (CPT1) and β-oxidation during lipid oversupply. The regular arrangement of GPAT1 in the spaces in which COX staining is absent may suggest that GPAT1 is present in ER membranes, as these have been suggested to play a role in lipid and phospholipid synthesis in several tissues (Lebiedzinska *et al.*, 2009). As there is a small amount of colocalisation of GPAT1 with some of the lipid droplets (Figure 3.7), it is tempting to speculate that GPAT1 plays a role in lipid droplet formation in skeletal muscle, thus depositing the lipid droplets at these regular positions in the gaps between the mitochondria, ready for use as a fuel by the mitochondria. This may imply that GPAT1 exerts its controlling effect on the LCFACoA concentration seen by CPT1 (and thus reducing β-oxidation) from a larger distance in skeletal muscle, or that part of GPAT1 can translocate to a position closer to the mitochondria in the fed state and during recovery from exercise when IMTG resynthesis rates are high (Sacchetti *et al.*, 2002;Sacchetti *et al.*, 2004;Summermatter *et al.*, 2010). This however is yet to be confirmed and should be addressed in future experiments.

Little is currently known about the regulation of GPAT1 and GPAT4 activity but it is likely that the subcellular location and association with related proteins and/or organelles as observed in the current study (Figure 3.8) are important. As the content/activity of GPAT isoforms will influence the concentration of the FA metabolites LCFACoA and DAG, variation in the content/activity of these enzymes may play a role in the mechanisms leading to insulin resistance and determine diabetes risk. The accumulation of these FA metabolites leads to insulin resistance through the activation of PKCβ and serine phosphorylation and inactivation of IRS1 (Itani *et al.*, 2002).

In summary, this study has revealed, for the first time, the subcellular and fibre type distribution of GPAT1 and GPAT4. Future studies comparing IMTG synthetic capacity and GPAT1 and DGAT1 distribution in lean, obese and obese type 2 diabetic subjects are warranted and may provide new information on the role of these enzymes in the control of FA metabolites that play a role in the development of insulin resistance in skeletal muscle.

3.6 Acknowledgements

We thank Professor Jan Oscarsson for donating the GPAT1 antibody and human GPAT1 protein and also providing expert advice on generating evidence of the specificity of the used antibodies to include the BLAST analysis.

The myosin heavy chain type I (A4.480) antibody developed by Dr. H.M. Blau was obtained from the Developmental Studies Hybridoma Bank developed under the auspices of the NICHD and maintained by The University of Iowa, Department of Biology, Iowa City, IA 52242

CHAPTER 4

SUBCELLULAR DISTRIBUTION AND FIBRE TYPE DIFFERENCES IN PROTEIN CONTENT OF DIACYLGLYCEROL ACYLTRANSFERASE-1 IN HUMAN SKELETAL MUSCLE

4.1 Abstract

Intramuscular triglycerides (IMTG) accumulate in skeletal muscle as discrete lipid droplets that are in close proximity to the mitochondria. The key enzymes in IMTG synthesis are glycerol-3-phosphate acyltransferase (GPAT) and diacylglycerol acyltransferase 1 (DGAT1). DGAT1 catalyses an acylation reaction that consumes the fatty acid metabolites diacylglycerol and long-chain fatty acyl-CoA, which both lead to insulin resistance. The aim of the present study was to develop methods that allow the investigation of the spatial and fibre type distribution of DGAT1 in human skeletal muscle. Percutaneous biopsies were obtained from the *m. vastus lateralis* of six lean, moderately active males at rest and following an overnight fast. Cryosections (5 µm) were stained using goat anti-DGAT1 in combination with mouse anti-myosin heavy chain type I. Mitochondria were stained using mouse anti-cytochrome c oxidase and IMTGs were stained using the neutral lipid dye oil red O. The stained sections were viewed using widefield and confocal microscopy. DGAT1 staining revealed a diffuse staining distribution within the fibres with some areas seemingly having more organised distribution. There were brighter spots visible throughout the diffuse staining in cross sections, and in longitudinally oriented sections striations were visible in the staining distribution. DGAT1 staining also showed a greater staining intensity in type I fibres ($P < 0.05$). IMTG staining revealed a greater IMTG content (expressed as area fraction stained) in type I compared to type II fibres ($P < 0.05$). Mitochondrial staining also showed a greater intensity in type I compared to type II fibres. The results of the present study show that DGAT1, the enzyme responsible for the final step of IMTG synthesis, has a higher protein content in type I than in type II fibres.

4.2 Introduction

Intramuscular triglycerides (IMTG) are synthesised via a series of sequential acylation reactions. Diacylglycerol acyltransferase 1 (DGAT1) catalyses the final step of IMTG synthesis (Choi *et al.*, 2007) which is the acylation of DAG with LCFACoA. In this role, DGAT1 can increase IMTG synthesis and reduce DAG and LCFACoA (Bagnato & Igal, 2003). Two DGAT isoforms are known to exist, DGAT1 and DGAT2 (Cases *et al.*, 1998;Cases *et al.*, 2001). It has recently been reported that an increase in IMTG synthesis resulting from increased content of DGAT1 (and the enzyme responsible for the first step of IMTG synthesis, glycerol-3-phosphate acyltransferase 1, GPAT1) occurs the day following a single bout of endurance exercise and prevents insulin resistance induced by infusion of lipid and heparin in healthy untrained women by reducing the content of the FA metabolites which lead to insulin resistance (Schenk *et al.*, 2005;Schenk & Horowitz, 2007;Newsom *et al.*, 2010). A 70% increase in muscle DGAT1 activity was also shown in a group of exercise trained mice (6 swimming sessions per day for one week) which coincided with an increased IMTG synthesis rate. Furthermore, overexpression of DGAT1 in skeletal muscle of a transgenic mouse model led to an acute protection against insulin resistance induced by switching to a high fat diet (Liu *et al.*, 2007). More recently, it has been shown that mice overexpressing DGAT1 in skeletal muscle are protected against skeletal muscle lipotoxicity via a mechanism involving both increases in triacylglycerol synthesis and FA oxidation (Liu *et al.*, 2009b)

DGAT1, therefore, may play an important role in the control of the concentration of FA metabolites in skeletal muscle and thus offer protection against insulin resistance. As there is currently little research (Schenk & Horowitz, 2007;Newsom *et al.,* 2010) into DGAT1 in

human skeletal muscle, the aim of the present study was to investigate the fibre type specific distribution of DGAT1 in human skeletal muscle obtained from lean, moderately active and healthy individuals.

4.3 Methods

Measurement of VO_{2max}

Subjects performed a progressive exercise test to exhaustion on an electronically braked cycle ergometer (Lode BV, Groningen, The Netherlands) in order to determine maximal oxygen consumption (VO_{2max}) using an online gas collection system (Oxycon Pro, Jaeger, Wuerzburg, Germany). The test consisted of initially cycling at 95 W, followed by sequential increments of 35 W every 3 minutes until cadence was reduced to < 50 rpm, at which point the test was terminated. VO_{2max} was taken as the highest value obtained in the last 30-seconds of the test.

Muscle Samples

Percutaneous muscle biopsies were obtained from the *m. vastus lateralis* of six lean, moderately active male subjects using the needle biopsy technique (Bergstrom, 1975). Subject characteristics can be seen in Table 4.1. Samples were prepared and stored as described previously in Chapter 2.2.

Table 4.1 Subject Characteristics

	Lean Male Participants
n	**6**
Age (y)	**20 ± 1**
Height (m)	**1.79 ± 0.03**
Body Mass (kg)	**72.0 ± 2.8**
Body Mass Index (BMI) (kg/m^2)	**22.4 ± 0.4**
VO_2 max (ml/min/kg)	**55.8 ± 1.8**
Wmax (W)	**282.0 ± 17.0**

Data are presented as means ± SEM.

Antibodies

DGAT1 was identified using goat anti-DGAT1 (Abcam, UK). This was used in combination with mouse anti-myosin heavy chain type I (MHCI) (A4.840 DSHB, developed by Dr. Blau) to investigate fibre type distribution. The secondary antibodies used in this case were donkey anti goat IgG (targeting DGAT1) and donkey anti mouse IgM (targeting MHCI). Mouse anti-cytochrome c oxidase (COX) (Invitrogen, Paisley, UK) was also used to visualise mitochondria. This stain was combined with MHCI. The secondary antibodies applied were goat anti mouse IgG_{2a} (targeting COX) and goat anti mouse IgM (targeting MHCI). Cell borders were marked using wheat germ agglutinin (WGA) (Invitrogen, Paisley, UK). IMTGs were stained using the neutral lipid dye oil red O in combination with immunofluorescence developed by Koopman *et al.,* (2001) as described previously in Chapter 2.3.1.4.

Immunofluorescence Staining

Cryosections were treated using fixation, permeabilisation and antibody application methods described in Chapter 2.4. For immunofluorescence staining anti-DGAT1 was used at a dilution of 1:50.

Fluorescence Microscopy

Images were captured using a Nikon E600 microscope coupled to a SPOT RT KE colour 3 shot CCD camera (Diagnostic instruments Inc, MI, USA) using the excitation filters described in Chapter 2.5 to visualise Alexa Fluor 350, 488 as well as oil red O. Digital images showing the distribution of DGAT1 and IMTG in longitudinally oriented and cross sections of muscle fibres were obtained. Detailed digital images demonstrating the cellular distribution of DGAT1 were obtained using an inverted confocal microscope (Leica DMIRE2, Leica

Microsystems) with a 63 x oil immersion objective. The excitation and emission wavelengths of each Alexa Fluor dye can be found in Chapter 2.5.

Image Processing

Images were processed using Image-Pro Plus 5.1 software (Media Cybernetics, MD, USA). A mean of 200 type I fibres and 164 type II fibres were analysed per participant. Fibre type differences in DGAT1 fluorescence intensity were quantified using measures of optical density using the WGA outline to mark the individual cells.

Automated Image Capture and Analysis

The routine analysis of IMTG and mitochondria was completed using automated image analysis as described in Chapter 2.5.2. In the widefield images obtained using automated analysis a mean of 684 type I fibres were analysed and a mean of 740 type II fibres were analysed per participant.

Antibody Validation

Antibodies were validated using Western Blotting in order to check the molecular weight of the bands stained by the antibody against DGAT1. The total protein fraction of the skeletal muscle sample was isolated as described in Chapter 2.6.1. Proteins were then loaded (50 µg) and separated in 10 % Tris - HCl Polyacrylamide Gel (Biorad, Hertfordshire, UK) and transferred to a PVDF membrane which was then blocked in 5 % bovine serum albumin (BSA) (Sigma Aldrich, UK) in TBST for 1 hour at room temperature. Membranes were then incubated for 2 hours at room temperature in polyclonal goat anti-DGAT1 (Abcam, Cambridge, UK) which is specifically targeted against amino acids 305-317 of human

DGAT1. Following washing, membranes were then incubated for 1 hour at room temperature with horseradish peroxidase linked donkey anti-goat IgG and developed using Super signal West Dura chemiluminescent substrate (Pierce Scientific, Northumberland, UK).

Western blot analysis completed using anti-DGAT1 revealed a dense band at ~50 kDa (Figure 4.1). The expected molecular weight of DGAT1 is 47 kDa. BLAST analysis for anti-DGAT1 returned a single 100 % sequence identity match to human DGAT1.

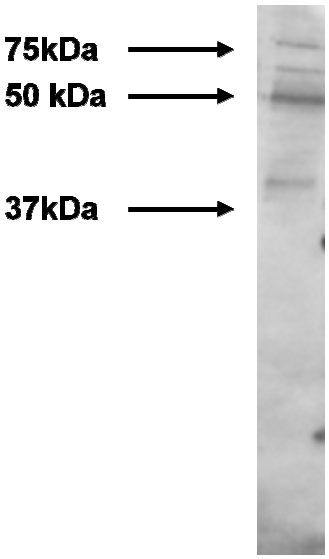

Figure 4.1. Western blot of an extract of a human skeletal muscle homogenate to determine the specificity of anti-DGAT1. The expected molecular weight of DGAT1 is 47 kDa. A dense band was seen at ~ 50 kDa.

In addition to the Western Blotting, a protein competition assay was also used to test the specificity of anti-DGAT1. Human DGAT1 protein was kindly donated by AstraZeneca R&D (Alderley Park, Macclesfield, UK) and was added in excess of the anti-DGAT1 and incubated together at 4 °C for 24 hours prior to immunohistochemical staining. The mixed DGAT1-antibody solution was then added in place of the primary antibody alone during the immunohistochemical staining procedures and this resulted in total elimination of the staining (Figure 4.2) adding further evidence of the specificity of the DGAT1 antibody.

Statistical analyses

In order to investigate fibre type differences in DGAT1 signal in type I and type II muscle fibres, a Student's paired samples t-test was undertaken on the fluorescence intensity analysis. Furthermore the lipid droplet area fraction and mitochondria content for both type I and type II fibres was also compared using a Student's paired samples t-test. Statistical significance was set at $P < 0.05$. All data are expressed as mean ± SEM.

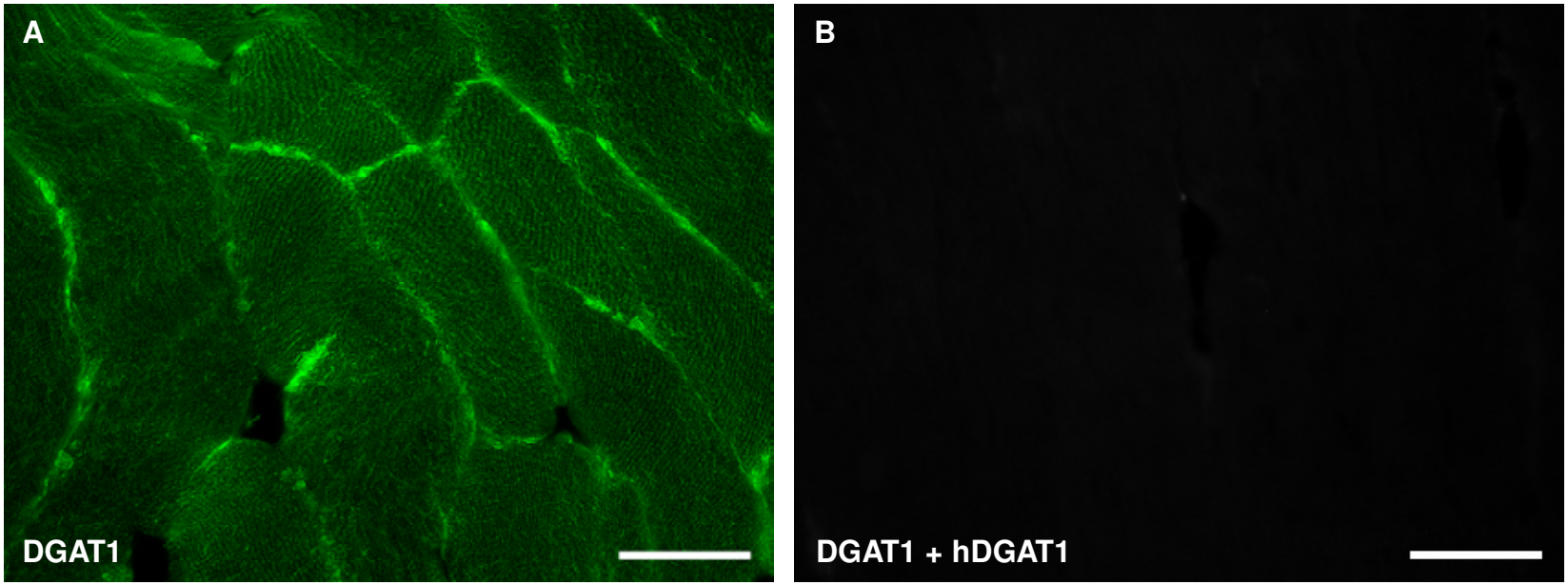

Figure 4.2. Immunostaining competition assay to generate evidence of the specificity of anti--DGAT1. Panel A shows anti-DGAT1 staining in human skeletal muscle. The image of Panel B was generated using exactly the same procedure except anti-DGAT1 was preincubated with human DGAT1 protein for 24 h prior to being used for immunostaining. Bar is 50 µm.

4.4 Results

DGAT1 staining revealed a diffuse staining distribution within the fibres with some areas showing a more specific distribution with brighter punctate staining within the diffuse intracellular staining. There was also intense staining in some peripheral areas of the cells (Figure 4.3A and 4.4A). There were brighter spots visible throughout the diffuse staining in cross sections (Figure 4.3A) and in longitudinally oriented sections striations were visible in the staining distribution (Figure 4.4A). When combined with a MHCI stain, it was found that the positively stained MHCI cells corresponded to the brighter DGAT1 stained fibres (Figure 4.3 and 4.4). Quantifying the images obtained from all the participants in this study, DGAT1 staining was, on average, 17 % more intense in type I fibres (66 ± 4) than in type II fibres (56 ± 3) ($P < 0.05$) (Figure 4.5).

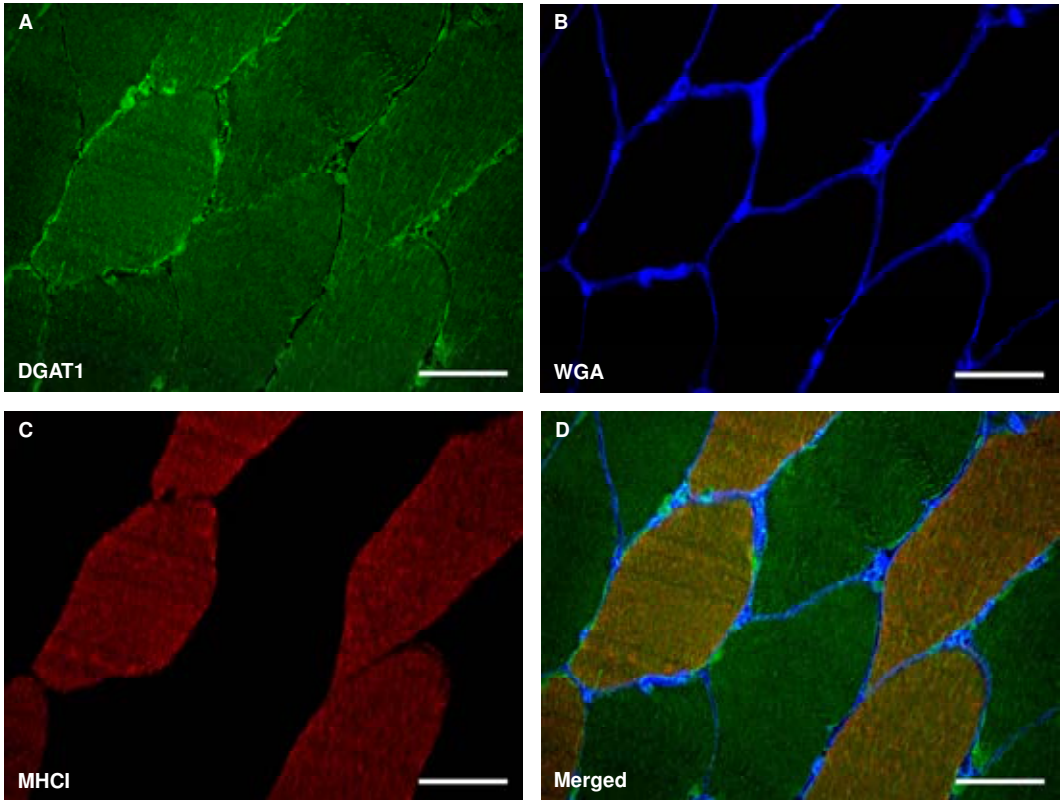

Figure 4.3. Widefield fluorescence microscopy of cross sections of human skeletal muscle showing anti-DGAT1 staining (panel A), cell borders stained in blue using WGA (panel B), type I fibres positively stained in red with anti-MHCI (panel C), and the merged image (panel D). Bar represents 50 µm.

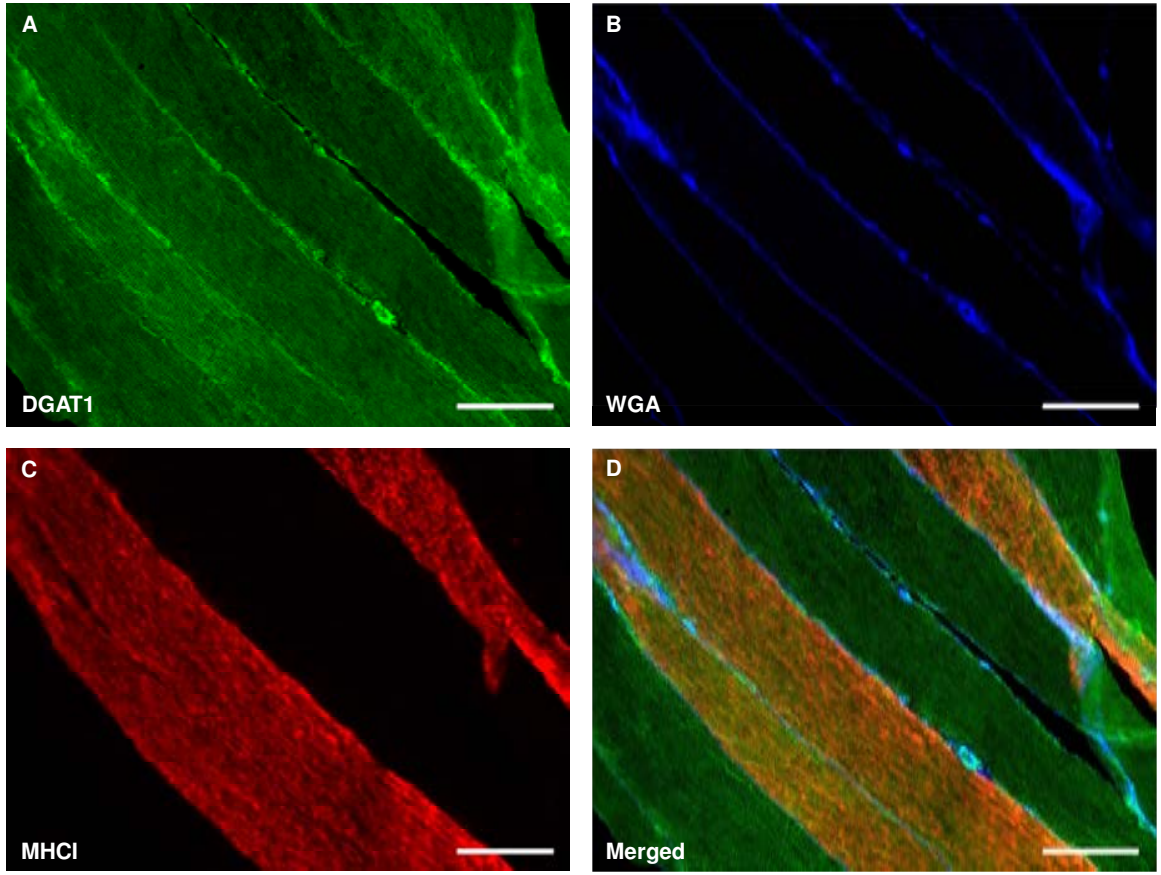

Figure 4.4. Widefield fluorescence microscopy of longitudinally oriented sections of human skeletal muscle showing anti-DGAT1 staining (panel A), cell borders stained in blue using WGA (panel B), type I fibres positively stained in red with anti-MHCI (panel C), and the merged image (panel D). Bar represents 50 µm.

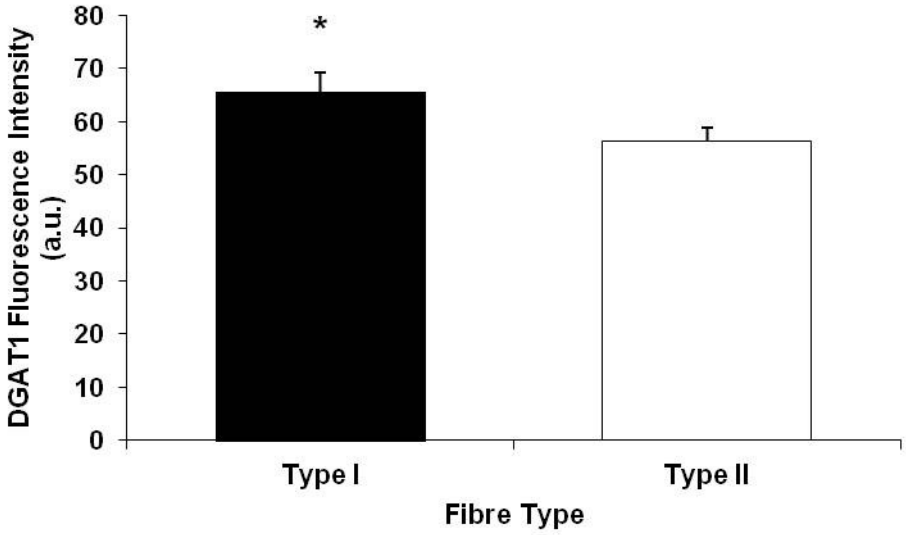

Figure 4.5. Fibre type specific distribution of DGAT1 in human skeletal muscle. Data are mean ± SEM. * Denotes significant difference between fibre types at P < 0.05.

Oil red O staining of IMTG showed the expected spotted distribution throughout the fibres (Figure 4.6A) and the automated analysis revealed that there was a significantly greater IMTG content (expressed as area fraction stained) in type I fibres (0.023 ± 0.002) compared to type II fibres (0.016 ± 0.002) ($P = 0.004$) (Figure 4.6B). These data are in line with data previously observed in our laboratory in a smaller number of cells using the traditional method of analysis (Shaw *et al.*, 2008).

The automated analysis of the mitochondrial staining using anti-COX also showed a distribution similar to that shown elsewhere in this thesis (Chapter 3, Chapter 7, Chapter 8) as well as in work previously published by our laboratory (Shaw *et al.*, 2008). In cross sections, the mitochondrial distribution was spotted in appearance with a greater density in the number of these spots towards the peripheral areas of the cells (Figure 4.7A). In longitudinally oriented sections, the distribution of COX staining appeared to show a network like distribution as previously observed by Shaw *et al.,* (2008), again with the greatest staining density in peripheral regions of the cell (Figure 4.7B). The staining intensity was greater in type I fibres (147 ± 7) compared to type II fibres (136 ± 7) *(*$P = 0.035$*)* (Figure 4.7C).

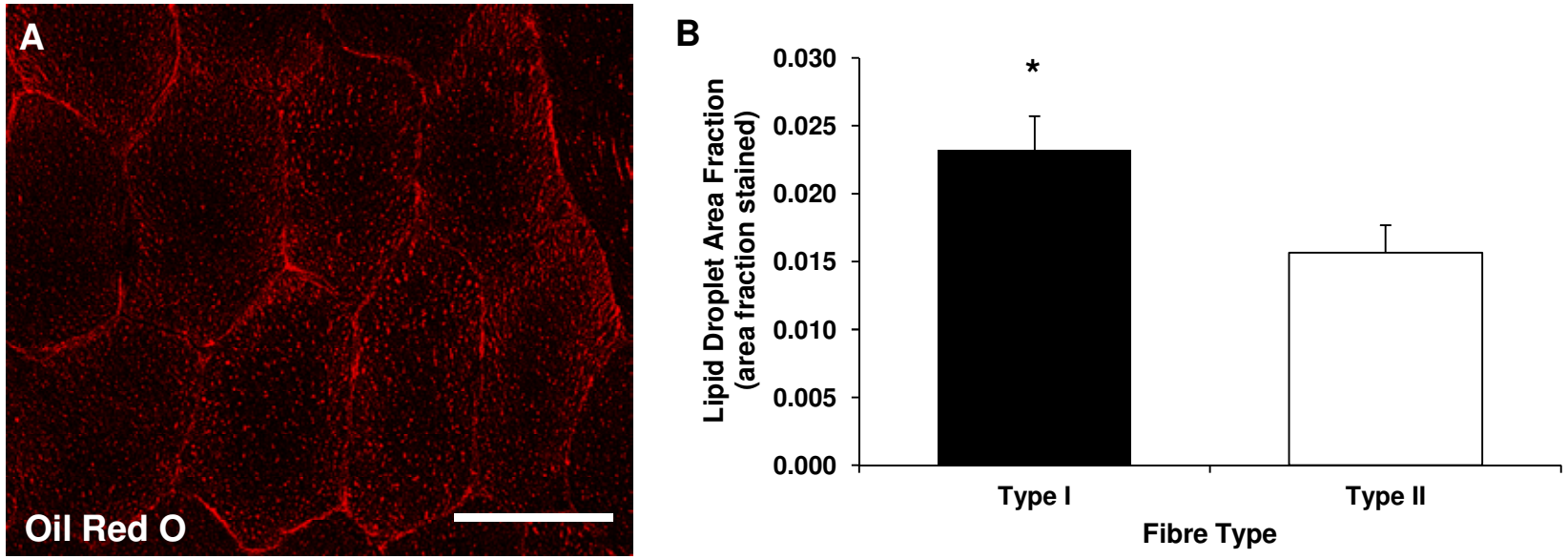

Figure 4.6. IMTG staining of human skeletal muscle using oil red O (A). Bar is 30 µm. Panel B shows graph of IMTG content (expressed as area fraction stained) in type I and type II fibres as obtained through the automated analysis. Data are mean ± SEM of 6 individuals. * Denotes significant difference between fibre types at P < 0.05.

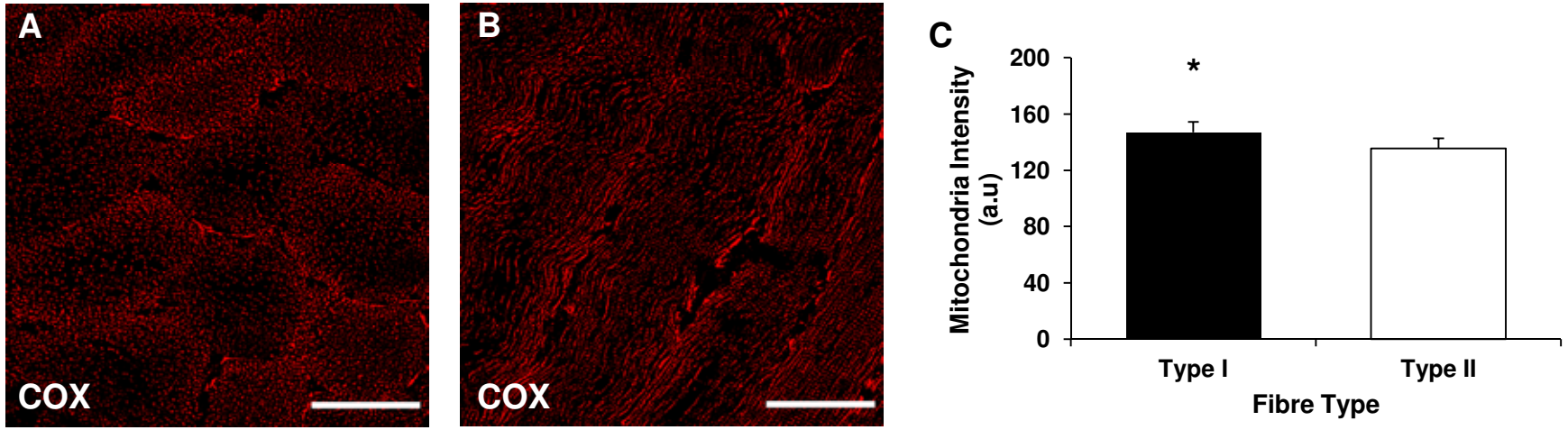

*Figure 4.7. Mitochondrial staining using anti-COX in cross sections (A) and longitudinally oriented sections (B) of human skeletal muscle using immunofluorescence microscopy. Bar is 30 µm. Panel C shows graph of mitochondrial staining intensity in type I and type II fibres obtained using the automated analysis. Data are mean ± SEM of six individuals. * Denotes significant difference between fibre types at P < 0.05.*

4.5 Discussion

DGAT1 is known to be responsible for the final step of IMTG synthesis; however the distribution of this enzyme had yet to be identified in human skeletal muscle at the start of this study. The results show that DGAT1 is present in both type I and type II skeletal muscle fibres with a 17 % greater signal in type I fibres compared to type II fibres (Figures 4.3, 4.4 and 4.5). These findings suggest that the higher DGAT1 protein content may contribute to the greater IMTG content of type I fibres in humans (Figure 4.6B) (Malenfant *et al.*, 2001;van Loon *et al.*, 2004) and to the higher IMTG synthesis rates in type I than in type II fibres of rats (Budohoski *et al.*, 1996).

In summary, the findings of this study show for the first time the subcellular and fibre type distribution of DGAT1. Future studies comparing IMTG synthetic capacity and GPAT1 and DGAT1 distribution in lean, obese and obese type 2 diabetic subjects are warranted and may provide new information on the role of these enzymes in the control of FA metabolites that play a role in the development of insulin resistance in skeletal muscle.

4.6 Acknowledgements

The myosin heavy chain type I (A4.480) antibody developed by Dr. H.M. Blau was obtained from the Developmental Studies Hybridoma Bank developed under the auspices of the NICHD and maintained by The University of Iowa, Department of Biology, Iowa City, IA 52242.

CHAPTER 5

GPAT AND DGAT DISTRIBUTION IN AGEING NON OBESE AND OBESE FEMALES

5.1 Abstract

The content and activity of the enzymes glycerol-3-phosphate acyltransferase 1 (GPAT1) and diacylglycerol acyltransferase 1 (DGAT1) could mediate the concentration of fatty acid (FA) metabolites and therefore muscle insulin sensitivity. The subcellular localisation of these enzymes could influence their activity, yet no studies in human skeletal muscle have investigated this. The aim of the present study was to investigate the distribution of GPAT1 and DGAT1 in skeletal muscle of six non obese and six obese ageing women. Biopsies were taken from the *m. gluteus maximus* during elective orthopaedic surgery under general anaesthesia. Cryosections (5 µm) were immunolabelled with antibodies against GPAT1 and DGAT1. Fibre type was determined through the use of anti-myosin heavy chain type I and mitochondria were labelled using anti-cytochrome c oxidase. Intramuscular triglycerides (IMTG) were stained using the neutral lipid dye oil red O in combination with immunofluorescence. There was no difference in IMTG content, mitochondria area fraction or mitochondria intensity between the non obese and obese individuals for either muscle fibre type. GPAT1 did not colocalise with IMTG in either group (non obese: $r = 0.09 \pm 0.02$; obese: $r = 0.08 \pm 0.02$) and mitochondria showed only a weak colocalisation with GPAT1 in both groups (non obese: $r = 0.12 \pm 0.02$; obese: $r = 0.10 \pm 0.02$). This study visualised the subcellular distribution of GPAT1 and DGAT1 for the first time in human skeletal muscle of obese females and did not observe differences in the distribution of these enzymes between non obese and obese women.

5.2 Introduction

Glycerol-3-phosphate acyltransferase 1 (GPAT1) catalyses the conversion of glycerol-3-phosphate and long-chain fatty acyl-coenzyme A (LCFACoA) into lysophosphatidic acid. Diacylglycerol acyltransferase 1 (DGAT1) catalyses the conversion of LCFACoA and diacylglycerol (DAG) into TAG. Both reactions, therefore, consume fatty acid (FA) metabolites that have been proposed to lead to insulin resistance in skeletal muscle (Ellis *et al.*, 2000;Itani *et al.*, 2002). It can, therefore, be expected that a high content of these enzymes will protect against insulin resistance, while a low content might contribute to insulin resistance. To test this hypothesis a number of animal studies have investigated the effect of gain or loss of function of these enzymes on insulin action in skeletal muscle.

Transgenic overexpression of DGAT1 in mouse skeletal muscle increased the IMTG content reduced the DAG content and protected the mice against high-fat diet-induced insulin resistance (Liu *et al.*, 2007). Moreover, in isolated muscle, DGAT1 deficiency exacerbated insulin resistance caused by FA, whereas DGAT1 overexpression mitigated the detrimental effect of fatty acids (Liu *et al.*, 2007). In a subsequent study (Liu *et al.*, 2009b) transgenic overexpression of DGAT1 in mouse skeletal muscle was shown to simultaneously lead to increased IMTG synthesis and increased FA oxidation rates. Transgenic overexpression in the mouse heart (Liu *et al.*, 2009a) simultaneously increased the TAG content, while substantially reducing FA, DAG and ceramide levels. In rats, unilateral overexpression of DGAT1 resulted in higher IMTG in the treated tibialis anterior muscle compared to control leg (Roorda *et al.*, 2005). Collectively, these animal studies strongly suggest that increasing the DGAT1 content in skeletal muscle can increase IMTG synthesis, reduce the concentration of FA metabolites and prevent insulin resistance.

Skeletal muscle DGAT1 activity was also found to be increased in mice in response to swimming exercise (six sessions a day (5-10 min each) for a week) (Liu *et al.*, 2007) and again resulted in increased TAG synthesis and decreases in DAG and ceramide concentrations. In a human study elevations in GPAT1 and DGAT1 content have also been observed the day following a single 90 minute bout of endurance exercise (Schenk & Horowitz, 2007). This increase in GPAT1 and DGAT1 also led to a higher TAG content, and reductions in DAG and ceramides the day following exercise and protected the muscle against insulin resistance induced by a lipid-heparin infusion. In a continuation of this work, using a similar protocol, Newsom *et al.,* (2010) found an increase in GPAT1 activity and a protection against lipid induced insulin resistance following the 90 minute bout of endurance exercise the day before an overnight lipid-heparin infusion. Taken together, these studies suggest that acute exercise and exercise training are natural means to increase the protein content and activity of GPAT1 and DGAT1 and increase IMTG content while offering protection against insulin resistance.

Two studies have measured the GPAT1 protein content in lean and obese individuals with Western blots and did not observe a difference between these groups (Thrush *et al.*, 2009;Li *et al.*, 2011). Again, using Western blots one study observed a lower DGAT1 content in obese than in lean individuals (Li *et al.*, 2011), while another study did not observe a difference (Thrush *et al.*, 2009). However, Western blots do not reveal whether there are differences in the subcellular distribution of these enzymes between lean and obese individuals that might explain the difference in skeletal muscle insulin resistance between these groups. The recent observation that high DAG concentrations in the compartment directly under the plasma membrane might lead to insulin resistance (Bergman *et al.*, 2012) makes it worthwhile to investigate this hypothesis.

Therefore, the present study aimed to investigate the total protein content and distribution of GPAT1 and DGAT1 using immunofluorescence microscopy in skeletal muscle obtained from non obese and obese women in order to investigate whether there are differences in the spatial distribution and protein content of these enzymes between these groups.

5.3 Methods

Muscle Samples

Muscle biopsies were obtained from the *m. gluteus maximus* of six non obese females and six obese females during elective orthopaedic surgery (total hip arthroplasty) under general anaesthesia. Subject characteristics can be seen in Table 5.1. All participants were undergoing surgery at Russells Hall Hospital (Dudley Group of Hospitals) and gave their informed consent for participation in this study. The study was approved by the local NHS Research Ethics Committee. A small sample of muscle (~ 200 mg) was taken by Consultant Surgeon Mr. Edward Davis immediately following the initial surgical incision.

Table 5.1 Subject Characteristics

	Non Obese Females	**Obese Females**
n	**6**	**6**
Age (y)	**62 ± 3**	**68 ± 3**
Height (m)	**1.59 ± 0.03**	**1.60 ± 0.03**
Body Mass (kg)	**57.36 ± 4.54**	**85.14 ± 4.73***
Body Mass Index (BMI) (kg/m^2)	**22.63 ± 1.40**	**33.3 ± 1.63***
Fasting plasma Glucose (mmol/L)	**6.98 ± 0.36**	**6.32 ± 0.36**
Fasting plasma Insulin (µU/ml)	**11.91 ± 3.23**	**21.53 ± 4.04**
HOMA IR	**3.92 ± 1.15**	**6.19 ± 1.25**

Data are presented as mean ± SEM. * $P < 0.05$

The sample preparation and storage procedures were performed as described in Chapter 2.2. Immunofluorescence methods are described in Chapter 2.4.

Blood Analyses

Following anaesthesia, blood was collected into two vacutainers, one containing EDTA (for plasma). Blood samples were centrifuged at 3,500 rpm for 15 minutes at 4 °C. Aliquots of serum and plasma were then frozen and stored at −80 °C until later analysis. Plasma glucose concentration was analysed using an ILAB automated analyser (Instrumentation Laboratory, Cheshire, UK). Serum insulin concentrations were measured using ELISA (Invitrogen, Paisley, UK).

Antibodies

All antibodies used in this chapter were identical to those used in Chapters 3 and 4. Anti-GPAT1 was a kind gift from Professor Jan Oscarsson (AstraZeneca R&D, Mölndal, Sweden) and anti-DGAT1 was obtained from a commercial source (Abcam, Cambridge, UK). Anti-myosin heavy chain type I (MHCI) was obtained from DSHB, Iowa, USA. Anti-cytochrome c oxidase (COX) (Invitrogen, Paisley, UK) was used to stain mitochondria using the procedure previously described by Shaw *et al.,* (2008). IMTG were stained using the neutral lipid dye oil red O in combination with immunofluorescence as described by Koopman and colleagues (2001).

Antibody Validation

Details of antibody validation are described in Chapter 2.3.1.1 and also in the antibody validation sections of the methods of Chapters 3 and 4.

Immunofluorescence Staining

Cryosections were stained using methods described in Chapter 2.4. Specifically, following formaldehyde fixing, and permeabilisation, samples were incubated in appropriate antibodies

for 1 hour. Subsequently, samples were incubated with appropriate Alexa Fluor conjugated secondary antibodies for 30 minutes (donkey anti rabbit IgG-488, donkey anti mouse IgM-594, goat anti rabbit IgG-488, goat anti mouse IgM 594). IMTG were stained as described in Chapter 2.3.1.4.

Fluorescence Microscopy

Images were captured using a Nikon E600 microscope coupled to a SPOT RT KE colour 3 shot CCD camera (Diagnostic instruments Inc, MI, USA) using the excitation filters described in Chapter 2.5 to visualise Alexa Fluor 350, 488, 594 as well as oil red O. To investigate fibre type specific contents, ORO, COX, GPAT1 and DGAT1 antibodies were each incubated with MHCI and WGA. To investigate GPAT1 colocalisation with lipid droplets and mitochondria, GPAT1 was co-incubated with ORO or COX, along with WGA. Digital images showing distribution in cross sections of muscle fibres were obtained. Detailed digital images were captured using an inverted confocal microscope (Leica DMIRE2, Leica Microsystems) using the excitation filters as described in Chapter 2.5.

Image Processing

Images were processed using Image-Pro Plus 5.1 software (Media Cybernetics, MD, USA), a description of which can be found in Chapter 2.5.1. Analysis was completed for fibre type specific lipid content and mitochondrial intensity. Colocalisation was investigated in confocal images of cross sections using Pearson's correlation analysis in the Image-Pro Plus 5.1 software.

Automated Image Capture and Analysis

For analysis of IMTG and mitochondria, and fibre type specific fluorescence of GPAT1 and DGAT1, automated image analysis was used. Details of automated image capture and analysis are described in Chapter 2.5.2. Images were captured using a 40 x oil objective.

Automated Image Processing

Details of automated image processing are described in Chapter 2.5.3. Images were analysed using Definiens Cellenger software (Munich, Germany) with the user defined algorithms which assigned whether the cell is fast or slow type, then (depending on the analysis required) the algorithm defined the fine detail objects using a watershed algorithm.

Statistics

Total mitochondria area fraction and intensity and total IMTG content (expressed as area fraction stained) of type I and type II fibres were compared using a paired samples t-test. Fibre type specific GPAT1 and DGAT1 distribution was investigated using a paired samples t-test. Between group differences in IMTG content, mitochondrial content and intensity and GPAT1 and DGAT1 fluorescence intensity were also investigated using an independent samples t-test. Colocalisation of GPAT1 with both lipid droplets and mitochondria was investigated using Pearson's correlation coefficient. Statistical significance was set at $P < 0.05$. All data are expressed as mean ± SEM.

5.4 Results

The distribution of GPAT1 was visually similar in both non obese (Figure 5.1A) and obese individuals (Figure 5.1B). There was intense staining in some fibres and little staining in other fibres. In longitudinally oriented fibres, the GPAT1 staining showed a striated distribution with striations running across the fibre in both non obese (Figure 5.1A) and obese (Figure 5.1B) individuals. Combination with the fibre type stain MHCI revealed that the fibres intensely stained for GPAT1 were the type I fibres. Quantitative analysis showed that the GPAT1 staining was significantly greater in type I than in type II fibres in both non obese (80 ± 5 vs. 43 ± 4, $P = 0.001$) and obese individuals (81 ± 6 vs. 42 ± 2, $P = 0.001$) (Figure 5.2). However, there was no difference between the non obese and obese individuals in either type I (non obese: 80 ± 5 vs. obese: 81 ± 6, $P = 0.86$) or type II (non obese: 43 ± 4 vs. obese: 42 ± 2, $P = 0.82$) fibres (Figure 5.2).

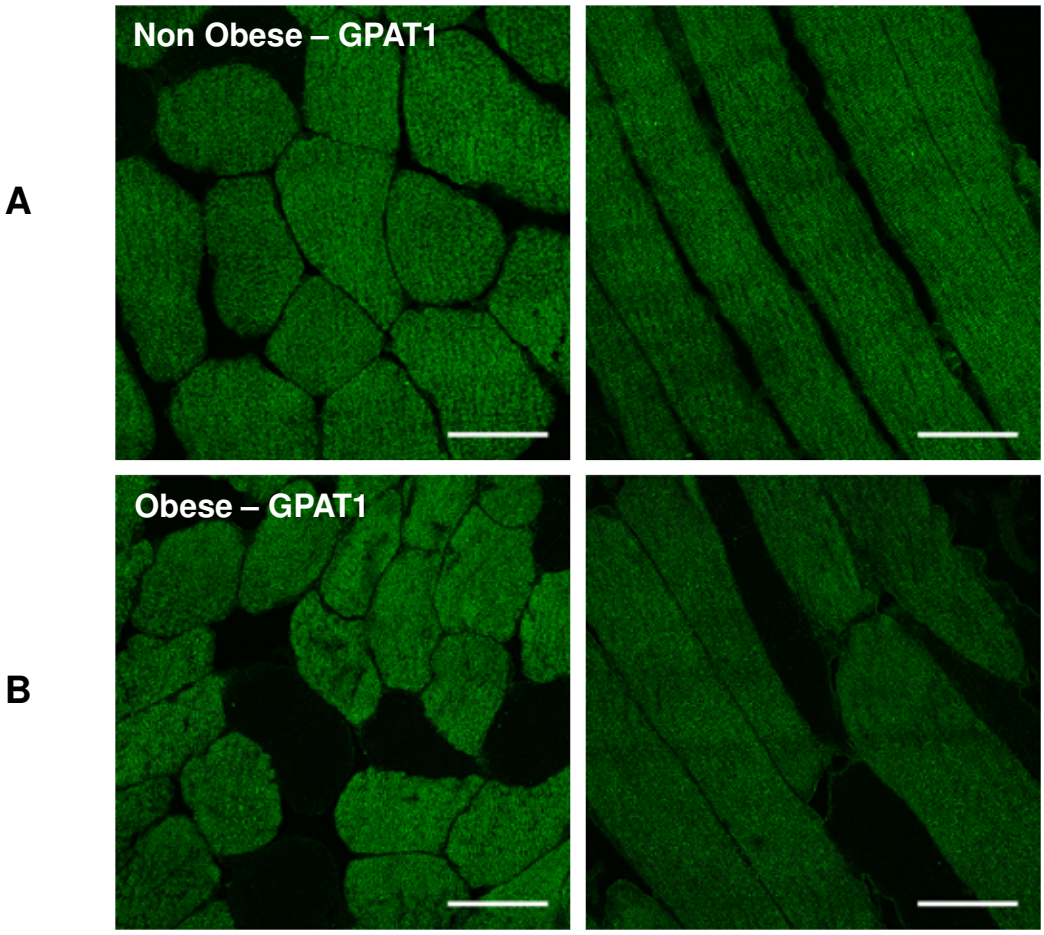

Figure 5.1 GPAT1 distribution in human skeletal muscle. Panel A shows the distribution of GPAT1 in skeletal muscle of non obese women in both cross sections (left image) and longitudinally oriented sections (right image). Panel B shows the distribution of GPAT1 in skeletal muscle obtained from obese women in both cross sections (left image) and longitudinally oriented sections (right image). Bar = 50 µm.

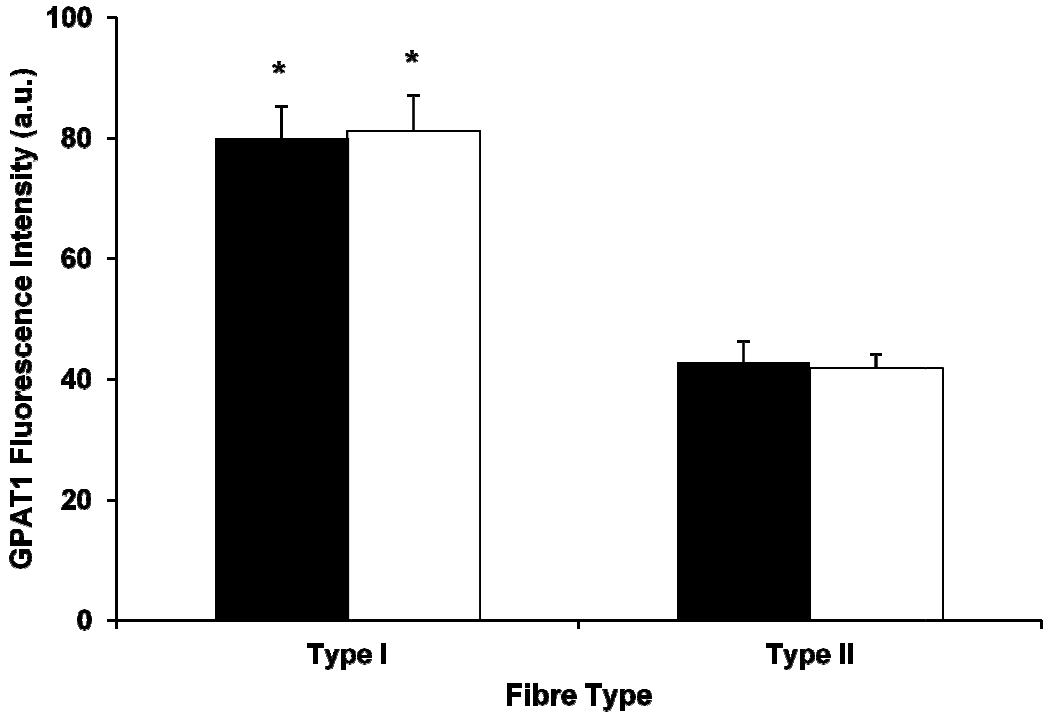

Figure 5.2 Fibre type specific distribution of GPAT1 in human skeletal muscle. Black bars represent mean values of non obese participants and white bars represent mean values of obese participants. GPAT1 was greater in type I compared to type II fibres in both non obese and obese individuals. Values are mean ± SEM. * Denotes a significant difference between fibre types at P < 0.05.

Given the role of GPAT1 in IMTG synthesis, co-staining of GPAT1 and IMTG, using oil red O, was completed in order to investigate their colocalisation. Visual inspection of GPAT1 and IMTG co-staining showed little colocalisation in both non obese (Figure 5.3A) and obese participants (Figure 5.3B) in the confocal microscopy images. The images were analysed using Pearson's correlation. This also revealed limited colocalisation in both non obese ($r = 0.09 \pm 0.02$) and obese individuals ($r = 0.08 \pm 0.02$) (Figure 5.3C). The observed values were significantly greater than the values of non matched, randomised images ($P < 0.05$) (Figure 5.3C).

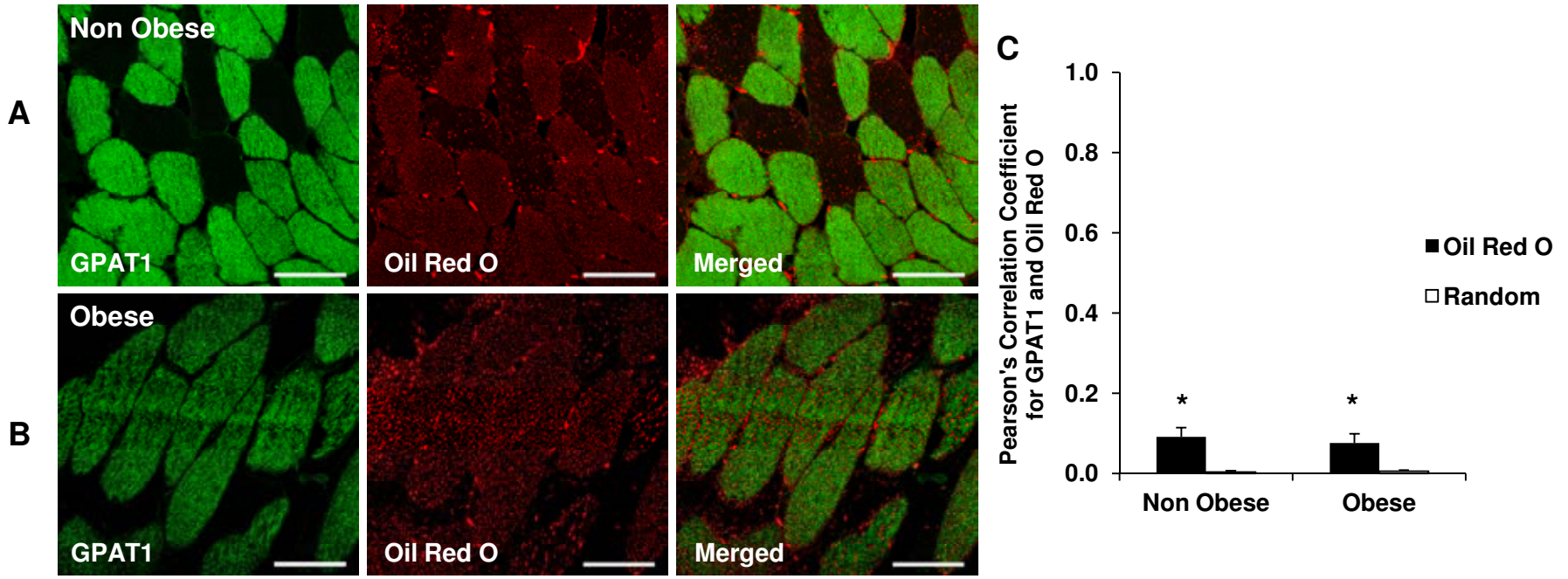

*Figure 5.3. GPAT1 and IMTG (stained with oil red O) colocalisation in skeletal muscle of non obese (A) and obese (B) females. Bar is 50 µm. Pearson's correlation was used to investigate the colocalisation of GPAT1 and oil red O (C). Colocalisation was deemed significant compared to randomised non matched pairs of images. Values are mean ± SEM. * Denotes a significant difference between matched and non matched pairs of images at P < 0.05.*

When examining fibre type differences in IMTG, there was no difference in lipid droplet area fraction in type I fibres (non obese: 0.034 ± 0.006 vs. obese: 0.034 ± 0.007, $P = 0.977$) or type II fibres (non obese: 0.020 ± 0.002 vs. obese: 0.020 ± 0.005, $P = 0.991$) between the non obese and obese individuals (Figure 5.4A). However, there was a fibre type difference in lipid droplet area fraction in both the non obese (type I fibres: 0.034 ± 0.006 vs. type II fibres: 0.020 ± 0.002, $P = 0.03$) and obese individuals (type I fibres: 0.034 ± 0.007 vs. type II fibres: 0.020 ± 0.005, $P = 0.01$) (Figure 5.4A). There was also no difference in lipid droplet size between the non obese and obese individuals (0.72 ± 0.04 μm^2 vs. 0.82 ± 0.08 μm^2, $P = 0.29$) (Figure 5.4B).

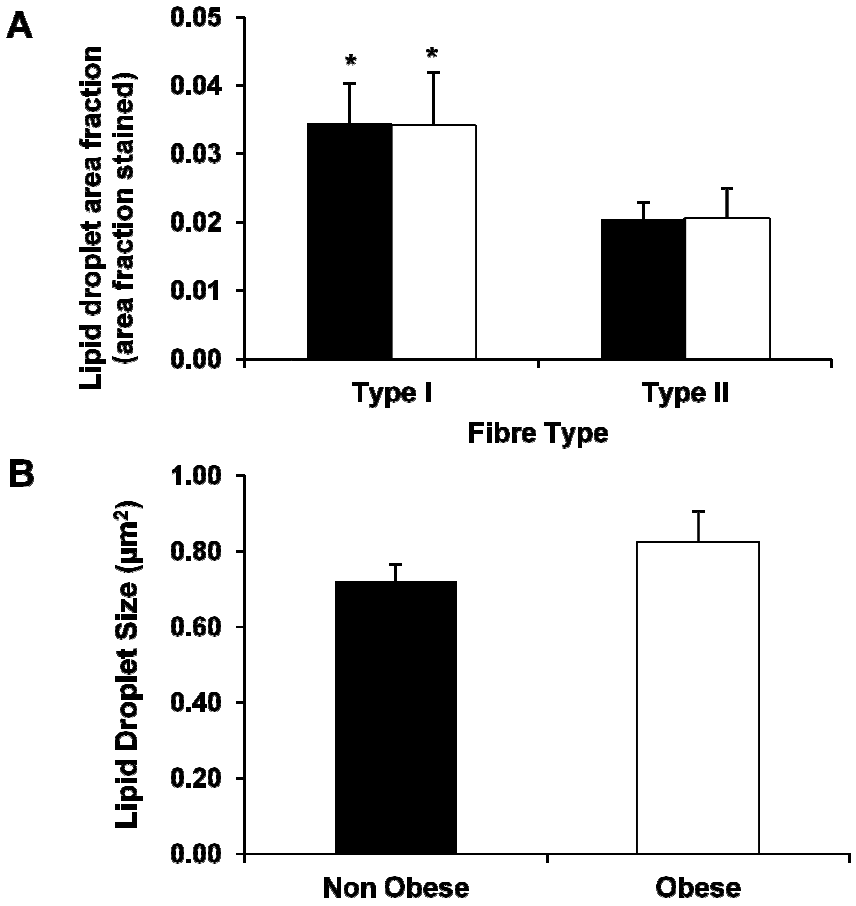

Figure 5.4. Lipid parameters in non obese and obese individuals where black bars represent mean values for non obese participants and white bars represent mean values for obese participants. Lipid droplet area fraction (A) was greater in type I fibres compared to type II fibres in both non obese and obese individuals. Lipid droplet size (B) was not different between non obese and obese individuals. Values are mean ± SEM. * Denotes significant difference between fibre types at P < 0.05.

GPAT1 is also known as mitochondrial GPAT and as such the GPAT1 stain was combined with the mitochondrial stain, COX, in order to investigate their colocalisation. Co-staining of GPAT1 and COX revealed little colocalisation in both non obese (Figure 5.5A) and obese (Figure 5.5B) individuals in the confocal microscopy images. This was confirmed by Pearson's correlation analysis ($r = 0.12 \pm 0.02$ and $r = 0.10 \pm 0.02$ for non obese and obese individuals respectively, $P = 0.581$) (Figure 5.5C). This Pearson's correlation coefficient for matched images was significantly higher for matched than for non matched pairs of images ($P < 0.05$) (Figure 5.5C).

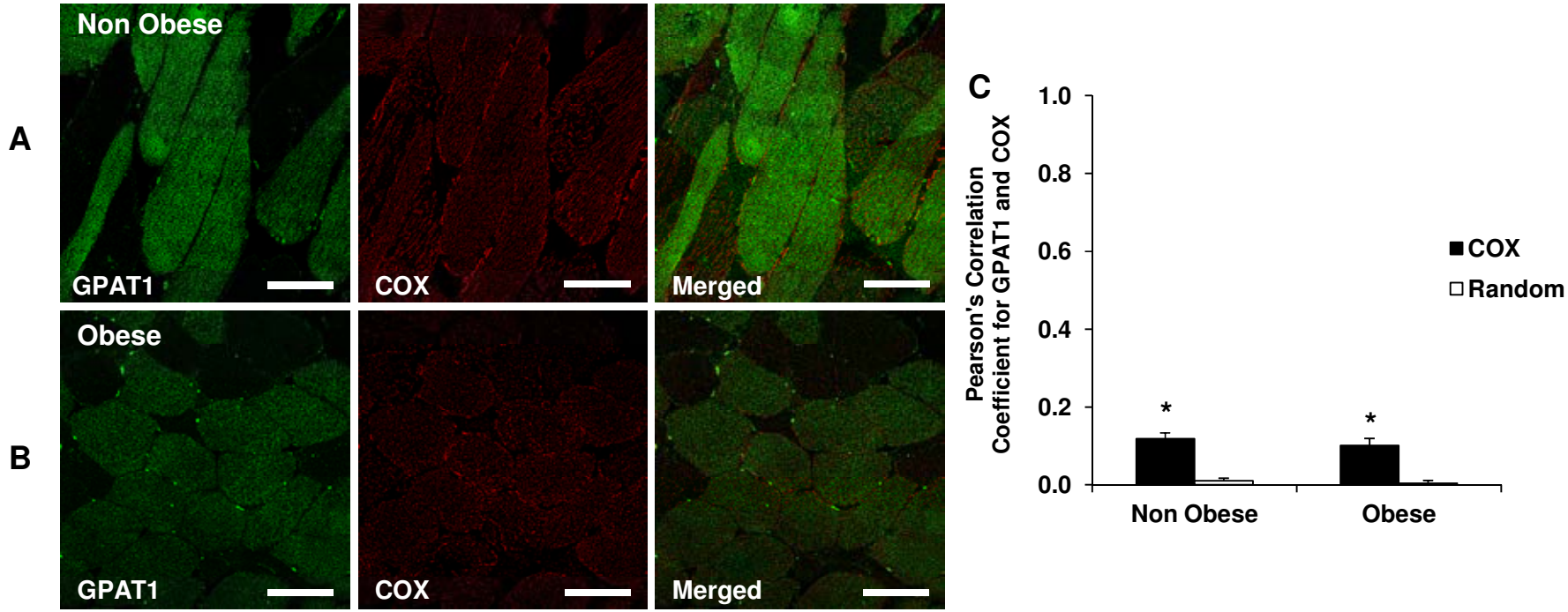

*Figure 5.5. GPAT1 and mitochondria (stained using COX) colocalisation in skeletal muscle of non obese (A) and obese (B) females. Bar is 50 µm. Pearson's correlation was used to investigate the colocalisation of GPAT1 and COX (C). Colocalisation was significant in both groups compared to randomised non matched pairs of images. Values are mean ± SEM. *Denotes a significant difference between overlapping and random images at P < 0.05.*

In the non obese individuals, mitochondria intensity was significantly greater in type I fibres than in type II fibres (type I: 98 ± 13 vs. type II: 80 ± 10, P = 0.01) (Figure 5.6A). Mitochondrial area fraction was also greater in type I fibres than in type II fibres (type I: 0.127 ± 0.03 vs. type II: 0.090 ± 0.02, P = 0.02) (Figure 5.6B). In obese individuals, both mitochondrial intensity (type I: 87 ± 11 vs. type II: 75 ± 9, P = 0.02) (Figure 5.6A) and mitochondrial area fraction (type I: 0.109 ± 0.02 vs. type II: 0.069 ± 0.01, P = 0.02) (Figure 5.6B) were significantly greater in type I than in type II fibres. However, there were no differences between non obese and obese individuals in either type I or type II fibres in mitochondria intensity or mitochondria area fraction ($P > 0.05$).

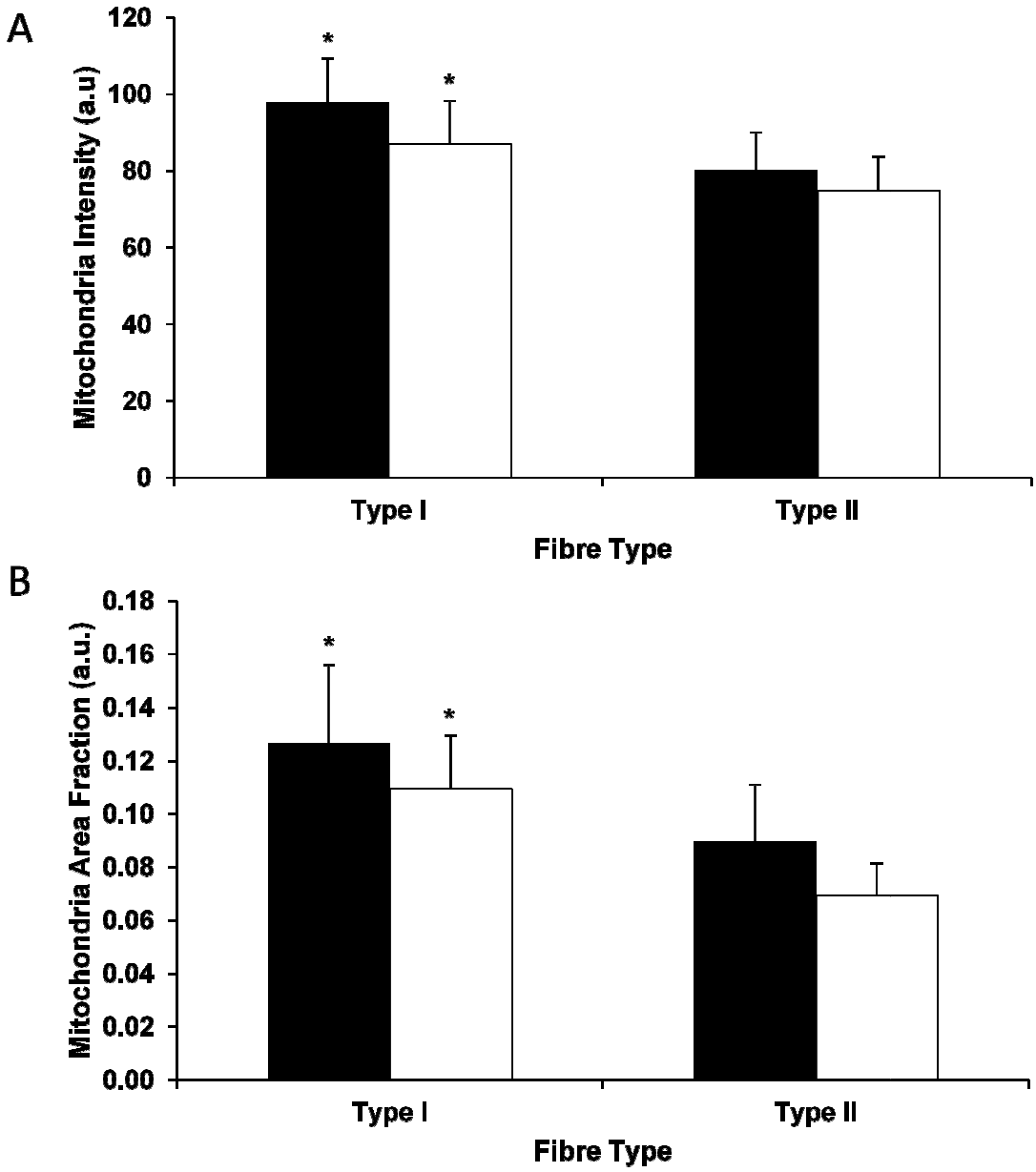

Figure 5.6. Mitochondrial variables in non obese and obese individuals. Black bars represent mean values for non obese participants and white bars represent mean values for obese participants. Mitochondria intensity (A) was greater in type I fibres in both non obese and obese individuals. Mitochondria area fraction (B) was greater in type I fibres than in type II fibres in both non obese and obese individuals. Values are mean ± SEM. * Denotes a significant difference between fibre types at P < 0.05.

The distribution of DGAT1 was similar in the non obese (Figure 5.7A) and obese individuals (Figure 5.7B). The staining was diffuse throughout the fibres with some areas of intense staining towards the cell borders. The DGAT1 stain also was stronger in some fibres than others but not to the same extent as GPAT1. There was also some brighter, intense punctate staining throughout the diffuse signal. Combining the DGAT1 staining with anti-MHCI revealed that DGAT1 staining was significantly greater in type I fibres than in type II fibres in both non obese (type I: 91 ± 5 vs. type II: 74 ± 5, $P = 0.001$) and obese individuals (type I: 85 ± 5 vs. type II: 70 ± 4, $P = 0.002$) (Figure 5.7C). There was also no difference between the groups in DGAT1 intensity in type I fibres (non obese: 91 ± 5 vs. obese: 85 ± 5, $P = 0.203$) and type II fibres (non obese: 74 ± 5 vs. obese: 70 ± 4, $P = 0.240$) (Figure 5.7C). In longitudinally oriented sections, there was no difference in the distribution between the non obese and obese individuals. Both groups showed areas of intense signal at the borders of the cells and clear striations running across the fibres (Figure 5.8).

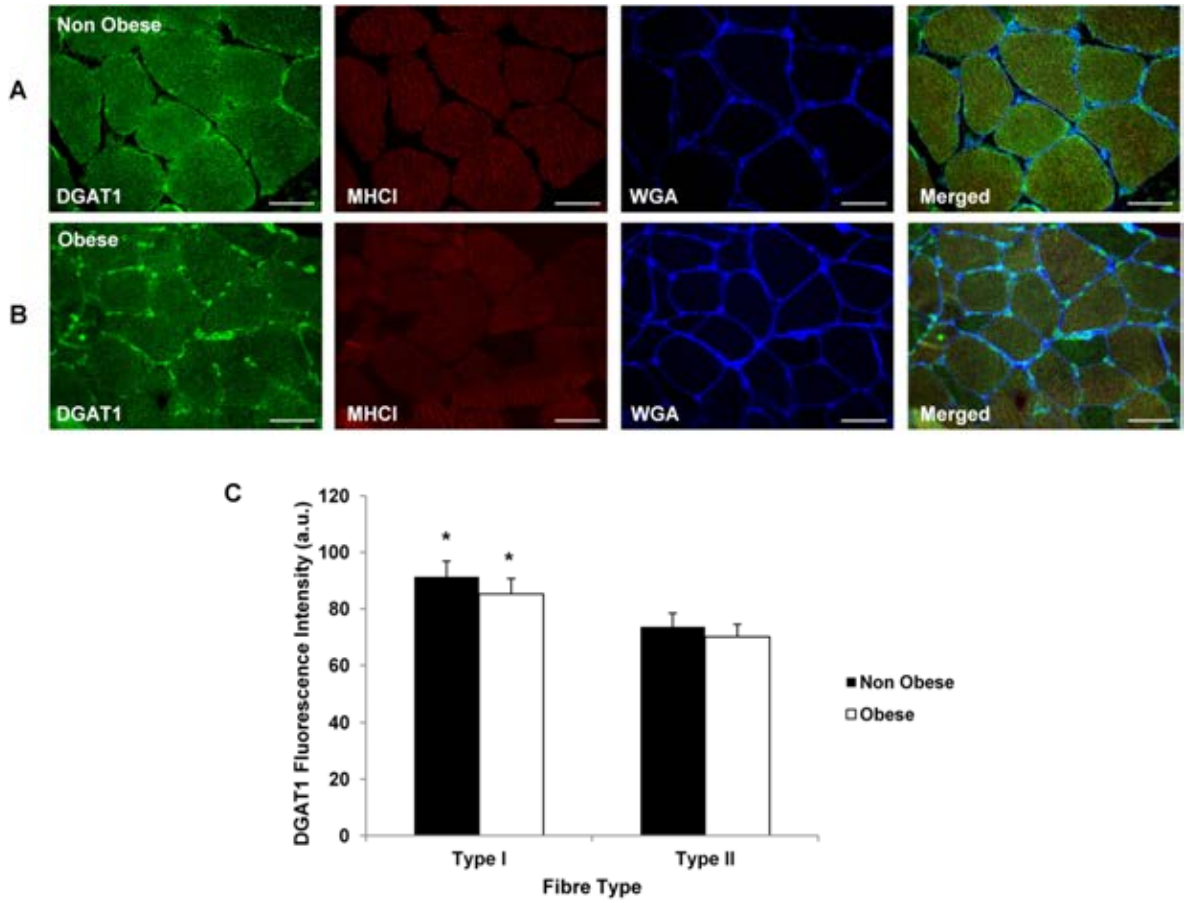

Figure 5.7 Visualisation of DGAT1 in human skeletal muscle of non obese (A) and obese individuals (B). DGAT1 was stained in combination with MHCI to identify type I fibres (red). Cell borders were stained using WGA (blue). Bar = 50 µm. DGAT1 had a greater intensity in type I compared to type II fibres in both non obese and obese individuals. All values are mean ± SEM. * denotes significant difference between fibre types at P < 0.05.

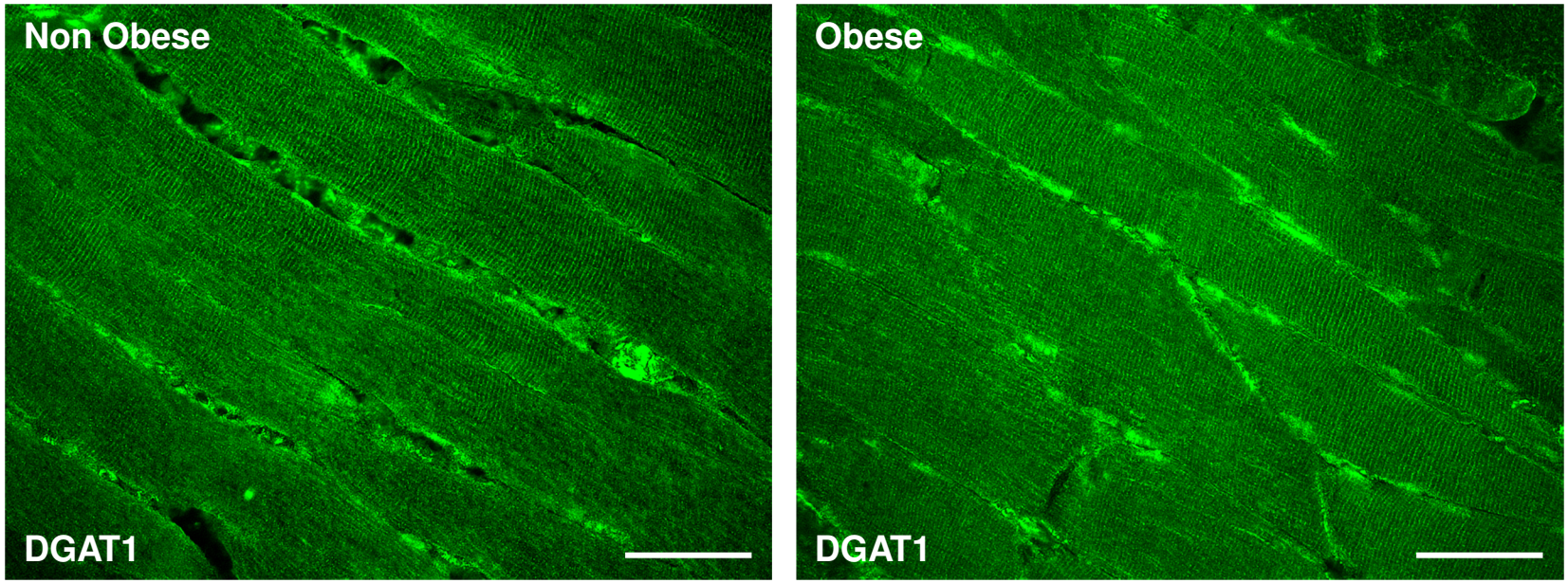

Figure 5.8 DGAT1 distribution in longitudinally oriented sections of skeletal muscle obtained from non obese and obese women. Bar = 50 µm.

5.5 Discussion

The present study is the first to show the distribution of GPAT1 and DGAT1 in human skeletal muscle. The data also show that there is no difference in the content and distribution of these enzymes between skeletal muscle obtained from non obese and obese women. In this study, it has also been observed that there appears to be a difference in the morphology of the cross sections compared to those in biopsies taken from lean men (see Figure 3.3 for example). Decreases in fibre number and fibre size have previously been reported in ageing, resulting in sarcopenia (Deschenes, 2004) which may explain why we see this different morphology in samples from ageing individuals.

This study showed a weak colocalisation of GPAT1 with the mitochondria and this observation is in agreement with the findings in lean, healthy men reported in Chapter 3 of this thesis. As described in Chapter 3, this is somewhat surprising given that the enzyme is named mitochondrial GPAT. GPAT1 was localised in close proximity to (but only weakly colocalised with) the mitochondria in both this study and in Chapter 3 of this thesis. The mitochondrial marker, COX, is an inner mitochondrial membrane enzyme involved in the electron transport chain which has been used previously to stain the mitochondrial network (Shaw *et al.*, 2008). This may therefore explain the lack of colocalisation of GPAT1 with the COX stain as GPAT1 was initially proposed to reside at the outer mitochondrial membrane. However, the resolving power of the microscope in this case is 0.2 μm and would therefore be unlikely to distinguish between the inner and outer mitochondrial membranes. In rat liver fractions the highest GPAT1 protein content has been observed in the mitochondrial associated vesicles (MAV), while the greatest GPAT1 activity was found in the outer mitochondrial membrane (OMM) fraction (Pellon-Maison *et al.*, 2007). It may be that in rat

liver, GPAT1 translocates from MAV to OMM when its activity is required for the reciprocal inhibition of carnitine palmitoyl transferase 1 (CPT1), thus directing LCFACoA towards IMTG storage. The data of the present study and that of Chapter 3 does suggest that GPAT1 in human skeletal muscle is in fact not directly tethered to the mitochondria in the overnight, fasted state in both non obese and obese individuals. It cannot be excluded that in response to feeding, GPAT1 translocates to the OMM in order to direct LCFACoA towards storage pathways, however this requires future verification.

DGAT1 is proposed to reside at the endoplasmic reticulum, shown to be the site of lipid droplet synthesis in chicken liver (Weiss *et al.*, 1960). This is likely to also be the case in rat skeletal muscle as immunofluoresence images showed that the distribution of DGAT1 observed in the present study was similar to that of the sarcoplasmic reticulum protein calsequestrin (Jorgensen *et al.*, 1979). The images in our human study clearly show striations running across the fibre in longitudinally oriented sections, which could well be in line with their presence in the ER. Definitive confirmation of this spatial location should be obtained using either DGAT1 colocalisation with markers of the ER or immunogold labelling of DGAT1 and transmission electron microscopy.

The results of the present study did not show a difference in the distribution or content of GPAT1 and DGAT1 between non obese and obese women. As has been mentioned previously in Chapter 1.3.1 of this thesis, accumulation of FA metabolites in the muscle of obese individuals has been suggested to play a key role in the development of insulin resistance (Chalkley *et al.*, 1998;Griffin *et al.*, 1999;Yu *et al.*, 2002;Itani *et al.*, 2002). As GPAT1 and DGAT1 are enzymes that catalyse reactions consuming FA metabolites,

differences in subcellular distribution and concentration between these groups could have explained the increased insulin resistance in the obese women. The absence of such a difference must imply that other aspects of lipid metabolism, such as a higher arterial exposure and uptake rate of FA in skeletal muscle, higher rates of IMTG lipolysis or reduced mitochondrial oxidation must lead to higher levels of muscle FA metabolites in the obese women. The absence of a difference in GPAT1 is in line with two earlier studies which did not show a difference in total GPAT1 protein expression measured with Western Blots between lean and obese individuals (Thrush et al 2009, Li et al 2011). The absence of a difference in DGAT1 is in line with one Western blot study (Thrush *et al.*, 2009), while another study found a lower content in obese than in non obese women (Li *et al.*, 2011).

The present study did not show differences in lipid droplet content between non obese and obese women. This is perhaps surprising given that a number of previous studies have shown that the IMTG content is greater in sedentary obese than in lean individuals (Goodpaster *et al.*, 2001;He *et al.*, 2001;Li *et al.*, 2011). The difference between this study and the previous study may be that the subjects of the present study were older (> 60 years) and were sedentary women. The women were awaiting orthopaedic surgery and had very limited mobility. The majority were able to move around using crutches or a frame however some were restricted to a wheelchair. In previous studies younger and potentially more active men and women were investigated (Goodpaster *et al.*, 2001;He *et al.*, 2001;Li *et al.*, 2011). Ageing shows a positive correlation with the accumulation of intramuscular lipid (Kim *et al.*, 2004a) and the development of muscle insulin resistance and a sedentary lifestyle also correlates with a decline in insulin sensitivity (Stuart *et al.*, 1988;Lipman *et al.*, 1972;Mikines *et al.*, 1991;Kim *et al.*, 2004a). A larger lipid droplet area fraction was observed in type I compared to type II

fibres in both non obese and obese women, a finding which is in line with previous reports on lean (Malenfant *et al.*, 2001;van Loon *et al.*, 2003a) and obese individuals (He *et al.*, 2001). There was no difference in mitochondrial content between the non obese and obese group neither in type I nor in type II fibres. This may indicate that both groups had very low activity levels. Mitochondrial content in both groups was greater in type I compared to type II fibres, confirming data previously reported in trained young men (Shaw *et al.*, 2008).

In conclusion, this study shows the first immunofluorescence staining images of GPAT1 and DGAT1 in human skeletal muscle obtained from obese females and demonstrates that both enzymes have a greater expression in type I compared to type II fibres. There was no difference in the protein content and distribution of GPAT1 and DGAT1 between non obese and obese sedentary elderly women.

CHAPTER 6

VISUALISATION OF ADIPOSE TRIGLYCERIDE LIPASE AND ITS ACTIVATOR COMPARATIVE GENE IDENTIFICATION-58 IN HUMAN SKELETAL MUSCLE

6.1 Abstract

Lipid droplets are present in skeletal muscle and the fatty acids (FA) liberated through lipolysis are utilised as a readily available fuel source, during exercise in lean trained individuals. Adipose triglyceride lipase (ATGL) is responsible for the first step of lipolysis in human skeletal muscle; the removal of a FA from triacylglycerol (TAG) to form diacylglycerol (DAG). Comparative gene identification-58 (CGI-58) is required for full activation of ATGL in a kidney cell line. The aims of the present study were to develop immunofluorescence methodology to visualise ATGL and, for the first time, its activator CGI-58 and potential colocalisation with ATGL in sections of human skeletal muscle. The acquired images showed that ATGL fluorescence was greater in type I compared to type II fibres ($P < 0.001$), while the fluorescence intensity of CGI-58 did not differ between the fibre types. The images also revealed that ATGL and CGI-58 only partially colocalised with lipid droplets in human skeletal muscle in the overnight fasted and resting state. IMTG content was greater in type I compared to type II fibres ($P < 0.001$). ATGL staining revealed a strong stain in peripheral regions of the cell and a weak diffuse intracellular stain. CGI-58 showed diffuse intracellular staining with more intense spots in peripheral regions, which colocalised with the nuclei. ATGL and CGI-58 partially colocalised, particularly in peripheral and nuclear regions of the cell. The intense staining of CGI-58 in the myonuclei suggests that the protein may play a role in the local DAG and/or FA generation at this site.

6.2 Introduction

In humans, excess caloric intake is stored as triacylglycerol (TAG) in lipid droplets, primarily in adipose tissue and to a lesser extent in skeletal muscle and liver. Lipid droplets are stores of neutral lipid in the cytosol surrounded by a phospholipid monolayer. The most abundantly stored lipid molecules are TAG followed by cholesteryl esters (Bostrom *et al.*, 2009). Data obtained in adipocytes have shown that lipid droplets are coated by a number of proteins including the so called PAT proteins (**p**erilipin 1, **a**dipocyte differentiation related protein (ADRP) and **t**ail interacting protein (TIP-47)). The PAT proteins have been suggested to regulate the access of the lipolytic enzymes to the stored TAG, to thus liberate FA that can then be released (adipose tissue) or oxidised to generate energy (muscle) (Prats *et al.*, 2006;Listenberger *et al.*, 2007;Bell *et al.*, 2008).

The first lipase discovered in skeletal muscle was hormone sensitive lipase (HSL) which for some time was believed to be the only lipase in skeletal muscle. Observations in HSL knockout mice showed that they do not accumulate TAG but instead accumulate diacylglycerol (DAG), suggesting that an additional lipase may be responsible for the removal of the first FA from TAG to form DAG (Haemmerle *et al.*, 2002;Schweiger *et al.*, 2006). This data initiated a search for an additional lipase generating DAG and led to the discovery of ATGL (Zimmermann *et al.*, 2004) also known as desnutrin or calcium-independent phospholipase A2ζ (Jenkins *et al.*, 2004;Villena *et al.*, 2004). ATGL plays a role in basal lipolysis in adipocytes (Ryden *et al.*, 2007;Langin *et al.*, 2005) and it has been shown in a kidney cell line that it requires an activator protein, comparative gene identification - 58 (CGI-58), to reach maximum activity (~ 20 fold increase) (Lass *et al.*, 2006).

ATGL has been suggested to play a crucial role in skeletal muscle TAG lipolysis; animals with a general ATGL knockout show significant TAG accumulation in all tissues (Haemmerle *et al.*, 2006). ATGL has been shown to be present in rat skeletal muscle (Zimmermann *et al.*, 2004) and more recently in human skeletal muscle (Jocken *et al.*, 2008;Alsted *et al.*, 2009) where it was demonstrated to be predominantly present in type I fibres (Jocken *et al.*, 2008).

Incomplete lipolysis, resulting from an imbalance between the activity of ATGL and HSL, may lead to the accumulation of DAG and generation of long-chain fatty acyl-coenzyme A (LCFACoA), which are both known to inhibit insulin signalling in obese (Itani *et al.*, 2000) and type 2 diabetic humans (Itani *et al.*, 2001). This imbalance has been seen in HSL knockout mice, which accumulate DAG in skeletal muscle and have reduced insulin sensitivity (Osuga *et al.*, 2000;Mulder *et al.*, 2003). ATGL deficiency on the other hand results in an accumulation of TAG (including ~ 20 fold increase in IMTG), but perhaps surprisingly improved insulin sensitivity (Haemmerle *et al.*, 2006). This finding seems to confirm that increases in FA metabolites in skeletal muscle, rather than increases in the total size of the IMTG pool play a key role in the mechanism that leads to insulin resistance in skeletal muscle. Further, DAG concentrations in skeletal muscle of ATGL knockout mice have been found to be normal despite an increased body weight resulting from excess fat accumulation (Hoy *et al.*, 2011). Conversely, HSL knockout mice have reduced fat mass and severe DAG accumulation in skeletal muscle (Haemmerle *et al.*, 2002;Zechner *et al.*, 2009). Therefore HSL is considered to be the rate limiting step for DAG hydrolysis whereas ATGL is responsible for cleavage of the first ester bond, liberating DAG from the stored TAG.

CGI-58 is ubiquitously expressed and has been shown to be present in skeletal muscle (Brown, 2001). CGI-58 is a 39 kDa protein and plays a role in facilitating the hydrolysis of TAG in almost all cell types (Lass *et al.*, 2006;Yamaguchi *et al.*, 2007), however it lacks intrinsic lipase activity due to the lack of a serine residue in its catalytic domain (Lass *et al.*, 2006;Yamaguchi *et al.*, 2007). In adipocytes, under basal conditions, CGI-58 interacts with the PAT protein, perilipin 1, at the surface of the lipid droplet. Upon catecholamine stimulation, PKA activity is increased which phosphorylates both HSL (Yamaguchi *et al.*, 2004;Subramanian *et al.*, 2004) and perilipin 1 (Yamaguchi *et al.*, 2007;Lass *et al.*, 2006). CGI-58 dissociates from perilipin 1, activating ATGL, and causing an increase in lipolysis. Lass *et al.,* (2006) demonstrated in a kidney cell line that CGI-58 acts as a coactivator of ATGL but not HSL. The mechanism of activation of ATGL by CGI-58 and its role in lipolytic regulation in skeletal muscle has currently not been investigated. In both kidney and adipocyte cell lines it has however been shown that CGI-58 coactivation of ATGL requires direct protein-protein interaction (Lass *et al.*, 2006;Granneman *et al.*, 2007). Further, in kidney cells, CGI-58 must bind to the lipid droplet (Gruber *et al.*, 2010) to bring about activation of ATGL. Given the importance of skeletal muscle lipolysis in fuel selection mechanisms and in the pathogenesis of insulin resistance and type 2 diabetes, the aim of this study was to develop a method that allows investigation of the spatial distribution of ATGL and its coactivator CGI-58 and their colocalisation with each other and with lipid droplets in human skeletal muscle. This method will be applied to the muscle of six lean, healthy individuals studied in the overnight fasted state to generate the first data on the spatial distribution of CGI-58 and its colocalisation with ATGL in man.

6.3 Methods

Measurement of VO_{2max}

Subjects performed a progressive exercise test to exhaustion on an electronically braked cycle ergometer (Lode BV, Groningen, The Netherlands) in order to determine maximal oxygen consumption (VO_{2max}) using an online gas collection system (Oxycon Pro, Jaeger, Wuerzburg, Germany). The test consisted of initially cycling at 95 W, followed by sequential increments of 35 W every 3 minutes until cadence was reduced to < 50 rpm, at which point the test was terminated. VO_{2max} was taken as the highest value obtained in the last 30 seconds of the test.

Muscle Samples

Percutaneous muscle biopsies were obtained from the vastus lateralis muscle of six healthy, lean and active male subjects using the needle biopsy technique (Bergstrom, 1975) as described in detail in Chapter 2.2. Subject characteristics are shown in Table 6.1.

Table 6.1 Subject Characteristics

	Male Participants
n	**6**
Age (y)	**26 ± 1**
Height (m)	**1.81 ± 0.02**
Body Mass (kg)	**72.0 ± 2.7**
Body Mass Index (BMI) (kg/m^2)	**22.0 ± 0.3**
VO_{2max} (ml/min/kg)	**60 ± 2**

Data are presented as means ± SEM.

Antibodies

ATGL staining was carried out using rabbit anti-ATGL (10006409, Cayman Chemical Michigan, USA) targeting amino acids 382-400 (KRKLGRHLPSRLPEQVELR) which, using BLAST (www.uniprot.org) showed 100% sequence identity to human ATGL (504 amino acids in length) as well as a shorter isoform (180 amino acids in length). This antibody has been validated in Western blotting (Figure 6.1) (unpublished data kindly shared by Dr Johan Jocken, Maastricht University, NL) and has been used in previously published research (Jocken *et al.*, 2008). CGI-58 staining was completed using rabbit anti-CGI-58 (NB110-41576, Novus Biologicals, Littleton, CO) produced from a synthetic peptide corresponding to residues 200-300 of the human protein (ALGAALTPFNPLAGLRIAGPFGLSLVQRLRPDFKRKYSSMFEDDTVTEYIYHCNVQT PSGETAFKNMTIPYGWAKRPMLQRIGKMHPDIPVSVIFGARSCI).

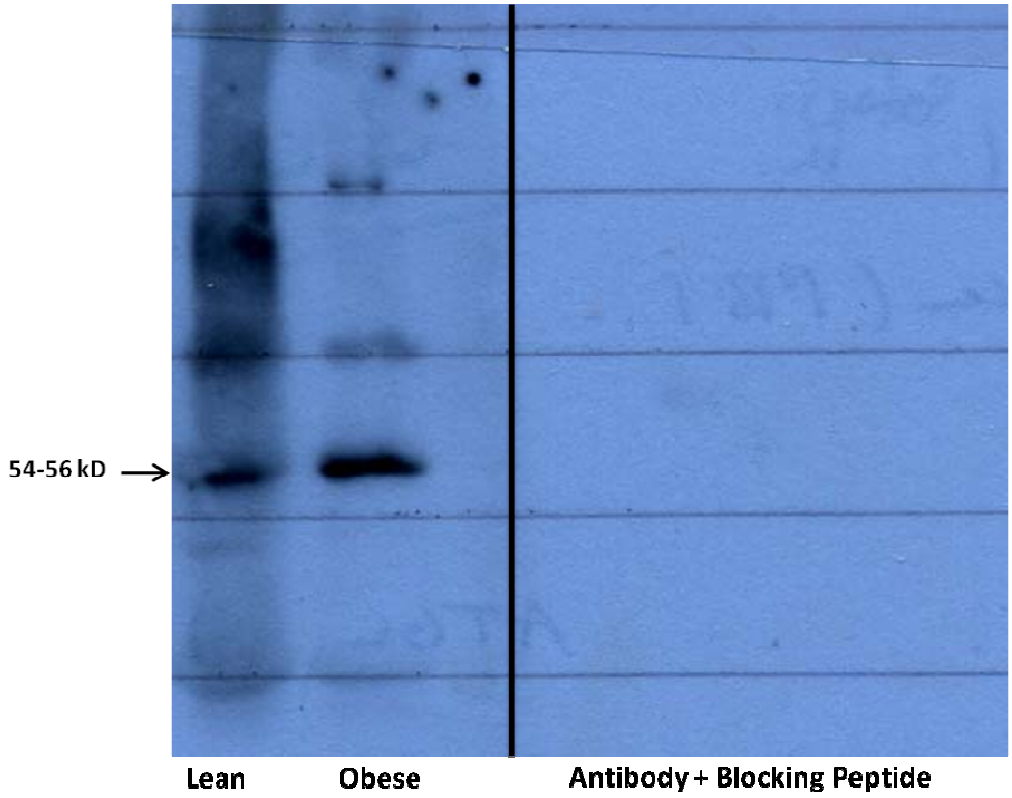

Figure 6.1 Validation of the ATGL antibody. Western blot shows a band at the correct molecular weight (54 kDa) in skeletal muscle of lean and obese individuals. Incubation with a blocking peptide as well as the primary antibody removes all visible bands. Data kindly provided courtesy of Dr Johan Jocken, Maastricht University, The Netherlands.

BLAST (www.uniprot.org) showed 100 % sequence identity to human CGI-58 as well as 58% sequence identity to ABHD4, a protein that is not present in skeletal muscle. Therefore the antibody is selective as it can detect only one protein in muscle. This antibody has also been validated for use in Western blotting (Figure 6.2), detecting a single band at the correct molecular weight in mesenchymal stem cells (kindly shared unpublished data, Dr. Johan Jocken, Maastricht University, NL). This antibody has been used in human skeletal muscle to assess CGI-58 protein content (Jocken *et al.*, 2010). Fibre type was determined by incubating sections in mouse anti-myosin heavy chain type I (MHCI) (A4.840 DSHB, developed by Dr. Blau). Nuclei were stained using the DNA stain 4',6-diamidino-2-phenylindole (DAPI). PBS was used for dilution of all antibodies and for use in the washing steps of the procedure. IMTGs were stained using the neutral lipid dye oil red O in combination with immunofluorescence as developed by Koopman *et al.,* (2001) and described in Chapter 2.3.1.4.

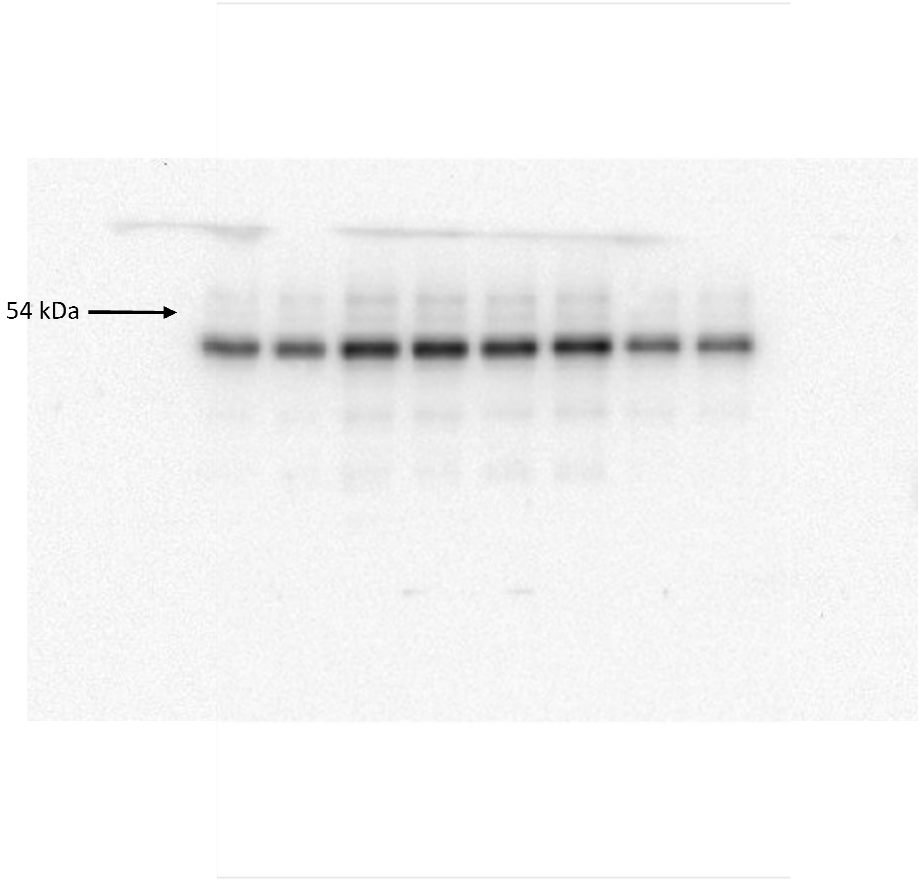

Figure 6.2 Validation of CGI-58 antibody. Western blot shows band at the correct molecular weight (39 kDa) in mesenchymal stem cells. Data kindly provided courtesy of Dr Johan Jocken, Maastricht University, The Netherlands.

Immunofluorescence Staining

Details of the immunofluorescence staining are described in Chapter 2.4. In staining procedures for CGI-58, samples were blocked for 30 minutes in 5 % normal goat serum (NGS) before the application of anti-CGI-58 (1:100) overnight at 4 °C. When identifying ATGL, anti-ATGL was applied at a dilution of 1:50 for 1 hour at room temperature. Following washing steps, all samples were then treated with the appropriate Alexa Fluor conjugated secondary antibody. Sections were then incubated in oil red O for 30 minutes at room temperature.

Sequential Staining of ATGL and CGI-58

Double staining of ATGL and CGI-58 was performed using a method which allows for application of two primary antibodies from the same host species (rabbit) (Granneman *et al.*, 2009b). Samples were incubated as follows. Anti-ATGL was applied for 1 hour at room temperature followed by an excess of Dylight 594 conjugated goat anti rabbit Fab (Stratech Scientific, Suffolk, UK) for one hour at room temperature. The Fab fragment covers the surface of the first primary antibody applied so that in the application of the whole IgG secondary antibody, the only available binding sites are those of the second primary antibody. Cryosections were then incubated in anti-CGI-58 before Alexa Fluor 488 conjugated secondary antibody (Invitrogen, Paisley, UK) was applied for 30 minutes at room temperature. Samples were washed thoroughly between antibody incubations as well as blocking for 30 minutes in 10 % NGS. Using this protocol, we aimed to eliminate cross-reactivity between the two sets of primary and secondary antibodies. Control experiments that omitted each primary antibody resulted in complete elimination of the fluorescent signal in the corresponding channel.

Fluorescence Microscopy

Images were captured using a Nikon E600 microscope coupled to a SPOT RT KE colour 3 shot CCD camera (Diagnostic instruments Inc, MI, USA) using the excitation filters described in Chapter 2.5 to visualise Alexa Fluor 350, DAPI, Alexa Fluor 488, Dylight 594 and oil red O. Digital images showing the distribution of ATGL, CGI-58 and IMTG in cross sections and longitudinally oriented muscle fibres were obtained.

Image Processing

Images were processed using Image-Pro Plus 5.1 software (Media Cybernetics, MD, USA) and intensity thresholds were selected to represent minimum values for lipid droplets. These were kept consistent throughout all image analysis. For each image, the muscle fibre area and the area occupied by lipid droplets was measured. Lipid content was expressed as area fraction stained by dividing the stained area in the fibre by the total area of that fibre. Fibre type differences in ATGL and CGI-58 fluorescence intensity were quantified using measures of optical density.

Statistical analyses

In order to compare fibre type differences in ATGL and CGI-58 signal and IMTG area fraction, a Student's paired samples t-test was undertaken on the fluorescence intensity analysis. Statistical significance was set at $P < 0.05$. All data are expressed as mean ± SEM unless otherwise stated.

6.4 Results

In order to investigate the distribution of ATGL and CGI-58 in human skeletal muscle, cryosections were stained with appropriately targeted antibodies. Representative images of immunofluorescence staining with anti-CGI-58 can be seen in Figure 6.3A. A weak, diffuse fluorescence signal was seen throughout all fibres with some spots of greater intensity in peripheral areas of the cells. When the CGI-58 stain was combined with anti-MHCI to denote fibre type, no differences in fibre type distribution of CGI-58 were seen (Figure 6.4) with a mean fluorescence of 67 ± 2 in type I fibres and a mean fluorescence of 62 ± 3 in type II fibres ($P = 0.292$) (Figure 6.3D). There was also greater intensity in large structures around the cell periphery which colocalised with nuclei stained using the DNA stain DAPI, showing that CGI-58 was present in the nuclei (Figure 6.5). There was also a more intense signal in some extranuclear areas of the cell periphery (Figure 6.3A). Oil red O staining revealed a relatively large number of small distinct spots demonstrating the presence of lipid droplets (Figure 6.3C). In line with previous observations ((Chapters 3, 4 and 5; (Malenfant *et al.*, 2001;van Loon *et al.*, 2003a;Shaw *et al.*, 2008)), there was a greater content of lipid in type I (0.027 ± 0.006) when compared to type II fibres (0.015 ± 0.005*)* ($P < 0.001$) (Figure 6.3B, 6.3C, 6.3E and 6.6). Combination of the CGI-58 stain with the oil red O staining revealed that lipid droplets only partially colocalised with CGI-58 (Figure 6.3E).

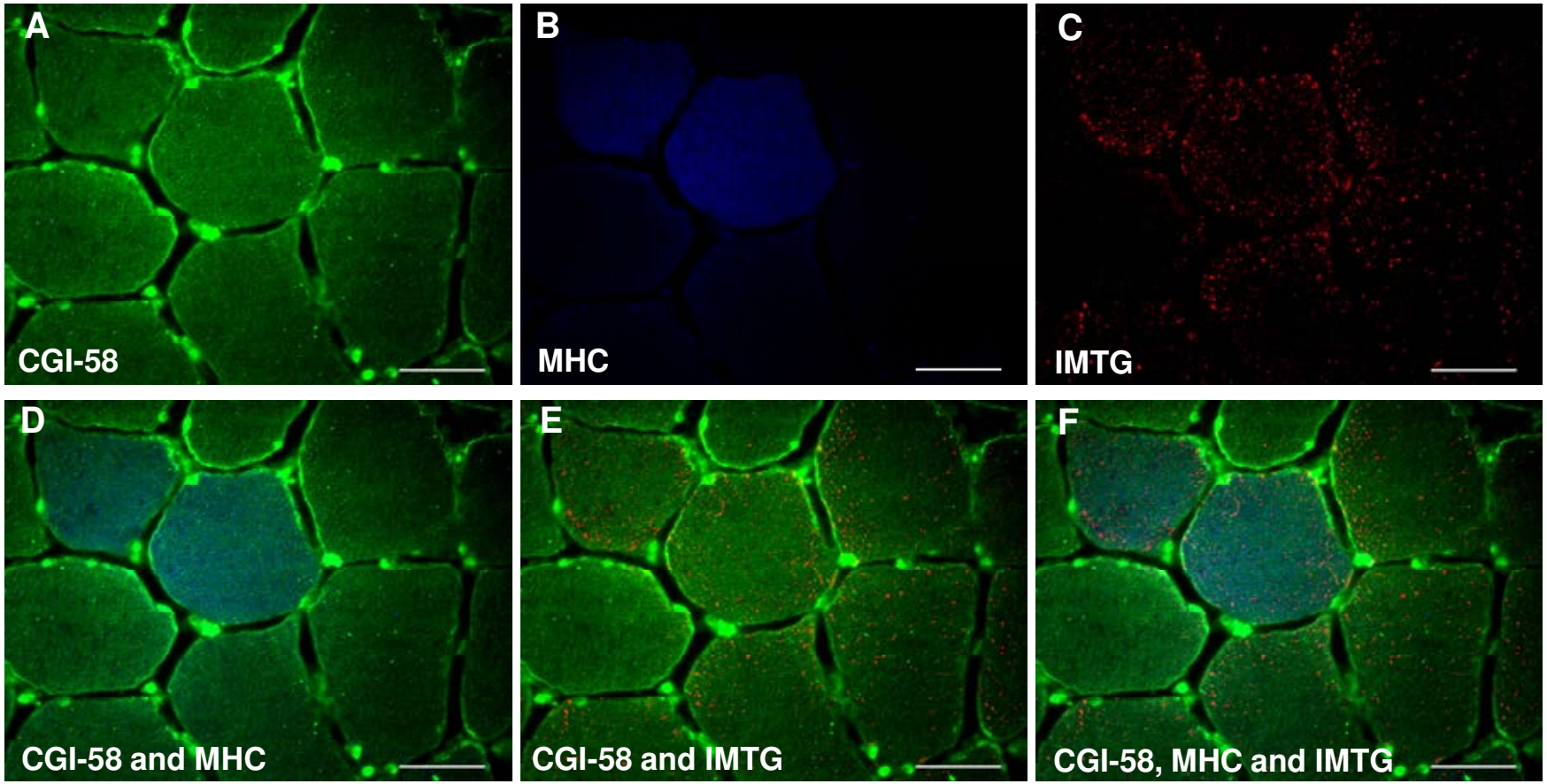

Figure 6.3. Widefield immunofluorescence microscopy to show visualisation of CGI-58 (A), MHC type I (B) and IMTG (C). Combinations of the merged images are also shown: CGI-58 merged with MHC type I (D), CGI-58 merged with IMTG (E) and the merging of all three images (F). Bar represents 50µm.

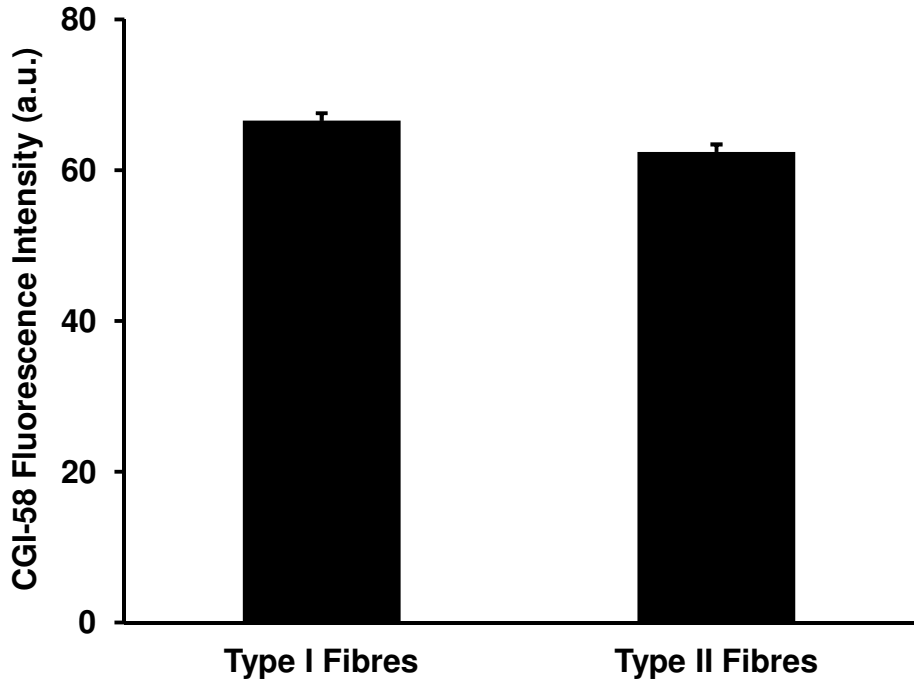

Figure 6.4. Fibre type specific CGI-58 fluorescence intensity. Data are mean ± SEM.

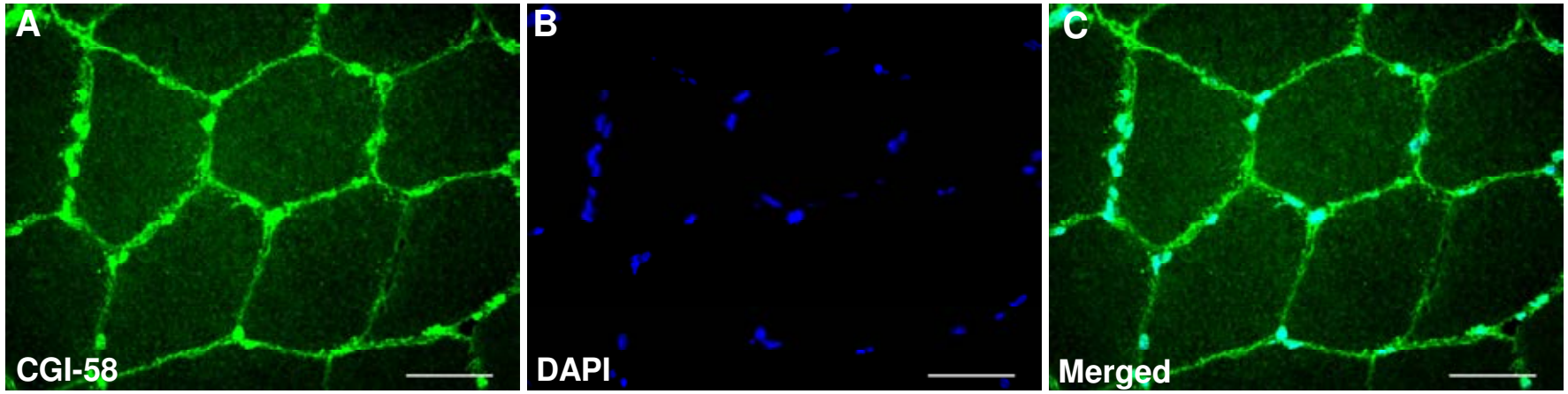

Figure 6.5. Representative images showing (A) distribution of CGI-58 in cross sections of human skeletal muscle, (B) nuclei stained with DAPI (B), and (C) merged images showing the colocalisation of CGI-58 with the nuclei. Bar is 50 µm.

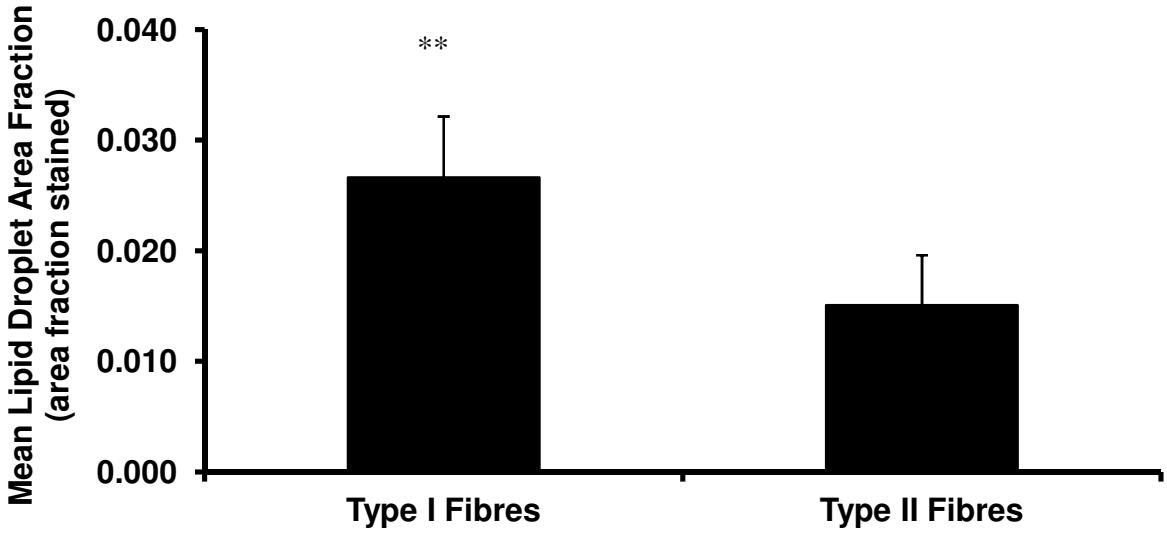

Figure 6.6. Fibre type specific lipid area fraction. ** Significant difference between fibre types (P < 0.001). Data are mean ± SEM.

Anti-ATGL staining showed a strong stain at peripheral regions of the cell (Figure 6.7A) and there was also a more diffuse and weaker fluorescence signal present in the interior of the cell. There did appear to be some spatial structure in the staining in the interior of the cell, however, this was not consistent across all subjects. ATGL staining was more intense in type I fibres compared to type II fibres (95 ± 4 vs. 57 ± 5, $P < 0.001$) (Figure 6.6 and 6.8). This was also true for lipid droplet distribution with a greater lipid content in type I compared to type II fibres ($P < 0.001$) (Figure 6.3 and 6.6), however there was also no obvious colocalisation between lipid droplets and ATGL (Figure 6.7). ATGL and CGI-58 co-staining is shown in Figure 6.9. ATGL and CGI-58 colocalise particularly at the cell periphery in subsarcolemmal and nuclear regions with little colocalisation within the cell interior. It seems that in longitudinally oriented sections ATGL is distributed in a striated network (Figure 6.9A). The distribution of CGI-58 also shows a regular distribution when viewed longitudinally (Figure 6.9B).

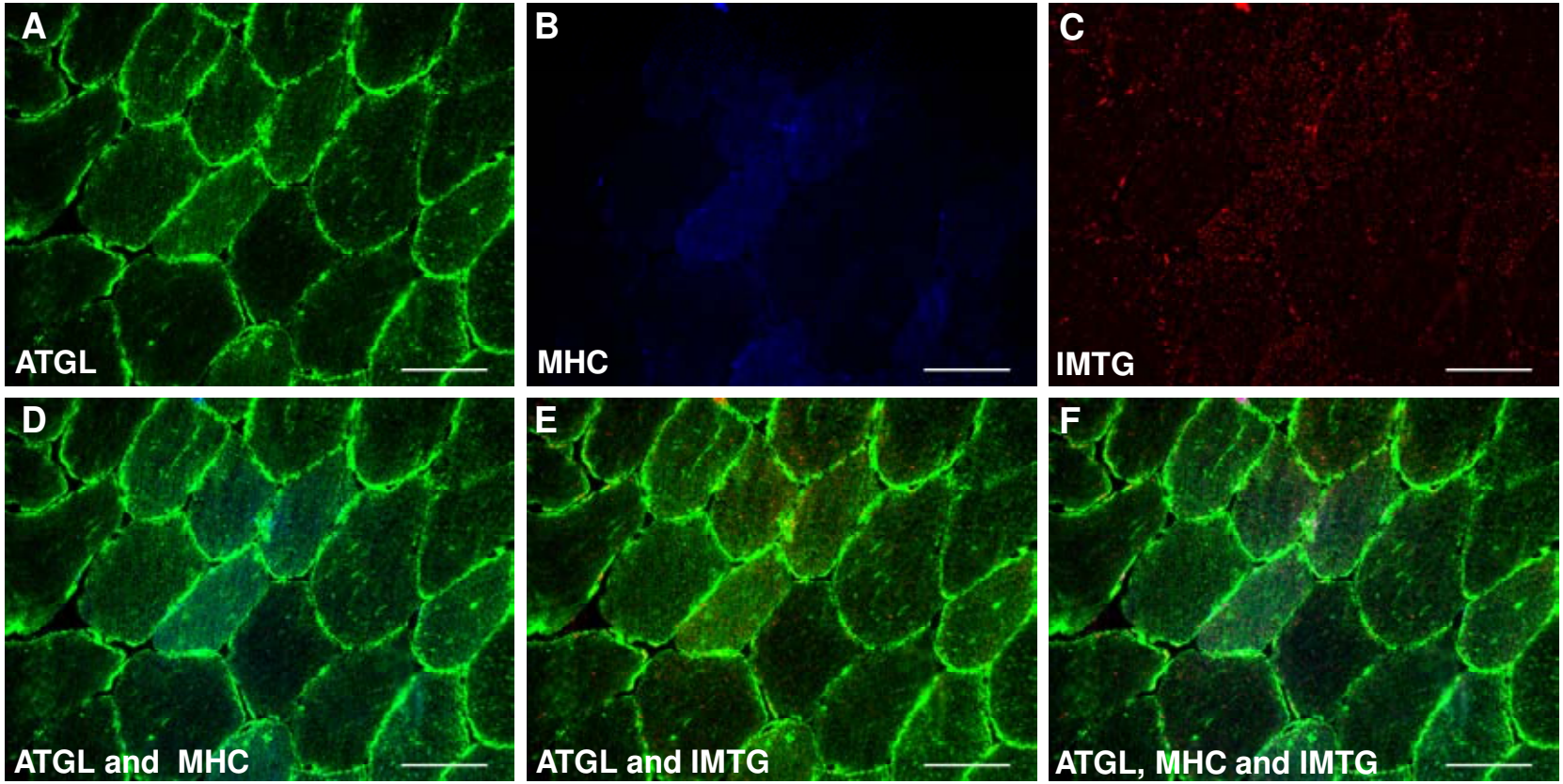

Figure 6.7. Cross sections showing (A) distribution of ATGL, (B) type I fibres using the MHCI stain, (C) IMTG stained with oil red O. Merged images of these stains are shown in panel D-F. Bar is 50 µm.

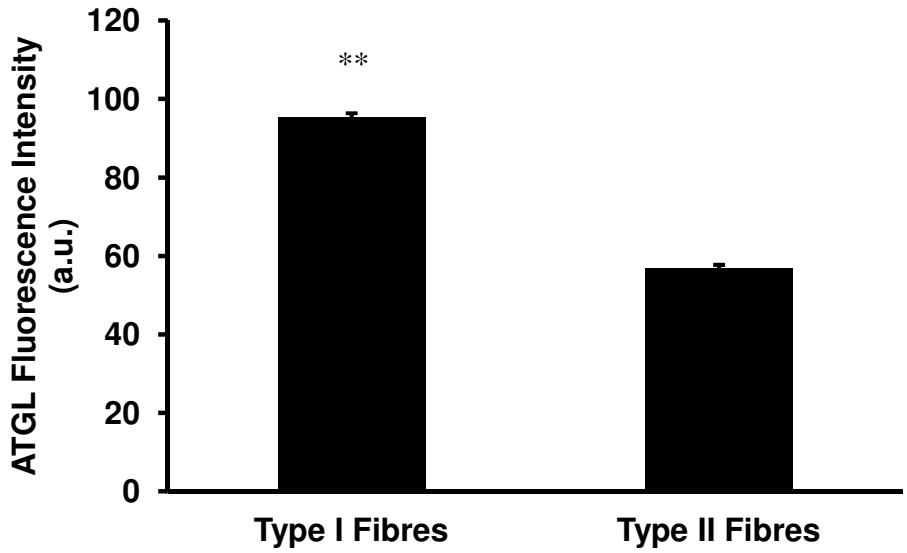

Figure 6.8. Fibre type specific ATGL fluorescence intensity. ** Significant difference between fibre types (P < 0.001). Data are mean ± SEM of 6 individuals.

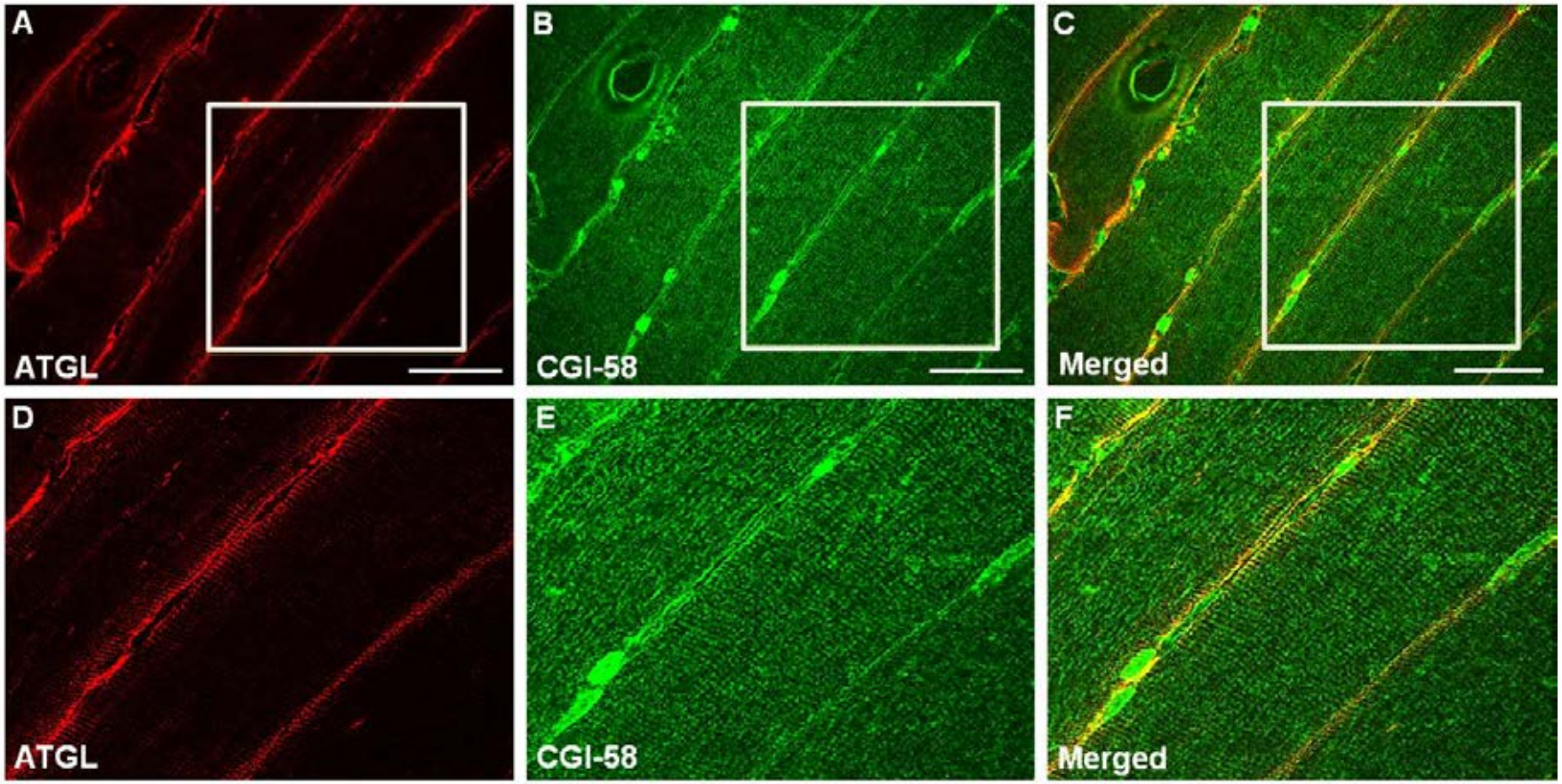

Figure 6.9. Representative images of costaining of ATGL (A) and CGI-58 (B) in human skeletal muscle. Merged images are shown in C. The area highlighted in white is shown at a larger magnification in images D, E and F. Bar is 50 µm.

6.5 Discussion

This study is the first to show spatial distribution of ATGL and CGI-58 in human skeletal muscle. Protein content of ATGL was higher in type I fibres and its staining intensity was greater in peripheral regions of the cells. Partial colocalisation of ATGL and CGI-58 was demonstrated within the cytosolic regions of the cell and a greater amount of colocalisation was seen at the cell periphery.

The observation that ATGL distribution is fibre type specific (Figure 6.8) is in line with earlier work of Jocken *et al.,* (2008) and was to be expected as lipid droplet content is greater in type I compared to type II fibres ((Figure 6.6; Chapters 3 and 4, and as shown in earlier work of others (Malenfant *et al.*, 2001;van Loon *et al.*, 2004;Shaw *et al.*, 2008)). There were no fibre type differences in the CGI-58 protein content. This may be related to the fact that CGI-58 has multiple roles, and apart from activating ATGL, is also involved in the acylation of lysophosphatidic acid (LPA) (Ghosh *et al.,* 2008;Montero-Moran *et al.,* 2009). For the distribution of ATGL, there did appear to be a difference in signal within the interior of the cells whether they were cross sections or longitudinally oriented. This, for the time being, remains unexplained. It may be that there were some problems with the penetration of the antibodies which could explain the weak signal in the cell interior in longitudinally oriented sections.

Colocalisation of CGI-58 with lipid droplets has been observed in adipocytes via a direct protein-protein interaction with perilipin 1 (Liu *et al.*, 2004). This colocalisation has also been observed in non lipid droplet compartments in adipocytes (Yamaguchi *et al.*, 2004;Subramanian *et al.*, 2004) and Chinese hamster ovary cells (Yamaguchi *et al.*, 2004).

Further, colocalisation of CGI-58 with the endoplasmic reticulum (ER) and golgi apparatus has been observed in hepatocytes (Brown *et al.*, 2007). However, very little colocalisation of CGI-58 and lipid droplets was observed in this study in human skeletal muscle (Figure 6.3). The staining of CGI-58 in the present study was diffuse throughout the muscle fibres on cross-sections (Figure 6.3) and a pattern with striations was observed in longitudinal sections (Figure 6.9E). This could potentially point at its presence at the ER in skeletal muscle. However, this would need confirmation in future studies through co-staining of an ER marker and CGI-58. There are still many gaps in our knowledge of lipolysis of lipid droplets in skeletal muscle, however, extrapolation of *in vitro* data (Murphy & Vance, 1999;Robenek *et al.*, 2006) suggests that the ER may be both the site of growth and lipolysis of small lipid droplets with the lipolytic enzymes ATGL, HSL and the activator CGI-58 potentially being located close to/at the ER for ease of access to the lipid droplets when lipolysis is required for FA generation during times of increased energy demand.

The absence of perilipin 1 in lipid droplets in skeletal muscle (Sztalryd *et al.*, 2003;Greenberg *et al.*, 1993;Londos *et al.*, 1995;Servetnick *et al.*, 1995) may explain why CGI-58 does not colocalise with lipid droplets in human skeletal muscle, as it has been shown in adipocytes that this interaction is dependent upon the presence of perilipin 1. In cardiomyocytes, CGI-58 binds specifically to lipid droplets containing perilipin 5 (MLDP/ OXPAT) (Granneman *et al.*, 2009a). It has been shown that ADRP (perilipin 2) regulates the access of ATGL to lipid droplets *in vitro* in human kidney cells and in mouse liver cells *(*Listenberger *et al.,* 2007;Bell *et al.,* 2008), however it is yet to be shown whether CGI-58 is also involved in this process.

The fact that CGI-58 was present in locations other than the lipid droplets was not unexpected as it has recently been suggested that CGI-58 may be involved in the regulation of other metabolic processes such as mediating the acylation of LPA (Ghosh *et al.*, 2008;Montero-Moran *et al.*, 2009). This would likely require localisation to the ER membrane which is the site where TAG synthesis occurs, as the acylation of LPA is one of the steps involved in this process (Takeuchi & Reue, 2009). The protein itself recently has also been shown to have enzymatic activity catalysing the CoA-dependent acylation of LPA (Montero-Moran *et al.*, 2010). The proposed function is that it channels FA released from hydrolysis of TAG into phospholipids (Montero-Moran *et al.*, 2010). This may explain its apparent homogenous distribution in the cytosol, presumably close to the ER where there may be small growing lipid droplets, as LPA (the substrate for CGI-58) is produced during phospholipid synthesis. Further, overexpression of CGI-58 leads to increased phospholipid content (Yamaguchi, 2010). Therefore it is possible that CGI-58 could be involved in both TAG hydrolysis (activating ATGL) and phospholipid synthesis dependent on the metabolic status of the cell (Lass *et al.*, 2010). The colocalisation of CGI-58 with myonuclei may be related to the observation that separate metabolically active pools of DAG (the product of the action of ATGL and CGI-58) exist in nuclei and are important in regulation of gene expression (D'Santos *et al.*, 1999).

The overall conclusion of this study is that ATGL content is higher in type I than in type II fibres, while a similar content was seen for CGI-58 in both fibre types. The merged images suggest that there is partial colocalisation of CGI-58 with lipid droplets however this requires further substantiation in future studies with the use of confocal microscopy which is the only valid method to quantitate colocalisation. ATGL however, did not appear to colocalise with

lipid droplets. These data suggest that, in the overnight fasted resting state, when lipolytic rates are low, ATGL and CGI-58 are not present in a high concentration in the lipid droplets in human skeletal muscle.

CHAPTER 7

VISUALISATION AND DISTRIBUTION OF SYNAPTOSOMAL-ASSOCIATED PROTEIN 23 IN SKELETAL MUSCLE OF LEAN, HEALTHY MALES

7.1 Abstract

Lipid droplets are present in skeletal muscle and provide a cellular store of lipid and a readily available fuel source during exercise in trained humans. SNARE proteins such as synaptosomal associated protein 23 (SNAP23) are also present in skeletal muscle and play a crucial role in docking and fusion processes including GLUT4 docking with the plasma membrane and fusion of lipid droplets. Recently, on the basis of *in vitro* observations in lipid loaded cardiomyocytes, suggestions have been made that in obesity, the lipid droplets may hijack SNAP23 from the plasma membrane and thus impair GLUT4 fusion and docking. The aim of this research was to develop methodology in order to visualise SNAP23 and investigate its subcellular distribution in human skeletal muscle using immunofluorescence microscopy. Percutaneous biopsies were obtained from the *m. vastus lateralis* of six lean, moderately active males in the rested, overnight fasted state. Cryosections (5µm) were then stained with antibodies targeting SNAP23, the mitochondrial marker, cytochrome c oxidase, and the plasma membrane marker, dystrophin. Intramuscular lipid droplets were stained using the neutral lipid dye oil red O in combination with immunofluorescence. Immunofluorescence staining of SNAP23 showed a diffuse stain throughout the fibres with additional areas of intense punctate staining within the cells. There was also intense staining at the peripheral regions of the cell. SNAP23 staining intensity was similar throughout both type I and type II fibres (P = 0.422). Confocal microscopy images showed colocalisation of SNAP23 with the plasma membrane (Pearson's correlation coefficient (r) = 0.499 ± 0.012) as well as diffuse and more intense punctate intracellular staining. The latter colocalised primarily with mitochondria (r = 0.504 ± 0.017) and to a lesser extent with lipid droplets (r = 0.208 ± 0.014). The distribution data are in line with the previously suggested main metabolic roles of

SNAP23, which are GLUT4 docking in the plasma membrane and shuttling of FAs generated by lipolysis of IMTG in lipid droplets into the mitochondria for subsequent β-oxidation.

7.2 Introduction

In humans, the SNAREs (Soluble N-Ethylmaleimide-Sensitive Factor (NSF) Attachment Protein Receptors) form a family of 36 proteins (Jahn & Scheller, 2006). Most SNARE proteins share a similar structure with a characteristic SNARE 'motif' which is a conserved sequence of 60 - 70 amino acids arranged in heptad repeats. The SNARE motif is connected by a short linker to the C-terminal end, which contains transmembrane domains. It is the SNARE motifs that mediate SNARE complex formation, forming helical core complexes which are extraordinarily stable. SNAREs are categorised according to the role they play in membrane fusion; vesicle-SNAREs (v-SNAREs) are found on the transport vesicles and target-SNAREs (t-SNAREs) are found at the plasma membrane. SNARE proteins play a crucial role in many intracellular docking and fusion processes, such as GLUT4 docking with the plasma membrane (Foster *et al.*, 1999;Kawanishi *et al.*, 2000b) and fusion of lipid droplets (Bostrom *et al.*, 2007).

Synaptosomal Associated Protein 23 (SNAP23) is a SNARE protein, which has been identified in non neural tissues and has been found to be an analogue of SNAP25 sharing high sequence homology (Ravichandran *et al.*, 1996). In its role as a SNARE protein, SNAP23 is able to bind with VAMP1 and 2 and also Syntaxin1, 2, 3 and 4 playing a role in targeted exocytosis. SNAP23 is a t-SNARE (for a review see (Bryant *et al.*, 2002) and it would therefore be expected to reside at the plasma membrane.

SNAP23 has also been proposed to play a role in lipid droplet-mitochondria interactions (Jagerstrom *et al.*, 2009) aiding the efficient delivery of fatty acids (FA) generated by lipolysis of intramuscular triglycerides (IMTG) of lipid droplets into the mitochondria for

subsequent β-oxidation. Therefore in both lean and trained individuals, it would also be expected that SNAP23 would reside within the cells specifically at the mitochondria and lipid droplets.

Lipid droplets are present in multiple cell types including skeletal muscle and provide a cellular store of lipid and a readily available fuel source during exercise in trained humans. It has been reported that one of the many adaptations to endurance training is a dispersal of larger lipid droplets into a larger number of smaller droplets (He *et al.*, 2004). This would increase the surface area making the IMTG more accessible to lipases and their activators and thus facilitate the utilisation of intramuscular lipids as a fuel during exercise. Electron microscopy has been used to demonstrate that in skeletal muscle, lipid droplets appear to be localised in close proximity to the mitochondria, presumably in order for efficient lipid oxidation during times of increased demand (Hoppeler, 1999). Further, using electron microscopy, an increased spatial contact between mitochondria and lipid droplets has been demonstrated following a seven week endurance training protocol in previously untrained individuals (Tarnopolsky *et al.*, 2007). In addition to this data, lipid droplets have been shown to be situated in close proximity to the mitochondrial network using confocal microscopy in skeletal muscle of lean, highly trained cyclists (Shaw *et al.*, 2008). This adaptation has been suggested to aid in the efficient oxidation of FAs liberated from lipid droplets upon lipolysis during exercise as it reduces the diffusion distance of the released FAs to the site of β-oxidation. In a recent study in fibroblasts, ablation of SNAP23 resulted in a decreased spatial complex formation between mitochondria and lipid droplets and decreased mitochondrial β-oxidation (Jagerstrom *et al.*, 2009). This has led to the suggestion that SNAP23 is implicated in the formation of functional lipid droplet-mitochondria complexes.

The purpose of the present study was to investigate whether the subcellular distribution of SNAP23 in human skeletal muscle is in agreement with the functional roles proposed above in the plasma membrane, mitochondria and lipid droplets. The developed staining methodologies are important as they generate the first detailed images of the distribution of SNAP23 in human skeletal muscle. The study was conducted using percutaneous muscle biopsies obtained in the resting, overnight fasted state from six lean, moderately active males and analysed using widefield and confocal fluorescence microscopy.

7.3 Methods

Measurement of VO_{2max}

Subjects performed a progressive exercise test to exhaustion on an electronically braked cycle ergometer to determine VO_{2max} as described in Chapter 4.3.

Muscle Samples

Percutaneous biopsies were obtained from the *m. vastus lateralis* of 6 lean, healthy, moderately active male subjects using the needle biopsy technique (Bergstrom, 1975). Subject characteristics can be seen in Table 7.1. Samples were prepared and stored as described previously in Chapter 2.2.

Table 7.1 Subject Characteristics

	Lean Male Participants
n	**6**
Age (y)	**20.2 ± 0.7**
Height (m)	**1.79 ± 0.03**
Body Mass (kg)	**72.0 ± 2.8**
Body Mass Index (BMI) (kg/m^2)	**22.4 ± 0.4**
VO_2 max (ml/min/kg)	**55.8 ± 1.8**
Wmax (W)	**282.0 ± 17.0**

Data are presented as means ± SEM.

Antibody Validation Overview

Validation of the selected antibody was completed using the methods described in Chapter 2.3.1.1. Western blotting revealed a single band at the correct molecular weight (23 kDa) as well as an additional band at ~ 75 kDa (Figure 7.1). This additional band may relate to an extracellular protein as extracellular staining was visible in Figure 7.5. Also, the BLAST analysis indicated a single match in human skeletal muscle of the target sequence to SNAP23 and its shorter isoform SNAP23B.

SNAP23 Green Fluorescent Protein – Transfection

In addition to the aforementioned techniques, a green fluorescent protein (GFP) transfection study was also completed. A human cancer cell line (HeLa cells) were transfected with human GFP-tagged SNAP23 cDNA (Amsbio, Abingdon UK). Cells were incubated with 100 µg SNAP23-GFP construct for 48 hours before fixing in 4 % paraformaldehyde for 20 minutes before washing 3 times, for 5 minutes each in PBS. The plate was then washed using PBS and 0.2 % triton X-100. The cells were then stained using anti-SNAP23 (Synaptic Systems, Germany) (1 hour incubation at room temperature). The primary antibody was applied in the dilution series 1:100, 1:200, 1:500 as well as a control with no primary antibody. This allowed for 4 repeats on the 96 well plate. The secondary antibody (donkey anti-rabbit IgG 647) (Invitrogen, Paisley, UK) was applied for 30 minutes at room temperature. The cells were also counterstained with the nuclear stain Hoechst. The plate was then imaged using ImageXpress software (California, USA).

The HeLa cells displayed a heterogenous expression of the plasmid. The antibody did successfully colocalise with the transfected GFP-tagged SNAP23 (Figure 7.2). The antibody

was also able to detect variations in SNAP23 (Figure 7.3) as quantification of the cytoplasmic intensities of SNAP23-GFP and of the immunostaining with anti-SNAP23 showed a linear relationship.

On the basis of these antibody validation tests this antibody (anti-SNAP23, Synaptic Systems) was selected for use in this study.

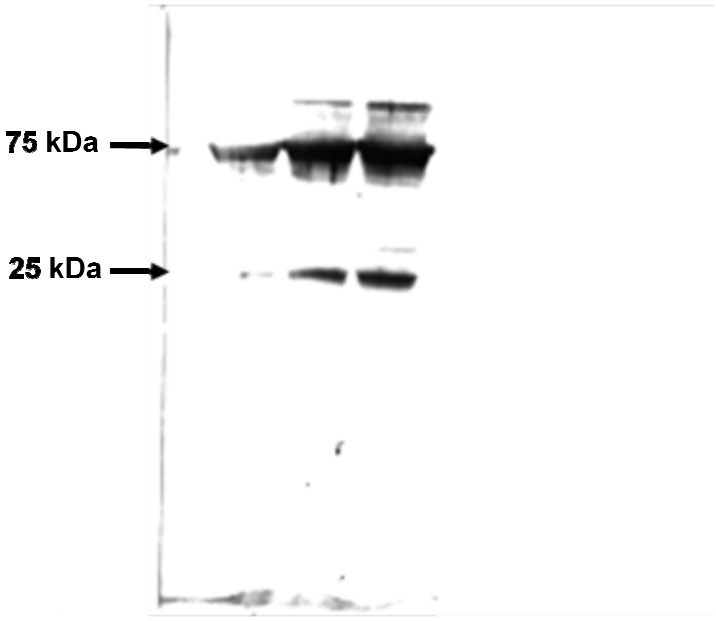

Figure 7.1. Immunoblot using anti-SNAP23 (Synaptic Systems, Germany) of a homogenate of human skeletal muscle from a lean individual.

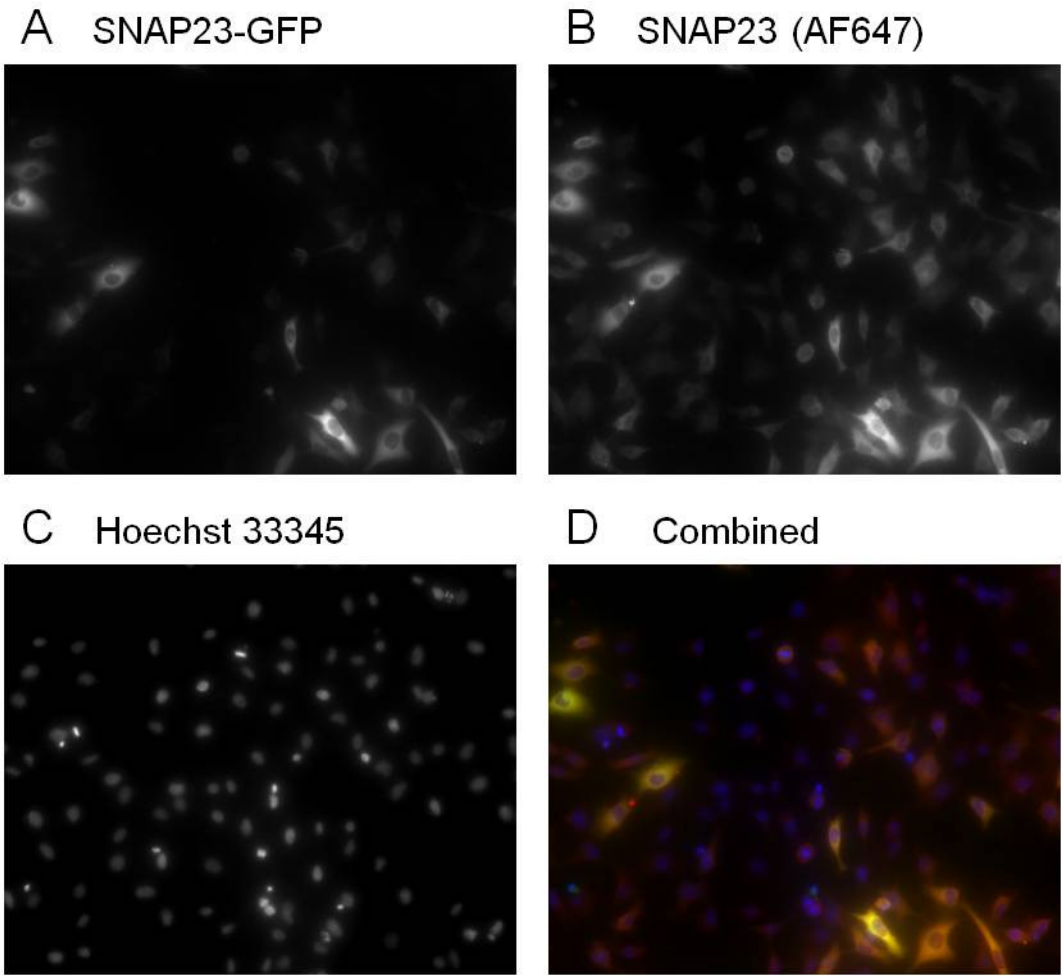

Figure 7.2. HeLa cells transfected with 100 µg SNAP23-GFP plasmid incubated for 48h. The cells displayed a heterogenous expression of the plasmid and show colocalisation of SNAP23-GFP and immunostaining for SNAP23 with anti-SNAP 23 (1:100 dilution). In the merged image (D) the SNAP23-GFP plasmid is visualised in green, SNAP23 stained with anti-SNAP23 in red, nuclei in blue, and colocalisation of SNAP23-GFP with anti-SNAP23 in yellow.

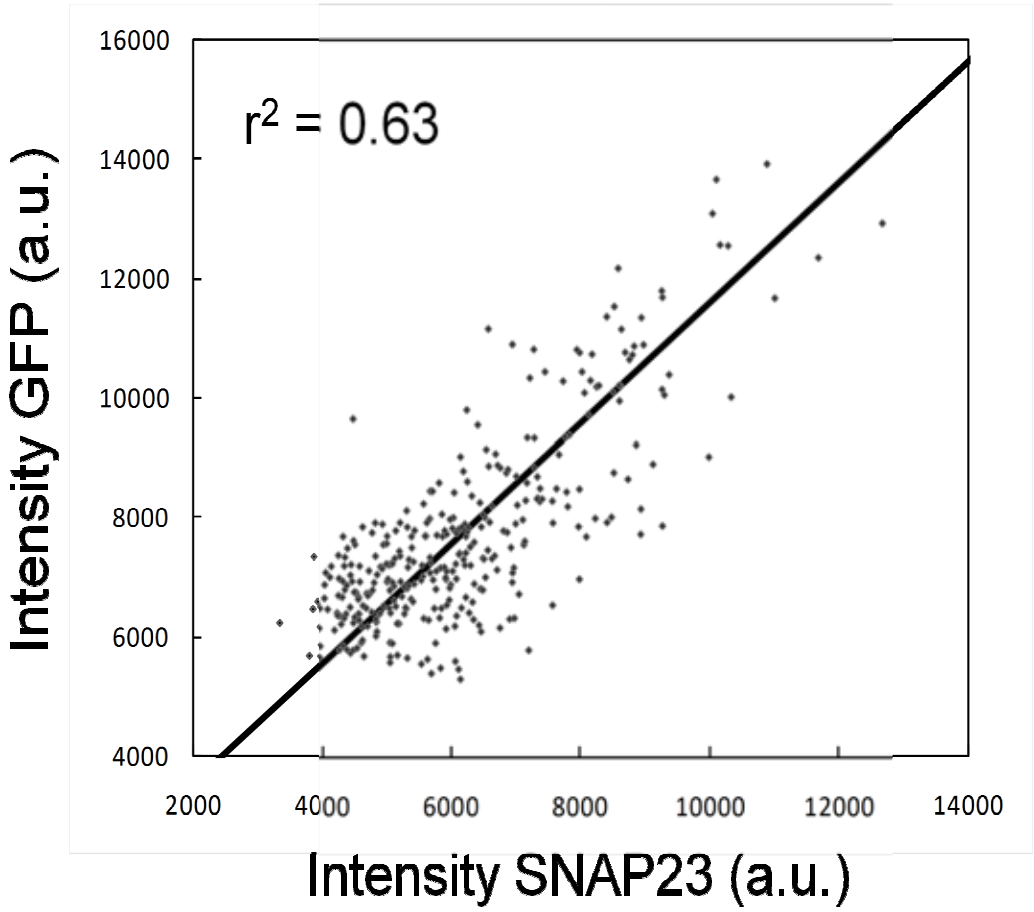

Figure 7.3. Quantification of the cytoplasmic fluorescence intensities of SNAP23-GFP and immunostaining with anti-SNAP23. Data points are obtained from 337 cells in 3 replicate wells and show a linear relationship.

Antibodies

Images of the spatial distribution of SNAP23 were obtained with anti-SNAP23 (Synaptic Systems, Goettingen, Germany). This antibody was used in combination with others in order to further investigate the specific subcellular distribution of SNAP23. Mitochondria were visualised using anti-cytochrome c oxidase (COX) (Invitrogen, Paisley, UK). The secondary Alexa Fluor conjugated antibodies applied were goat anti rabbit IgG (targeting SNAP23) and goat anti mouse IgG_{2a} (targeting COX). The plasma membrane of the cells was visualised using anti-dystrophin (Sigma Aldrich, UK). The secondary Alexa Fluor conjugated antibodies applied were goat anti rabbit IgG (targeting SNAP23) and goat anti mouse IgG_{2b} (targeting dystrophin). Fibre type was determined using anti-myosin heavy chain type I (MHCI) (developed by Dr. Blau, DSHB, Iowa, USA). The secondary Alexa Fluor conjugated antibodies applied were goat anti rabbit IgG (targeting SNAP23) and goat anti mouse IgM (targeting MHCI). IMTGs were stained using the neutral lipid dye oil red O in combination with immunofluorescence using the method developed by Koopman *et al.,* (2001) as described previously in Chapter 2.3.1.4.

Immunofluorescence Staining

Cryosections were treated using fixation, permeabilisation and antibody application methods described in Chapter 2.4. For immunofluorescence staining, anti-SNAP23 was used at a dilution of 1:50.

Fluorescence Microscopy

Images were captured using a Nikon E600 microscope coupled to a SPOT RT KE colour 3 shot CCD camera (Diagnostic instruments Inc, MI, USA) using the excitation filters described

in Chapter 2.5 to visualise Alexa Fluor 350, 488, 594 as well as oil red O. Widefield images were obtained in order to examine the fibre type specificity of SNAP23 using MHCI. Digital images showing the distribution of SNAP23 and IMTG in longitudinally oriented and cross sections of muscle fibres were obtained. Detailed digital images demonstrating the cellular distribution of SNAP23, COX, IMTG and dystrophin were obtained using an inverted confocal microscope (Leica DMIRE2, Leica Microsystems) with a 63 x oil immersion objective using the excitation wavelengths described in Chapter 2.5.

Image Processing

Images were processed using Image-Pro Plus 5.1 software (Media Cybernetics, MD, USA). Lipid and mitochondria content was expressed as the area fraction stained by dividing the stained area in the fibre by the total area of that fibre. Colocalisation was investigated in the confocal microscopy images using Pearson's correlation analysis using Image-Pro Plus 5.1 software. An average of 14 images were investigated per participant. Each image contained approximately seven fibres leading to a total of 98 fibres analysed for colocalisation. The significance of this colocalisation was also investigated by overlaying staining of non-matched sections and analysing these images using the same method as matched images as described previously by Lachmanovich *et al.,* (2003). This enabled us to investigate whether the colocalisation was significantly higher in matched than non matched images.

Automated Image Capture and Analysis

The routine analysis of IMTG and mitochondria was completed using automated image analysis as described in detail in Chapter 2.5.2. In the widefield images obtained using

automated analysis a mean of 684 type I fibres were analysed and a mean of 740 type II fibres were analysed per participant.

Automated Image Processing

Images were analysed in detail using Definiens Cellenger software (Munich, Germany) as described in Chapter 2.5.3.

Statistics

Total mitochondria and total IMTG content of type I and type II fibres were compared using a paired samples t-test. Comparisons of both mitochondria and IMTG content was also compared using a paired samples t-test. The fibre type specific SNAP23 distribution was investigated using a paired samples t-test. Colocalisation was investigated using Pearson's correlation coefficient. Statistical significance was set at $P < 0.05$. All data are expressed as mean ± SEM.

7.4 Results

SNAP23 Distribution.

Immunofluorescence staining of human skeletal muscle obtained from 6 lean individuals showed diffuse staining throughout the individual fibres with some more intense puncta stained within the cells (Figure 7.4A). Some parts of the cell border regions were also stained with a greater intensity than other regions of the cell (Figure 7.4A). In longitudinally oriented sections, SNAP23 appeared to show a regular distribution with a network like structure (Figure 7.4B), similar to that shown previously for mitochondria in skeletal muscle (Shaw *et al.*, 2008). The staining was of similar intensity throughout both type I and type II fibres (Figure 7.4C) with no significant difference (type I: 57 ± 2 vs. type II: 56 ± 2, $P = 0.422$) in SNAP23 fibres positively stained as type I fibres and MHCI negative fibres.

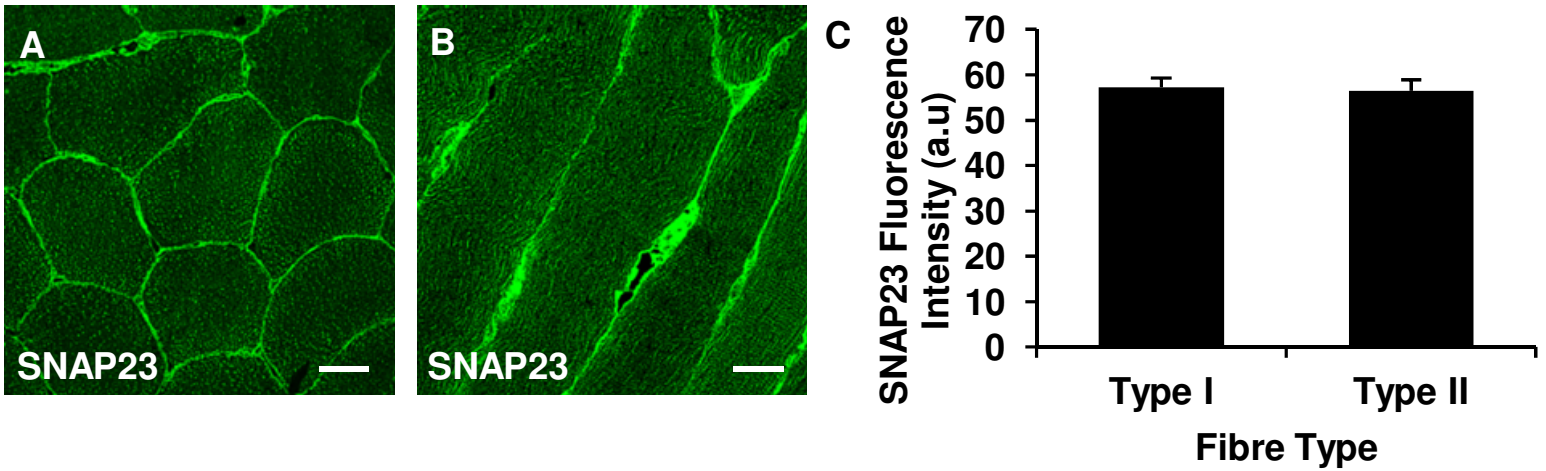

Figure 7.4. SNAP23 distribution in cross sections (A) and longitudinally oriented sections (B) of human skeletal muscle. Images were obtained using a 63 x oil immersion objective of a confocal microscope. Bar is 30µm. There was no difference in the fluorescence intensity of SNAP23 between type I and type II fibres (C) where type I fibres were positively labelled with anti-MHCI.

SNAP23 and Dystrophin

Immunofluorescence staining in cross sections of human skeletal muscle revealed an intense stain in peripheral regions of the cell. Combined staining of SNAP23 with the plasma membrane marker dystrophin revealed partial colocalisation (r = 0.499 ± 0.012) (Figure 7.5A). When comparing non-matched image overlays, to determine whether the colocalisation was significant, an r of 0.007 ± 0.003 was obtained, implying that the colocalisation in the matched overlays was significant ($P < 0.001$) (Figure 7.6A).

SNAP23 and COX

Immunofluorescence staining of SNAP23 in cross sections of human skeletal muscle also showed a diffuse intracellular stain interspersed with some intense punctate staining. When stained in combination with the mitochondrial marker COX, it was shown that the punctate staining partially colocalised with mitochondria (r = 0.504 ± 0.017) (Figure 7.5B). For the SNAP23 and COX non matched images an r of 0.006 ± 0.005 was obtained, implying that the colocalisation in the matched overlays was significant ($P < 0.001$) (Figure 7.6B). It was also found that the staining intensity of the COX stain was greater in type I fibres (147 ± 7) compared to type II fibres (136 ± 7) ($P = 0.035$) (Figure 7.7A).

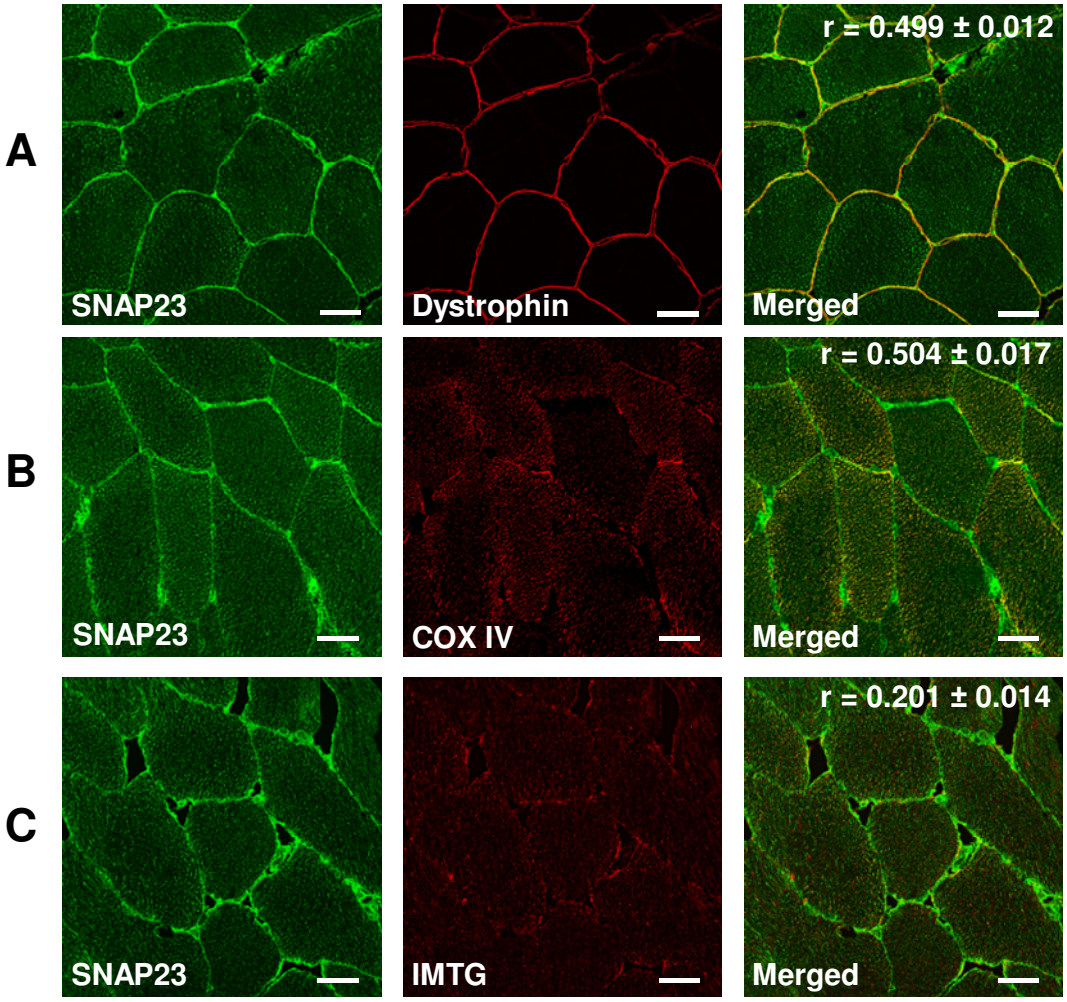

Figure 7.5 Representative images showing SNAP23 colocalisation with the plasma membrane marker dystrophin (A), mitochondrial marker COX (B) and IMTG staining using oil red O (C). All images were obtained using a 63x oil objective of a confocal microscope. Bar = 30 µm. Mean Pearson's correlation values are shown on the merged images.

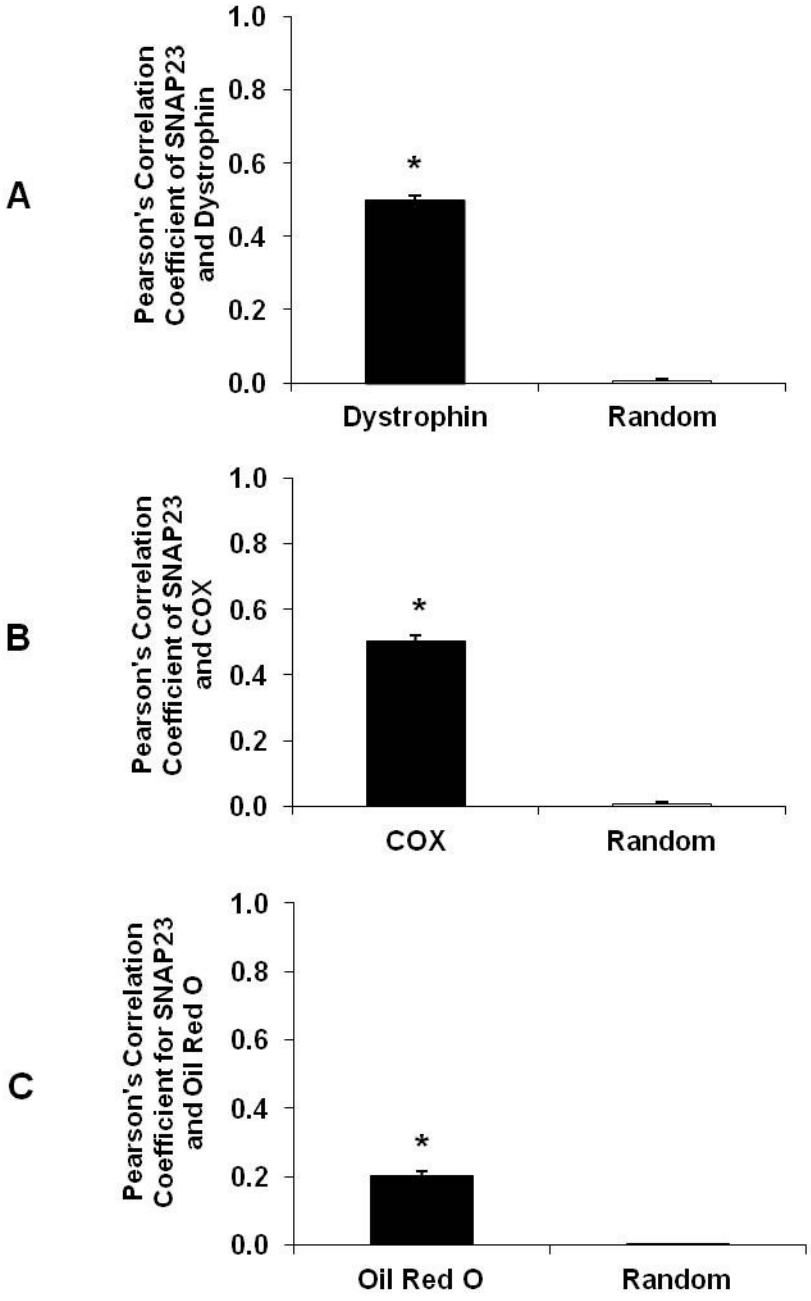

Figure 7.6. SNAP23 colocalisation with the plasma membrane labelled with anti-dystrophin (A), the mitochondria labelled with COX (B) and lipid droplets labelled with oil red O (C). Random bar represents the mean colocalisation of non matched pairs of images. Data are mean ± SEM. * Denotes a significant difference between matched and non matched images at P < 0.05.

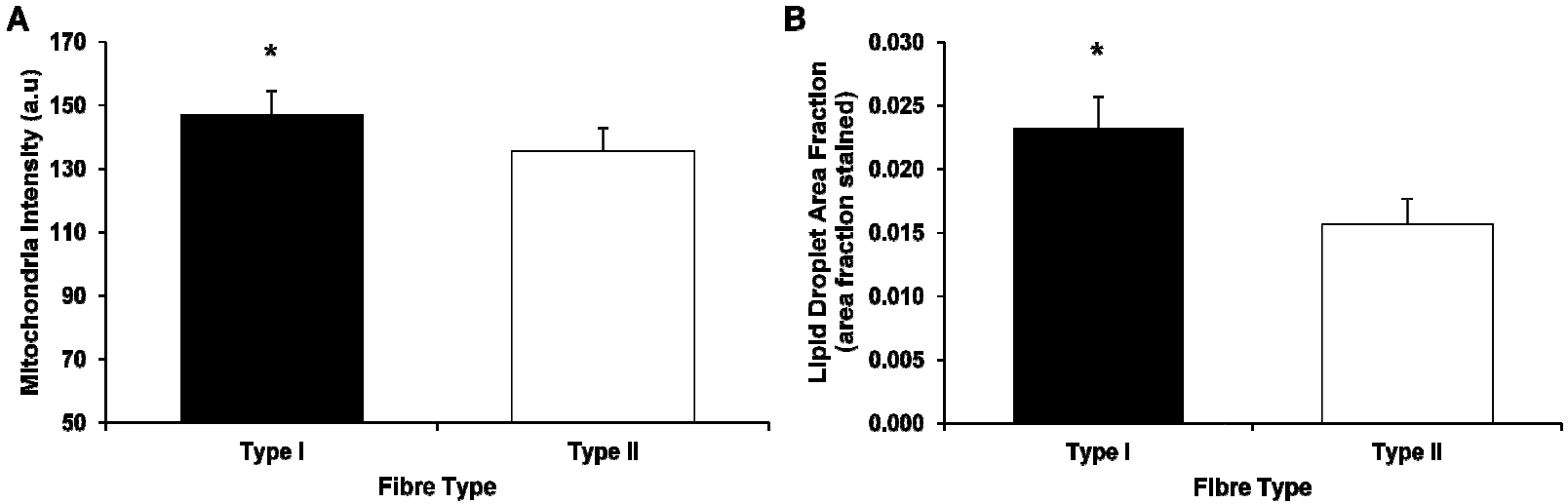

*Figure 7.7. Fibre type specific mitochondria intensity (A) and lipid droplet area fraction (B) (expressed as area fraction stained). Data are mean ± SEM. * Denotes a significant difference between fibre types (P < 0.05).*

SNAP23 and Oil Red O

SNAP23 was also stained in combination with the neutral lipid dye oil red O in order to investigate its colocalisation with the intramuscular lipid droplets. SNAP23 showed a weak, partial colocalisation with oil red O (r = 0.201 ± 0.014) (Figure 7.5C). For the non matched images the mean colocalisation was r = 0.000 ± 0.003, implying that the colocalisation in the matched images was significant (P = 0.0001) (Figure 7.6C).

Quantitative analysis of the lipid droplets revealed no difference in lipid droplet size between the type I (15.17 ± 0.63) and type II (16.09 ± 0.79) fibres (P = 0.086). It was however shown that type I lipid droplet area fraction (0.023 ± 0.002) was significantly greater than type II lipid droplet area fraction (0.016 ± 0.002) (P = 0.004) (Figure 7.7B).

7.5 Discussion

As SNAP23 is a t-SNARE and has been proposed to play a role in the docking and fusion of GLUT4 vesicles into the plasma membrane (Foster *et al.*, 1999;Kawanishi *et al.*, 2000b), a high degree of colocalisation with the plasma membrane would be expected. This indeed was confirmed in the images (Figure 7.5), which show a partial colocalisation with the plasma membrane marker dystrophin. Our data are in line with results recently obtained in human skeletal muscle from lean individuals using widefield immunofluorescence microscopy (Bostrom *et al.*, 2010). A high SNAP23 content has also been observed in the plasma membrane of cardiomyocytes (Bostrom *et al.*, 2007) and in plasma membrane fractions of rat adipocytes (St-Denis *et al.*, 1999). Collectively these data suggest that SNAP23 resides at the plasma membrane ready to enable GLUT4 docking with the membrane in the basal fasted state before meal ingestion or exercise both of which enhance GLUT4 docking and fusion.

The hypothesis that SNAP23 is involved in the formation of lipid droplet-mitochondria complexes is based on recent observations in fibroblasts (Jagerstrom *et al.*, 2009). It has been proposed that these complexes play a functional role in the channelling of FA liberated by lipolysis into the mitochondria for subsequent β-oxidation. The partial colocalisation between SNAP23 and the mitochondrial stain COX observed in this study has a higher Pearson's correlation coefficient than the colocalisation with lipid droplets and is the first evidence in humans that SNAP23 may also exert this FA channelling role in human skeletal muscle *in vivo* (Figure 7.5).

In conclusion, this study reveals that in the muscle of lean, healthy, moderately active men, SNAP23 primarily resides at the plasma membrane and in close proximity to the

mitochondria. A weak colocalisation was observed with the lipid droplets. These distribution data are in line with the previously suggested main metabolic roles of SNAP23; GLUT4 docking in the plasma membrane and shuttling of FAs generated by lipolysis of IMTG of lipid droplets into the mitochondria for subsequent β-oxidation.

7.6 Acknowledgements

I would like to thank Dr Ed Ainscow (AstraZeneca, UK) for expertise and guidance in the running the GFP-Transfection experiment.

I would also like to thank James Pilling (AstraZeneca, UK) for the expertise in the automated image acquisition and analysis using algorithms written for the Definiens software.

CHAPTER 8

SYNAPTOSOMAL-ASSOCIATED PROTEIN 23 DISTRIBUTION IN AGEING NON OBESE AND OBESE FEMALES

8.1 Abstract

The aim of this study was to investigate the distribution of SNAP23 in skeletal muscle of non obese and obese women using immunofluorescence microscopy to generate evidence for the hijacking hypothesis and to investigate the potential role of SNAP23 in mitochondrial FA oxidation. Participants were six non obese (age: 62 ± 3 years, BMI: 22.6 ± 1.4, HOMA-IR 3.9 ± 1.2) and six obese women (age: 68 ± 3 years, BMI: 33.3 ± 1.6, HOMA-IR: 6.2 ± 1.3) undergoing elective orthopaedic surgery. Biopsies were obtained from the *m. gluteus maximus* during hip arthroplasty. Cryosections (5µm) were stained with antibodies targeting SNAP23, mitochondria and the plasma membrane. Lipid droplets were visualised using oil red O. There was no difference in lipid droplet or mitochondria content between non obese and obese individuals in either type I or type II fibres. In both groups SNAP23 showed partial colocalisation with the plasma membrane (Pearson's correlation non obese: r = 0.39 ± 0.01, obese: r = 0.37 ± 0.03, P = 0.640) and with the mitochondria with significantly more colocalisation with the mitochondria in the non obese women (non obese: r = 0.34 ± 0.03, obese: r = 0.27 ± 0.03, P=0.037). SNAP23 showed a more weak colocalisation with lipid droplets with no difference between groups (non obese: r = 0.12 ± 0.02, obese: r = 0.07 ± 0.02, P = 0.277). This study does not confirm the hypothesis that more SNAP23 hijacking would occur in obese than non obese elderly women as there was no difference in the colocalisation of SNAP23 with the lipid droplets or the plasma membrane between the groups. The reduced colocalisation of SNAP23 with the mitochondria in the obese women may suggest a target for investigation of the reduced IMTG oxidation in obesity, and for larger increases in the concentration of FA metabolites that have been proposed to lead to insulin resistance of skeletal muscle.

8.2 Introduction

SNAP23 has also been proposed to play a role in lipid droplet fusion as addition of short interfering RNA inhibiting SNAP23, syntaxin 5 and VAMP4 led to a decrease in the rate of lipid droplet fusion in cardiomyocytes (Bostrom *et al.*, 2007). Furthermore, incubation of cardiomyocytes with oleic acid resulted in an increase in lipid droplet fusion, the growth of lipid droplets and a decrease in insulin sensitivity. It was proposed that the process of lipid droplet fusion reduces the SNAP23 content in the plasma membrane and subsequently limits GLUT4 docking and inhibits insulin-mediated glucose uptake. This impairment in glucose uptake was overcome with SNAP23 transfection and subsequent replenishment of the plasma membrane SNAP23 pool (Bostrom *et al.*, 2007). These *in vitro* findings led to the proposal of the hypothesis that fusing lipid droplets in the muscle of obese sedentary individuals and patients with type 2 diabetes might be able to hijack SNAP23 and thus reduce its content in the plasma membrane and impair GLUT4 fusion and docking (Sollner, 2007). Bostrom *et al.,* (2010) generated evidence in support of the hijacking hypothesis in patients with type 2 diabetes as, using immunofluorescence microscopy they observed a redistribution of SNAP23 away from the plasma membrane to the cell interior (specifically, to the microsomal/cytosolic compartment) in comparison with results obtained in healthy, lean, insulin sensitive individuals.

It has been known for a long time that there is close spatial contact between the phospholipid monolayer of the lipid droplets and the mitochondrial outer membrane (Hoppeler, 1999;Shaw *et al.*, 2008) and the total contact area is known to increase following a period of exercise training (Tarnopolsky *et al.*, 2007). SNAP23 has been proposed to play a role in increasing the efficiency of mitochondrial β-oxidation of FA by forming complexes between lipid

droplets and mitochondria which channel the FA derived from IMTG lipolysis into the mitochondria for oxidation. This suggestion is based on observations by Jagerstrom *et al.,* (2009) in fibroblasts. Ablation of SNAP23 using siRNA reduced complex formation and β-oxidation, which suggested that these lipid droplet-mitochondria complexes are functional in living cells (Jagerstrom *et al.*, 2009). It may be that exercise training leads to a more efficient SNAP23 mediated fusion process between lipid droplets and mitochondria then it could also be part of the mechanism that allows trained individuals to utilise IMTG at much higher rates than sedentary and obese individuals (Schrauwen-Hinderling *et al.*, 2003;Van Proeyen *et al.*, 2011), while simultaneously keeping the intramuscular concentration of FA metabolites low and therefore insulin sensitivity high. The high colocalisation between SNAP23 and mitochondria observed in Chapter 7 in lean, healthy, moderately trained men would be in line with the proposed role of SNAP23 in establishing these functional lipid droplet-mitochondria complexes.

This study had two main aims. The first aim was to investigate the hypothesis that SNAP23 hijacking by lipid droplets is more pronounced in obese ageing women than in age-matched non obese controls and leads to a larger reduction in the colocalisation of SNAP23 with the plasma membrane. The second aim was to investigate the hypothesis that SNAP23 colocalisation with the mitochondria is lower in the obese ageing women than in age-matched non obese controls. Both of these mechanisms might lead to larger impairments in glucose tolerance and insulin sensitivity in the obese women. In order to investigate these hypotheses the methods described in Chapter 7 will be applied to percutaneous muscle biopsies of obese and non obese women to measure colocalisation of SNAP23 with lipid droplets, the plasma membrane and mitochondria.

8.3 Methods

Muscle Samples

Percutaneous muscle biopsies were obtained from the *m. gluteus maximus* of six non obese women and six obese women during elective orthopaedic surgery. Subject characteristics can be seen in Table 8.1. All participants were undergoing total hip arthroplasty at Russells Hall Hospital (Dudley Group of Hospitals) and gave their informed consent for participation in this study. The study was approved by the local NHS Research Ethics Committee. An ~ 300mg muscle biopsy was taken by Consultant Surgeon, Mr. Edward Davis immediately following the initial incision.

Table 8.1 Subject Characteristics

	Non Obese Females	Obese Females
n	**6**	**6**
Age (y)	**62 ± 3**	**68 ± 3**
Height (m)	**1.59 ± 0.03**	**1.60 ± 0.03**
Body Mass (kg)	**57.4 ± 4.5**	**85.1 ± 4.7***
Body Mass Index (BMI) (kg/m^2)	**22.6 ± 1.4**	**33.3 ± 1.6***
Fasting plasma glucose (mmol/L)	**6.98 ± 0.36**	**6.32 ± 0.36**
Fasting serum insulin (µU/ml)	**11.91 ± 3.23**	**21.53 ± 4.04**
HOMA IR	**3.92 ± 1.15**	**6.19 ± 1.25**

Data are presented as means ± SEM. * $P < 0.05$

Samples were prepared and stored at -80 °C as described previously in Chapter 2.2. For immunofluorescence analysis, cryosections (5 µm) were cut using a microtome (Bright Instrument Company Limited, Huntingdon, England).

Blood Analyses

Following anaesthesia, blood was collected into two vacutainers, one containing EDTA (for plasma). Blood samples were centrifuged at 3,500 rpm for 15 min at 4°C. Aliquots of serum and plasma were then frozen and stored at −80°C until later analysis. Plasma glucose concentration was analyzed using an ILAB automated analyzer (Instrumentation Laboratory, Cheshire, UK). Serum insulin concentrations were measured using ELISA (Invitrogen, Paisley, UK).

Antibodies

The antibodies used in this study are the same as those used in Chapter 7. Each antibody used is detailed in Chapter 7.3. Details of SNAP23 antibody validation procedures can also be found in Chapter 7.3.

Immunofluorescence Staining

Cryosections were stained using methods described in Chapter 2.4. Identical methods to those used in this chapter can be found in Chapter 7.3.

Fluorescence Microscopy

Images were captured using a Nikon E600 microscope coupled to a SPOT RT KE colour 3 shot CCD camera (Diagnostic instruments Inc, MI, USA) using the excitation filters described in Chapter 2.5 and 7.3. For colocalisation analyses, detailed digital images were captured using an inverted confocal microscope (Leica DMIRE2, Leica Microsystems) as described in Chapter 2.5 and 7.3.

Image Processing

Image processing was completed in this Chapter using methods identical to Chapter 7. For details of lipid and mitochondrial image processing and colocalisation analyses see Chapter 7.3.

Automated Image Capture and Analysis

Details of automated image capture and analysis can be found in Chapter 2.5.2 and 7.3. Automated image analysis was used for fluorescence intensity, lipid and mitochondria analysis. Images were captured with widefield microscopy using a 40 x oil objective.

Automated Image Processing

Details of automated image processing using Definiens Cellenger software (Munich, Germany) can be found in Chapter 2.5.3 and 7.3.

Statistics

The total IMTG content (expressed as area fraction stained) and the total mitochondria area fraction and intensity of type I and type II fibres were compared using an independent samples t-test. Between group differences in IMTG content and mitochondrial content and intensity were also investigated using an independent samples t-test. Colocalisation of SNAP23 with lipid droplets, plasma membrane and mitochondria was investigated using Pearson's correlation coefficient. Statistical significance was set at $P < 0.05$. All data are expressed as mean ± SEM.

8.4 Results

Non obese and obese women were recruited with significantly different body mass and BMI (48 % and 47 % higher respectively in the obese group) (Table 8.1). However, the groups were not significantly different in their fasting plasma glucose and serum insulin concentrations nor insulin resistance as assessed by HOMA-IR (Table 8.1).

The overall staining patterns of SNAP23 appeared to be similar in both the non obese and obese individuals. The distribution of SNAP23 showed a diffuse stain throughout the fibres, some of which were speckled with some more intense punctate signal. Interestingly in some fibres, there appeared to be a strong, diffuse stain of SNAP23, far stronger than that observed in the 'speckled' fibres however this particular distribution was not present in every section examined. There was no difference between the groups in the detection of these bright fibres ($P > 0.05$). Of the fibres examined, the intense staining was detected in 17 ± 7 % of fibres investigated in non obese individuals whereas in obese individuals the intense staining was detected in 25 ± 4 % of fibres examined. There was also an intense stain in peripheral regions of the cell.

Cell area was greater in type I fibres compared to type II fibres in non obese individuals (type I: 12580.16 ± 804.77 μm^2 vs. type II: 11135.17 ± 643.35 μm^2, $P = 0.05$) however this relationship only tended towards significance in the obese individuals (type I: 12569.44 ±756.15 μm^2 vs. type II: 11354.95 ± 758.56 μm^2, $P = 0.07$). There was no difference in cell area between the groups in either type I or type II fibres ($P > 0.05$).

SNAP23 and Dystrophin

In both non obese and obese individuals, SNAP23 showed a strong stain in some regions at the cell borders (Figure 8.1A and 8.1B). SNAP23 was stained in combination with anti-dystrophin to determine its colocalisation with the plasma membrane. In skeletal muscle of non obese women, SNAP23 partially colocalised with the plasma membrane marker dystrophin (r = 0.387 ± 0.014) (Figure 8.1A and 8.1C). A similar degree of colocalisation was seen in skeletal muscle obtained from obese women (r = 0.368 ± 0.029) (P = 0.643) (Figure 8.1B and 8.1C). Both of these values were significantly higher (P = 0.001) than the colocalisation seen in non matched pairs of images (non obese r = 0.004 ± 0.004 and obese r = 0.003 ± 0.004) (Figure 8.1C).

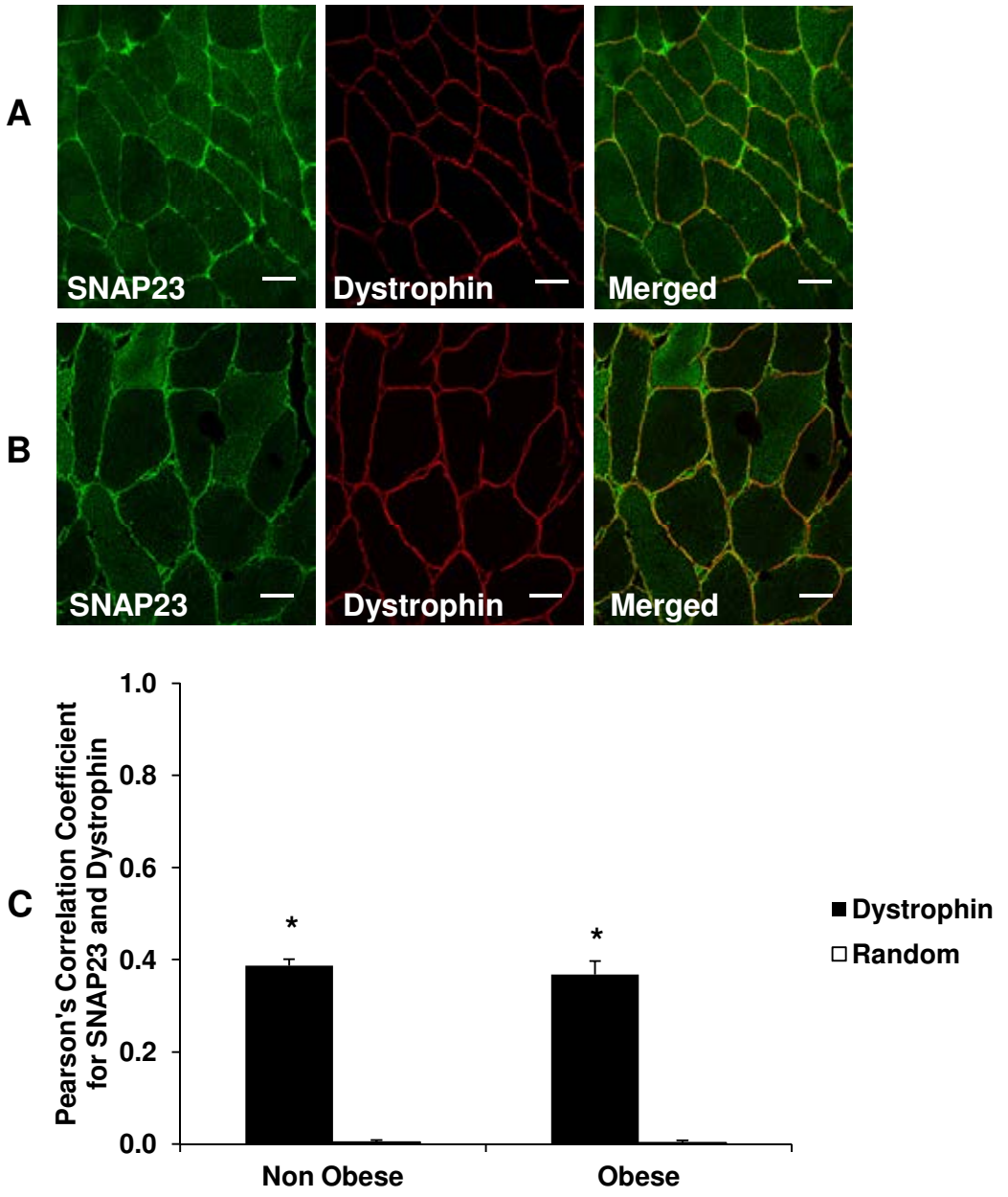

*Figure 8.1. Representative images showing colocalisation of SNAP23 with the plasma membrane (stained using anti-dystrophin) in skeletal muscle of non obese women (A) and obese women (B). Bar is 30 µm. Pearson's correlation coefficients are shown in panel C. * Denotes a significant difference between matched and non matched images at P < 0.05.*

SNAP23 and COX

In both the non obese and obese women, immunofluorescence staining of SNAP23 showed a diffuse intracellular stain interspersed with more intense punctate staining. When stained in combination with the mitochondrial marker COX, it was shown that the punctate staining partially colocalised with mitochondria. Mitochondrial staining showed similar images to those shown in an earlier publication from our laboratory (Shaw *et al.*, 2008), with a punctate appearance that was more dense in the peripheral regions of the cell (Figure 8.2A and 8.2B). In skeletal muscle obtained from non obese women, SNAP23 partially colocalised with mitochondria (r = 0.344 ± 0.030) (Figure 8.2A and 8.2C). This value was significantly greater than the colocalisation occurring in non-matched images (r = 0.015 ± 0.002, P = 0.0001) (Figure 8.2C). In the skeletal muscle obtained from obese women, SNAP23 also partially colocalised with mitochondria (r = 0.265 ± 0.027) (Figure 8.2B and 8.2C) which was again significantly greater than the colocalisation of non matched images (r = 0.006 ± 0.005, P = 0.0002) (Figure 8.2C). The degree of colocalisation between SNAP23 and mitochondria in the skeletal muscle of the non obese women was significantly greater than of the obese women (non obese: r = 0.344 ± 0.030 vs. obese: r = 0.265 ± 0.027, P = 0.037).

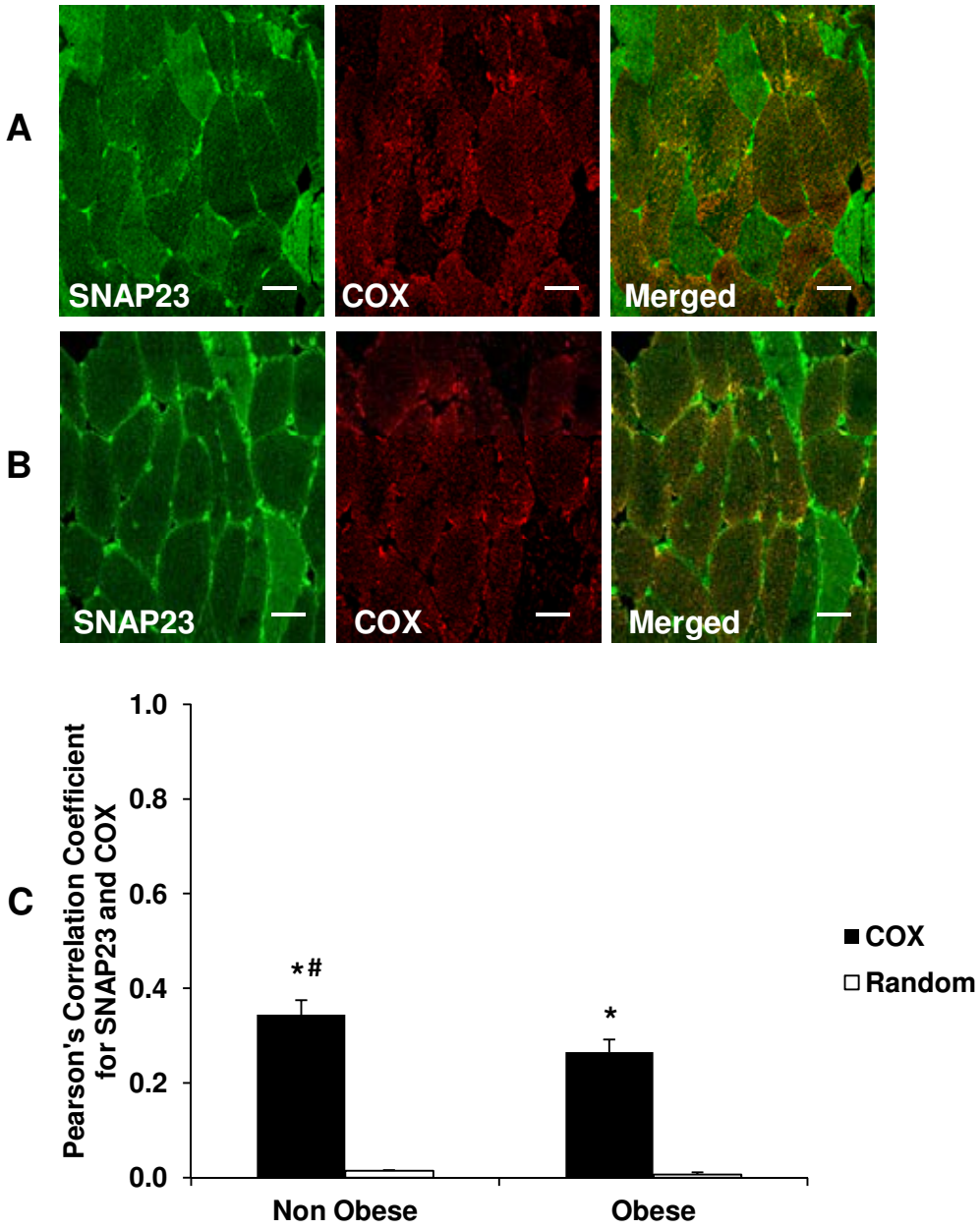

*Figure 8.2. Representative images showing colocalisation of SNAP23 with mitochondria (stained with anti-COX) in skeletal muscle of non obese women (A) and obese women (B). Bar is 30 µm. Pearson's correlation coefficients are shown in panel C. * Denotes a significant difference between matched and non matched images at P < 0.05. # Denotes a significant difference between obese and non obese individuals at P < 0.05.*

When examining fibre type differences in mitochondrial intensity, it was found that there was no difference between non obese and obese individuals in mitochondrial intensity in type I fibres (non obese: 98 ± 13 vs. obese: 87 ± 11, $P = 0.545$) or type II fibres (non obese: 80 ± 10 vs. obese: 75 ± 9, $P = 0.698$) (Figure 8.3A). However there was a fibre type difference in mitochondrial intensity in both the non obese ($P = 0.01$) and obese ($P = 0.02$) individuals with a greater intensity measured in type I fibres compared to type II fibres (Figure 8.3A). These findings were also similar for mitochondrial area fraction, with no difference between groups in either type I (non obese: 0.127 ± 0.03 vs. obese: 0.109 ± 0.02, $P = 0.633$) or type II fibres (non obese: 0.090 ± 0.02 vs. obese: 0.069 ± 0.01, $P = 0.428$) (Figure 8.3B). However both groups did show a greater mitochondrial content (expressed as mitochondria area fraction) in type I fibres compared to type II fibres (non obese: $P = 0.02$; obese: $P = 0.02$) (Figure 8.3B).

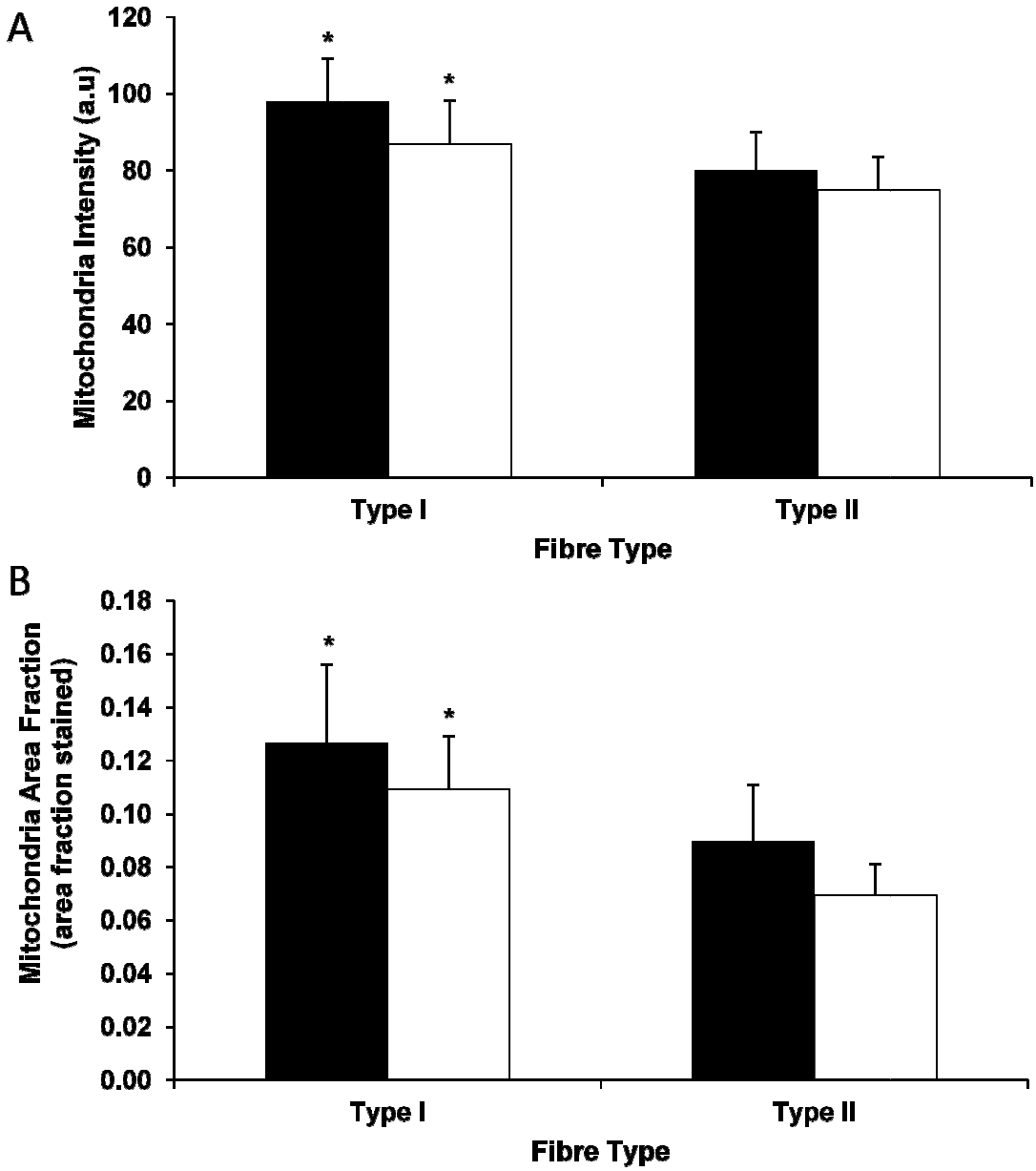

Figure 8.3. Mitochondrial variables in non obese and obese individuals. Black bars represent mean values for non obese participants and white bars represent mean values for obese participants. Mitochondria intensity (A) and mitochondria area fraction (B) were greater in type I than in type II fibres in both non obese and obese individuals. Values are mean ± SEM. * Denotes a significant difference compared to type II fibres (P < 0.05).

SNAP23 and IMTG

In both the non obese and obese individuals, the IMTG were stained using the neutral lipid dye oil red O and the distribution showed a number of small droplets distributed through the fibres. There was more intense staining in some fibres compared to others and in both the non obese and obese individuals, there were some larger lipid droplets present in addition to the smaller droplets (Figure 8.4A and 8.4B). In skeletal muscle obtained from non obese women, SNAP23 showed a weak colocalisation with lipid droplets ($r = 0.105 \pm 0.019$) (Figure 8.4A and 8.4C). This value was significantly greater than the colocalisation in non matched pairs of images ($r = 0.001 \pm 0.004$, $P = 0.003$) (Figure 8.4C). In the skeletal muscle obtained from obese women, SNAP23 also showed a weak colocalisation with lipid droplets ($r = 0.073 \pm 0.021$) (Figure 8.4 B and 8.4C) which was again significantly greater than the colocalisation of non matched images ($r = -0.001 \pm 0.002$, $P = 0.012$) (Figure 8.4C). There was no difference in the degree of colocalisation in the skeletal muscle of the non obese women compared to the obese women (non obese: $r = 0.105 \pm 0.019$ vs. obese: $r = 0.073 \pm 0.021$, $P = 0.645$).

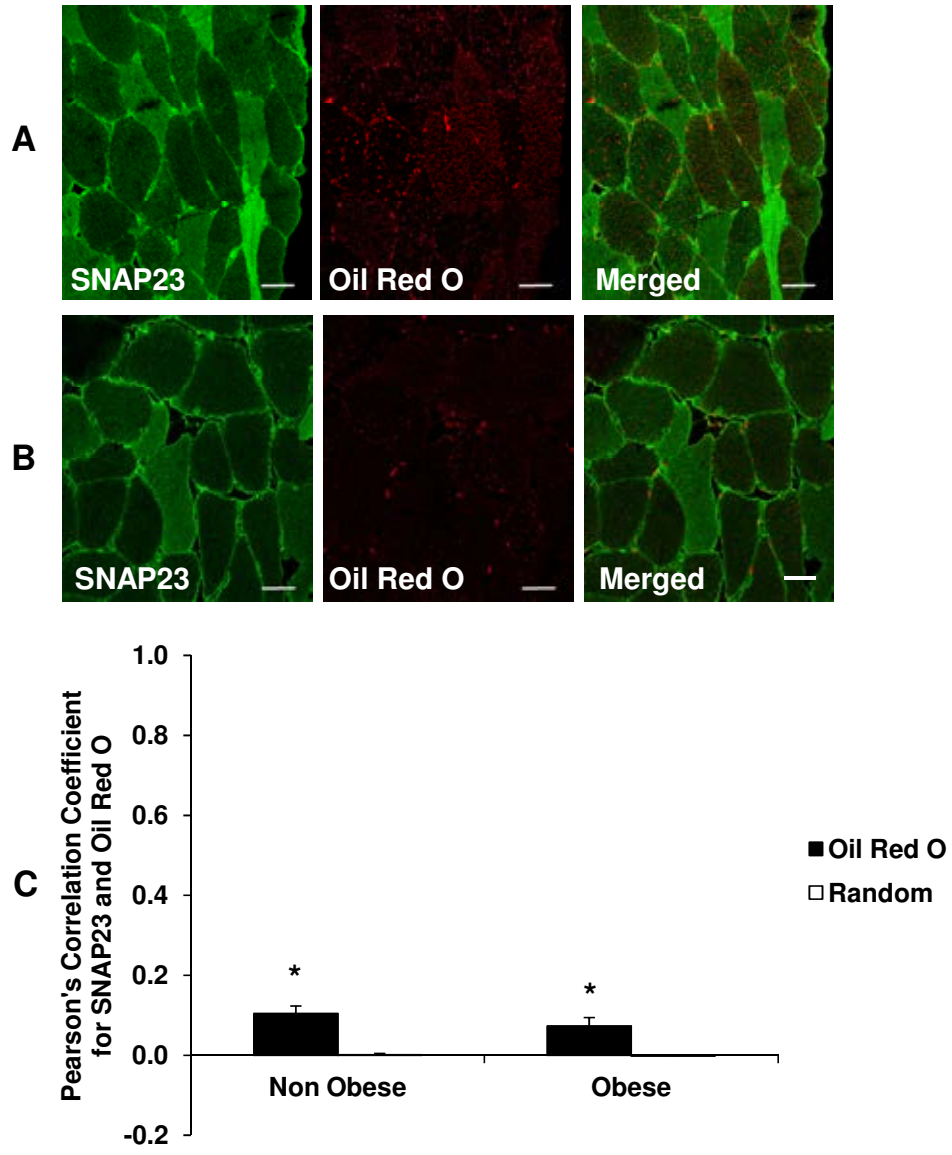

Figure 8.4. Representative images showing colocalisation of SNAP23 with IMTG (stained with oil red O) in skeletal muscle of non obese women (A) and obese women (B). Bar is 30 µm. Pearson's correlation coefficients are shown in panel C. Denotes a significant difference between matched and non matched images at P < 0.05.*

When examining fibre type differences in IMTG, there was also no difference reported in lipid droplet area fraction in type I fibres (non obese: 0.034 ± 0.006 vs. obese: 0.034 ± 0.007, $P = 0.977$) or type II fibres (non obese: 0.020 ± 0.002 vs. obese: 0.020 ± 0.005, $P = 0.991$) between the non obese and obese individuals (Figure 8.5A). However, there was a fibre type difference in lipid droplet area fraction in both the non obese (type I fibres: 0.034 ± 0.006 vs. type II fibres: 0.020 ± 0.002, $P = 0.03$) and obese individuals (type I fibres: 0.034 ± 0.007 vs. type II fibres: 0.020 ± 0.005, $P = 0.01$) (Figure 8.5A). It was also found that there was no difference in lipid droplet size between the non obese and obese individuals (0.72 ± 0.04 μm^2 vs. 0.82 ± 0.08 μm^2, $P = 0.29$) (Figure 8.5B).

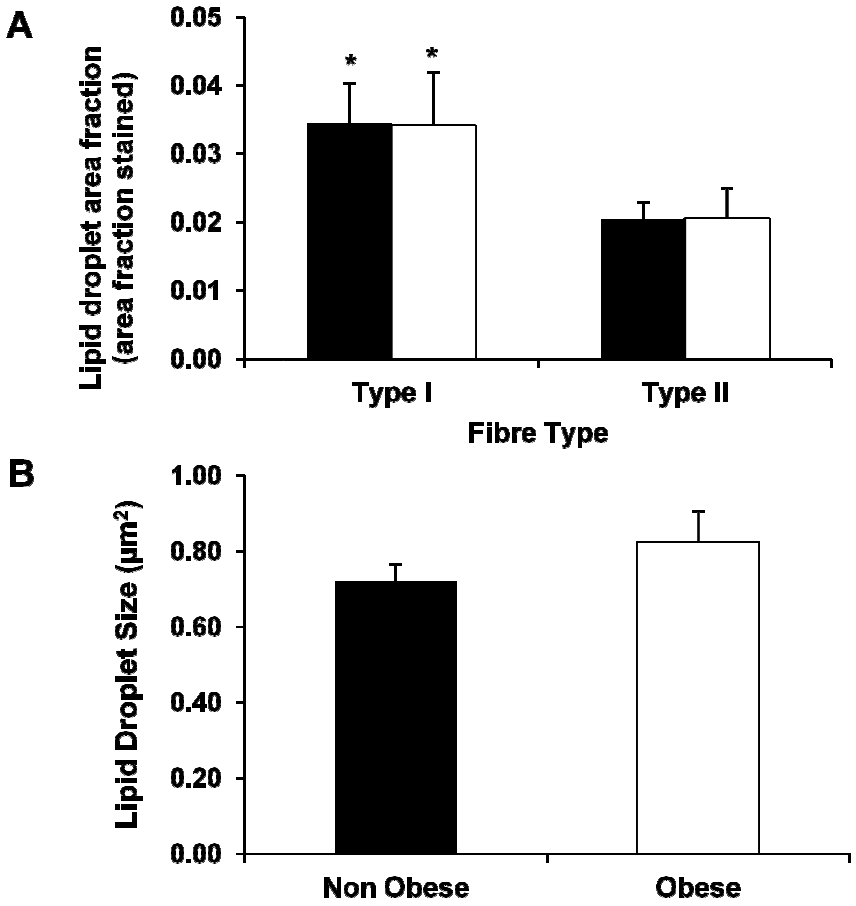

Figure 8.5. Lipid parameters in non obese and obese individuals where black bars represent mean values for non obese participants and white bars represent mean values for obese participants. Lipid droplet area fraction (A) was greater in type I fibres compared to type II fibres in both non obese and obese individuals. Lipid droplet size (B) was not different between non obese and obese individuals. Values are mean ± SEM. * Denotes a significant difference compared to type II fibres at P < 0.05.

8.5 Discussion

The results of this study did not confirm the hypothesis that SNAP23 hijacking by lipid droplets would be more pronounced in obese, ageing women than in age-matched non obese controls and would lead to a larger reduction in the colocalisation of SNAP23 with the plasma membrane. In fact, there was no difference in the colocalisation of SNAP23 with either the plasma membrane or with lipid droplets between the non obese and obese women. The results, on the other hand, did confirm the hypothesis that SNAP23 colocalisation with the mitochondria would be lower in the obese, ageing women than in age-matched non obese controls.

The main limitation of the present study was that the individuals in both groups were inactive as they were awaiting orthopaedic surgery. It is possible that this inactivity may therefore negate any changes which may otherwise have been seen due to obesity. Perhaps the most surprising finding of this study was that there was no difference between the non obese and obese elderly women in the lipid droplet area fraction and size of the lipid droplets. Many previous studies, primarily in younger individuals, have shown that there are increased concentrations of plasma FA and TAG in obese individuals and a higher FA flux from the enlarged adipose tissue stores to skeletal muscle (Opie & Walfish, 1963;Frayn, 2002;Mittendorfer *et al.*, 2009). This would predict that more and potentially larger lipid droplets would accumulate in the muscle of obese individuals. More of the lipid droplets could also be expected to be in the active fusing stage, which requires the presence of SNAP23. Larger lipid droplets have indeed been observed in obese and obese type 2 diabetes patients compared to lean individuals in previous studies (He *et al.*, 2004). There, however, also are a number of other studies that fail to observe an elevated IMTG content in obese

and/or type 2 diabetic compared to age-matched controls (Goodpaster *et al.*, 2001;van Loon *et al.*, 2004;Meex *et al.*, 2010;Bostrom *et al.*, 2010).

As has been discussed previously in Chapter 5.5 of this thesis, the difference between the earlier studies and our study is that most of these studies involved younger men and women, who most likely were more active, and that in several cases a comparison was made between obese and truely lean individuals. The women recruited to our study were older (mean age 65) and as the women in both groups were scheduled for orthopaedic surgery they were very inactive with many only able to walk using crutches or a frame. A small number were even restricted to a wheelchair whilst they awaited the surgery. It is well known that normal ageing in non obese individuals is also associated with muscle lipid accumulation (Nakagawa *et al.*, 2007;Crane *et al.*, 2010). The non obese elderly women in our study are representative for an elderly sedentary UK population and despite the BMI of 22.6 they cannot be qualified as lean and are likely to combine a significant fat mass with a low muscle mass. This may well be the reason that the two groups had a similar lipid droplet area fraction, lipid droplet size and also similar mitochondrial area fraction and intensity, despite a massive difference in body mass. This is probably also the reason that both groups had reduced insulin sensitivity and that there was no significant difference between the two groups in plasma glucose, serum insulin and the HOMA-IR score (Table 8.1). The latter is in part due to the fact that the non obese group does not have an optimal insulin sensitivity and in part due to the fact that the study is underpowered. A retrospective power calculation has shown that at least 10 subjects per group would be required to obtain a significant difference in the HOMA-IR score (calculation conducted using G Power (Erdfelder *et al.*, 1996)).

The data in this study did not confirm the hypothesis that SNAP23 hijacking by lipid droplets occurs in obese and inactive ageing women however in a direct comparison between the obese group and an age-matched lean but physically active group the conclusion might well be different. This in fact may also be the reason that Bostrom *et al.,* (2010) found evidence of a redistribution of SNAP23 from the plasma membrane to the microsomal/cytosolic compartment in a comparison between patients with type diabetes and lean (potentially more physically active) controls. Unfortunately Bostrom *et al.,* (2010) did not present the results from a BMI-matched control group.

SNAP23 primarily resides at the plasma membrane and at the mitochondria, while a weaker colocalisation was observed with the lipid droplets (also seen in Chapter 7). This implies that the results of Bostrom *et al.,* (2010) of an increased SNAP23 content in the microsomal/cytosolic compartment need to be reevaluated and split into the amount present in lipid droplets and in the mitochondria before it can be concluded that it is the lipid droplets that hijack SNAP23.

The results of this study show that there is a significant reduction in colocalisation of SNAP23 with the mitochondria in the obese individuals in comparison with the non obese individuals. This observation is important given the role that has been proposed for SNAP23 associated with the mitochondria discussed in Chapter 7.5. Reduced colocalisation of SNAP23 with the mitochondria of the obese women would imply that more FA would escape from mitochondrial β-oxidation and this would then lead to higher cytosolic concentrations of long-chain fatty acyl CoA, diacylglycerol and ceramides in the muscle of the obese than the non obese women. These fatty acid metabolites have been proposed to lead to insulin

resistance in skeletal muscle *(see Introduction section 1.3)* via a mechanism that involves activation of PKC and IRS-1 serine phosphorylation. Impairment of the formation of these lipid droplet-mitochondria complexes most likely also reduces lipolysis of the IMTG and may provide a mechanism for the very low IMTG oxidation rates that have been observed during bouts of endurance exercise in obese, sedentary individuals and patients with type 2 diabetes (Blaak *et al.*, 2000;Borghouts *et al.*, 2002;van Loon *et al.*, 2005).

In summary, there was no difference in this study in the colocalisation of SNAP23 with either the plasma membrane or lipid droplets between obese and non obese elderly women. Therefore, the data generated do not support the hypothesis that obesity in elderly women leads to impaired glucose tolerance and insulin sensitivity via a mechanism that involves hijacking of SNAP23 by lipid droplets. However, there was a significant reduction in the colocalisation of SNAP23 with the mitochondria in the obese women in comparison to non obese controls. This may lead to an increased escape of FA generated by IMTG lipolysis from mitochondrial β-oxidation, cytosolic accumulation of FA metabolites, skeletal muscle insulin resistance and a decreased capacity to oxidise IMTG during endurance exercise.

CHAPTER 9

GENERAL DISCUSSION

9.1 Introduction

Impairments in intramuscular triglyceride (IMTG) turnover in skeletal muscle have been proposed to be important for the development of insulin resistance. A reduced ability to use IMTG during exercise and low IMTG resynthesis rates following exercise are seen in sedentary and obese individuals and patients with type 2 diabetes, and may be the cause of the accumulation of fatty acid (FA) metabolites that lead to insulin resistance. Acute bouts of exercise and long-term training interventions have lead to increased protein expression of lipogenic and lipolytic enzymes in skeletal muscle of humans (Schenk *et al.*, 2005;Schenk & Horowitz, 2007;Thrush *et al.*, 2009;Newsom *et al.*, 2010;Bergman *et al.*, 2010;Jocken *et al.*, 2010;Li *et al.*, 2011). Exercise also leads to increased IMTG resynthesis and turnover rates and offers protection against skeletal muscle insulin resistance induced by acute lipid-heparin infusions. As the understanding of the underlying mechanisms was incomplete at the start of this PhD work, the aim of this thesis was to further current knowledge via the development of novel immunofluorescence microscopy methods, which are able to reveal the spatial distribution of these enzymes in skeletal muscle fibres, their colocalisation with lipid droplets, mitochondria and membranes and differences between fibre types. After development of these methods in biopsies of lean trained or moderately active men, this thesis specifically aimed to investigate if there were differences between non obese and obese elderly women that might explain the increased insulin resistance of the skeletal muscle of the obese women. A further aim was to investigate whether the recently proposed SNAP23 hijacking hypothesis (Sollner, 2007) observed in cultured cardiomyocytes also operates in human skeletal muscle of obese women *in vivo*. Immunofluorescence microscopy has been used to investigate whether hijacking of SNAP23 by fusing lipid droplets would reduce the content of SNAP23 in the

plasma membrane and whether this leads to a lower SNAP23 plasma membrane content in the muscle of obese than of non obese elderly women.

9.2 Summary of the novel findings of this thesis

9.2.1 IMTG Synthesis

In Chapter 3, GPAT1, the enzyme responsible for the first committed step of IMTG synthesis, was visualised in skeletal muscle and was shown to have a fibre type specific distribution with higher concentrations in type I compared to type II fibres. As GPAT1, on the basis of its presence in rat liver mitochondria, has been given the name mitochondrial GPAT it came as a surprise that it did not colocalise with the mitochondria in human skeletal muscle taken in the overnight fasted state. Instead GPAT1 appeared to reside at regular locations in the mitochondrial network in close proximity to, but not colocalising with, the mitochondria. In Chapter 4, DGAT1 distribution was investigated. DGAT1 is the enzyme responsible for the final step in triglyceride synthesis, which is the conversion of diacylglycerol (DAG) and long chain fatty acyl CoA (LCFACoA) to IMTG. DGAT1 showed a diffuse cytoplasmic staining in cross sections and a striated distribution in longitudinally oriented sections. There were also some intense spots of staining in the cells. DGAT1 also showed a greater content in oxidative type I fibres, which are the muscle fibres with the greatest lipid content (Malenfant *et al.*, 2001;van Loon *et al.*, 2001). Chapter 5 showed that the distribution of GPAT1 and DGAT1 did not differ between non obese and obese elderly women. GPAT1 also did not colocalise with mitochondria and lipid droplets in these groups.

9.2.2 IMTG hydrolysis

In Chapter 6 of this thesis the distribution of ATGL and CGI-58 was investigated using immunofluorescence microscopy in healthy, lean, moderately active males. It was found that neither ATGL nor CGI-58 colocalised with lipid droplets in muscle biopsies taken in the fasted, resting state. ATGL was distributed in a fibre type specific manner with higher concentrations in type I fibres, however, CGI-58 was not.

9.2.3 SNARE Proteins

Chapter 7 details the distribution of SNAP23 in the muscle of healthy, lean, moderately active men. A diffuse distribution was observed which was speckled with more intense staining. This speckled staining colocalised with the mitochondrial stain anti-cytochrome c oxidase. This is the first time that colocalisation of SNAP23 and mitochondria has been observed in images of human skeletal muscle. Intense staining of SNAP23 was also observed at the plasma membrane with a high degree of colocalisation with the plasma membrane marker dystrophin in lean, moderately active males. This again is the first visualisation of this colocalisation in human muscle. A low colocalisation was observed for SNAP23 with lipid droplets stained with oil red O.

As a continuation of this work, thesubcellular distribution of SNAP23 in skeletal muscle samples obtained from non obese and obese elderly women was compared in Chapter 8. The images showed that there was a reduced colocalisation of SNAP23 with the mitochondria in the obese compared to the non obese women, whereas the degree of SNAP23 colocalisation with both the plasma membrane and the lipid droplets was the same between the two groups. The data also showed that in both groups the highest Pearson correlation coefficient was

observed for SNAP23 and the plasma membrane marker dystrophin, followed by SNAP23 colocalisation with the mitochondria and relatively low Pearson's correlation coefficients for SNAP23 and lipid droplets stained with oil red O.

9.3 Findings in the context of existing literature

9.3.1 IMTG Synthesis

Chapters 3 and 4 of this thesis provide a description of robust methods by which to investigate the distribution of the lipogenic enzymes GPAT1 and DGAT1 in human skeletal muscle. The data presented in Chapters 3 and 5 provide new evidence that GPAT1 is not localised at the mitochondrial outer membrane in human skeletal muscle in the overnight fasted state, but is instead localised in close proximity to the mitochondria, probably at sites in the endoplasmic reticulum (ER) with small growing lipid droplets. Earlier work in rat liver mitochondria (Lewin *et al.*, 2004) suggested that GPAT1 is present in the outer mitochondrial membrane and therefore the enzyme was named mitochondrial GPAT. The present observations on the localisation of GPAT1 in human skeletal muscle are in line with a more recent study by Pellon-Maison and colleagues (2007) which found that the majority of the GPAT1 protein in rat liver mitochondria was found in mitochondria associated vesicles, which are assumed to be part of the ER (Lebiedzinska *et al.*, 2009), rather than in the mitochondrial outer membrane. Future studies should investigate whether GPAT1 translocates to the mitochondria outer membrane in human skeletal muscle in conditions that lead to activation of IMTG synthesis, such as in the period after endurance exercise and ingestion of lipid containing mixed meals.

The data presented in Chapter 5 shows that there is no difference in the content of GPAT1 and DGAT1 in non obese and obese elderly women. This is in agreement with previous human studies using Western blots to measure the whole muscle protein content of these enzymes (Thrush *et al.*, 2009;Li *et al.*, 2011). The aim of the study in Chapter 5 also was to investigate if there were differences in the spatial distribution of GPAT1 and DGAT1 between the two groups. A recent study has provided evidence that higher DAG concentrations occur in the plasma membrane fraction of obese men with and without type 2 diabetes than in athletes, and that this explained the increased insulin resistance in the obese group (Bergman *et al.*, 2012). On the basis of this observation, it was hypothesised that a lower content of GPAT1 and DGAT1 in subsarcolemmal areas in the obese women might lead to higher FA metabolites, but this hypothesis was not confirmed as there was no difference between the two groups both in total protein content and subcellular distribution.

9.3.2 IMTG Hydrolysis

Chapter 6 of this thesis developed methods by which to investigate the total protein content and spatial distribution of ATGL and CGI-58 in skeletal muscle of lean humans and the potential difference between fibre types. This study showed that ATGL was distributed in a fibre type specific manner with higher concentrations in type I fibres, however the CGI-58 protein content did not differ between fibre types. A potential reason for the absence of a difference in CGI-58 content between fibre types is that there is substantial evidence that CGI-58 is also involved in alternative metabolic processes such as the acylation of LPA (Ghosh *et al.*, 2008;Montero-Moran *et al.*, 2010) and the channelling of FA into phospholipids (Montero-Moran *et al.*, 2010). Such processes may well have similar metabolic capacity requirements in type I and type II fibres.

9.3.3 SNARE Proteins

Pearson's correlation coefficients are a recognised quantitative measure of colocalisation of matched immunofluorescence images. The highest Pearson's correlation coefficients ($r = 0.50 \pm 0.01$ in lean active males, $r = 0.39 \pm 0.01$ in non obese women and $r = 0.37 \pm 0.03$ in obese elderly women) were observed for colocalisation between SNAP23 and dystrophin (as a marker of the plasma membrane). This observation is in line with the proposed role of SNAP23 in the docking and fusion of GLUT4 with the plasma membrane (Foster *et al.*, 1999;Kawanishi *et al.*, 2000a).

Relatively high Pearson's correlation coefficients were also found for colocalisation of SNAP23 and the mitochondrial marker COX ($r = 0.50 \pm 0.02$ in lean active males, $r = 0.34 \pm 0.03$ in non obese women and $r = 0.27 \pm 0.03$ in obese women). This observation is in line with the recent work of Jagerstrom and colleagues (2009) who observed colocalisation of SNAP23 and mitochondria in fibroblasts. This observation has led to the hypothesis that SNAP23 is involved in the formation of lipid droplet-mitochondria complexes. It has been proposed that these complexes play a functional role in the channelling of FA liberated by lipolysis of IMTG present in lipid droplets into the mitochondria for subsequent β-oxidation. The partial colocalisation between SNAP23 and the mitochondrial stain COX observed in Chapters 7 and 8 provides the first evidence in humans that SNAP23 may also exert this FA channelling role in human skeletal muscle *in vivo*. Further, the findings of Chapter 8 show that this colocalisation of SNAP23 with the mitochondria is lower in the obese than in the non obese elderly women, potentially leading to less efficient channelling of FA into the mitochondria for oxidation and higher levels of FA metabolites in skeletal muscle. This therefore may explain the greater insulin resistance in the obese than in the non obese women.

The lowest Pearson's correlation coefficients were actually observed for SNAP23 and lipid droplets stained with oil red O ($r = 0.20 \pm 0.01$ in lean active males, $r = 0.11 \pm 0.02$ in non obese women and $r = 0.07 \pm 0.02$ in obese elderly women). This observation was unexpected as the aim of the study was to investigate whether the lipid droplets were a main location of SNAP23, especially in the obese women, and whether hijacking of SNAP23 by the lipid droplets in fact reduced the SNAP23 content of the plasma membrane, thus preventing GLUT4 docking and fusion. This expectation was based on the observation of Bostrom *et al.,* (2010) which showed a redistribution of SNAP23 from the plasma membrane regions to the microsomal/cytosolic regions of the muscle fibres in type 2 diabetic patients. However, the data in Chapter 8 convincingly show that there was no difference in the colocalisation of SNAP23 with either the plasma membrane or the lipid droplets between the obese and non obese group. These data, therefore, do not support that the hijacking hypothesis (Sollner, 2007), which was based on research in cultured cardiomyocytes (Bostrom *et al.*, 2007), operates and contributes more to muscle insulin resistance in obese than non obese elderly women with low habitual physical activity levels.

9.4 Suggestions for future studies

9.4.1 Gaps in current knowledge about IMTG metabolism

Most of the studies that have investigated the role of IMTG content and use as a fuel during exercise have been executed in male individuals. However, the few studies that have been executed in women have shown large gender differences (Kiens, 2006;Haugaard *et al.*, 2009;Moro *et al.*, 2009;Perreault *et al.*, 2010). Therefore a systematic evaluation of IMTG content, IMTG use during exercise, mitochondrial density, as well as all of the assays described in this thesis are needed in five groups of both male and female participants; 1) lean

sedentary, 2) obese sedentary, 3) obese type 2 diabetes patients, 4) lean habitually active individuals, and 5) highly trained individuals. As age, BMI and habitual physical activity are main determinants of IMTG turnover and insulin sensitivity, the use of properly matched control groups is of crucial importance. To be optimally informative the results in these group comparisons should be related to total skeletal muscle levels of FA metabolites, levels of subspecies of FA metabolites and the subcellular distribution of these FA metabolites as the FA metabolites are the strongest predictors of insulin resistance in human skeletal muscle (Bergman *et al.*, 2012).

Differences in the total protein content of GPAT1 and DGAT1 and in the gradients in the protein concentration of these enzymes between the indicated groups could generate novel information on the mechanisms by which FA metabolites accumulate in the muscle and lead to the large range in insulin sensitivity between these groups. *In situ* measurements of the activity of GPAT1 and DGAT1 would be the ultimate aim of this type of research, but are not yet possible. As the work in Chapter 5 revealed no difference in the spatial distribution of GPAT1 and DGAT1 between non obese and obese women and also in the COX content as a marker of mitochondrial density, it may be that the increased FA uptake that has previously been observed in obesity (Bonen *et al.*, 2004), cannot be matched by IMTG synthesis and mitochondrial β-oxidation rates. It may be this mismatch that leads to accumulation of FA metabolites. Future studies comparing lipid metabolism in different groups in muscle biopsies should, therefore, also be complemented by measurements of whole body lipolysis rates using stable isotope methodologies and the arterial extraction of FA and glycerol using limb arteriovenous difference measurements.

In studies investigating the SNAP23 hijacking hypothesis it would be important to also measure total SNAP23 content in skeletal muscle. It should be noted that in the non obese and obese elderly women the Pearson's correlation was lower than in the lean, moderately active younger men at all three sites (plasma membrane, mitochondria and lipid droplets). This could imply that the total amount of SNAP23 is reduced and that the risk of a shortage of SNAP23 at the plasma membrane is lower in young, moderately active men than in obese and non obese elderly women. Again, such information would be required in gender-matched groups as well, as there also may be a difference between genders and between young and old as suggested above. A very important unanswered question is the amount of SNAP23, or the degree of colocalisation with the plasma membrane, that is required to allow maximal rates of GLUT4 docking and fusion in response to meal induced increases in insulin and contraction induced GLUT4 translocation. Without such knowledge it will be difficult to determine whether a redistribution of SNAP23 to sites other than the plasma membrane might lead to a functional shortage of SNAP23 in the plasma membrane. In the first instance, this of course also would require the development of an immunofluorescence method to visualise GLUT4 in human skeletal muscle, which is further reflected upon in section 9.4.2.

The lipid droplet-mitochondria interactions reported by Jagerstrom *et al.,* (2009) may be an essential part of the mechanism that allows trained athletes to oxidise IMTG at high rates without developing high levels of FA in their muscles, and therefore may be part of the metabolic adaptation in highly trained athletes behind the 'athletes paradox' (Goodpaster *et al.*, 2001;van Loon *et al.*, 2004). Following a discussion regarding the potential molecular mechanism behind this interaction with the late Professor Sven Olof Olofsson, it was hypothesised that the mechanism may involve the fusion of the lipid monolayer of the lipid

droplets with the outer layer of the lipid bilayer of the mitochondrial outer membrane. Such a functional fusion would channel FA released by the lipid droplets directly to LCFACoA synthase and, via the carnitine shuttle system of the mitochondria, into the mitochondrial matrix and β-oxidation. This functional interaction would prevent FA generated by IMTG lipolysis and LCFACoA from entering the cytosol and thus reduce the cytosolic levels of FA metabolites (LCFACoA, DAG and ceramides), which have been implicated in the mechanisms that lead to IRS-1 serine phosphorylation and insulin resistance in skeletal muscle (Ellis *et al.*, 2000;Itani *et al.*, 2002).

9.4.2 The need for a GLUT-4 translocation assay in humans skeletal

Surprisingly little research has been performed in humans to investigate the spatial distribution and translocation of GLUT4, the ultimate target and endpoint of the insulin signalling cascade, with immunofluorescence microscopy methods. The distribution of GLUT4 has been examined in skeletal muscle of animal models (Wang *et al.*, 1996;Ploug *et al.*, 1998;Hansen *et al.*, 1998;Lauritzen *et al.*, 2006;Lauritzen *et al.*, 2008b;Lauritzen & Schertzer, 2010;Lauritzen *et al.*, 2010) and in cultured adipocytes (Bai *et al.,* 2007). However research in human skeletal muscle is, to the best of our knowledge, limited to published abstracts. The t-tubules, in mice at least, appear to be the most important target of GLUT4 fusion and docking (Lauritzen *et al.*, 2006). Upon insulin stimulation of mouse muscles *in vivo*, it has been shown that there is a delay of approximately 10 minutes in the appearance of GLUT4 in the t-tubules compared to the sarcolemma (Lauritzen *et al.*, 2006). It is very important that this research is extended to man to thus generate a better understanding of the mechanisms behind the glucose uptake kinetics in human skeletal muscle after oral glucose or

mixed meal ingestion and after the start of a hyperinsulinaemic euglycaemic clamp and of the differences in glucose uptake kinetics between the groups mentioned in 9.4.1.

It has also been suggested that high fat feeding leads to a further delay in GLUT4 translocation to the t-tubules and contributes to the reduced insulin action and insulin signalling (Lauritzen *et al.*, 2008a). Experiments in obese individuals and patients with type 2 diabetes should determine if a delay in GLUT4 translocation to plasma and t-tubular membranes contributes to the process known as metabolic inflexibility (Storlien *et al.*, 2004), which is the slower switching from fat as the main fuel in the fasted state to glucose as the main fuel after ingestion of a carbohydrate containing meal and vice versa. Metabolic inflexibility is seen as an early indicator of the development of the metabolic syndrome and again impairments in lipid metabolism play an important role in it, but the underlying mechanisms in the muscle are poorly understood. Ideally, in such studies GLUT4 colocalisation with SNAP23 (due to its role in GLUT4 docking in the plasma membrane) should be investigated and related to insulin signalling intermediates such as IRS-1 tyrosine and serine phosphorylation, Akt phosphorylation and AS160 (TBC1D4) phosphorylation. In fact, co-staining of SNAP23 with GLUT4 would be ideal in order to corroborate the suggestion that SNAP23 hijacking by lipid droplets in obese individuals and patients with type 2 diabetes actually limits GLUT4 docking with the plasma membrane and thus would allow for a more thorough investigation of the hijacking hypothesis (Sollner, 2007). It would be of interest to investigate whether the appearance of GLUT4 in the t-tubules is paralleled by the appearance of SNAP23 in the t-tubules, given its role in GLUT4 docking. In addition to this, further fluorescence microscopy investigation of the SNARE complex (SNAP23, syntaxin 4 and VAMP2) proposed to be involved in GLUT4 docking at the plasma membrane

in skeletal muscle would also be important in terms of investigating exactly how this process occurs and the defects that occur with the development of insulin resistance. This would require the development of new immunofluorescence assays of a number of additional SNARE proteins.

9.4.3 Enzymes that may play a role in reduced lipolysis and fatty acid oxidation in obesity and type 2 diabetes

The isolation of lipid droplets from skeletal muscle homogenates requires drastic homogenisation and isolation procedures. This carries a high risk of artifactual protein loss or protein associations and therefore, colocalisation with immunohistochemical methods for the time being remains to be the preferred analytical method to identify the proteins that are naturally present in and play functional roles in lipid droplets.

Future studies measuring lipases in skeletal muscle should also measure HSL protein content as well as subcellular and fibre type distribution, as suggestions have been made that accumulation of DAG may in fact result from incomplete lipolysis resulting from an imbalance between the activity of ATGL and HSL. The largest possible imbalance has been observed in HSL knockout mice, which as expected, accumulate a high DAG concentration in skeletal muscle and have reduced insulin sensitivity (Osuga *et al.*, 2000;Mulder *et al.*, 2003). Studies investigating HSL protein content and distribution should also include potential regulator or facilitator proteins, which in skeletal muscle, among others, include the PAT proteins perilipin 2 (ADRP) (Prats *et al.*, 2006;Shaw *et al.*, 2009). Another PAT protein, perilipin 5, has recently been proposed to play a role in the formation of functional lipid-droplet mitochondria complexes and helps to determine whether FA are either used for IMTG

synthesis or for mitochondrial β-oxidation (Wang *et al.*, 2011). Cardiomyocytes overexpressing perilipin 5 in basal conditions showed decreased lipid droplet lipolysis, decreased palmitate β-oxidation and increased palmitate incorporation into TAG. Whereas in stimulated conditions, lipid droplet hydrolysis inhibition was lifted and the released FA were channelled into the mitochondria for β-oxidation.

Future studies using the methods developed in this thesis and complementary methods should not only make measurements in the fasted unstimulated state, but especially under conditions that are known to increase IMTG lipolysis, such as exercise and adrenaline infusion. The observation made by Prats *et al.,* (2006) that *in vitro* electrical stimulation of rat soleus muscles and incubation with adrenaline (stimulating PKA) both led to HSL translocation from a cytosolic/microsomal site to the lipid droplets and to increased colocalisation of HSL with perilipin 2 still needs confirmation during dynamic exercise and adrenaline infusion in humans. A recent observation of my colleagues in Birmingham that lipid droplets containing perilipin 2 are preferentially used (oxidised) during one hour of endurance-type exercise in trained men (Shepherd *et al.,* 2012) confirms that the PAT proteins present in the protein coat surrounding the lipid droplets probably should be regarded as lipid droplet scaffolding proteins that need to recruit the right environment (either neighbouring mitochondria or neighbouring ER binding sites containing GPAT1 and DGAT1) to determine if lipolysis or lipid synthesis prevails and whether IMTG can be oxidised during exercise (trained athletes) or not (obese sedentary and type 2 diabetes).

9.5 Final Conclusions

The work contained within this thesis has demonstrated that a variety of immunofluorescence microscopy methods can be successfully developed and applied to sections of human skeletal muscle to thus generate novel information. These methods have also been used to make the first comparisons between obese and non obese elderly women. In future research these methods will be used to address some of the important unanswered questions on the mechanisms behind the impairments in lipid metabolism which prevent IMTG use in sedentary, obese and type 2 diabetic individuals and the mechanistic link between the inability to use IMTG during exercise, accumulation of FA metabolites in skeletal muscle and the development of insulin resistance. The added value of these immunofluorescence methods to traditional methods which focus on fuel use and insulin sensitivity, is that they provide a tool to investigate whether hypotheses generated in cultured cells and/or animal models (in which the expression and function of single proteins can be experimentally increased or decreased) also operate in skeletal muscle of human beings *in vivo*. In combination with the traditional methodologies to investigate regulation of metabolism in man (mentioned in earlier sections of this Chapter), these novel complementary immunohistochemical staining methods will help to identify novel drug targets and allow for more relevant metabolic evaluations of the effect and efficiency of life style interventions. Therefore these methods are expected to help and support medicine based evidence for the effectiveness of clinical trials and lifestyle interventions and to thus make a significant contribution to get improved control on the worldwide health threat of obesity and type 2 diabetes.

CHAPTER 10

REFERENCES

Alsted TJ, Nybo L, Schweiger M, Fledelius C, Jacobsen P, Zimmermann R, Zechner R, & Kiens B (2009). Adipose triglyceride lipase in human skeletal muscle is upregulated by exercise training. *Am J Physiol Endocrinol Metab* **296**, E445-E453.

Andersson L, Bostrom P, Ericson J, Rutberg M, Magnusson B, Marchesan D, Ruiz M, Asp L, Huang P, Frohman MA, Boren J, & Olofsson SO (2006). PLD1 and ERK2 regulate cytosolic lipid droplet formation. *J Cell Sci* **119**, 2246-2257.

Anthonsen MW, Ronnstrand L, Wernstedt C, Degerman E, & Holm C (1998). Identification of Novel Phosphorylation Sites in Hormone-sensitive Lipase That Are Phosphorylated in Response to Isoproterenol and Govern Activation Properties in Vitro. *J Biol Chem* **273**, 215-221.

Bagnato C & Igal RA (2003). Overexpression of Diacylglycerol Acyltransferase-1 Reduces Phospholipid Synthesis, Proliferation, and Invasiveness in Simian Virus 40-transformed Human Lung Fibroblasts. *J Biol Chem* **278**, 52203-52211.

Bai L, Wang Y, Fan J, Chen Y, Ji W, Qu A, Xu P, James DE, & Xu T (2007). Dissecting Multiple Steps of GLUT4 Trafficking and Identifying the Sites of Insulin Action. *Cell Metabolism* **5**, 47-57.

Bansal S, Buring JE, Rifai N, Mora S, Sacks FM, & Ridker PM (2007). Fasting Compared With Nonfasting Triglycerides and Risk of Cardiovascular Events in Women. *JAMA: The Journal of the American Medical Association* **298**, 309-316.

Bao Y, Lopez JA, James DE, & Hunziker W (2008). Snapin interacts with the Exo70 subunit of the exocyst and modulates GLUT4 trafficking. *J Biol Chem* **283**, 324-331.

Barrett EJ, Eggleston EM, Inyard AC, Wang H, Li G, Chai W, & Liu Z (2009). The vascular actions of insulin control its delivery to muscle and regulate the rate-limiting step in skeletal muscle insulin action. *Diabetologia* **52**, 752-764.

Bartz R, Zehmer JK, Zhu M, Chen Y, Serrero G, Zhao Y, & Liu P (2007a). Dynamic activity of lipid droplets: protein phosphorylation and GTP-mediated protein translocation. *J Proteome Res* **6**, 3256-3265.

Bartz R, Li WH, Venables B, Zehmer JK, Roth MR, Welti R, Anderson RGW, Liu P, & Chapman KD (2007b). Lipidomics reveals that adiposomes store ether lipids and mediate phospholipid traffic. *J Lipid Res* **48**, 837-847.

Bell M, Wang H, Chen H, McLenithan JC, Gong DW, Yang RZ, Yu D, Fried SK, Quon MJ, Londos C, & Sztalryd C (2008). Consequences of Lipid Droplet Coat Protein Downregulation in Liver Cells. *Diabetes* **57**, 2037-2045.

Bell RM & Coleman RA (1980). Enzymes of glycerolipid synthesis in eukaryotes. *Annu Rev Biochem* **49**, 459-487.

Bergman BC, Hunerdosse DM, Kerege A, Playdon MC, & Perreault L (2012). Localisation and composition of skeletal muscle diacylglycerol predicts insulin resistance in humans. *Diabetologia* **55**, 1140-1150.

Bergman BC, Perreault L, Hunerdosse DM, Koehler MC, Samek AM, & Eckel RH (2010). Increased intramuscular lipid synthesis and low saturation relate to insulin sensitivity in endurance-trained athletes. *J Appl Physiol* **108**, 1134-1141.

Bergstrom (1975). Percutaneous needle biopsy of skeletal muscle in physiological and clinical research. *Scandinavian Journal of Clinical Laboratory Investigation* **35**, 609-616.

Bickerton AS, Roberts R, Fielding BA, Tornqvist H, Blaak EE, Wagenmakers AJ, Gilbert M, Humphreys SM, Karpe F, & Frayn KN (2008). Adipose tissue fatty acid metabolism in insulin-resistant men. *Diabetologia* **51**, 1466-1474.

Blaak EE, van Aggel-Leijssen DP, Wagenmakers AJ, Saris WH, & van Baak MA (2000). Impaired oxidation of plasma-derived fatty acids in type 2 diabetic subjects during moderate-intensity exercise. *Diabetes* **49**, 2102-2107.

Boden G (1999). Free fatty acids, insulin resistance, and type 2 diabetes mellitus. *Proc Assoc Am Physicians* **111**, 241-248.

Boden G, Chen X, Ruiz J, White JV, & Rossetti L (1994). Mechanisms of fatty acid-induced inhibition of glucose uptake. *J Clin Invest* **93**, 2438-2446.

Boden G, Jadali F, White J, Liang Y, Mozzoli M, Chen X, Coleman E, & Smith C (1991). Effects of fat on insulin-stimulated carbohydrate metabolism in normal men. *J Clin Invest* **88**, 960-966.

Boesch C, Decombaz J, Slotboom J, & Kreis R (1999). Observation of intramyocellular lipids by means of 1H magnetic resonance spectroscopy. *Proc Nutr Soc* **58**, 841-850.

Boesch C, Slotboom J, Hoppeler H, & Kreis R (1997). In vivo determination of intra-myocellular lipids in human muscle by means of localized 1H-MR-spectroscopy. *Magn Reson Med* **37**, 484-493.

Bonen A, Parolin ML, Steinberg GR, Calles-Escandon J, Tandon NN, Glatz JFC, Luiken JJFP, Heigenhauser G, & Dyck DJ (2004). Triacylglycerol accumulation in human obesity and type 2 diabetes is associated with increased rates of skeletal muscle fatty acid transport and increased sarcolemmal FAT/CD36. *FASEB J*.

Borghouts LB, Wagenmakers AJ, Goyens PL, & Keizer HA (2002). Substrate utilization in non-obese Type II diabetic patients at rest and during exercise. *Clin Sci (Lond)* **103**, 559-566.

Bostrom P, Andersson L, Li L, Perkins R, Hojlund K, Boren J, & Olofsson SO (2009). The assembly of lipid droplets and its relation to cellular insulin sensitivity. *Biochem Soc Trans* **37**, 981-985.

Bostrom P, Andersson L, Rutberg M, Perman J, Lidberg U, Johansson BR, Fernandez-Rodriguez J, Ericson J, Nilsson T, Boren J, & Olofsson SO (2007). SNARE proteins mediate fusion between cytosolic lipid droplets and are implicated in insulin sensitivity. *Nat Cell Biol* **9**, 1286-1293.

Bostrom P, Andersson L, Vind B, Haverson L, Rutberg M, Wickstrom Y, Larsson E, Jansson PA, Svensson MK, Branemark R, Ling C, Beck-Nielsen H, Boron J, Hojlund K, & Olofsson SO (2010). The SNARE protein SNAP23 and the SNARE-interacting protein Munc18c in human skeletal muscle are implicated in insulin resistance/type 2 diabetes. *Diabetes*.

Bostrom P, Rutberg M, Ericsson J, Holmdahl P, Andersson L, Frohman MA, Boren J, & Olofsson SO (2005). Cytosolic Lipid Droplets Increase in Size by Microtubule-Dependent Complex Formation. *Arterioscler Thromb Vasc Biol* **25**, 1945-1951.

Brasaemle DL, Dolios G, Shapiro L, & Wang R (2004). Proteomic Analysis of Proteins Associated with Lipid Droplets of Basal and Lipolytically Stimulated 3T3-L1 Adipocytes. *J Biol Chem* **279**, 46835-46842.

Brasaemle DL, Levin DM, dler-Wailes DC, & Londos C (2000a). The lipolytic stimulation of 3T3-L1 adipocytes promotes the translocation of hormone-sensitive lipase to the surfaces of lipid storage droplets. *Biochimica et Biophysica Acta (BBA) - Molecular and Cell Biology of Lipids* **1483**, 251-262.

Brasaemle DL, Rubin B, Harten IA, Gruia-Gray J, Kimmel AR, & Londos C (2000b). Perilipin A Increases Triacylglycerol Storage by Decreasing the Rate of Triacylglycerol Hydrolysis. *J Biol Chem* **275**, 38486-38493.

Brechtel K, Niess AM, Machann J, Rett K, Schick F, Claussen CD, Dickhuth HH, Haering HU, & Jacob S (2001). Utilisation of intramyocellular lipids (IMCLs) during exercise as assessed by proton magnetic resonance spectroscopy (1H-MRS). *Horm Metab Res* **33**, 63-66.

Brown DA (2001). Lipid droplets: Proteins floating on a pool of fat. *Current Biology* **11**, R446-R449.

Brown JM, Chung S, Das A, Shelness GS, Rudel LL, & Yu L (2007). CGI-58 facilitates the mobilization of cytoplasmic triglyceride for lipoprotein secretion in hepatoma cells. *J Lipid Res* **48**, 2295-2305.

Bryant NJ, Govers R, & James DE (2002). Regulated transport of the glucose transporter GLUT4. *Nat Rev Mol Cell Biol* **3**, 267-277.

Budohoski L, Gorski J, Nazar K, Kaciuba-Uscilko H, & Terjung RL (1996). Triacylglycerol synthesis in the different skeletal muscle fiber sections of the rat. *Am J Physiol* **271**, E574-E581.

Campbell PJ, Carlson MG, & Nurjhan N (1994). Fat metabolism in human obesity. *Am J Physiol* **266**, E600-E605.

Cao J, Li JL, Li D, Tobin JF, & Gimeno RE (2006). Molecular identification of microsomal acyl-CoA:glycerol-3-phosphate acyltransferase, a key enzyme in de novo triacylglycerol synthesis. *Proceedings of the National Academy of Sciences* **103**, 19695-19700.

Cases S, Smith SJ, Zheng YW, Myers HM, Lear SR, Sande E, Novak S, Collins C, Welch CB, Lusis AJ, Erickson SK, & Farese RV, Jr. (1998). Identification of a gene encoding an acyl CoA:diacylglycerol acyltransferase, a key enzyme in triacylglycerol synthesis. *Proc Natl Acad Sci U S A* **95**, 13018-13023.

Cases S, Stone SJ, Zhou P, Yen E, Tow B, Lardizabal KD, Voelker T, & Farese RV, Jr. (2001). Cloning of DGAT2, a Second Mammalian Diacylglycerol Acyltransferase, and Related Family Members. *J Biol Chem* **276**, 38870-38876.

Chalkley SM, Hettiarachchi M, Chisholm DJ, & Kraegen EW (1998). Five-hour fatty acid elevation increases muscle lipids and impairs glycogen synthesis in the rat. *Metabolism* **47**, 1121-1126.

Chamberlain LH & Gould GW (2002). The vesicle- and target-SNARE proteins that mediate Glut4 vesicle fusion are localized in detergent-insoluble lipid rafts present on distinct intracellular membranes. *J Biol Chem* **277**, 49750-49754.

Chang L, Chiang SH & Saltiel AR (2004). Insulin signaling and the regulation of glucose transport. *Mol Med* **10**, 65-71.

Cheatham B, Vlahos CJ, Cheatham L, Wang L, Blenis J, & Kahn CR (1994). Phosphatidylinositol 3-kinase activation is required for insulin stimulation of pp70 S6 kinase, DNA synthesis, and glucose transporter translocation. *Mol Cell Biol* **14**, 4902-4911.

Chen HC, Smith SJ, Ladha Z, Jensen DR, Ferreira LD, Pulawa LK, McGuire JG, Pitas RE, Eckel RH, & Farese RV, Jr. (2002). Increased insulin and leptin sensitivity in mice lacking acyl CoA:diacylglycerol acyltransferase 1. *J Clin Invest* **109**, 1049-1055.

Chen YQ, Kuo MS, Li S, Bui HH, Peake DA, Sanders PE, Thibodeaux SJ, Chu S, Qian YW, Zhao Y, Bredt DS, Moller DE, Konrad RJ, Beigneux AP, Young SG, & Cao G (2008). AGPAT6 Is a Novel Microsomal Glycerol-3-phosphate Acyltransferase. *J Biol Chem* **283**, 10048-10057.

Choi CS, Savage DB, Kulkarni A, Yu XX, Liu ZX, Morino K, Kim S, Distefano A, Samuel VT, Neschen S, Zhang D, Wang A, Zhang XM, Kahn M, Cline GW, Pandey SK, Geisler JG, Bhanot S, Monia BP, & Shulman GI (2007). Suppression of Diacylglycerol Acyltransferase-2 (DGAT2), but Not DGAT1, with Antisense Oligonucleotides Reverses Diet-induced Hepatic Steatosis and Insulin Resistance. *J Biol Chem* **282**, 22678-22688.

Coleman RA & Lee DP (2004). Enzymes of triacylglycerol synthesis and their regulation. *Progress in Lipid Research* **43**, 134-176.

Coll T, Eyre E, Rodriguez-Calvo R, Palomer X, Sanchez RM, Merlos M, Laguna JC, & Vazquez-Carrera M (2008). Oleate Reverses Palmitate-induced Insulin Resistance and Inflammation in Skeletal Muscle Cells. *J Biol Chem* **283**, 11107-11116.

Corpeleijn E, Saris WH, & Blaak EE (2009). Metabolic flexibility in the development of insulin resistance and type 2 diabetes: effects of lifestyle. *Obes Rev* **10**, 178-193.

Crane JD, Devries MC, Safdar A, Hamadeh MJ, & Tarnopolsky MA (2010). The effect of aging on human skeletal muscle mitochondrial and intramyocellular lipid ultrastructure. *J Gerontol A Biol Sci Med Sci* **65**, 119-128.

Cushman SW & Wardzala LJ (1980). Potential mechanism of insulin action on glucose transport in the isolated rat adipose cell. Apparent translocation of intracellular transport systems to the plasma membrane. *J Biol Chem* **255**, 4758-4762.

D'Santos CS, Clarke JH, Irvine RF, & Divecha N (1999). Nuclei contain two differentially regulated pools of diacylglycerol. *Current Biology* **9**, 437-440.

Daval M, Diot-Dupuy F, Bazin R, Hainault I, Viollet Bt, Vaulont S, Hajduch E, Ferre P, & Foufelle F (2005). Anti-lipolytic Action of AMP-activated Protein Kinase in Rodent Adipocytes. *J Biol Chem* **280**, 25250-25257.

De FK & Roth RA (1997). Protein kinase C modulation of insulin receptor substrate-1 tyrosine phosphorylation requires serine 612. *Biochemistry* **36**, 12939-12947.

Decombaz J, Schmitt B, Ith M, Decarli B, Diem P, Kreis R, Hoppeler H, & Boesch C (2001). Postexercise fat intake repletes intramyocellular lipids but no faster in trained than in sedentary subjects. *Am J Physiol Regul Integr Comp Physiol* **281**, R760-R769.

Department for Health. Foresight Report. 2007. London, Department for Health.
Ref Type: Report

Deschenes MR (2004). Effects of aging on muscle fibre type and size. *Sports Med* **34**, 809-824.

Diabetes UK. Diabetes in the UK 2010. 2010. Diabetes UK.
Ref Type: Report

Douen AG, Ramlal T, Cartee GD, & Klip A (1990). Exercise modulates the insulin-induced translocation of glucose transporters in rat skeletal muscle. *FEBS Lett* **261**, 256-260.

Dresner A, Laurent D, Marcucci M, Griffin ME, Dufour S, Cline GW, Slezak LA, Andersen DK, Hundal RS, Rothman DL, Petersen KF, & Shulman GI (1999). Effects of free fatty acids on glucose transport and IRS-1-associated phosphatidylinositol 3-kinase activity. *J Clin Invest* **103**, 253-259.

Egan JJ, Greenberg AS, Chang MK, Wek SA, Moos MC, Jr., & Londos C (1992). Mechanism of hormone-stimulated lipolysis in adipocytes: translocation of hormone-sensitive lipase to the lipid storage droplet. *Proc Natl Acad Sci U S A* **89**, 8537-8541.

Ellis BA, Poynten A, Lowy AJ, Furler SM, Chisholm DJ, Kraegen EW, & Cooney GJ (2000). Long-chain acyl-CoA esters as indicators of lipid metabolism and insulin sensitivity in rat and human muscle. *Am J Physiol Endocrinol Metab* **279**, E554-E560.

Enoksson S, Degerman E, Hagstrom-Toft E, Large V, & Arner P (1998). Various phosphodiesterase subtypes mediate the in vivo antilipolytic effect of insulin on adipose tissue and skeletal muscle in man. *Diabetologia* **41**, 560-568.

Erdfelder E, Faul F, & Buchner A (1996). GPOWER A general power analysis program. *Behaviour Research Methods* **28**, 1-11.

Ferrannini E, Smith JD, Cobelli C, Toffolo G, Pilo A, & DeFronzo RA (1985). Effect of insulin on the distribution and disposition of glucose in man. *J Clin Invest* **76**, 357-364.

Fery F, d'Attellis NP, & Balasse EO (1990). Mechanisms of starvation diabetes: a study with double tracer and indirect calorimetry. *Am J Physiol* **259**, E770-E777.

Foster LJ, Yaworsky K, Trimble WS, & Klip A (1999). SNAP23 promotes insulin-dependent glucose uptake in 3T3-L1 adipocytes: possible interaction with cytoskeleton. *Am J Physiol Cell Physiol* **276**, C1108-C1114.

Fox CH, Johnson FB, Whiting J, & Roller PP (1985). Formaldehyde fixation. *J Histochem Cytochem* **33**, 845-853.

Frangioudakis G, Ye JM, & Cooney GJ (2005). Both Saturated and n-6 Polyunsaturated Fat Diets Reduce Phosphorylation of Insulin Receptor Substrate-1 and Protein Kinase B in Muscle during the Initial Stages of in Vivo Insulin Stimulation. *Endocrinology* **146**, 5596-5603.

Frayn KN (2002). Adipose tissue as a buffer for daily lipid flux. *Diabetologia* **45**, 1201-1210.

Fredrikson G, Stralfors P, Nilsson NO, & Belfrage P (1981a). Hormone-sensitive lipase from adipose tissue of rat. *Methods Enzymol* **71 Pt C**, 636-646.

Fredrikson G, Stralfors P, Nilsson NO, & Belfrage P (1981b). Hormone-sensitive lipase of rat adipose tissue. Purification and some properties. *J Biol Chem* **256**, 6311-6320.

Garton AJ, Campbell DG, Carling D, Hardie DG, Colbran RJ, & Yeaman SJ (1989). Phosphorylation of bovine hormone-sensitive lipase by the AMP-activated protein kinase. A possible antilipolytic mechanism. *Eur J Biochem* **179**, 249-254.

Garton AJ, Campbell DG, Cohen P, & Yeaman SJ (1988). Primary structure of the site on bovine hormone-sensitive lipase phosphorylated by cyclic AMP-dependent protein kinase. *FEBS Lett* **229**, 68-72.

Ghosh AK, Ramakrishnan G, Chandramohan C, & Rajasekharan R (2008). CGI-58, the Causative Gene for Chanarin-Dorfman Syndrome, Mediates Acylation of Lysophosphatidic Acid. *J Biol Chem* **283**, 24525-24533.

Gimeno RE & Cao J (2008). Mammalian glycerol-3-phosphate acyltransferases (GPATs): new genes for an old activity. *J Lipid Res* **49**, 2079-2088.

Gonzalez-Baro MR, Lewin TM, & Coleman RA (2007). Regulation of Triglyceride Metabolism II. Function of mitochondrial GPAT1 in the regulation of triacylglycerol biosynthesis and insulin action. *Am J Physiol Gastrointest Liver Physiol* **292**, G1195-G1199.

Goodpaster BH, He J, Watkins S, & Kelley DE (2001). Skeletal Muscle Lipid Content and Insulin Resistance: Evidence for a Paradox in Endurance-Trained Athletes. *J Clin Endocrinol Metab* **86**, 5755-5761.

Goodpaster BH, Kelley DE, Thaete FL, He J, & Ross R (2000). Skeletal muscle attenuation determined by computed tomography is associated with skeletal muscle lipid content. *J Appl Physiol* **89**, 104-110.

Granneman JG, Moore HP, Granneman RL, Greenberg AS, Obin MS, & Zhu Z (2007). Analysis of Lipolytic Protein Trafficking and Interactions in Adipocytes. *J Biol Chem* **282**, 5726-5735.

Granneman JG, Moore HP, Krishnamoorthy R, & Rathod M (2009a). Perilipin controls lipolysis by regulating the interactions of ab-hydrolase containing 5 (Abhd5) and adipose trigylceride lipase (ATGL). *J Biol Chem*.

Granneman JG, Moore HP, Mottillo EP, & Zhu Z (2009b). Functional Interactions between Mldp (LSDP5) and Abhd5 in the Control of Intracellular Lipid Accumulation. *J Biol Chem* **284**, 3049-3057.

Gray RE, Tanner CJ, Pories WJ, MacDonald KG, & Houmard JA (2003). Effect of weight loss on muscle lipid content in morbidly obese subjects. *Am J Physiol Endocrinol Metab* **284**, E726-E732.

Greco AV, Mingrone G, Giancaterini A, Manco M, Morroni M, Cinti S, Granzotto M, Vettor R, Camastra S, & Ferrannini E (2002). Insulin Resistance in Morbid Obesity. *Diabetes* **51**, 144-151.

Greenberg AS, Egan JJ, Wek SA, Moos MC, Jr., Londos C, & Kimmel AR (1993). Isolation of cDNAs for perilipins A and B: sequence and expression of lipid droplet-associated proteins of adipocytes. *Proc Natl Acad Sci U S A* **90**, 12035-12039.

Greenberg AS, Shen WJ, Muliro K, Patel S, Souza SC, Roth RA, & Kraemer FB (2001). Stimulation of Lipolysis and Hormone-sensitive Lipase via the Extracellular Signal-regulated Kinase Pathway. *J Biol Chem* **276**, 45456-45461.

Griffin ME, Marcucci MJ, Cline GW, Bell K, Barucci N, Lee D, Goodyear LJ, Kraegen EW, White MF, & Shulman GI (1999). Free fatty acid-induced insulin resistance is associated with activation of protein kinase C theta and alterations in the insulin signaling cascade. *Diabetes* **48**, 1270-1274.

Groop LC, Bonadonna RC, DelPrato S, Ratheiser K, Zyck K, Ferrannini E, & DeFronzo RA (1989). Glucose and free fatty acid metabolism in non-insulin-dependent diabetes mellitus. Evidence for multiple sites of insulin resistance. *J Clin Invest* **84**, 205-213.

Gruber A, Cornaciu I, Lass A, Schweiger M, Poeschl M, Eder C, Kumari M, Schoiswohl G, Wolinski H, Kohlwein SD, Zechner R, Zimmermann R, & Oberer M (2010). The N-terminal region of comparative gene identification-58 (CGI-58) is important for lipid droplet binding and activation of adipose triglyceride lipase. *J Biol Chem*.

Guo Y, Cordes KR, Farese RV, Jr., & Walther TC (2009). Lipid droplets at a glance. *J Cell Sci* **122**, 749-752.

Guo Z (2001). Triglyceride Content in Skeletal Muscle: Variability and the Source. *Analytical Biochemistry* **296**, 1-8.

Haemmerle G, Lass A, Zimmermann R, Gorkiewicz G, Meyer C, Rozman J, Heldmaier G, Maier R, Theussl C, Eder S, Kratky D, Wagner EF, Klingenspor M, Hoefler G, & Zechner R (2006). Defective Lipolysis and Altered Energy Metabolism in Mice Lacking Adipose Triglyceride Lipase. *Science* **312**, 734-737.

Haemmerle G, Zimmermann R, Hayn M, Theussl C, Waeg G, Wagner E, Sattler W, Magin TM, Wagner EF, & Zechner R (2002). Hormone-sensitive Lipase Deficiency in Mice Causes Diglyceride Accumulation in Adipose Tissue, Muscle, and Testis. *J Biol Chem* **277**, 4806-4815.

Hammond LE, Gallagher PA, Wang S, Hiller S, Kluckman KD, Posey-Marcos EL, Maeda N, & Coleman RA (2002). Mitochondrial Glycerol-3-Phosphate Acyltransferase-Deficient Mice Have Reduced Weight and Liver Triacylglycerol Content and Altered Glycerolipid Fatty Acid Composition. *Mol Cell Biol* **22**, 8204-8214.

Hansen PA, Wang W, Marshall BA, Holloszy JO, & Mueckler M (1998). Dissociation of GLUT4 Translocation and Insulin-stimulated Glucose Transport in Transgenic Mice Overexpressing GLUT1 in Skeletal Muscle. *J Biol Chem* **273**, 18173-18179.

Hardie DG, Carling D, & Carlson M (1998). The AMP-activated/SNF1 protein kinase subfamily: metabolic sensors of the eukaryotic cell? *Annu Rev Biochem* **67**, 821-855.

Haugaard SB, Mu H, Vaag A, & Madsbad S (2009). Intramyocellular triglyceride content in man, influence of sex, obesity and glycaemic control. *Eur J Endocrinol* **161**, 57-64.

Havel RJ, Pernow B, & Jones NL (1967). Uptake and release of free fatty acids and other metabolites in the legs of exercising men. *J Appl Physiol* **23**, 90-99.

He J, Goodpaster BH, & Kelley DE (2004). Effects of Weight Loss and Physical Activity on Muscle Lipid Content and Droplet Size. *Obesity Res* **12**, 761-769.

He J, Watkins S, & Kelley DE (2001). Skeletal Muscle Lipid Content and Oxidative Enzyme Activity in Relation to Muscle Fiber Type in Type 2 Diabetes and Obesity. *Diabetes* **50**, 817-823.

Helge JW, Watt PW, Richter EA, Rennie MJ, & Kiens B (2001). Fat utilization during exercise: adaptation to a fat-rich diet increases utilization of plasma fatty acids and very low density lipoprotein-triacylglycerol in humans. *J Physiol* **537**, 1009-1020.

Helmrich SP, Ragland DR, Leung RW, & Paffenbarger RS, Jr. (1991). Physical activity and reduced occurrence of non-insulin-dependent diabetes mellitus. *N Engl J Med* **325**, 147-152.

Hirsch AH & Rosen OM (1984). Lipolytic stimulation modulates the subcellular distribution of hormone- sensitive lipase in 3T3-L1 cells. *J Lipid Res* **25**, 665-677.

Hodson L, McQuaid SE, Humphreys SM, Milne R, Fielding BA, Frayn KN, & Karpe F (2010). Greater dietary fat oxidation in obese compared with lean men: an adaptive mechanism to prevent liver fat accumulation? *American Journal of Physiology - Endocrinology And Metabolism* **299**, E584-E592.

Hoeg L, Roepstorff C, Thiele M, Richter EA, Wojtaszewski JFP, & Kiens B (2009). Higher intramuscular triacylglycerol in women does not impair insulin sensitivity and proximal insulin signaling. *J Appl Physiol* **107**, 824-831.

Hokanson JE & Austin MA (1996). Plasma triglyceride level is a risk factor for cardiovascular disease independent of high-density lipoprotein cholesterol level: a meta-analysis of population-based prospective studies. *J Cardiovasc Risk* **3**, 213-219.

Hoppeler H (1999). Skeletal muscle substrate metabolism. *Int J Obes Relat Metab Disord* **23 Suppl 3**, S7-10.

Houmard JA, Tanner CJ, Yu C, Cunningham PG, Pories WJ, MacDonald KG, & Shulman GI (2002). Effect of Weight Loss on Insulin Sensitivity and Intramuscular Long-Chain Fatty Acyl-CoAs in Morbidly Obese Subjects. *Diabetes* **51**, 2959-2963.

Hoy AJ, Bruce CR, Turpin SM, Morris AJ, Febbraio MA, & Watt MJ (2011). Adipose Triglyceride Lipase-Null Mice Are Resistant to High-Fat Diet-Induced Insulin Resistance Despite Reduced Energy Expenditure and Ectopic Lipid Accumulation. *Endocrinology* **152**, 48-58.

Igal RA, Wang S, Gonzalez-Baro M, & Coleman RA (2001). Mitochondrial Glycerol Phosphate Acyltransferase Directs the Incorporation of Exogenous Fatty Acids into Triacylglycerol. *J Biol Chem* **276**, 42205-42212.

Itani SI, Zhou Q, Pories WJ, MacDonald KG, & Dohm GL (2000). Involvement of protein kinase C in human skeletal muscle insulin resistance and obesity. *Diabetes* **49**, 1353-1358.

Itani SI, Pories WJ, MacDonald KG, & Dohm GL (2001). Increased protein kinase C theta in skeletal muscle of diabetic patients. *Metabolism* **50**, 553-557.

Itani SI, Ruderman NB, Schmieder F, & Boden G (2002). Lipid-Induced Insulin Resistance in Human Muscle Is Associated With Changes in Diacylglycerol, Protein Kinase C, and I{kappa}B-{alpha}. *Diabetes* **51**, 2005-2011.

Jagerstrom S, Polesie S, Wickstrom Y, Johansson BR, Schroder HD, Hojlund K, & Bostrom P (2009). Lipid droplets interact with mitochondria using SNAP23. *Cell Biol Int* **33**, 934-940.

Jahn R & Scheller RH (2006). SNAREs - engines for membrane fusion. *Nat Rev Mol Cell Biol* **7**, 631-643.

Jenkins CM, Mancuso DJ, Yan W, Sims HF, Gibson B, & Gross RW (2004). Identification, Cloning, Expression, and Purification of Three Novel Human Calcium-independent Phospholipase A2 Family Members Possessing Triacylglycerol Lipase and Acylglycerol Transacylase Activities. *J Biol Chem* **279**, 48968-48975.

Jocken JW, Moro C, Goossens GH, Hansen D, Mairal A, Hesselink MK, Langin D, van Loon LJ, & Blaak EE (2010). Skeletal Muscle Lipase Content and Activity in Obesity and Type 2 Diabetes. *J Clin Endocrinol Metab*.

Jocken JW, Smit E, Goossens GH, Essers YP, van Baak MA, Mensink M, Saris WH, & Blaak EE (2008). Adipose triglyceride lipase (ATGL) expression in human skeletal muscle is type I (oxidative) fiber specific. *Histochem Cell Biol*.

Johnson NA, Stannard SR, Mehalski K, Trenell MI, Sachinwalla T, Thompson CH, & Thompson MW (2003). Intramyocellular triacylglycerol in prolonged cycling with high- and low-carbohydrate availability. *J Appl Physiol* **94**, 1365-1372.

Johnson NA, Stannard SR, Rowlands DS, Chapman PG, Thompson CH, Sachinwalla T, & Thompson MW (2006). Short-term suppression of plasma free fatty acids fails to improve insulin sensitivity when intramyocellular lipid is elevated. *Diabetic Medicine* **23**, 1061-1068.

Jorgensen AO, Kalnins V, & MacLennan DH (1979). Localization of sarcoplasmic reticulum proteins in rat skeletal muscle by immunofluorescence. *J Cell Biol* **80**, 372-384.

Jucker BM, Rennings AJM, Cline GW, & Shulman GI (1997). 13C and 31P NMR Studies on the Effects of Increased Plasma Free Fatty Acids on Intramuscular Glucose Metabolism in the Awake Rat. *J Biol Chem* **272**, 10464-10473.

Kanzaki M (2006). Insulin receptor signals regulating GLUT4 translocation and actin dynamics. *Endocr J* **53**, 267-293.

Katz LD, Glickman MG, Rapoport S, Ferrannini E, & DeFronzo RA (1983). Splanchnic and peripheral disposal of oral glucose in man. *Diabetes* **32**, 675-679.

Kawanishi M, Tamori Y, Okazawa H, Araki S, Shinoda H, & Kasuga M (2000a). Role of SNAP23 in Insulin-induced Translocation of GLUT4 in 3T3-L1 Adipocytes. Mediation of complex formation between syntaxin4 and VAMP2. *J Biol Chem* **275**, 8240-8247.

Kawanishi M, Tamori Y, Okazawa H, Araki S, Shinoda H, & Kasuga M (2000b). Role of SNAP23 in Insulin-induced Translocation of GLUT4 in 3T3-L1 Adipocytes. Mediation of Complex Formation between Syntaxin4 and VAMP2. *J Biol Chem* **275**, 8240-8247.

Kelemen BR, Hsiao K, & Goueli SA (2002). Selective in Vivo Inhibition of Mitogen-activated Protein Kinase Activation Using Cell-permeable Peptides . *J Biol Chem* **277**, 8741-8748.

Kelley DE, Goodpaster BH, & Storlien L (2002). Muscle triglyceride and insulin resistance. *Annu Rev Nutr* **22**, 325-346.

Kelley DE, Mokan M, Simoneau JA, & Mandarino LJ (1993). Interaction between glucose and free fatty acid metabolism in human skeletal muscle. *J Clin Invest* **92**, 91-98.

Khayat ZA, Tong P, Yaworsky K, Bloch RJ, & Klip A (2000). Insulin-induced actin filament remodeling colocalizes actin with phosphatidylinositol 3-kinase and GLUT4 in L6 myotubes. *J Cell Sci* **113**, 279-290.

Kiens B (2006). Skeletal Muscle Lipid Metabolism in Exercise and Insulin Resistance. *Physiol Rev* **86**, 205-243.

Kim HJ, Lee JS, & Kim CK (2004a). Effect of exercise training on muscle glucose transporter 4 protein and intramuscular lipid content in elderly men with impaired glucose tolerance. *Eur J Appl Physiol* **93**, 353-358.

Kim JK, Fillmore JJ, Sunshine MJ, Albrecht B, Higashimori T, Kim DW, Liu ZX, Soos TJ, Cline GW, O'Brien WR, Littman DR, & Shulman GI (2004b). PKC-theta knockout mice are protected from fat-induced insulin resistance. *J Clin Invest* **114**, 823-827.

Klein S, Coyle EF, & Wolfe RR (1994). Fat metabolism during low-intensity exercise in endurance-trained and untrained men. *Am J Physiol* **267**, E934-E940.

Knudson CM & Campbell KP (1989). Albumin is a major protein component of transverse tubule vesicles isolated from skeletal muscle. *J Biol Chem* **264**, 10795-10798.

Kobayashi K, Inoguchi T, Maeda Y, Nakashima N, Kuwano A, Eto E, Ueno N, Sasaki S, Sawada F, Fujii M, Matoba Y, Sumiyoshi S, Kawate H, & Takayanagi R (2008). The Lack of the C-Terminal Domain of Adipose Triglyceride Lipase Causes Neutral Lipid Storage Disease through Impaired Interactions with Lipid Droplets. *J Clin Endocrinol Metab* **93**, 2877-2884.

Koopman R, Schaart G, & Hesselink MK (2001). Optimisation of oil red O staining permits combination with immunofluorescence and automated quantification of lipids. *Histochem Cell Biol* **116**, 63-68.

Krssak M, Petersen KF, Bergeron R, Price T, Laurent D, Rothman DL, Roden M, & Shulman GI (2000). Intramuscular Glycogen and Intramyocellular Lipid Utilization during Prolonged Exercise and Recovery in Man: A 13C and 1H Nuclear Magnetic Resonance Spectroscopy Study. *J Clin Endocrinol Metab* **85**, 748-754.

Kruszynska YT, Worrall DS, Ofrecio J, Frias JP, Macaraeg G, & Olefsky JM (2002). Fatty Acid-Induced Insulin Resistance: Decreased Muscle PI3K Activation But Unchanged Akt Phosphorylation. *J Clin Endocrinol Metab* **87**, 226-234.

Langin D, Dicker A, Tavernier G, Hoffstedt J, Mairal A, Ryden M, Arner E, Sicard A, Jenkins CM, Viguerie N, van Harmelen V, Gross RW, Holm C, & Arner P (2005). Adipocyte Lipases and Defect of Lipolysis in Human Obesity. *Diabetes* **54**, 3190-3197.

Lara-Castro C, Newcomer BR, Rowell J, Wallace P, Shaughnessy SM, Munoz AJ, Shiflett AM, Rigsby DY, Lawrence JC, Bohning DE, Buchthal S, & Garvey WT (2008). Effects of short-term very low-calorie diet on intramyocellular lipid and insulin sensitivity in nondiabetic and type 2 diabetic subjects. *Metabolism* **57**, 1-8.

Larson-Meyer DE, Newcomer BR, & Hunter GR (2002). Influence of endurance running and recovery diet on intramyocellular lipid content in women: a 1H NMR study. *Am J Physiol Endocrinol Metab* **282**, E95-106.

Lass A, Zimmermann R, Haemmerle G, Riederer M, Schoiswohl G, Schweiger M, Kienesberger P, Strauss JG, Gorkiewicz G, & Zechner R (2006). Adipose triglyceride lipase-mediated lipolysis of cellular fat stores is activated by CGI-58 and defective in Chanarin-Dorfman Syndrome. *Cell Metabolism* **3**, 309-319.

Lass A, Zimmermann R, Oberer M, & Zechner R (2010). Lipolysis - a highly regulated multi-enzyme complex mediates the catabolism of cellular fat stores. *Progress in Lipid Research* **In Press, Accepted Manuscript**.

Lauritzen HPM, Ploug T, Ai H, Donsmark M, Prats C, & Galbo H (2008a). Denervation and High-Fat Diet Reduce Insulin Signaling in T-Tubules in Skeletal Muscle of Living Mice. *Diabetes* **57**, 13-23.

Lauritzen HPMM, Galbo H, Brandauer J, Goodyear LJ, & Ploug T (2008b). Large GLUT4 Vesicles Are Stationary While Locally and Reversibly Depleted During Transient Insulin Stimulation of Skeletal Muscle of Living Mice. *Diabetes* **57**, 315-324.

Lauritzen HPMM, Galbo H, Toyoda T, & Goodyear LJ (2010). Kinetics of Contraction-Induced GLUT4 Translocation in Skeletal Muscle Fibers From Living Mice. *Diabetes* **59**, 2134-2144.

Lauritzen HPMM, Ploug T, Prats C, Tavare JM, & Galbo H (2006). Imaging of Insulin Signaling in Skeletal Muscle of Living Mice Shows Major Role of T-Tubules. *Diabetes* **55**, 1300-1306.

Lauritzen HPMM & Schertzer JD (2010). Measuring GLUT4 translocation in mature muscle fibers. *Am J Physiol Endocrinol Metab* **299**, E169-E179.

Lebiedzinska M, Szabadkai G, Jones AW, Duszynski J, & Wieckowski MR (2009). Interactions between the endoplasmic reticulum, mitochondria, plasma membrane and other subcellular organelles. *Int J Biochem Cell Biol* **41**, 1805-1816.

Lewin TM, Granger DA, Kim JH, & Coleman RA (2001). Regulation of Mitochondrial sn-Glycerol-3-phosphate Acyltransferase Activity: Response to Feeding Status Is Unique in Various Rat Tissues and Is Discordant with Protein Expression. *Archives of Biochemistry and Biophysics* **396**, 119-127.

Lewin TM, Schwerbrock NMJ, Lee DP, & Coleman RA (2004). Identification of a New Glycerol-3-phosphate Acyltransferase Isoenzyme, mtGPAT2, in Mitochondria. *J Biol Chem* **279**, 13488-13495.

Lewin TM, Wang S, Nagle CA, Van Horn CG, & Coleman RA (2005). Mitochondrial glycerol-3-phosphate acyltransferase-1 directs the metabolic fate of exogenous fatty acids in hepatocytes. *Am J Physiol Endocrinol Metab* **288**, E835-E844.

Lewis GF, Carpentier A, Adeli K, & Giacca A (2002). Disordered Fat Storage and Mobilization in the Pathogenesis of Insulin Resistance and Type 2 Diabetes. *Endocr Rev* **23**, 201-229.

Li M, Paran C, Wolins NE, & Horowitz JF (2011). High muscle lipid content in obesity is not due to enhanced activation of key triglyceride esterification enzymes or to the suppression of lipolytic proteins. *American Journal of Physiology - Endocrinology And Metabolism*.

Linden D, William-Olsson L, Ahnmark A, Ekroos K, Hallberg C, Sjogren HP, Becker B, Svensson L, Clapham JC, Oscarsson J, & Schreyer S (2006). Liver-directed overexpression of mitochondrial glycerol-3-phosphate acyltransferase results in hepatic steatosis, increased triacylglycerol secretion and reduced fatty acid oxidation. *FASEB J* **20**, 434-443.

Lipman RL, Raskin P, Love T, Triebwasser J, Lecocq FR, & Schnure JJ (1972). Glucose intolerance during decreased physical activity in man. *Diabetes* **21**, 101-107.

Listenberger LL, Ostermeyer-Fay AG, Goldberg EB, Brown WJ, & Brown DA (2007). Adipocyte differentiation-related protein reduces the lipid droplet association of adipose triglyceride lipase and slows triacylglycerol turnover. *J Lipid Res* **48**, 2751-2761.

Liu L, Shi X, Bharadwaj KG, Ikeda S, Yamashita H, Yagyu H, Schaffer JE, Yu YH, & Goldberg IJ (2009a). DGAT1 Expression Increases Heart Triglyceride Content but Ameliorates Lipotoxicity. *J Biol Chem* **284**, 36312-36323.

Liu L, Shi X, Choi CS, Shulman GI, Klaus K, Nair KS, Schwartz GJ, Zhang Y, Goldberg IJ, & Yu YH (2009b). Paradoxical coupling of triglyceride synthesis and fatty acid oxidation in skeletal muscle overexpressing DGAT1. *Diabetes*.

Liu L, Zhang Y, Chen N, Shi X, Tsang B, & Yu YH (2007). Upregulation of myocellular DGAT1 augments triglyceride synthesis in skeletal muscle and protects against fat-induced insulin resistance. *J Clin Invest* **117**, 1679-1689.

Liu LZ, Zhao HL, Zuo J, Ho SKS, Chan JCN, Meng Y, Fang FD, & Tong PCY (2006). Protein Kinase C{zeta} Mediates Insulin-induced Glucose Transport through Actin Remodeling in L6 Muscle Cells. *Mol Biol Cell* **17**, 2322-2330.

Liu P, Ying Y, Zhao Y, Mundy DI, Zhu M, & Anderson RG (2004). Chinese hamster ovary K2 cell lipid droplets appear to be metabolic organelles involved in membrane traffic. *J Biol Chem* **279**, 3787-3792.

Londos C, Brasaemle DL, Gruia-Gray J, Servetnick DA, Schultz CJ, Levin DM, & Kimmel AR (1995). Perilipin: unique proteins associated with intracellular neutral lipid droplets in adipocytes and steroidogenic cells. *Biochem Soc Trans* **23**, 611-615.

Malenfant P, Joanisse DR, Theriault R, Goodpaster BH, Kelley DE, & Simoneau JA (2001). Fat content in individual muscle fibers of lean and obese subjects. *Int J Obes Relat Metab Disord* **25**, 1316-1321.

Mansell PI & Macdonald IA (1990). The effect of starvation on insulin-induced glucose disposal and thermogenesis in humans. *Metabolism* **39**, 502-510.

Marchesan D, Rutberg M, Andersson L, Asp L, Larsson T, Boren J, Johansson BR, & Olofsson SO (2003). A phospholipase D-dependent process forms lipid droplets containing caveolin, adipocyte differentiation-related protein, and vimentin in a cell-free system. *J Biol Chem* **278**, 27293-27300.

Marette A, Burdett E, Douen A, Vranic M, & Klip A (1992). Insulin induces the translocation of GLUT4 from a unique intracellular organelle to transverse tubules in rat skeletal muscle. *Diabetes* **41**, 1562-1569.

Martin S, Tellam J, Livingstone C, Slot JW, Gould GW, & James DE (1996). The glucose transporter (GLUT-4) and vesicle-associated membrane protein-2 (VAMP-2) are segregated from recycling endosomes in insulin- sensitive cells. *J Cell Biol* **134**, 625-635.

Martin S, Driessen K, Nixon SJ, Zerial M, & Parton RG (2005). Regulated Localization of Rab18 to Lipid Droplets. *J Biol Chem* **280**, 42325-42335.

Martin S & Parton RG (2006). Lipid droplets: a unified view of a dynamic organelle. *Nat Rev Mol Cell Biol* **7**, 373-378.

Martinez O & Goud B (1998). Rab proteins. *Biochim Biophys Acta* **1404**, 101-112.

McQuaid SE, Hodson L, Neville MJ, Dennis AL, Cheeseman J, Humphreys SM, Ruge T, Gilbert M, Fielding BA, Frayn KN, & Karpe F (2011). Downregulation of Adipose Tissue Fatty Acid Trafficking in Obesity. *Diabetes* **60**, 47-55.

Meex RCR, Schrauwen-Hinderling VB, Moonen-Kornips E, Schaart G, Mensink M, Phielix E, van de Weijer T, Sels JP, Schrauwen P, & Hesselink MKC (2010). Restoration of Muscle Mitochondrial Function and Metabolic Flexibility in Type 2 Diabetes by Exercise Training Is Paralleled by Increased Myocellular Fat Storage and Improved Insulin Sensitivity. *Diabetes* **59**, 572-579.

Mikines KJ, Richter EA, Dela F, & Galbo H (1991). Seven days of bed rest decrease insulin action on glucose uptake in leg and whole body. *J Appl Physiol* **70**, 1245-1254.

Mittendorfer B, Magkos F, Fabbrini E, Mohammed BS, & Klein S (2009). Relationship Between Body Fat Mass and Free Fatty Acid Kinetics in Men and Women. *Obesity Res* **17**, 1872-1877.

Monroy G, Kelker HC, & Pullman ME (1973). Partial Purification and Properties of an Acyl Coenzyme A:sn-Glycerol 3-Phosphate Acyltransferase from Rat Liver Mitochondria. *J Biol Chem* **248**, 2845-2852.

Montero-Moran G, Caviglia JM, McMahon D, Rothenberg A, Subramanian V, Xu Z, Lara-Gonzalez S, Storch J, Carman GM, & Brasaemle DL (2010). CGI-58/ABHD5 is a coenzyme A-dependent lysophosphatidic acid acyltransferase. *J Lipid Res* **51**, 709-719.

Montero-Moran G, Caviglia JM, McMahon D, Rothenberg A, Subramanian V, Xu Z, Lara-Gonzalez S, Storch J, Carman GM, & Brasaemle DL (2009). CGI-58/ABHD5 is a coenzyme A-dependent lysophosphatidic acid acyltransferase. *J Lipid Res* jlr.

Moro C, Bajpeyi S, & Smith SR (2008). Determinants of intramyocellular triglyceride turnover: implications for insulin sensitivity. *Am J Physiol Endocrinol Metab* **294**, E203-E213.

Moro C, Galgani JE, Luu L, Pasarica M, Mairal A, Bajpeyi S, Schmitz G, Langin D, Liebisch G, & Smith SR (2009). Influence of gender, obesity, and muscle lipase activity on intramyocellular lipids in sedentary individuals. *J Clin Endocrinol Metab* jc.

Mulder H, Sorhede-Wizell M, Contreras JA, Fex M, Strom K, Ploug T, Galbo H, Arner P, Lundberg C, Sundler F, Ahren B, & Holm C (2003). Hormone-sensitive Lipase Null Mice Exhibit Signs of Impaired Insulin Sensitivity whereas Insulin Secretion Is Intact. *J Biol Chem* **278**, 36380-36388.

Murphy DJ & Vance J (1999). Mechanisms of lipid-body formation. *Trends in Biochemical Sciences* **24**, 109-115.

Nagle CA, Vergnes L, DeJong H, Wang S, Lewin TM, Reue K, & Coleman RA (2008). Identification of a novel sn-glycerol-3-phosphate acyltransferase isoform, GPAT4, as the enzyme deficient in Agpat6-/- mice. *J Lipid Res* **49**, 823-831.

Nakagawa Y, Hattori M, Harada K, Shirase R, Bando M, & Okano G (2007). Age-related changes in intramyocellular lipid in humans by in vivo H-MR spectroscopy. *Gerontology* **53**, 218-223.

Narkar VA, Downes M, Yu RT, Embler E, Wang YX, Banayo E, Mihaylova MM, Nelson MC, Zou Y, Juguilon H, Kang H, Shaw RJ, & Evans RM (2008). AMPK and PPARdelta agonists are exercise mimetics. *Cell* **134**, 405-415.

Nebl T, Oh SW, & Luna EJ (2000). Membrane cytoskeleton: PIP(2) pulls the strings. *Curr Biol* **10**, R351-R354.

Newsom SA, Schenk S, Li M, Everett AC, & Horowitz JF (2010). High fatty acid availability after exercise alters the regulation of muscle lipid metabolism. *Metabolism*.

NHS Information Centre. Health Survey for England 2007: Healthy Lifestyles: Knowledge, Attitudes and Behaviour. 2008. NHS Information Centre.
Ref Type: Report

NHS Information Centre. Prescribing for Diabetes in England: Supplement - January 2002 - March 2009. 2009. NHS Information Centre.
Ref Type: Report

Nolte LA, Galuska D, Martin IK, Zierath JR, & Wallberg-Henriksson H (1994). Elevated free fatty acid levels inhibit glucose phosphorylation in slow-twitch rat skeletal muscle. *Acta Physiol Scand* **151**, 51-59.

Oakes ND, Bell KS, Furler SM, Camilleri S, Saha AK, Ruderman NB, Chisholm DJ, & Kraegen EW (1997a). Diet-induced muscle insulin resistance in rats is ameliorated by acute dietary lipid withdrawal or a single bout of exercise: parallel relationship between insulin stimulation of glucose uptake and suppression of long-chain fatty acyl-CoA. *Diabetes* **46**, 2022-2028.

Oakes ND, Cooney GJ, Camilleri S, Chisholm DJ, & Kraegen EW (1997b). Mechanisms of liver and muscle insulin resistance induced by chronic high-fat feeding. *Diabetes* **46**, 1768-1774.

Oakes ND, Kennedy CJ, Jenkins AB, Laybutt DR, Chisholm DJ, & Kraegen EW (1994). A new antidiabetic agent, BRL 49653, reduces lipid availability and improves insulin action and glucoregulation in the rat. *Diabetes* **43**, 1203-1210.

Ohsaki Y, Cheng J, Suzuki M, Shinohara Y, Fujita A, & Fujimoto T (2009). Biogenesis of cytoplasmic lipid droplets: from the lipid ester globule in the membrane to the visible structure. *Biochim Biophys Acta* **1791**, 399-407.

Oja P (1995). Descriptive epidemiology of health-related physical activity and fitness. *Research Quarterly for Exercise and Sport* **66**, 303-312.

Okada T, Kawano Y, Sakakibara T, Hazeki O, & Ui M (1994). Essential role of phosphatidylinositol 3-kinase in insulin-induced glucose transport and antilipolysis in rat adipocytes. Studies with a selective inhibitor wortmannin. *J Biol Chem* **269**, 3568-3573.

Ong JM & Kern PA (1989). Effect of feeding and obesity on lipoprotein lipase activity, immunoreactive protein, and messenger RNA levels in human adipose tissue. *J Clin Invest* **84**, 305-311.

Opie LH & Walfish PG (1963). Plasma free fatty acid concentrations in obesity. *N Engl J Med* **268**, 757-760.

Oscai LB, Essig DA, & Palmer WK (1990). Lipase regulation of muscle triglyceride hydrolysis. *J Appl Physiol* **69**, 1571-1577.

Osuga Ji, Ishibashi S, Oka T, Yagyu H, Tozawa R, Fujimoto A, Shionoiri F, Yahagi N, Kraemer FB, Tsutsumi O, & Yamada N (2000). Targeted disruption of hormone-sensitive

lipase results in male sterility and adipocyte hypertrophy, but not in obesity. *Proceedings of the National Academy of Sciences of the United States of America* **97**, 787-792.

Ozeki S, Cheng J, Tauchi-Sato K, Hatano N, Taniguchi H, & Fujimoto T (2005). Rab18 localizes to lipid droplets and induces their close apposition to the endoplasmic reticulum-derived membrane. *J Cell Sci* **118**, 2601-2611.

Pan DA, Lillioja S, Kriketos AD, Milner MR, Baur LA, Bogardus C, Jenkins AB, & Storlien LH (1997). Skeletal muscle triglyceride levels are inversely related to insulin action. *Diabetes* **46**, 983-988.

Park H, Kaushik VK, Constant S, Prentki M, Przybytkowski E, Ruderman NB, & Saha AK (2002). Coordinate Regulation of Malonyl-CoA Decarboxylase, sn-Glycerol-3-phosphate Acyltransferase, and Acetyl-CoA Carboxylase by AMP-activated Protein Kinase in Rat Tissues in Response to Exercise. *J Biol Chem* **277**, 32571-32577.

Patsch JR, Miesenbock G, Hopferwieser T, Muhlberger V, Knapp E, Dunn JK, Gotto AM, Jr., & Patsch W (1992). Relation of triglyceride metabolism and coronary artery disease. Studies in the postprandial state. *Arterioscler Thromb* **12**, 1336-1345.

Pellon-Maison M, Montanaro MA, Coleman RA, & Gonzalez-Baro MR (2007). Mitochondrial glycerol-3-P acyltransferase 1 is most active in outer mitochondrial membrane but not in mitochondrial associated vesicles (MAV). *Biochimica et Biophysica Acta (BBA) - Molecular and Cell Biology of Lipids* **1771**, 830-838.

Perreault L, Bergman BC, Hunerdosse DM, & Eckel RH (2010). Altered Intramuscular Lipid Metabolism Relates to Diminished Insulin Action in Men, but Not Women, in Progression to Diabetes. *Obesity Res*.

Pessin JE & Saltiel AR (2000). Signaling pathways in insulin action: molecular targets of insulin resistance. *J Clin Invest* **106**, 165-169.

Petersen KF, Dufour S, Befroy D, Lehrke M, Hendler RE, & Shulman GI (2005). Reversal of Nonalcoholic Hepatic Steatosis, Hepatic Insulin Resistance, and Hyperglycemia by Moderate Weight Reduction in Patients With Type 2 Diabetes. *Diabetes* **54**, 603-608.

Ploug T, van Deurs B, Ai H, Cushman SW, & Ralston E (1998). Analysis of GLUT4 Distribution in Whole Skeletal Muscle Fibers: Identification of Distinct Storage Compartments That Are Recruited by Insulin and Muscle Contractions. *J Cell Biol* **142**, 1429-1446.

Potts JL, Coppack SW, Fisher RM, Humphreys SM, Gibbons GF, & Frayn KN (1995). Impaired postprandial clearance of triacylglycerol-rich lipoproteins in adipose tissue in obese subjects. *Am J Physiol* **268**, E588-E594.

Prats C, Donsmark M, Qvortrup K, Londos C, Sztalryd C, Holm C, Galbo H, & Ploug T (2006). Decrease in intramuscular lipid droplets and translocation of HSL in response to muscle contraction and epinephrine. *J Lipid Res* **47**, 2392-2399.

Prentice AM & Jebb SA (1995). Obesity in Britain: gluttony or sloth? *BMJ* **311**, 437-439.

Rabol R, Svendsen PF, Skovbro M, Boushel R, Haugaard SB, Schjerling P, Schrauwen P, Hesselink MK, Nilas L, Madsbad S, & Dela F (2009). Reduced skeletal muscle mitochondrial respiration and improved glucose metabolism in nondiabetic obese women during a very low calorie dietary intervention leading to rapid weight loss. *Metabolism* **58**, 1145-1152.

Randle PJ, Garland PB, Hales CN, & Newsholme EA (1963). The glucose fatty-acid cycle. Its role in insulin sensitivity and the metabolic disturbances of diabetes mellitus. *Lancet* **1**, 785-789.

Ravichandran V, Chawla A, & Roche PA (1996). Identification of a novel syntaxin- and synaptobrevin/VAMP-binding protein, SNAP-23, expressed in non-neuronal tissues. *J Biol Chem* **271**, 13300-13303.

Rea S, Martin LB, McIntosh S, Macaulay SL, Ramsdale T, Baldini G, & James DE (1998). Syndet, an Adipocyte Target SNARE Involved in the Insulin-induced Translocation of GLUT4 to the Cell Surface. *J Biol Chem* **273**, 18784-18792.

Richelsen B, Pedersen SB, Moller-Pedersen T, Schmitz O, Moller N, & Borglum JD (1993). Lipoprotein lipase activity in muscle tissue influenced by fatness, fat distribution and insulin in obese females. *Eur J Clin Invest* **23**, 226-233.

Rico-Sanz J, Moosavi M, Thomas EL, McCarthy J, Coutts GA, Saeed N, & Bell JD (2000). In vivo evaluation of the effects of continuous exercise on skeletal muscle triglycerides in trained humans. *Lipids* **35**, 1313-1318.

Robenek H, Hofnagel O, Buers I, Robenek MJ, Troyer D, & Severs NJ (2006). Adipophilin-enriched domains in the ER membrane are sites of lipid droplet biogenesis. *J Cell Sci* **119**, 4215-4224.

Robenek H, Robenek MJ, & Troyer D (2005). PAT family proteins pervade lipid droplet cores. *J Lipid Res* **46**, 1331-1338.

Roden M, Krssak M, Stingl H, Gruber S, Hofer A, Furnsinn C, Moser E, & Waldhausl W (1999). Rapid impairment of skeletal muscle glucose transport/phosphorylation by free fatty acids in humans. *Diabetes* **48**, 358-364.

Roden M, Price TB, Perseghin G, Petersen KF, Rothman DL, Cline GW, & Shulman GI (1996). Mechanism of free fatty acid-induced insulin resistance in humans. *J Clin Invest* **97**, 2859-2865.

Roepstorff C, Donsmark M, Thiele M, Vistisen B, Stewart G, Vissing K, Schjerling P, Hardie DG, Galbo H, & Kiens B (2006). Sex differences in hormone-sensitive lipase expression, activity, and phosphorylation in skeletal muscle at rest and during exercise. *Am J Physiol Endocrinol Metab* **291**, E1106-E1114.

Roepstorff C, Steffensen CH, Madsen M, Stallknecht B, Kanstrup IL, Richter EA, & Kiens B (2002). Gender differences in substrate utilization during submaximal exercise in endurance-trained subjects. *Am J Physiol Endocrinol Metab* **282**, E435-E447.

Roorda BD, Hesselink MKC, Schaart G, Moonen-Kornips E, Martinez-Martinez P, Losen M, De Baets MH, Mensink RP, & Schrauwen P (2005). DGAT1 overexpression in muscle by in vivo DNA electroporation increases intramyocellular lipid content. *J Lipid Res* **46**, 230-236.

Ruderman NB, Saha AK, Vavvas D, & Witters LA (1999). Malonyl-CoA, fuel sensing, and insulin resistance. *Am J Physiol* **276**, E1-E18.

Ruge T, Hodson L, Cheeseman J, Dennis AL, Fielding BA, Humphreys SM, Frayn KN, & Karpe F (2009). Fasted to Fed Trafficking of Fatty Acids in Human Adipose Tissue Reveals a Novel Regulatory Step for Enhanced Fat Storage. *J Clin Endocrinol Metab* **94**, 1781-1788.

Ryden M, Jocken J, van Harmelen V, Dicker A, Hoffstedt J, Wiren M, Blomqvist L, Mairal A, Langin D, Blaak E, & Arner P (2007). Comparative studies of the role of hormone-sensitive lipase and adipose triglyceride lipase in human fat cell lipolysis. *Am J Physiol Endocrinol Metab* **292**, E1847-E1855.

Sacchetti M, Saltin B, Olsen DB, & van HG (2004). High triacylglycerol turnover rate in human skeletal muscle. *J Physiol* **561**, 883-891.

Sacchetti M, Saltin B, Osada T, & van HG (2002). Intramuscular fatty acid metabolism in contracting and non-contracting human skeletal muscle. *J Physiol* **540**, 387-395.

Sadur CN, Yost TJ, & Eckel RH (1984). Insulin responsiveness of adipose tissue lipoprotein lipase is delayed but preserved in obesity. *J Clin Endocrinol Metab* **59**, 1176-1182.

Schenk S, Cook JN, Kaufman AE, & Horowitz JF (2005). Postexercise insulin sensitivity is not impaired after an overnight lipid infusion. *Am J Physiol Endocrinol Metab* **288**, E519-E525.

Schenk S & Horowitz JF (2007). Acute exercise increases triglyceride synthesis in skeletal muscle and prevents fatty acid-induced insulin resistance. *J Clin Invest* **117**, 1690-1698.

Schmitz-Peiffer C, Browne CL, Oakes ND, Watkinson A, Chisholm DJ, Kraegen EW, & Biden TJ (1997). Alterations in the expression and cellular localization of protein kinase C isozymes epsilon and theta are associated with insulin resistance in skeletal muscle of the high-fat-fed rat. *Diabetes* **46**, 169-178.

Schmitz-Peiffer C, Craig DL, & Biden TJ (1999). Ceramide Generation Is Sufficient to Account for the Inhibition of the Insulin-stimulated PKB Pathway in C2C12 Skeletal Muscle Cells Pretreated with Palmitate. *J Biol Chem* **274**, 24202-24210.

Schrauwen-Hinderling VB, Schrauwen P, Hesselink MKC, van Engelshoven JMA, Nicolay K, Saris WHM, Kessels AGH, & Kooi ME (2003). The Increase in Intramyocellular Lipid Content Is a Very Early Response to Training. *Journal of Clinical Endocrinology & Metabolism* **88**, 1610-1616.

Schrauwen-Hinderling VB, Kooi ME, Hesselink MKC, Moonen-Kornips E, Schaart G, Mustard KJ, Hardie DG, Saris WHM, Nicolay K, & Schrauwen P (2005). Intramyocellular Lipid Content and Molecular Adaptations in Response to a 1-Week High-Fat Diet. *Obesity Res* **13**, 2088-2094.

Schweiger M, Schoiswohl G, Lass A, Radner FPW, Haemmerle G, Malli R, Graier W, Cornaciu I, Oberer M, Salvayre R, Fischer J, Zechner R, & Zimmermann R (2008). The C-terminal Region of Human Adipose Triglyceride Lipase Affects Enzyme Activity and Lipid Droplet Binding. *J Biol Chem* **283**, 17211-17220.

Schweiger M, Schreiber R, Haemmerle G, Lass A, Fledelius C, Jacobsen P, Tornqvist H, Zechner R, & Zimmermann R (2006). Adipose Triglyceride Lipase and Hormone-sensitive Lipase Are the Major Enzymes in Adipose Tissue Triacylglycerol Catabolism. *J Biol Chem* **281**, 40236-40241.

Servetnick DA, Brasaemle DL, Gruia-Gray J, Kimmel AR, Wolff J, & Londos C (1995). Perilipins are associated with cholesteryl ester droplets in steroidogenic adrenal cortical and Leydig cells. *J Biol Chem* **270**, 16970-16973.

Shaw CS, Jones DA, & Wagenmakers AJ (2008). Network distribution of mitochondria and lipid droplets in human muscle fibres. *Histochem Cell Biol*.

Shaw CS, Sherlock M, Stewart PM, & Wagenmakers AJ (2009). Adipophilin distribution and colocalization with lipid droplets in skeletal muscle. *Histochem Cell Biol* **131**, 575-581.

Shen WJ, Patel S, Natu V, & Kraemer FB (1998). Mutational analysis of structural features of rat hormone-sensitive lipase. *Biochemistry* **37**, 8973-8979.

Shepherd SO, Cocks M, Tipton KD, Ranasinghe AM, Barker TA, Burniston JG, Wagenmakers AJM & Shaw CS (2012). Preferential utilisation of perilipin 2 associated intramuscular triglycerides during one hour of moderate intensity endurance-type exercise. *Exp Physiol* ePub ahead of print.

Shin DH, Paulauskis JD, Moustaid N, & Sul HS (1991). Transcriptional regulation of p90 with sequence homology to Escherichia coli glycerol-3-phosphate acyltransferase. *J Biol Chem* **266**, 23834-23839.

Sollner T, Whiteheart SW, Brunner M, Erdjument-Bromage H, Geromanos S, Tempst P, & Rothman JE (1993). SNAP receptors implicated in vesicle targeting and fusion. *Nature* **362**, 318-324.

Sollner TH (2007). Lipid droplets highjack SNAREs. *Nat Cell Biol* **9**, 1219-1220.

Solomon TPJ, Sistrun SN, Krishnan RK, Del Aguila LF, Marchetti CM, O'Carroll SM, O'Leary VB, & Kirwan JP (2008). Exercise and diet enhance fat oxidation and reduce insulin resistance in older obese adults. *J Appl Physiol* **104**, 1313-1319.

St-Denis JF, Cabaniols JP, Cushman SW, & Roche PA (1999). SNAP-23 participates in SNARE complex assembly in rat adipose cells. *Biochem J* **338**, 709-715.

Stannard SR, Thompson MW, Fairbairn K, Huard B, Sachinwalla T, & Thompson CH (2002). Fasting for 72 h increases intramyocellular lipid content in nondiabetic, physically fit men. *Am J Physiol Endocrinol Metab* **283**, E1185-E1191.

Starling RD, Trappe TA, Parcell AC, Kerr CG, Fink WJ, & Costill DL (1997). Effects of diet on muscle triglyceride and endurance performance. *J Appl Physiol* **82**, 1185-1189.

Steffensen CH, Roepstorff C, Madsen M, & Kiens B (2002). Myocellular triacylglycerol breakdown in females but not in males during exercise. *Am J Physiol Endocrinol Metab* **282**, E634-E642.

Stellingwerff T, Boon H, Jonkers RAM, Senden JM, Spriet LL, Koopman R, & van Loon LJC (2007). Significant intramyocellular lipid use during prolonged cycling in endurance-trained males as assessed by three different methodologies. *Am J Physiol Endocrinol Metab* **292**, E1715-E1723.

Stern W & Pullman ME (1978). Acyl-CoA:sn-glycerol-3-phosphate acyltransferase and the positional distribution of fatty acids in phospholipids of cultured cells. *J Biol Chem* **253**, 8047-8055.

Stettler R, Ith M, Acheson KJ, Decombaz J, Boesch C, Tappy L, & Binnert C (2005). Interaction Between Dietary Lipids and Physical Inactivity on Insulin Sensitivity and on Intramyocellular Lipids in Healthy Men. *Diabetes Care* **28**, 1404-1409.

Stockli J, Davey JR, Hohnen-Behrens C, Xu A, James DE, & Ramm G (2008). Regulation of Glucose Transporter 4 Translocation by the Rab Guanosine Triphosphatase-Activating Protein AS160/TBC1D4: Role of Phosphorylation and Membrane Association. *Mol Endocrinol* **22**, 2703-2715.

Stone SJ, Levin MC, Zhou P, Han J, Walther TC, & Farese RV, Jr. (2009). The Endoplasmic Reticulum Enzyme DGAT2 Is Found in Mitochondria-associated Membranes and Has a Mitochondrial Targeting Signal That Promotes Its Association with Mitochondria. *J Biol Chem* **284**, 5352-5361.

Storlien L, Oakes ND, & Kelley DE (2004). Metabolic flexibility. *Proc Nutr Soc* **63**, 363-368.

Stralfors P, Bjorgell P, & Belfrage P (1984). Hormonal regulation of hormone-sensitive lipase in intact adipocytes: identification of phosphorylated sites and effects on the phosphorylation by lipolytic hormones and insulin. *Proc Natl Acad Sci U S A* **81**, 3317-3321.

Stuart CA, Shangraw RE, Prince MJ, Peters EJ, & Wolfe RR (1988). Bed-rest-induced insulin resistance occurs primarily in muscle. *Metabolism* **37**, 802-806.

Subramanian V, Rothenberg A, Gomez C, Cohen AW, Garcia A, Bhattacharyya S, Shapiro L, Dolios G, Wang R, Lisanti MP, & Brasaemle DL (2004). Perilipin A Mediates the Reversible Binding of CGI-58 to Lipid Droplets in 3T3-L1 Adipocytes. *J Biol Chem* **279**, 42062-42071.

Summermatter S, Baum O, Santos G, Hoppeler H, & Handschin C (2010). Peroxisome proliferator-activated receptor {gamma} coactivator 1{alpha} (PGC-1{alpha}) promotes skeletal muscle lipid refueling in vivo by activating de novo lipogenesis and the pentose phosphate pathway. *J Biol Chem* **285**, 32793-32800.

Sun Y, Bilan PJ, Liu Z, & Klip A (2010). Rab8A and Rab13 are activated by insulin and regulate GLUT4 translocation in muscle cells. *Proc Natl Acad Sci U S A* **107**, 19909-19914.

Sztalryd C, Xu G, Dorward H, Tansey JT, Contreras JA, Kimmel AR, & Londos C (2003). Perilipin A is essential for the translocation of hormone-sensitive lipase during lipolytic activation. *J Cell Biol* **161**, 1093-1103.

Takeuchi K & Reue K (2009). Biochemistry, Physiology, and Genetics of GPAT, AGPAT, and Lipin Enzymes in Triglyceride Synthesis. *Am J Physiol Endocrinol Metab* 90958.

Tamura Y, Tanaka Y, Sato F, Choi JB, Watada H, Niwa M, Kinoshita J, Ooka A, Kumashiro N, Igarashi Y, Kyogoku S, Maehara T, Kawasumi M, Hirose T, & Kawamori R (2005). Effects of Diet and Exercise on Muscle and Liver Intracellular Lipid Contents and Insulin Sensitivity in Type 2 Diabetic Patients. *J Clin Endocrinol Metab* **90**, 3191-3196.

Tarnopolsky MA, Rennie C, Robertshaw HA, Fedak-Tarnopolsky SN, Devries MC, & Hamadeh MJ (2007). Influence of endurance exercise training and sex on intramyocellular lipid and mitochondrial ultrastructure, substrate use, and mitochondrial enzyme activity. *Am J Physiol Regul Integr Comp Physiol* **292**, R1271-R1278.

Taskinen MR (2003). LDL-cholesterol, HDL-cholesterol or triglycerides--which is the culprit? *Diabetes Research and Clinical Practice* **61**, S19-S26.

Thrush AB, Brindley DN, Chabowski A, Heigenhauser GJ, & Dyck DJ (2009). Skeletal Muscle Lipogenic Protein Expression Is Not Different between Lean and Obese Individuals; A Potential Factor in Ceramide Accumulation. *J Clin Endocrinol Metab* jc.

Toledo FGS, Menshikova EV, Azuma K, Radikova Z, Kelley CA, Ritov VB, & Kelley DE (2008). Mitochondrial Capacity in Skeletal Muscle Is Not Stimulated by Weight Loss Despite Increases in Insulin Action and Decreases in Intramyocellular Lipid Content. *Diabetes* **57**, 987-994.

van Loon LJ & Goodpaster BH (2006). Increased intramuscular lipid storage in the insulin-resistant and endurance-trained state. *Pflugers Arch* **451**, 606-616.

van Loon LJ, Manders RJ, Koopman R, Kaastra B, Stegen JH, Gijsen AP, Saris WH, & Keizer HA (2005). Inhibition of adipose tissue lipolysis increases intramuscular lipid use in type 2 diabetic patients. *Diabetologia* **48**, 2097-2107.

van Loon LJC (2004). Use of intramuscular triacylglycerol as a substrate source during exercise in humans. *J Appl Physiol* **97**, 1170-1187.

van Loon LJC, Greenhaff PL, Constantin-Teodosiu D, Saris WHM, & Wagenmakers AJM (2001). The effects of increasing exercise intensity on muscle fuel utilisation in humans. *J Physiol* **536**, 295-304.

van Loon LJC, Koopman R, Stegen JHCH, Wagenmakers AJM, Keizer HA, & Saris WHM (2003a). Intramyocellular lipids form an important substrate source during moderate intensity exercise in endurance-trained males in a fasted state. *The Journal of Physiology* **553**, 611-625.

van Loon LJC, Koopman R, Manders R, van der Weegen W, van Kranenburg GP, & Keizer HA (2004). Intramyocellular lipid content in type 2 diabetes patients compared with overweight sedentary men and highly trained endurance athletes. *Am J Physiol Endocrinol Metab* **287**, E558-E565.

van Loon LJC, Schrauwen-Hinderling VB, Koopman R, Wagenmakers AJM, Hesselink MKC, Schaart G, Kooi ME, & Saris WHM (2003b). Influence of prolonged endurance cycling and recovery diet on intramuscular triglyceride content in trained males. *Am J Physiol Endocrinol Metab* **285**, E804-E811.

Van Proeyen K, Szlufcik K, Nielens H, Ramaekers M, & Hespel P (2011). Beneficial metabolic adaptations due to endurance exercise training in the fasted state. *J Appl Physiol* **110**, 236-245.

Vessby B, Unsitupa M, Hermansen K, Riccardi G, Rivellese AA, Tapsell LC, Nalsen C, Berglund L, Louheranta A, Rasmussen BM, Calvert GD, Maffetone A, Pedersen E, Gustafsson IB, & Storlien LH (2001). Substituting dietary saturated for monounsaturated fat impairs insulin sensitivity in healthy men and women: The KANWU Study. *Diabetologia* **44**, 312-319.

Villena JA, Roy S, Sarkadi-Nagy E, Kim KH, & Sul HS (2004). Desnutrin, an Adipocyte Gene Encoding a Novel Patatin Domain-containing Protein, Is Induced by Fasting and Glucocorticoids: Ectopic Expression of Desnutrin Increases Triglyceride Hydrolysis. *J Biol Chem* **279**, 47066-47075.

Vogt M, Puntschart A, Howald H, Mueller B, Mannhart C, Gfeller-Tuescher L, Mullis P, & Hoppeler H (2003). Effects of dietary fat on muscle substrates, metabolism, and performance in athletes. *Med Sci Sports Exerc* **35**, 952-960.

Wang H, Bell M, Sreenevasan U, Hu H, Liu J, Dalen K, Londos C, Yamaguchi T, Rizzo MA, Coleman R, Gong D, Brasaemle D, & Sztalryd C (2011). Unique Regulation of Adipose Triglyceride Lipase (ATGL) by Perilipin 5, a Lipid Droplet-associated Protein. *J Biol Chem* **286**, 15707-15715.

Wang W, Hansen PA, Marshall BA, Holloszy JO, & Mueckler M (1996). Insulin unmasks a COOH-terminal Glut4 epitope and increases glucose transport across T-tubules in skeletal muscle. *J Cell Biol* **135**, 415-430.

Wardzala LJ & Jeanrenaud B (1981). Potential mechanism of insulin action on glucose transport in the isolated rat diaphragm. Apparent translocation of intracellular transport units to the plasma membrane. *J Biol Chem* **256**, 7090-7093.

Watson RT & Pessin JE (2001). Subcellular Compartmentalization and Trafficking of the Insulin-Responsive Glucose Transporter, GLUT4. *Experimental Cell Research* **271**, 75-83.

Watt MJ & Spriet LL (2010). Triacylglycerol lipases and metabolic control: implications for health and disease. *Am J Physiol Endocrinol Metab* **299**, E162-E168.

Webber J, Taylor J, Greathead H, Dawson J, Buttery PJ, & Macdonald IA (1994). Effects of fasting on fatty acid kinetics and on the cardiovascular, thermogenic and metabolic responses to the glucose clamp. *Clin Sci (Lond)* **87**, 697-706.

Weber T, Zemelman BV, McNew JA, Westermann B, Gmachl M, Parlati F, Sollner TH, & Rothman JE (1998). SNAREpins: minimal machinery for membrane fusion. *Cell* **92**, 759-772.

Weis J, Johansson L, Courivaud F, Karlsson FA, & Ahlstrom H (2007). Quantification of intramyocellular lipids in obese subjects using spectroscopic imaging with high spatial resolution. *Magn Reson Med* **57**, 22-28.

Weiss SB, Kennedy EP, & Kiyasu JY (1960). The Enzymatic Synthesis of Triglycerides. *J Biol Chem* **235**, 40-44.

Welsh GI, Hers I, Berwick DC, Dell G, Wherlock M, Birkin R, Leney S, & Tavare JM (2005). Role of protein kinase B in insulin-regulated glucose uptake. *Biochem Soc Trans* **33**, 346-349.

White MF (1998). The IRS-signalling system: a network of docking proteins that mediate insulin action. *Mol Cell Biochem* **182**, 3-11.

Winder WW & Hardie DG (1999). AMP-activated protein kinase, a metabolic master switch: possible roles in type 2 diabetes. *Am J Physiol* **277**, E1-10.

World Health Organisation. Obesity and Overweight Fact Sheet. 2003. World Health Organisation.

Ref Type: Report

World Health Organisation. Definition and Diagnosis of Diabetes Mellitus and Intermediate Hyperglycaemia. 2006. World Health Organisation.
Ref Type: Report

World Health Organisation. Diabetes Fact Sheet 312. 2008. World Health Organisation.
Ref Type: Report

Yamaguchi T (2010). Crucial Role of CGI-58/alpha/beta Hydrolase Domain-Containing Protein 5 in Lipid Metabolism. *Biol Pharm Bull* **33**, 342-345.

Yamaguchi T, Omatsu N, Matsushita S, & Osumi T (2004). CGI-58 Interacts with Perilipin and Is Localized to Lipid Droplets. *J Biol Chem* **279**, 30490-30497.

Yamaguchi T, Omatsu N, Morimoto E, Nakashima H, Ueno K, Tanaka T, Satouchi K, Hirose F, & Osumi T (2007). CGI-58 facilitates lipolysis on lipid droplets but is not involved in the vesiculation of lipid droplets caused by hormonal stimulation. *J Lipid Res* **48**, 1078-1089.

Yamashita S, Hosaka K, & Numa S (1972). Resolution and reconstitution of the phosphatidate-synthesizing system of rat-liver microsomes. *Proc Natl Acad Sci U S A* **69**, 3490-3492.

Yamashita S & Numa S (1972). Partial purification and properties of glycerophosphate acyltransferase from rat liver. Formation of 1-acylglycerol 3-phosphate from sn-glycerol 3-phosphate and palmityl coenzyme A. *Eur J Biochem* **31**, 565-573.

Yang C, Coker KJ, Kim JK, Mora S, Thurmond DC, Davis AC, Yang B, Williamson RA, Shulman GI, & Pessin JE (2001). Syntaxin 4 heterozygous knockout mice develop muscle insulin resistance. *J Clin Invest* **107**, 1311-1318.

Yu C, Chen Y, Cline GW, Zhang D, Zong H, Wang Y, Bergeron R, Kim JK, Cushman SW, Cooney GJ, Atcheson B, White MF, Kraegen EW, & Shulman GI (2002). Mechanism by Which Fatty Acids Inhibit Insulin Activation of Insulin Receptor Substrate-1 (IRS-1)-associated Phosphatidylinositol 3-Kinase Activity in Muscle. *J Biol Chem* **277**, 50230-50236.

Zderic TW, Davidson CJ, Schenk S, Byerley LO, & Coyle EF (2004). High-fat diet elevates resting intramuscular triglyceride concentration and whole body lipolysis during exercise. *Am J Physiol Endocrinol Metab* **286**, E217-E225.

Zechner R, Kienesberger PC, Haemmerle G, Zimmermann R, & Lass A (2009). Adipose triglyceride lipase and the lipolytic catabolism of cellular fat stores. *J Lipid Res* **50**, 3-21.

Zeigerer A, McBrayer MK, & McGraw TE (2004). Insulin Stimulation of GLUT4 Exocytosis, but Not Its Inhibition of Endocytosis, Is Dependent on RabGAP AS160. *Mol Biol Cell* **15**, 4406-4415.

Zimmermann R, Strauss JG, Haemmerle G, Schoiswohl G, Birner-Gruenberger R, Riederer M, Lass A, Neuberger G, Eisenhaber F, Hermetter A, & Zechner R (2004). Fat Mobilization in Adipose Tissue Is Promoted by Adipose Triglyceride Lipase. *Science* **306**, 1383-1386.